Renato Miguel Rodrigues Pereira

Mestre em Engenharia Civil

Probabilistic-based structural safety analysis of concrete gravity dams

Dissertação para obtenção do Grau de Doutor em

Engenharia Civil

Orientador:	António Lopes Batista, Professor Associado Convidado, Universidade Nova de Lisboa
Co-orientador:	Luís Armando Canhoto Neves, Assistant Professor, University of Nottingham

Júri

Presidente:	Doutor Fernando Manuel dos Anjos Henriques
Arguentes:	Doutor Eduardo Soares Ribeiro Gomes Cavaco
	Doutora Laura Maria Mello Saraiva Caldeira
Vogais:	Doutor António Abel Ribeiro Henriques
	Doutor António Lopes Batista
	Doutora Carla Alexandra da Cruz Marchão
	Doutor José Antero Senra Vieira de Lemos

FACULDADE DE CIÊNCIAS E TECNOLOGIA
UNIVERSIDADE NOVA DE LISBOA

Março, 2019

Renato Miguel Rodrigues Pereira

Probabilistic-based structural safety analysis of concrete gravity dams

Março, 2019

Probabilistic-based structural safety analysis of concrete gravity dams

To my grandparents,

José Pereira and

Maria Júlia da Silva Matos

Acknowledgements

I would first like to thank my advisor, Dr. António Lopes Batista, Associate Professor of the Faculty of Science and Technology of the New University of Lisbon (FCT/UNL) and Head of the Concrete Dams Department of the National Laboratory for Civil Engineering (LNEC), and my co-advisor, Dr. Luís Canhoto Neves, Assistant Professor of the University of Nottingham, for their guidance throughout the development of this work. To Dr. António Lopes Batista, I would like to thank for his friendship, continuous support and motivation. The door to his office was always open. To Dr. Luís Canhoto Neves, I would thank for the insightful suggestions and the hospitality which he received me at his house in Nottingham, UK.

My acknowledgments go to: (i) the Department of Civil Engineering (DEC) at FCT/UNL, for the support provided during the elaboration of the thesis; (ii) LNEC, as host institution, for enabling the valuable resources required; and (iii) the Science and Technology Foundation (FCT), for granting the doctoral fellowship to develop this work.

I am grateful to the members of the Technical Advisory Committee, Dr. Laura Caldeira and Dr. José Vieira de Lemos, for their observations and recommendations. To Dr. José Vieira de Lemos, I am specially thankful for the introduction to the discrete element method and his constant solicitude on the work progress.

A very special acknowledgment goes to Dr. João Casaca, for the scientific and technical advices, providing his expertise, knowledge and hard work which were directly related to the development of this thesis.

I would also like to thank all my colleagues in the Concrete Dams Department, especially to Dr. Nuno Monteiro Azevedo, Dr. Maria Luísa Braga Farinha, Dr. Sérgio Oliveira, Dr. Jorge Pereira Gomes, Dr. Ivo Dias, Dr. Juan Mata, Dr. João Conde da Silva, Eng. Miguel Rodrigues, Eng. David Pereira, Eng. Tiago Henriques and Dr. Eduardo Bretas. Especial thanks are due to Dr. Carlos Serra, Eng. André Alegre and Eng. Margarida Espada for their friendship and material and emotional support. Thanks are also due to Dr. Alexandra

Carvalho, from the Earthquake Engineering and Structural Dynamics Unit (NESDE) of LNEC, for providing the seismic histograms.

I am grateful to my friends Dr. Filipe Ribeiro, Dr. Leonardo Rodrigues, Dr. Cláudia Ferreira, Valter Rodrigues, Pedro Félix Carvalho and Frederico Gomes for their support and encouragement.

Finally, my special gratitude belongs to my family. I am forever grateful to my parents, my sister and my girlfriend for their love, support and encouragement.

Abstract

The construction and operation of dams, associated with the use of water resources, aims generically at water supplying, the energy producing and, in many cases, flow regulating and flood controlling.

Considering the dam dimensions and the potential risks associated with its structural failure, due to the occupation of the downstream valley, and to the costs of the construction, maintenance and rehabilitation, the use of probabilistic principles in its design, as it is already performed for other type of structures, is justified considering adequate levels of safety.

The objections shared throughout the dam engineering community, regarding the difficulty in estimating the probability of failure for concrete dams, are expectedly overcome by the failure mode and uncertainty modeling, allowing the application of probabilistic principles for their safety analysis, based on conservative simplifications regarding the structural behavior, namely: (i) the definition of the failure surface (dam-foundation interface); (ii) the consideration of rigid body failure mechanisms; and (iii) the consideration of the residual shear strength, given only by the frictional component, corresponding to a limit analysis valid for ultimate limit states.

For that purpose, the failure modes are derived from the current construction and design practice by comparing analytical and numerical models of a generic, though representative, case study. The uncertainties involved in the safety of concrete dams are statistically quantified, through the definition of probabilistic distributions for loads and material properties, using, in addition to the elements found in the literature, the information available at LNEC about those features, resulting from the monitoring of the concrete dam behavior during the construction, first filling and operation periods.

This work explores the required tasks for the adoption of the partial safety factor

method for the safety analysis of concrete gravity dams, at the design phase. Two representative studies regarding the reliability-based design of concrete gravity dams and partial safety factor calibration are presented, intending to stimulate the discussion on the applicability of probabilistic principles for the design of concrete dams, as well as, to influence the safety criteria to be considered in a future revision of the dam safety regulation.

The obtained results confirm that the seismic load combination and the sliding failure modes are the most conditioning situations. It is also observed that cross-sections profiles flatter than currently used may be needed for high intensity seismic zones. Partial safety factors that approximate reasonably the reliability-based results could be derived.

Keywords: Concrete gravity dams, Failure mode modeling, Uncertainty modeling, Reliability-based design, Partial safety factor calibration

Resumo

A construção e exploração de barragens, que está associada ao aproveitamento dos recursos hídricos, visa essencialmente o abastecimento de água às populações, a produção de energia e, em muitos casos, a regularização de caudais e o controlo de cheias.

Por serem obras de engenharia a que estão associados consideráveis riscos potenciais, principalmente relacionados com a segurança das populações no vale de jusante, mas também custos de construção, manutenção e reabilitação de monta, justifica-se que as barragens sejam dimensionadas considerando níveis de segurança adequados, sendo que tal pode ser conseguido, com vantagem, usando princípios probabilísticos, à semelhança do que acontece correntemente com outros tipos de estruturas.

Pretendem-se ultrapassar as objeções levantadas pela comunidade da engenharia de barragens relativamente à dificuldade de estimar a probabilidade de falha de barragens de betão, através da definição analítica dos modos de falha e da modelação das fontes de incerteza. Estas ferramentas permitem a análise probabilística da segurança estrutural de barragens gravidade de betão com base em simplificações relativas ao seu comportamento estrutural, nomeadamente: (i) a definição da superfície de falha (neste caso a interface barragem-fundação); (ii) a consideração de mecanismos de rotura de corpo rígido; e (iii) a consideração da resistência residual, contabilizando apenas a contribuição da componente atrítica, correspondente a uma análise limite.

Com este propósito definem-se os modos de falha através da comparação de modelos analíticos e numéricos de um caso de estudo genérico mas representativo. Faz-se previamente a caracterização estatística das fontes de incerteza envolvidas na segurança de barragens de betão, através da definição de distribuições de probabilidade de ações e resistências, recorrendo-se, para além dos elementos disponíveis na literatura técnica e científica afim, à informação disponível no LNEC resultante do acompanhamento e monitorização

do comportamento deste tipo de estruturas.

O trabalho focou-se nas tarefas necessárias para a adoção do método dos coeficientes parciais de segurança para análise da segurança estrutural de barragens gravidade de betão, na fase de projeto. Apresentam-se dois estudos representativos do dimensionamento de barragens gravidade de betão com base nos princípios probabilísticos e da calibração de coeficientes parciais de segurança para os estados limites últimos. Estas aplicações pretendem estimular a discussão sobre a aplicabilidade destes conceitos no dimensionamento de barragens de betão, bem como influenciar os critérios de projeto com vista à sua consideração em futuras revisões da regulamentação portuguesa de segurança de barragens.

Os resultados obtidos confirmam que a combinação sísmica e o modos de falha relativos aos deslizamento da estrutura são as situações mais condicionantes. Conclui-se também que perfis transversais com paramento de jusante menos inclinado, deverão ser necessários em zonas sísmicas mais gravosas. Conseguiu-se uma calibração coerente dos coeficientes parcias de segurança que aproximam bem os resultados obtidos por via probabilística.

Palavras-chave: Barragens de betão, Modelação dos modos de falha, Quantificação das incertezas, Análise probabilística da segurança, Calibração de coeficientes parciais de segurança

Contents

List of Figures

List of Tables

List of Acronyms

Abbreviations

ALARP	As low as reasonable practicable
DDO	Deterministic design optimization
DEM	Discrete-element method
FORM	First-order reliability method
FWL	Flood water level
GLM	Generalized linear model
LAH	Portuguese law for the hydraulic exploitation
LRFD	Load and resistance factor design
LSM	Least-square method
MCE	Maximum credible earthquake
MDE	Maximum design earthquake
MLE	Maximum likelihood estimation
MM	Moment-matching
MOL	Minimum operation level
NCB	Portuguese code of practice for construction of dams
NOIB	Portuguese code of practice for observation and inspection of dams
NPB	Portuguese code of practice for dam design

NTPCS	Italian technical rules for the design and construction of dams
NWL	Normal water level
PNBEPH	Portuguese national programme for dams of great hydroelectric potential
RBDO	Reliability-based design optimization
RCC	Roller-compacted concrete
RO	Risk optimization
RSB	Portuguese dam safety regulation
SORM	Second-order reliability method
UDEC	Universal distinct element code

Official Bodies

ACI	American Concrete Institute
ANCOLD	Australian Committee on Large Dams
APA	Agência Portuguesa do Ambiente (Portuguese Environment Agency)
CDA	Canadian Dam Association
CEN	Comité Européen de Normalisation (European Committee for Standardization)
CFBR	Comité Français des Barrages et Réservoirs (French Committee of Dams and Reservoirs)
EPRI	Eletric Power Research Institute
FERC	Federal Energy Regulatory Commission
FIB	Fédération Internationale du Béton (International Federation for Structural Concrete)
HSE	Health and Safety Executive
ICOLD	International Committee on Large Dams

ISO	International Organization for Standardization
JCSS	Joint Committee on Structural Safety
JRC	Joint Research Centre
LNEC	Laboratório Nacional de Engenharia Civil (National Laboratory for Civil Engineering)
SPANCOLD	Spanish Committee on Large Dams
USACE	United States Army Corps of Engineers
USBR	United States Bureau of Reclamation

List of Symbols

Alphanumeric

a_g	Peak ground acceleration
a_{gr}	Reference peak ground acceleration
a_k	Characteristic value of geometric parameters
A_p	Hydrodynamic force coefficient
$\boldsymbol{a}$	Vector of unknown regression parameters of the model representing the relative reservoir water level variation over the year
B_1	Portion of p_0 that acts in the fundamental vibration mode
c	Cohesion
C	Consequences; velocity of pressure waves in water
D	Damage
$\boldsymbol{d}$	Search direction vector (FORM)
$\boldsymbol{D}$	Hessian matrix
E	Load effects; load event
E_c	Dam concrete Young's modulus
E_f	Foundation Young's modulus
E_m	Numerically calibrated Young's modulus
E_P	Average potential Young's modulus
f	Annual probability of failure; material properties

$f^{(1)}(\cdot)$	Merit function 1
$f^{(2)}(\cdot)$	Merit function 2
f_1	Pseudo-dynamic equivalent lateral forces for the fundamental vibration mode
f_c	Concrete compressive strength
$f_{c,c150}$	Concrete compressive strength of cubic specimens of wet-screened concrete
$f_{c,y150}$	Concrete compressive strength of cylindric specimens of wet-screened concrete
$f_{c,y450}$	Concrete compressive strength of cylindric specimens of full-mixed concrete
f_d	Design values of material properties
f_f	Concrete flexural strength
$f_{f,p150}$	Concrete flexural strength of prismatic specimens of wet-screened concrete
$f(\cdot)$	Model function
F_h	Horizontal component of the net force acting on the dam body
f_k	Representative (characteristic) values of material properties
$F_{n,w}$	Normal net force acting on the downstream rock wedge slope
f_s	Concrete splitting strength
F_s	Seismic equivalent pseudo-static or pseudo-dynamic forces
$f_{s,y150}$	Concrete splitting strength of cylindric specimens of wet-screened concrete
$f_{s,y450}$	Concrete splitting strength of cylindric specimens of full-mixed concrete

f_{sc}	Pseudo-dynamic equivalent lateral forces associated with higher vibration modes
f_t	Concrete tensile strength
$f_{t,y150}$	Concrete tensile strength of cylindric specimens of wet-screened concrete
$f_{t,y450}$	Concrete tensile strength of cylindric specimens of full-mixed concrete
$F_{t,w}$	Tangential net force acting on the downstream rock wedge slope
F_v	Vertical component of the net force acting on the dam body
$f_X(\cdot)$	Probability distribution function
$F_X(\cdot)$	Cumulative distribution function
$f_{\boldsymbol{X}}(\cdot)$	Joint probability distribution function
g	Gravity acceleration
$g(\cdot)$	Limit state function in the standard normal space; link function
$G(\cdot)$	Limit state function
$g(\cdot)^{-1}$	Inverse link function
G_k	Characteristic value for the permanent loads
h	Cylindric or prismatic concrete specimen height
H	Hazard; dam height
H_d	Hydraulic head at the drainage line
H_g	Gallery level
H_p	Hydraulic head at the piezometric line
H_r	Reservoir water level
h_s	Silt deposit height
H_t	Tailwater level

h_w	Keyed depth
$h_X(\cdot)$	Importance sampling probability distribution function
$\boldsymbol{H}$	Fisher information matrix
i_1	Partial seismic risk index related to the reservoir capacity
i_2	Partial seismic risk index related to the dam height
i_3	Partial seismic risk index related to the potential risks
$I(\cdot)$	Indicator function
i_r	Global seismic risk index
I_s	Total silt force
I_w	Total hydrostatic force
I_{ws}	Total hydrodynamic force
$\boldsymbol{J}$	Jacobian matrix
k	Curvature parameter; seismicity-dependent parameter
K_0	Coefficient of earth pressure at rest
k_{fwl}	Relative flood water level
k_{nwl}	Relative normal water level
k_r	Relative reservoir water level
k_u	Uplift factor
L	Dam base width
L_1	Earthquake force coefficient, with empty reservoir
$\tilde{L}_1$	Earthquake force coefficient, including the effect of the impounded water
$L(\cdot)$	Likelihood function
$\boldsymbol{L}$	Lower triangular matrix obtained from $\boldsymbol{\Sigma}$ by Cholesky decomposition
$\log L(\cdot)$	Log-likelihood function
m	Sample mean

M_1	Generalized mass coefficient, with empty reservoir
$\tilde{M}_1$	Generalized mass coefficient, including the effect of the impounded water
$M(\cdot)$	Penalty function
M_{ins}	Instabilizing moment
M_{sta}	Stabilizing moment
N	Number of fatalities; normal net force
N_{pz}	Number of piezometers
p	Probability of exceedance of a seismic action
P	Probability
$p_0(\cdot)$	Real-valued and frequency-independent hydrodynamic pressure, per unit weight, on a rigid dam under unit acceleration
p_f	Probability of failure
p_{ft}	Target probability of failure
$p(\cdot)$	Hydrodynamic pressure, per unit weight, of a full reservoir due to harmonic acceleration of period $\hat{T}_r$
p_u	Uplift pressure
p_w	Hydrostatic pressure
p_{ws}	Hydrodynamic pressure
Q	Applied loads
Q_k	Characteristic value for the variable loads
R	Risk; resistance or structural carrying capacity
r	Radius of a hyper-spheric region in the standard normal space
R_f	Period lengthening ratio due to the dam-foundation interaction

r_{in}	Internal radius of a hyper-spheric ring in the standard normal space
r_{out}	External radius of a hyper-spheric ring in the standard normal space
R_P	Plastic strength
R_r	Period lengthening ratio due to the impounded water
R_w	Period ratio of the dam-foundation interaction
$\boldsymbol{R}$	Rotation matrix
S	Loads; soil factor for the computation of the seismic elastic response spectrum; sliding forces; shear net force
s^2	Sample variance
S_a	Semi-amplitude of the model considering a sinusoidal variation of the reservoir water level over the year; pseudo-acceleration ordinate of the design spectrum
s_d	Downstream face slope
S_d	Design values of loads
S_e	Elastic response spectrum
$S(\cdot)$	Load effect function
S_k	Representative (characteristic) values of loads
T	Vibration period of a linear single-degree-of-freedom system
T_1	Dam fundamental vibration period
T_1^r	Fundamental vibration period of the impounded water
$\hat{T}_1$	Dam fundamental vibration period with impounded water and flexible foundation
T_B	Lower limit of the period of the constant spectral acceleration branch

T_C	Upper limit of the period of the constant spectral acceleration branch
T_d	Design return period
T_D	Value defining the beginning of the constant displacement response range of the elastic response spectrum
t_l	Structure service life
T_r	Reference return period
$\hat{T}_r$	Dam fundamental vibration period with impounded water
$\boldsymbol{T}$	Vector of independent variables of the model representing the relative reservoir water level variation over the year
U	Total uplift force
$\boldsymbol{u}^*$	Design point in the standard normal space
$\boldsymbol{u}$	Vector of random variables in the standard normal space
V	Reservoir capacity/volume; dam volume
W	Valley width at the crest level; dam weight
$w(\cdot)$	Dam weight per unit height
$W_Q(\cdot)$	External work function
$W_R(\cdot)$	Internal work function
x	Random variable
X	Factor characterizing the hazard associated with the dam operation
x_0	Application point of the horizontal component of the net force acting on the dam body
x_U	Application point of the total uplift force
$\boldsymbol{x}^*$	Design point
$\boldsymbol{x}$	Vector of random variables
$\boldsymbol{x}_d$	Vector of design values of random variables

$\boldsymbol{x}_k$	Vector of characteristic values of random variables
$\hat{\boldsymbol{x}}$	Generated sample of $\boldsymbol{x}$
Y	Number of permanent edifications
y_0	Application point of the horizontal component of the net force acting on the dam body
y_{F_s}	Application point of the seismic equivalent pseudo-static or pseudo-dynamic forces
y_{I_w}	Application point of the total hydrostatic force
$y_{I_{ws}}$	Application point of the total hydrodynamic force
z	Unit random number; water depth
$\boldsymbol{z}$	Vector of unit random numbers
$\hat{\boldsymbol{z}}$	Generated sample of $\boldsymbol{z}$

Greek letters

α	Downstream rock wedge slope; seismic coefficient; wave reflection coefficient
$\boldsymbol{\alpha}$	Vector of direction cosines
$\hat{\boldsymbol{\alpha}}$	Generated sample of $\boldsymbol{\alpha}$
β	Reliability index
β_T	Target reliability index
$\chi^2_n(\cdot)$	Chi-square distribution function with n degrees of freedom
Δ	Total expected losses
$\boldsymbol{\delta}$	Replacement vector
η	Damping correction factor for the computation of the seismic elastic response spectrum; constant hysteretic damping factor
γ_c	Strength reduction factor for the cohesion; concrete unit weight

γ_{cq}	Construction quality factor
γ_d	Structural coefficient for ultimate limit states (Chinese standards); model coefficient (French guidelines)
$\gamma_{E,1}$	Partial safety factor for the seismic action type I
$\gamma_{E,2}$	Partial safety factor for the seismic action type II
γ_f	Partial safety factor associated with the material property f
γ_G	Partial safety factor for the permanent loads
γ_I	Seismic importance factor; partial safety factor for the hydrostatic pressure
γ_m	Partial safety factor for friction coefficient
γ_Q	Partial safety factor for the variable loads
γ_r	Rock mass unit weight
γ_S	Partial safety factor associated with the load S
$\gamma_{\tan(\phi)}$	Strength reduction factor for the friction coefficient
γ_U	Partial safety factor for the uplift pressure
γ_w	Water unit weight
$\boldsymbol{\kappa}$	Vector of the limit state function curvature
λ	Safety factor; step size (FORM)
μ_X or $E[X]$	Expected (or mean) value of a random variable X
ω	Importance factor
$\mathbf{\Omega}$	Unknown weights of the mixture of beta distributions
ϕ	Friction angle
Φ	Cylindric specimen diameter; phase of the model considering a sinusoidal variation of the reservoir water level over the year
$\Phi(\cdot)$	Standard normal distribution function

ϕ_r	Residual friction angle
ϕ_s	Internal friction angle of silt deposit
φ	Beta distribution precision parameter
$\phi(y)$	Displacement of the fundamental mode shape of a standard monolith
ψ	Dilatancy angle; Design situation factor (Chinese standards)
ρ_c	Concrete density
σ	Normal stresses
σ_A	Applied stresses
σ_P	Permissible stresses
σ_U	Ultimate stresses
σ_X^2 or $V[X]$	Second central moment or variance of a random variable X
$\mathbf{\Sigma}$	Variance-covariance matrix
$\tan\phi$	Friction coefficient
$\tan\phi_c$	Critical friction coefficient
θ	Model uncertainty; design variable
θ_e	Seismic load model uncertainty
θ_S	Model uncertainty due to the rigid body formulation
θ_R	Mohr-Coulomb shear strength model uncertainty
θ_u	Uplift model uncertainty
θ^*	Vector of optimum values of the design variable
$\boldsymbol{\theta}$	Vector of the probability distribution parameters
$\mathbf{\Theta}$	Unknown parameters of the mixture of beta distributions
$\hat{\boldsymbol{\theta}}$	Best estimators of the probability distribution parameters
ξ_1	Dam damping ratio

$\hat{\xi}_1$	Dam damping ratio with impounded water and flexible foundation
ξ_f	Additional damping due to the dam-foundation interaction
ξ_r	Additional damping due to the added hydrodynamic mass
$\hat{\xi}_r$	Dam damping ratio with impounded water
ζ	Degree-of-fit parameter
ζ_T	Target degree-of-fit parameter

CHAPTER 1

Introduction

1.1 General framework

1.1.1 The role of dams in society

River regulation, since times immemorial, is linked to the formation of human settlements, ensuring water supply and the development of first agrarian civilizations, based on earliest irrigation systems. Flood mitigation, eliminating or reducing the damage to people/assets in case of floods, were also intended with dam construction.

The need for hydropower, initially used for small local projects such as milling grain and lifting water, has grown exponentially since the industrial revolution, in the 19^{th} century. Industrialization also inspired the mechanization of agriculture and stimulated demand for a variety of products (Billington *et al.* 2005), which could only be ensured with large-scaled irrigation systems.

As a renewable source of energy, hydropower, coming from the transformation of potential energy into kinetic energy, due to the hydraulic gradient installed, plays a crucial role in modern societies. The marked increase of dams, in number and size, in the last two centuries reflects the growing energy demand and the concerns related to energy dependence, sustainability and economy.

After the last census, the world register of dams (ICOLD 2018) includes more than 58000 large dams throughout the world, distributed as illustrated in Figure 1.1.

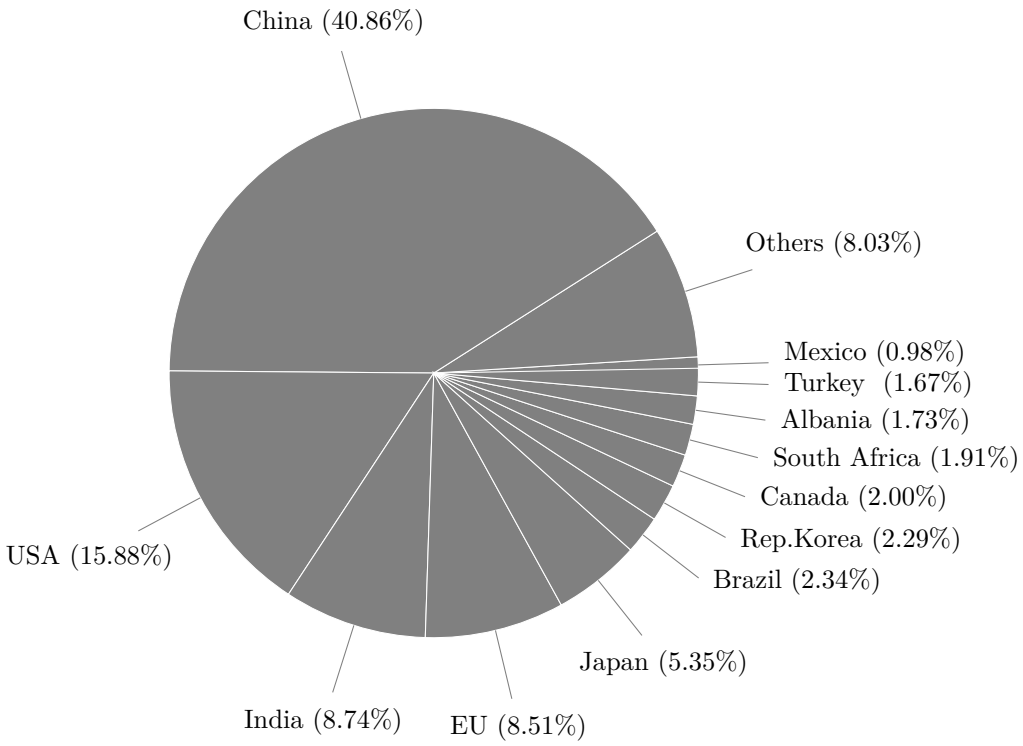

Figure 1.1: Countries by proportion of large dams (ICOLD 2018).

1.1.2 Dams in Portugal

The construction of dams and the exploitation of the water resources for hydroelectricity production grew, in Portugal, since the end of the 19$^{\text{th}}$ century.

First projects of small dimensions, from private initiative, aimed to provide energy for the operation of local industrial facilities. Later, in order to legislate the production, transport and distribution of energy and achieve the electrification of the country, the law for the hydraulic exploitation (LAH 1926), based on the construction of larger hydropower plants, was published. In the period following the second world war, some of the highest dams in service today were built and began operating, such as, for instance, Cabril dam (132 m) in 1954, Castelo do Bode dam (115 m) in 1951, Paradela dam (112 m) in 1956, Picote dam (100 m) in 1958 and Venda Nova dam (97 m) in 1951.

Facing the increased energy demand that characterizes the modern lifestyle, several dams were built since then such as, for instance, Alto Lindoso dam (110 m) and Alqueva dam (96 m), which began operating in 1992 and 2002, respectively.

Nowadays, in Portugal, there are 258 large dams in operation, most of them built during the second half of the last century. Following the national program for dams of

great hydroelectric potential (PNBEPH 2007), some dams were built and began operating in the last years, aiming to reduce the unexploited hydro potential from 54% to 33%, such as, for instance, Baixo Sabor dam (123 m) in 2016, Foz Tua dam (108 m) in 2017 and Ribeiradio dam (83 m) in 2014.

Some of the referred dams have multiple purposes, mainly related to water supply and flood control. A significant number of dams, with smaller dimensions, were also built for irrigation, mostly located in the center-south of Portugal.

1.1.3 Classical approach to dam safety

As the dam population grew throughout the world and increasingly higher dams were being built, engineers faced new challenges in conceiving proper solutions and maintaining adequate levels of safety, given that consequences of structural failure may be catastrophic according to the social, environmental, political and/or economical perspectives.

In 1928, recognizing the benefits taken from experience and collaboration, a number of countries formed the International Commission on Large Dams (ICOLD) aiming to encourage advances in planning, design, construction, operation and maintenance of large dams and associated civil works, by collecting and disseminating relevant information and studying related technical questions (ICOLD 2011).

While structural and material behavior were extensively studied in the early years of the scientific debates, during ICOLD congresses, dam safety was analyzed based exclusively on the judgment and experience of the practitioner (Donnelly 2006), who should implicitly account for the potential consequences of the structural failure in the choice of safety factors and magnitude of loads. The design and construction principles, dependent on the local experience, were progressively adapted as scientific advances were being achieved, especially after some dam accidents that promoted discussions. The difference of interpretation found in different regulatory instructions, such as, for instance, regarding the uplift pressures and the associated reduction works (Andrade 1982) before the contribution of Casagrande (1961), reflects the lack of consensus and orientation.

This orientation came formally at the late 1960s, when focus was put on subjects of current concern such as dam safety, monitoring, aging and environmental impact. The starting point for a common approach was the guidelines for dam safety (ICOLD 1987), which intended to stimulate the development of national dam safety regulations by detailing a comprehensive framework on dam design, operation, maintenance and monitoring that

should be considered against all scenarios expected to occur during the life of a dam, given (ICOLD 1987): (i) the several dam incidents, caused by inadequate design or construction, with severe consequences; (ii) the growing dimensions of new dams and the aging of older dams; and (iii) the increasing number of dams being built in countries with little or no tradition and experience in dam engineering.

Although recognizing the merit of risk analysis in the mathematical optimization of a problem that balances safety and economy, it is claimed that the calculation of the overall probability of failure for a given dam, within meaningful confidence limits, would not yet be possible (ICOLD 1987), since dam behavior highly depends on the foundation characteristics which are only roughly known. As large dams are, among the class of structures whose failure may lead to catastrophic consequences, those whose structural behavior is predicted with the highest degree of uncertainty (Kreuzer 2005), analytical models would require such assumptions that conclusions from a probabilistic assessment would not have any practical value. Thus, the classical approach to dam safety, according to these guidelines (ICOLD 1987), consists in a combination of deterministic criteria, based on the concept of safety factor, and continuous monitoring. Nonetheless, this approach has produced satisfactory results (Donnelly 2006) mainly because the uncertain nature of the dam safety problem is masked by considering: (i) exceptional load events, such as flood and earthquake, characterized by design values with high return period; (ii) a dam classification system, according to the potential consequences of a failure, providing guidance with respect to the conditions that a dam needs to resist to ensure that it does not present an unacceptable danger to the environment or the public (Donnelly 2006); and (iii) conservative safety factors, based on the allowable stress philosophy, intending to absorb the unexpected uncertainties or some unforeseeable phenomena (Lombardi 1993).

1.1.4 Probabilistic approach to dam safety

Since the second half of the last century, the societal concern about welfare, safety, sustainability and economy was extended to several domains of civil engineering including not only dams but also other types of structures. At that time, there was a theoretical development when the concepts of classical structural reliability emerged (Elingwood 1994), due to a convergence between the theoretical reliability (Cornell 1969) and the design/standards communities.

In the 1970s, the structural design approach changed from considering a safety factor

applied within the strength, corresponding to the allowable stress philosophy, to the limit state design, in which a safety factor was applied within the loads (Vrouwenvelder and Siemes 1987). By influence of the Joint Committee on Structural Safety (JCSS), created to improve the general knowledge on structural safety, there was a changed-over to the partial safety factor approach in which the safety margin was distributed on both the strength and the load sides, by means of partial safety factors defined proportionally to the uncertainty and influence of each quantity in the desired level of safety. Although safety analysis is still performed using deterministic safety criteria, this approach is commonly denoted as semi-probabilistic approach, since the partial safety factors are quantified preferentially by probabilistic calculations.

The JCSS probabilistic model code (JCSS 2001) provided the basis for the development of the European Standards (EN1990 2002), in which, to keep the design process practicable, a verification process based on partial safety factors (or semi-probabilistic approach) is considered. In these standards, a structure classification system, differentiating the safety requirements according to the possible consequences of failure, is employed. Nonetheless, for the design of large dams, as well as other special structures with possible catastrophic consequences, other dispositions shall be considered, indicating that, on one hand, the inherent simplifications of these standards may not be adequate for the design of these types of structures and, on the other hand, a more hazardous consequence class may be suitable.

Regarding large dams, although stimulating the development of national dam safety regulations based on the classical approach, ICOLD (1987) encouraged theoretical investigations for future adoption of a probabilistic approach to dam safety and states that the logical trend, in the design phase, goes from the predominantly deterministic concept of global safety factors to the semi-probabilistic method of partial safety factors. For existing dams, however, it is recognized that the standards-based approach is becoming increasingly inadequate (ICOLD 2005). Due to the inherent conservatism of a wide range domain of application, it may be costly ineffective (Bowles *et al.* 1998) for a single dam or a portfolio of dams. In those cases, risk-based approach has gained acceptance for the safety management of specific dams, as it allows a more focused deployment of finite resources to deal with dam safety issues on a priority basis (Donnelly 2006).

Thenceforth, legislators, regulators, institutions and working groups have studied and,

in some cases, implemented probabilistic approaches to dam safety. The limit state approach and the partial safety factor method for dam safety are already in: (i) the Chinese standards for the reliability-based design of hydraulic structures (GB50199 1994); (ii) the French guidelines for the justification of the stability of gravity dams (CFBR 2012); and (iii) the Italian technical rules for the design and construction of dams (NTPCS 2014). On the other hand, risk-based approach has been considered systematically for support decision-making regarding the operation of dams, even though it is not used as a substitute for the standards-based approach (ICOLD 2005). Nonetheless, as the dam building era is coming to an end (Westberg 2010) and maintenance and rehabilitation have become a priority, the aging of dams has been handled from a risk perspective. In Australia (ANCOLD 2003), Canada (CDA 2007), USA (USBR 2011) and Spain (SPANCOLD 2013), guidelines for the dam safety management, based on risk analysis techniques, are currently used.

1.2 Motivation, objectives and contribution

In Portugal, the preventive, safety control and civil protection measures for dams were established in the first version of the dam safety regulation (RSB 1990). This document formalizes the dam engineering practice, under the guidance of the ICOLD (1987), regarding the design, construction, operation and monitoring, based on complementary codes of practice (NPB 1993; NOIB 1993; NCB 1998). In this regulation, the classical approach to dam safety, based on the definition of safety factors supported by monitoring and inspection, was considered.

In the first revision of the dam safety regulation (RSB 2007), intending to incorporate the experience gained from the application of the previous regulation, the dams were classified according to the potential damage to lives, assets and environment in the downstream valley. However, the dam safety approach has not changed and the complementary codes of practice were still valid.

Recently, the dam safety regulation was revised again (RSB 2018), intending to include the scientific advances achieved with the Portuguese experience in dam engineering. The former codes of practice were revoked and reviewed codes were included in the RSB (2018). In this revised version, explicit formula was included to classify dams and redefine the return period of the design flood and the design earthquake, according to its height, reservoir capacity and permanent edifications in the downstream valley. The dam safety

approach has changed for embankment dams, where the limit state approach and the semi-probabilistic format for the dam safety analysis are now considered, whereas for concrete dams the classical approach was maintained.

Meanwhile, the risk-based approach in embankment dams has been increasingly discussed in Portugal. On this subject, a program for the application of concepts associated with the risk analysis to embankment dams was proposed (Caldeira 2005) and methodologies for the risk analysis were developed and applied to 36 Portuguese embankment dams in operation (Pimenta 2009).

For concrete dams, as mentioned, the possibility of incorporating probabilistic principles in the safety analysis has been recently explored worldwide, including Portugal (Ramos 1994; Farinha *et al.* 2014; Pereira *et al.* 2014; Pereira *et al.* 2015; Pereira *et al.* 2017), having been implemented in design standards or guidelines for support the risk-informed decision-making. However, the estimation of their probability of failure is one of the critical aspects for the dam engineering community, which has serious objections regarding its validity (Altarejos *et al.* 2015), since it was traditionally made by historic performance methods or by a combination of expert judgment techniques with deterministic analysis (Bowles *et al.* 1998), introducing relevant subjectiveness. The consideration of reliability theory to estimate the probability of failure of concrete dams has been increasingly tested, such as in the 11^{th} and the 14^{th} international benchmarks workshop on numerical analysis of dams organized by the ICOLD, with theme C "Estimation of the probability of failure of a gravity dam for the sliding failure mode" (Escuder *et al.* 2011) and theme D "Risk analysis-assessment of reliability for concrete dams" (Westberg *et al.* 2017), respectively. Furthermore, reliability theory has been successfully used to compute conditional probabilities within the risk analysis tools to dam safety management (Serrano 2011), based on the work of Altarejos (2009).

The success of the reliability methods in obtaining a realistic estimation of the probability of failure of concrete dams depends intrinsically on the proper modeling of the sources of uncertainties involved in the structural safety problem and the ability to model the structural behavior in limit conditions, and the associated failure modes, through analytical or numerical models. Regarding the uncertainty modeling, which requires a judicious combination of objective (data) and subjective (expert judgment) informations, guidance can be found in Westberg (2010) which compiled statistical information for material properties and loads and present a reliability-based methodology for safety assessment of new

and existing dams. This work was the basis for the development of a probabilistic model code for concrete dams (Westberg and Johansson 2016), following the same structure as the probabilistic model code (JCSS 2001), in an attempt to put together guidelines and regulations and to provide background that may be used for future development towards the application of the partial safety factor method for the dam safety analysis. Regarding the structural behavior, the known works refer to concrete gravity (Altarejos 2009; Westberg 2010) or buttress (Westberg 2010) dams, whose structural analysis can be based on two-dimensional simplifications, with well-defined failure surfaces and corresponding failure mechanisms. Extension to arch dams is more difficult since their structural behavior depends on the valley shape and the dam-foundation interaction. In those cases, estimations of the probability of failure could only be made by historic performance methods (Pedro 2007).

Having been recognized as the logical evolution of the classical approach (ICOLD 1987), this thesis aims to explore the tasks required for the adoption of the partial factors method for the safety analysis of concrete gravity dams, at the design phase, namely the failure mode identification and the uncertainty modeling. Simple developments regarding the reliability-based design of concrete gravity dams and partial safety factor calibration are also presented. It intends to stimulate the discussion on the applicability of probabilistic principles for the design of concrete dams, as well as, to justify a future revision of the dam safety regulation in the same direction as other regulations (GB50199 1994; CFBR 2012; NTPCS 2014). Although not intending to address the dam safety problem from a risk perspective, it is recognized that most of these tasks can also be considered within a risk analysis framework, particularly with regard to the failure mode identification, the uncertainty modeling and the estimation of conditional probabilities of failure. Briefly, this thesis aims at contributing with the following aspects:

- Identification of failure modes, corresponding to the actual practice of dam engineering, based on the physical perception of the gravity dam stability problem.
- Proposal of ultimate limit states, that explicitly set the boundary between the occurrence of consequences in the downstream valley and its avoidance;
- Proposal of probabilistic models for the quantitative characterization of uncertainties, related not only to loads and material properties but also to model simplifications,

which can be used as a priori information allowing a recurrent utilization of probabilistic (or risk) approach in the safety assessment and re-assessment of concrete dams;

- Testing a reliability-based methodology for structural safety analysis of concrete dams;
- Exploring the code calibration tasks for the quantification of partial safety factors and design rules towards the formulation of a semi-probabilistic verification process based on probabilistic principles;
- Promoting the discussion on this subject aiming to reformulate the Portuguese dam safety regulation.

1.3 Thesis outline

This thesis is organized into 7 chapters, as illustrated in Figure 1.2.

In Chapter 1, the thesis is introduced. An overall review on the application of probabilistic principles for structural safety analysis is made. The thesis motivation, objectives and contribution are discussed.

In Chapter 2, the probabilistic formulation of the structural safety problem is addressed. An historical review on the structural design is presented. Later, related subjects, namely uncertainty modeling, approaches for the structural safety analysis, reliability methods and procedure for reliability-based design and code calibration, are presented.

In Chapter 3, the methods for assessing the structural safety of concrete gravity dams are presented. After a review on the historical background on concrete dam design and construction, the constructive aspects and design principles, the loads acting on concrete gravity dams and the philosophy of the design codes are detailed. At the end, failure modes are modeled by comparing analytical and numerical solutions of representative, though generic, case studies.

In Chapter 4, the sources of uncertainty associated with the safety of concrete gravity dams are detailed. Data from monitoring and quality control tests are used to derive probabilistic models for water loads and concrete mechanical properties, respectively. The quantification of other sources of physical uncertainties, such as concrete density and

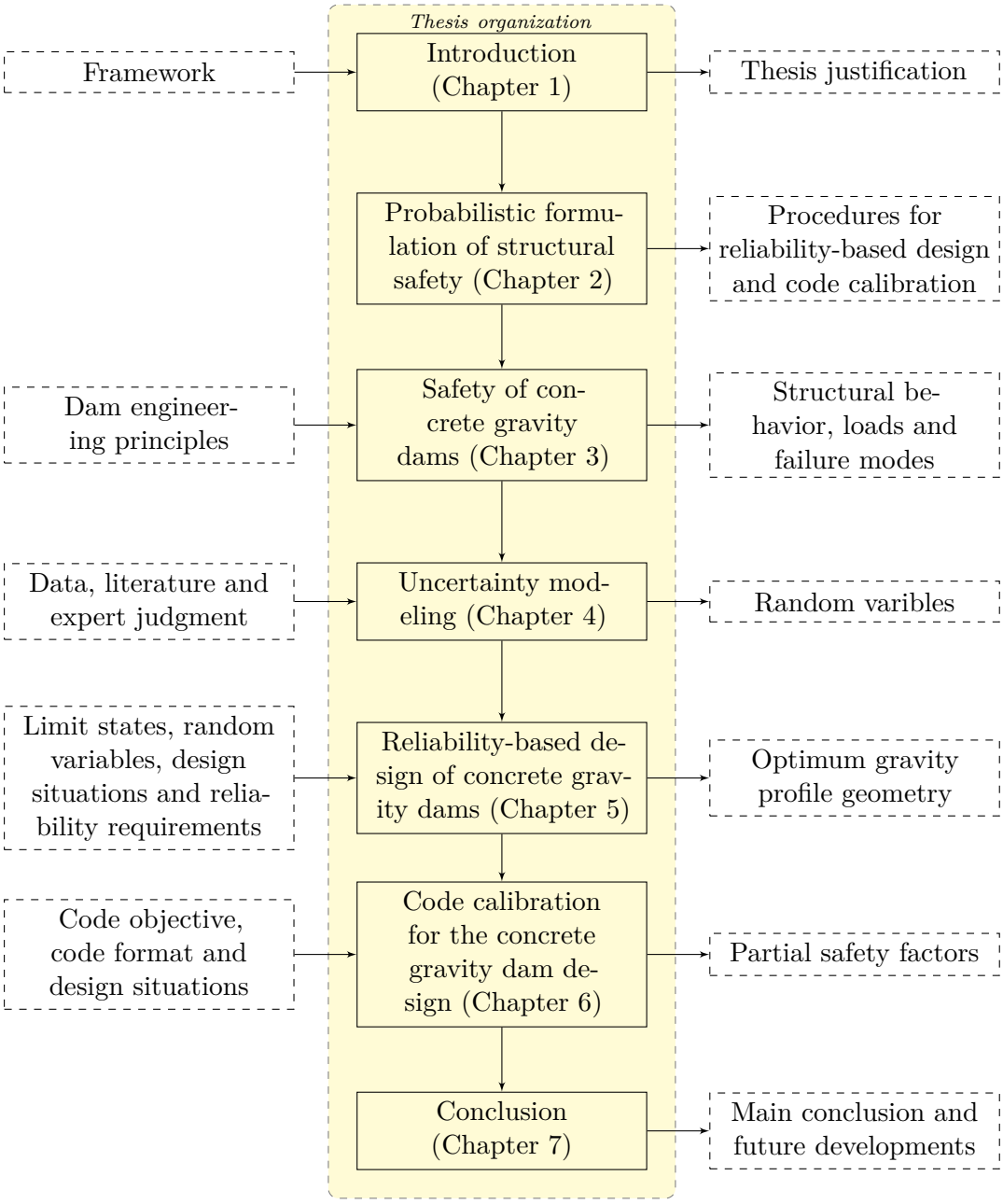

Figure 1.2: Thesis organization chart.

concrete-rock interface shear strength, is based on the literature. Sources of model uncertainty are also analyzed, mainly those related to the consideration of analytical seismic load models that approximate the structural response to seismic actions.

In Chapter 5, the reliability-based design principles are applied to a theoretical case study representing the structural class of large concrete gravity dams. After the definitions of limit states, random variables and reliability requirements, the reliability-based design procedure is applied to the design situations derived from all possible load combinations

started by flood or earthquake load events.

In Chapter 6, the code calibration procedure is applied to derive partial safety factors for the safety analysis of concrete gravity dams, at the design phase. For that, the results of the previous chapter are used, considering the techniques presented in Chapter 2.

In Chapter 7, the main conclusions and future developments on this subject are presented.

1.4 Software used

In this thesis, the MatLab scripting language (The Mathworks Inc. 2010) was used for data manipulation and algorithm development, regarding the failure modeling, uncertainty modeling, reliability-based design and code calibration.

The numerical analysis of discrete element models was performed in the Universal distinct element code (UDEC) software, version v5.0 (Itasca 2011).

CHAPTER 2

Probabilistic formulation of structural safety

2.1 General considerations

Civil engineering structures play a central role in modern society, providing infrastructures and facilities directly or indirectly necessary for our modern lifestyle. Furthermore, sustainability and economical optimality are increasingly required, since environmental and financial resources are limited. The benefits from the construction of structures must then be balanced with the non-negligible risks related to their use and/or operation.

Integrated in that process, structural safety analysis is the subject that deals with the verification whether structures can face expected load situations in safe conditions. However, due to the unavoidable uncertainties involved, absolute safety is not achievable for the structure itself. For that reason, structural safety shall be understood as fulfilling structural requirements that guarantee that failure would only occur at very low probability.

Besides its uncertain nature, structural safety is also a time-dependent problem, due to both time-variant loading conditions and deterioration of material strength properties. Figure 2.1 illustrates the time-variant structural safety problem.

Structural engineering in general, and standards community in particular, has dealt with the complex and uncertain nature of the structural safety problem by: (i) transforming it to a time-invariant equivalent problem, deriving combined effects of loads, know as the load combination problem (see, e.g., Ferry-Borges and Castanheta (1983)), which shall realistically represent the most conditioning situations that a structure faces during its

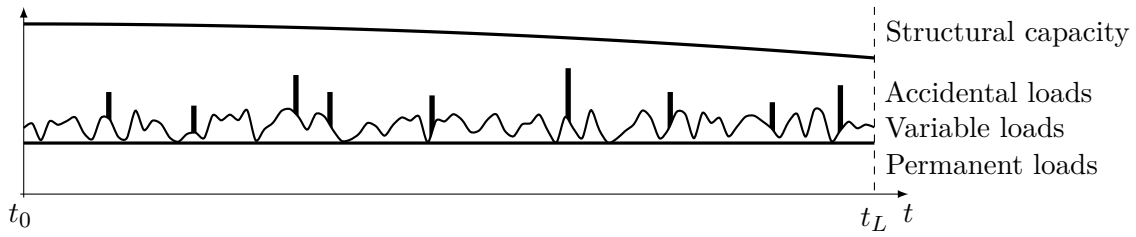

Figure 2.1: Illustration of the time-variant structural safety problem.

expected service life (t_L); (ii) considering reliability theory as the appropriate tool for a probabilistic quantification of safety; and (iii) defining target values of the probability of failure (or reliability index) based on risk acceptance criteria.

Reliability or risk-based approaches to structural safety analysis, which considers explicitly the uncertainty in the computation of the probability of failure, highly depend on the engineer performing them since they are conditional on the information available (Baravalle 2017). To keep the design process practicable, however, structural codes consider practical safety criteria, using the partial safety (or semi-probabilistic) format, calibrated to meet the reliability requirements. The intended wide-ranging domain of application of structural codes comes at a cost of optimality loss which shall be minimized during the calibration process.

In this thesis, these principles are applied to concrete gravity dams. To achieve that, some fundamental aspects are explored in the following sections, after a review of the historical background on structural design, namely: (i) sources of uncertainty and their modeling; (ii) approaches in structural safety analysis; (iii) methods to quantify reliability; (iv) reliability-based design procedure; and (v) code calibration procedure.

2.2 Historical background on structural design

Engineers have dealt with uncertainty by means of conservative design or risk-aversion strategies (Kübler 2007). Although the general acceptance of conservative design among population due to the severe consequences of structural failure, this strategy is irrational, from an economic perspective, when all the hazards, uncertainties and consequences are included in the decision making (Baravalle 2017).

Until the 20^{th} century, design solutions were frequently based on the experience accumulated from a long trial and error process. Mayer (1926) is frequently mentioned as the first to propose a rational design by considering pertinent limit states and probability

theory to quantify uncertainty. Ferry-Borges (1997) stated that these proposals were far ahead of their time since applied methods of structural reliability were not developed yet. Only after Freudenthal (1947), the scientific debate was initiated. Several works explored this new perspective (see, e.g., Costa 1948; Pugsley 1951; Ferry-Borges 1954). Yet, probabilistic concepts were addressed mainly in qualitative terms and sensitivity analysis was often taken to study the effects of variability. Cornell (1969) provoked a paradigm shift by introducing the reliability index as a quantitative measure of safety during a period of theoretical development of structural reliability theory. Since reliability is defined as the probability of a structure or element performing its intended function during its service life and under predicted conditions, safety could then be quantified.

After the theoretical developments of the 1960s, the Joint Committee on Structural Safety (JCSS), composed by five international associations in civil engineering, was created in 1971, aiming at improving the general knowledge in structural safety and providing sound basis for the formulation of structural design recommendations. Several meetings and studies on structural safety lead to the publication of the JCSS probabilistic model code (JCSS 2001), supplying the tools for probabilistic design and background for the preparation of guidance documents concerning the design and construction of different types of structures and materials. Also a guideline, addressed to decision makers, containing the basic premises for the use of risk assessment in establishing rational decisions for the benefit of and in consistency with the preferences of society and other stakeholders, was published (JCSS 2008).

The publication of the European Standards, the Eurocodes (EN1990 2002), which consider the reliability theory as the appropriate tool for the evaluation of structural safety, reflects the increasing awareness of the engineering society for the importance of risk-based decision making in design and maintenance (Vrouwenvelder 2008). These standards establish a set of harmonized technical rules for the design of construction works, aimed at unifying and replacing several national rules. Nowadays, according to JRC (2015), Eurocodes (EN1990 2002) are implemented in most European countries. In Portugal, however, a decree-law, establishing the period of coexistence with the current national regulations for design of structures and encouraging its use to future definitive adoption, has not been published yet. Meanwhile, the second generation of Eurocodes (EN1990 2018) has been under development since 2015, aiming for a more oriented design by expanding the application field, simplifying procedures and limiting alternative rules

(European Commission 2012).

Eurocodes (EN1990 2002), as well as, most other modern standards for structural design, are based on the concepts of limit state, as a demarcation between desired and adverse states of the structure, and partial safety factor (or semi-probabilistic) format for structural safety analysis. Although leading to deterministic measures of safety, this approach is considered as a consistent simplification of fully probabilistic methods (Vrouwenvelder 2008) since the selection of partial safety factors, through code calibration, ensures that the designed structures present a reliability index as close as possible to the target values. Due to its simplicity, a semi-probabilistic code reduces the engineering costs and the dependency on the engineer interpretation.

2.3 Uncertainty modeling

2.3.1 General considerations

In the context of structural safety, following the Bayesian interpretation, probability expresses a degree of belief or rational expectation, representing a state of knowledge. As knowledge cannot be absolute, sources of uncertainty shall be properly taken into account by probabilistic models that combine both data available (objective information) and physical arguments, experience and judgment (subjective information).

Uncertainty is typically classified into two types:

- aleatory (or inherent or type I) uncertainty, related to the natural variation due to unpredictable phenomena, which cannot be reduced;
- epistemic (or type II) uncertainty, due to the insufficient knowledge, which may be reduced through more investigation and improve understanding.

The distinction between these two types of uncertainty, although not consensual over the probability community, is often considered irrelevant in rational choices (Paté-Cornell 1996), making this more a philosophical than a practical question (Kiureghian and Ditlevsen 2009).

In practice, all fundamental variables with recognized uncertainty, whether from the aleatoric or epistemic type, involved in the structural safety problem, such as material properties, dimensions or loads, are considered as random or basic variables (non-stationary

random processes and fields are also used in complex cases). The sources of uncertainty are frequently divided into:

- physical uncertainty, related to the random nature of the random variable;
- statistical uncertainty, due to the consideration of sample statistic estimators to infer on probabilistic models;
- modeling uncertainty, due to the consideration of simplified mathematical models to represent real phenomena, such as the load effects on structures and the structural response, based on random variables;
- human-related uncertainty resulting from the human involvement in the design, construction, maintenance and use of structures. It is usually not explicitly considered in reliability analysis (Schneider 1997), since understanding of human error is mostly qualitative and limited (Melchers 1999).

Random variables are modeled by probabilistic distributions, characterized by a density function f_X and related parameters $\boldsymbol{\theta}$, in order to describe all relevant unknown quantities, interpreting the probability of an event as a conditional measure of uncertainty on an unitary scale (Bernardo 2009).

The moments, given in terms of the distribution parameters $\boldsymbol{\theta}$, are alternatives descriptors. The first moment, or mean (or expected) value $E[X]$, and the second central moment, or variance $V[X]$, are usually sufficient to describe a distribution. The third and forth normalized moments, skewness and kurtosis, respectively, are complementary descriptors.

Although the number of potential distribution models is very large, in practice a relatively small set have come to prominence, either because they have desirable mathematical characteristics or because they adjust particularly well to reality (Forbes *et al.* 2000).

The probabilistic distributions used for the reliability-based applications presented in this thesis are the normal, lognormal, uniform, Weibull and beta distributions, whose properties are synthesized in Table 2.1.

In the following sections, strategies to model the different sources of uncertainty are presented.

Table 2.1: Properties of the probabilistic distributions used for the reliability-based applications presented in the thesis.

Distribution	Probability density function	Moments
Normal	$f_X(x\|\mu,\sigma) = \frac{1}{\sqrt{2\pi\sigma^2}} \cdot e^{-\frac{(x-\mu)^2}{2\sigma^2}}$ parameters: μ, $\sigma > 0$ range: x $\in]-\infty,+\infty[$	$E(X) = \mu$ $V(X) = \sigma^2$
Lognormal	$f_X(x\|\mu,\sigma) = \frac{1}{x\sqrt{2\pi\sigma^2}} \cdot e^{-\frac{(\ln x-\mu)^2}{2\sigma^2}}$ parameters: μ, $\sigma > 0$ range: x $\in]0,+\infty[$	$E(X) = e^{\mu+\sigma^2/2}$ $V(X) = e^{2\mu+\sigma^2} \cdot \left(e^{\sigma^2} - 1\right)$
Uniform	$f_X(x\|a,b) = \frac{1}{(b-a)}$ parameters: a, b range: x $\in [a,b]$	$E(X) = \frac{a+b}{2}$ $V(X) = \frac{(b-a)^2}{12}$
Weibull	$f_X(x\|\lambda,k) = 1 - e^{-\left(x/\lambda\right)^k}$ parameters: $\lambda > 0$, $k > 0$ range: x $\in]0,+\infty[$	$E(X) = \lambda\Gamma\left[\frac{k+1}{k}\right]$ $V(X) = \lambda^2\left(\Gamma\left[\frac{k+2}{k}\right] - \Gamma\left[\frac{k+1}{k}\right]^2\right)$
Beta	$f_X(x\|\alpha,\beta) = \frac{x^{\alpha-1}(1-x)^{\beta-1}}{B(\alpha,\beta)}$ parameters: $\alpha > 0$, $\beta > 0$ range: x $\in]0,1[$	$E(X) = \frac{\alpha}{(\alpha+\beta)}$ $V(X) = \frac{\alpha\beta}{(\alpha+\beta)^2(\alpha+\beta+1)}$

where B is the beta function and Γ is the gamma function.

2.3.2 Physical uncertainty

Generally, physical uncertainty for any random variable is not known *a priori* and must be inferred from observations or be assessed subjectively (Melchers 1999). Any subjective information can be used to define a conservative probabilistic model, such as a summary estimation from expert judgment, fuzzy numbers or theoretical characteristic values (Lemaire 2009). On the presence of observations, the parameters of a probabilistic model can be estimated through statistical inference.

Considering a sample $\hat{\boldsymbol{x}}$ of a random variable x, its most important empiric parameters are the sample mean m and sample variance s^2, given, respectively, by,

$$m = \frac{1}{N}\sum_{i=1}^{N} x_i \tag{2.1}$$

$$s^2 = \frac{1}{N-1}\sum_{i=1}^{N} (x_i - m)^2 \tag{2.2}$$

The estimation of the parameters $\boldsymbol{\theta}$ of a chosen distribution can be made by using:

- the moment-matching (MM) method which estimates the distribution parameters by equating the theoretical moments of the distribution to the corresponding sample moments;
- the maximum likelihood estimation (MLE) method which considers the best estimators of the distribution parameters those that maximize the likelihood function L, i.e.,

$$\hat{\boldsymbol{\theta}} = \max_{\boldsymbol{\theta}} L\left(\boldsymbol{\theta}|\hat{\boldsymbol{x}}\right) \tag{2.3}$$

where $\hat{\boldsymbol{\theta}}$ are the best estimators of the distribution parameters and $L\left(\boldsymbol{\theta}|\hat{\boldsymbol{x}}\right)$ is given by,

$$L\left(\boldsymbol{\theta}|\hat{\boldsymbol{x}}\right) = \prod_{i=1}^{N} f_X\left(\hat{x}_i|\boldsymbol{\theta}\right) \tag{2.4}$$

Often its logarithm is conveniently considered instead, since the logarithmic is a strictly monotonically increasing function sharing the solution of the maximization problem. The log-likelihood function is then given by,

$$\log L\left(\boldsymbol{\theta}|\hat{\boldsymbol{x}}\right) = \sum_{i=1}^{N} \log\left[f_X\left(\hat{x}_i|\boldsymbol{\theta}\right)\right] \tag{2.5}$$

For some distributions, an analytical solution of the maximization problem exists, as the derivatives of the log-likelihood function in order to the distribution parameters can be obtained by closed-form expressions. For other distributions, numerical maximization must be performed.

The suitability of the selected distribution, with the parameters inferred from the sample, can then be measured by goodness-of-fit tests, such as the Kolmogorov-Smirnov or chi-squared tests.

2.3.3 Statistical uncertainty

In practice, very large samples are required to obtain representative estimates of the distribution parameters. The insufficient information results in statistical uncertainties whose relevancy in the outcome increases as the amount of data decreases.

In probabilistic modeling, it is then possible to take statistical uncertainty into account by considering the distribution parameters as random variables. Information about their uncertainty can be taken from the covariance matrix determined through the Fisher information matrix H, containing the negative second-order partial derivatives of the likelihood (or log-likelihood) function, whose elements are given by,

$$H_{ij} = -\frac{\partial^2 logL\left(\hat{\boldsymbol{\theta}}|\hat{\boldsymbol{x}}\right)}{\partial\theta_i \partial\theta_j} \tag{2.6}$$

Alternatively, samples of the distribution parameters can be obtained by bootstrapping (Efron and Tibshirani 1993) and a probabilistic model can be assigned to them, considering a method for parameter estimation.

2.3.4 Modelling uncertainty

Structural analysis makes use of simplified mathematical models, given in terms of random variables, to represent real phenomena, such as the load effects on structures and the structural response, based on either the mechanic formulation of the problem or empirical relations based on experience (Thoft-Christensen and Baker 1982).

However, apart from the physical and statistical uncertainties in the quantification of random variables, the prediction of real phenomena contains an additional model uncertainty, due to simplifying assumptions, unknown boundary conditions and neglected random effects which are not included in the model.

Ideally, model uncertainties, which can be modeled as random variables, should be obtained from a set of laboratory experiments or "in situ" measurements. However, in most cases, such information is lacking and statistical properties of model uncertainties are based purely on engineering judgment.

The most common ways of introducing the model uncertainty into the calculation model are,

$$Y = \theta \cdot f\left(x_1, \cdots, x_n\right) \tag{2.7}$$

or,

$$Y = \theta + f\left(x_1, \cdots, x_n\right) \tag{2.8}$$

where θ is the model uncertainty and f is a model function.

However, with these formulations, the statistical properties of the model uncertainties depend on the exact definition of the model output. A useful way to avoid this definition dependency is to link model uncertainties directly to the random variables (JCSS 2001),

$$Y = f\left(\theta_1 \cdot x_1, \cdots, \theta_n \cdot x_n\right) \tag{2.9}$$

2.4 Structural safety analysis

2.4.1 General considerations

Structural safety analysis addresses the tasks to be performed for estimating the structural response, through numerical or analytical methods, and assess whether the response is satisfactory or not depending on the performance requirements.

When explicitly referring to the boundary between the occurrence of consequences and its avoidance, performance requirements are properly represented by limit states, which are defined as states beyond which structures attained undesirable conditions (Melchers 1999). The limit state philosophy, already considered in the Eurocodes, has replaced the allowable stress, which reduces the allowable stresses to a fraction of the real structural capacity producing uneconomical designed structures, and the ultimate load philosophies, which, although considering the ultimate load capacity, is too severe for serviceability requirements.

Some limit states represent immediate collapse, such as brittle fracture or loss of equilibrium, while other cases involve slow or progressive failure, such as ductile fracture or cracking (Calgaro 2011). Taking that into account, limit states are generally divided into two major categories: (i) ultimate (or safety) limit states, concerning global or partial structural collapse associated with human, economical and environmental losses, which are expectedly achieved only after abnormal load conditions; and (ii) serviceability limit states, concerning the functionality, durability and aesthetics of the structure and the comfort of people, which must be considered during normal operation conditions.

Performance requirements must represent the structural response in face of foreseeable load conditions. Given the involved uncertainties, structural safety can be analyzed considering three main approaches, listed below in descending order in terms of complexity (Melchers 1999):

- Risk-based (or level 4) approach: Safety is analyzed based on a full risk analysis which considers explicitly both the probabilities and the consequences of hazardous events. Due to its complexity, only directives for its application to each particular case are often given;

- Reliability-based (or level 2 and 3) approach: Safety is analyzed based on reliability requirements. Probabilities are computed through reliability theory, considering the probabilistic modelling of uncertainties, and classes of consequences are considered in order to distinguish structures with different levels of consequences. Classes of structures can be analyzed, being the models and principles of the probabilistic model code (JCSS 2001) a sound basis for this approach;

- Deterministic or standards-based approach (or level 0 and 1) approach: Safety is analyzed based on a deterministic criteria which can be calibrated considering probabilistic principles (semi-probabilistic or level 1) or expert judgment (level 0). Due to its simplicity, standard codes are generally based on this approach.

Although covering a wide range of structures, building materials, ground conditions and design situations, the Eurocodes (EN1990 2002) still recommends: (i) the use of risk-based approach, when both uncertainties and consequences are outside common ranges, under the guidance of ISO 2394 (2015); (ii) the reliability-based approach, applied when it gives a significantly better representation of reality than the partial factor design format; and (iii) for the common cases, the semi-probabilistic approach (via the partial safety factor design format).

In the following sections these approaches are presented.

2.4.2 Risk-based approach

Within a risk-based approach to structural safety analysis, decisions are taken based on the estimated risks. Risks are estimated through the combination of all triplets of probability of a hazard event, probability of an adverse structural response and related consequences (ICOLD 2005; Ang 2011), generically translated as,

$$R = \int P(H) \cdot P(D|H) \cdot C(D|H) \tag{2.10}$$

where $P(H)$ is the probability of occurrence of a hazard H and $P(D|H)$ and $C(D|H)$ are the associated probability and consequences of damage (or failure), respectively, given in terms of injury to humans and environment or economic losses.

The process of evaluating if estimated risks are acceptable, tolerable or unacceptable, when several ethical/economical criteria are contemplated, is denoted as risk evaluation. For instance, the Health and Safety Executive (HSE) adopt a risk tolerability framework (Figure 2.2), accommodating different perspectives, on which most of the decision-makers are based (Serrano 2011).

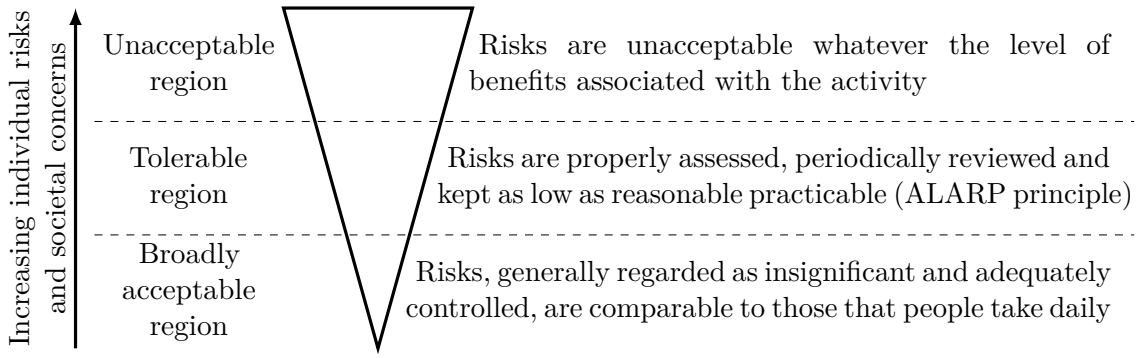

Figure 2.2: Tolerability for risk according to HSE (2001).

Variations on risk evaluation guidelines are expected from country to country, or even within a country, since societal, regulatory, legal, owners and other value judgment are introduced at this stage (ICOLD 2005). The guidelines may differ according to the (Vrouwenvelder *et al.* 2001): (i) individual perspective, which generally indicates that much higher risks are acceptable for voluntary than for involuntary activities; (ii) societal perspective, which indicates a greater social aversion to large disasters; and (iii) economic perspective, based on a rational cost-benefit analysis, intrinsically connected to the ALARP (as low as reasonable practicable) principle, which states that risks are tolerable if the costs of further risk reduction would be grossly disproportionate to the benefit gained.

Usually, regulators use risk curves or f-N charts (annualized failure probability vs number of fatalities), as a tool for risk evaluation. Figure 2.3 shows some examples of dam risk criteria considered by international associations.

2.4.3 Reliability-based approach

The reliability-based approach to structural safety analysis focus on ensuring that the reliability of a structure, i.e. the probability of performing its intended function during a

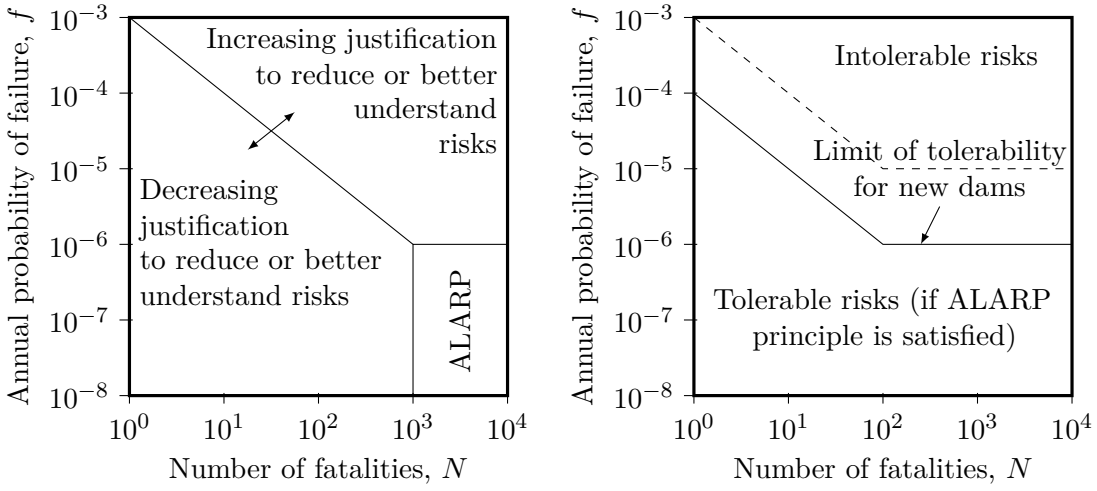

(a) USBR (2011) (b) ANCOLD (2003)

Figure 2.3: Dam risk criteria adopted by some international associations (adapted from Hariri-Ardebili (2018)).

specific time period, meets defined reliability requirements. Consequences are indirectly taken into account by the definition of adequate reliability levels to be achieved. Therefore, considering a predicted load combination, a limit state defining the boundary between desired and undesired structural performance, and the probabilistic models to quantify the uncertainties involved, the reliability index of a structure, β, computed through reliability analysis, must be greater than a defined target reliability index, β_T, within a simplified version of the risk acceptance criteria, i.e.,

$$\beta > \beta_T \tag{2.11}$$

The definition of the target reliability index, β_T, taking into account the possible cause (load event) of attaining a limit state and the possible consequences of failure in terms of risk to life, injury, potential economical losses, public aversion to failure, the expense and procedures necessary to reduce the risk of failure (Calgaro 2011), follows the reliability differentiation principle needed in order to account properly the consequences of failure (Schneider 1997).

The risk acceptance criteria introduced in the Eurocodes, in terms of target reliability indexes, have been derived from long studies by combining various approaches including human safety evaluation, optimization and calibration (Diamantidis and Holický 2010). The second generation of the Eurocodes (EN1990 2018) extends the reliability classification,

considered originally (EN1990 2002), to higher consequence classes. Table 2.2 presents the classification proposed in EN1990 (2018).

Table 2.2: Qualification of consequence class and target reliability index according to EN1990 (2018).

Consequence class	Indicative qualification of consequences		Target reliability index (probability of failure), for one year reference period
	Loss of human life or personal injury	Economic, social and environmental consequences	
CC4 - Highest	Extreme	Huge	-
CC3 - Higher	High	Very great	5.2 ($\sim 10^{-7}$)
CC2 - Normal	Medium	Considerable	4.7 ($\sim 10^{-6}$)
CC1 - Lower	Low	Small	4.2 ($\sim 10^{-5}$)
CC0 - Lowest	Very low	Insignificant	-

Although consequences classes CC0 and CC4 were added, the corresponding values for the target reliability index are not mentioned. For CC4 class, however, EN1990 (2018) states that additional provisions to those given can be needed.

2.4.4 Standards-based approach

2.4.4.1 General considerations

Deterministic measures of structural safety are based on the definition of explicit safety criteria, whose violation represents the structural failure, with determined values for loads and material properties. In this approach, reliability analysis is not performed since it is expected that the safety criteria represent properly the performance requirements.

Distinction is made between two deterministic methods:

- Global safety factor (or level 0) method, considered in the traditional allowable stress and ultimate load philosophies, which concentrates, in a single safety factor, all sources of uncertainty;
- Partial safety factor (or semi-probabilistic or level 1) method, considered in the limit state philosophy, which distributes the associated uncertainties for a set of partial safety factors applied to the loads, load effects, material properties, simplified models, etc, separately.

In the following sections, these methods are described in detail.

2.4.4.2 Global safety factor method

In the global safety factor method, structural safety is guaranteed by means of a safety factor λ given by the ratio between the structural carrying capacity R, and the load effect S, i.e.,

$$\lambda = R/S \tag{2.12}$$

Although this method is essentially deterministic, the concept of carrying capacity and/or load effects differs according to the allowable stress and ultimate load philosophies, since safety factors are be defined based on mean or representative (low probability) values.

For the allowable stress method, which considers only a fraction of the real structural capacity in order to ensure an elastic behavior, the safety factor is applied to the limit material capacity in serviceability conditions. The resulting permissible stresses shall be greater than the applied stresses, i.e.,

$$\sigma_A \leq \sigma_P \left(= \sigma_U/\lambda\right) \tag{2.13}$$

where σ_A, σ_P and σ_U are the applied, the permissible and the failure stresses, respectively.

This philosophy is still punctually followed worldwide. In Portugal, for instance, the dam safety regulation (RSB 2018) considers safety factors applied to material properties, aiming to keep stresses below the elastic limit.

The adoption of the limit state concept, after Streletskii in 1937 (Elishakoff 2004), led to the consideration of the ultimate structural capacity, computed in failure conditions, moving the safety factor to the load side, into the so-called ultimate load method. In this method, considered originally in the plastic theory of structures, the safety factor (also know as load factor) multiplies the acting load just enough to cause the structural collapse, while the material capacity is determined from the idealized plastic material properties, i.e.,

$$W_Q\left(\lambda \cdot Q\right) \leq W_R\left(R_P\right) \tag{2.14}$$

where W_Q and W_R are the external and internal work functions, described by the collapse mode considered, and Q and R_P are the applied loads and the plastic strength, respectively.

The safety factor may be selected on the basis of experimental observations, previous practical experience, economic and political considerations (Melchers 1999), and scaled such that it expectedly absorbs uncertainties and guarantees adequate safety (Ponslet 1994), which generally results in a satisfactory design (Lemaire 2009). However, this method incorporates all sources of uncertainty into a single coefficient, which penalizes the consistency of the safety levels for the cases covered by a structural code. For that purpose, partial safety factor method is more suitable.

2.4.4.3 Partial safety factor (semi-probabilistic) method

The partial safety factor method, also called load and resistance factor design (LRFD) method, was proposed by Ravindra and Galambos (1978) for the design safety evaluation of steel buildings. It emerged as the solution to incorporate reliability principles into the safety analysis. Moreover, together with the limit state philosophy, it results in a combined alternative to the allowable stress and ultimate load methods, since both the elastic behavior can be considered for the serviceability limit states and the ultimate strength can be accounted for the ultimate limit states, respectively. These are accomplished by considering partial safety factors, applied to both the loads and the material strength, so that reliability requirements are approximately fulfilled.

This method assigns a set of partial safety factors to the loads and material properties, according to their uncertainty and influence to the desired safety level (Vrouwenvelder and Siemes 1987). The structural safety is verified by means of criteria that compare the load effects, E, and resistance, R, given in terms of design values of random variables $\boldsymbol{x}_d = \{S_d, f_d, a_d, \theta_d\}$ (loads, material properties, geometry parameters and model uncertainties), such as,

$$E(\boldsymbol{x}_d) \leq R(\boldsymbol{x}_d) \tag{2.15}$$

or, equivalently,

$$R(\boldsymbol{x}_d) - E(\boldsymbol{x}_d) \geq 0 \tag{2.16}$$

Generally, the safety criteria are simplified such that partial safety factors are applied to representative (characteristic) values of loads $S_{k1}, \cdots, S_{kn}$ and material properties $f_{k1}, \cdots, f_{km}$, with associated small probabilities of exceedance and non-exceedance, respectively, comprising also all other sources of uncertainty (such as geometry and model

uncertainties), given, respectively, by,

$$S_{di} = S_{ki} \cdot \gamma_{Si} \tag{2.17}$$

$$f_{dj} = f_{kj}/\gamma_{fj} \tag{2.18}$$

where S_{di} and f_{dj} are the design values of the load S_i and the material property f_j, respectively, and γ_{Si} and γ_{fj} are the partial safety factor associated with the load S_i and the material property f_j.

The formal link between partial safety factors and probabilistic methods, can be established through the theory of code calibration (Vrouwenvelder 2008). Performing a probabilistic-based evaluation, the partial safety factors are determined such that the difference between the reliability for the different structures of the same consequence class and the target reliability level is minimized (Sørensen *et al.* 1994).

In the case of the Eurocodes, the partial safety factors have been determined on the basis of a combination of theory and calibration to existing practice in a large number of European countries (Vrouwenvelder 2008).

2.5 Reliability methods

2.5.1 General considerations

In order to perform structural reliability analysis, it is convenient to describe, explicitly, failure events in terms of functional relations between random variables, $\boldsymbol{x} = (x_1, \ldots, x_n)$. These relations are called performance functions, $G(\boldsymbol{x})$, as they represent the performance of a structural system or element. The limit state function, $G = 0$, sets the boundary between failure ($G < 0$) and non-failure ($G > 0$) states.

Reliability analysis aims at quantifying the probability of failure, p_f, of a limit state function, given the probabilistic description of the random variables $\boldsymbol{x}$. An illustration of the two-dimensional case is presented in Figure 2.4.

The probability of failure is obtained by the integration of the joint probability density function, $f_{\boldsymbol{X}}(\boldsymbol{x})$, over the failure domain (the hyperspace limited to $G(\boldsymbol{x}) < 0$), i.e,

$$p_f = P\{G(\boldsymbol{x}) < 0\} = \int_{G(\boldsymbol{x})<0} f_{\boldsymbol{X}}(\boldsymbol{x})\, d\boldsymbol{x} \tag{2.19}$$

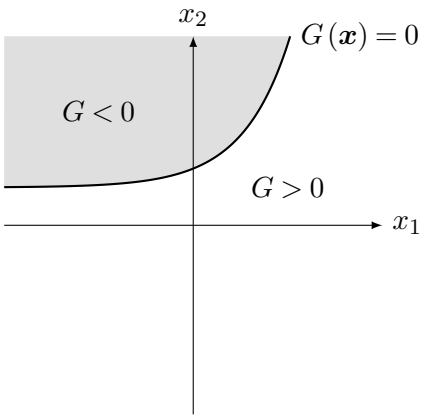

Figure 2.4: Illustration of a two-dimensional limit state function.

Analytical solution of equation 2.19 only exists in particular cases of limited practical interest. In most practical applications, in which limit state functions are explicitly defined, approximate methods must be used. These are divided into:

- Gradient-based (or level 2) methods which approximate well-defined differentiable functions, with known solution, to complex limit state functions;
- Simulation-based (or level 3) methods, instead of numerical integration which become cumbersome for typical complex structural reliability problems as the dimension (n) of the integration space increases, whose accuracy depend on the number of realizations performed.

Details about the procedure of several methods are presented in reference works (Ditlevsen and Madsen 1996; Schneider 1997; Melchers 1999; Haldar and Mahadevan 2000; Lemaire 2009; Faber 2012). In the following sections, some concepts about these methods are highlighted.

2.5.2 Gradient-based methods

2.5.2.1 General considerations

The gist of gradient-based methods is set on second-moment fundamentals, which only considers the first and second moments of the random variables. However, these are rarely sufficient to obtain the real probability of failure, p_f, as their range of applicability is limited to linear limit state functions and normal random variables.

Their extension to generic reliability problems requires, first and foremost, the Hasofer-Lind transformation, which makes their solution invariant to the limit state formulation.

To deal with non-linearity, limit state functions can be approximated by simpler functions about some point $\boldsymbol{x}'$, advantageously the design point ($\boldsymbol{x}^*$) which corresponds to the point on the limit state surface closer to the origin, representing the worst combination of random variables. The use of linear functions (or first-order Taylor expansion) is denoted as "first-order methods". If the approximation by linear functions is not satisfactory, parabolic, quadratic or high-order Taylor expansions can be used in a procedure denoted as "second-order methods".

Finally, the extension to non-normal variables, through variable transformation to independent standard normal variables, lead to the generalization of the reliability problem into the First-Order Reliability Methods (FORM) and Second-Order Reliability Methods (SORM), according to the order of the approximation function.

2.5.2.2 Second-moment fundamentals

Lets consider a limit state function given by a linear combination of random variables $\boldsymbol{x}$, i.e.,

$$G(\boldsymbol{x}) = \boldsymbol{a}^T \cdot \boldsymbol{x} \tag{2.20}$$

where $\boldsymbol{a}$ is a vector of known coefficients. If the random variables $\boldsymbol{x}$ are normally distributed, the limit state function G is then also normally distributed with the first two moments (mean value and variance) given, respectively, by,

$$\mu_G = \boldsymbol{a}^T \cdot \boldsymbol{\mu} \tag{2.21}$$

$$\sigma_G^2 = \boldsymbol{a}^T \cdot \boldsymbol{\Sigma} \cdot \boldsymbol{a} \tag{2.22}$$

where $\boldsymbol{\mu}$ and $\boldsymbol{\Sigma}$ are the vector of means and the variance-covariance matrix, respectively, of the random variables.

The probability of failure (equation 2.19) can then be rewritten as,

$$p_f = P\left\{G(\boldsymbol{x}) < 0\right\} = \Phi\left(-\frac{\mu_G}{\sigma_G}\right) = \Phi\left(-\beta\right) \tag{2.23}$$

where Φ is the standard normal distribution function, and β is the reliability index,

conceptually introduced by Cornell (1969), which indicates the distance, in number of standard deviations σ_G, between the mean value, $G = \mu_G$, and the limit state, $G = 0$.

2.5.2.3 Hasofer-Lind transformation

The reliability index, as defined by Cornell (1969), is not invariant to the definition of the limit state (Lind 1973), i.e., it is not constant for distinct, although mechanically equivalent, reformulations of the same problem.

To handle it, Hasofer and Lind (1974) proposed an invariant definition of the reliability index, considering the transformation of the limit state function into the standard normal space (Figure 2.5) by replacing the normal variables, $\boldsymbol{x}$, with independent standard normal variables (normal distribution with zero mean and unit standard deviation), $\boldsymbol{u}$, such as,

$$\boldsymbol{u} = \boldsymbol{L}^{-1} \cdot (\boldsymbol{x} - \boldsymbol{\mu}) \tag{2.24}$$

where $\boldsymbol{L}$ is a lower triangular matrix obtained from $\boldsymbol{\Sigma}$, by Cholesky decomposition, i.e.,

$$\boldsymbol{\Sigma} = \boldsymbol{L} \cdot \boldsymbol{L}^T \tag{2.25}$$

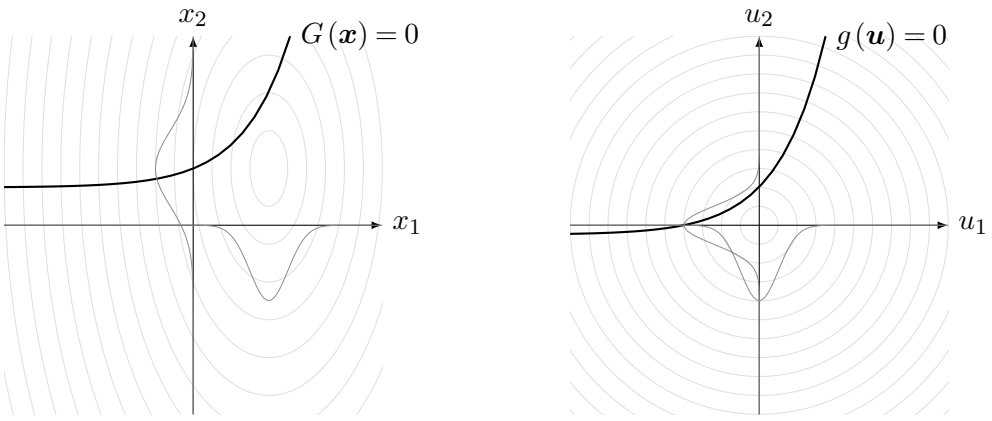

(a) Original variable space (b) Standard normal space

Figure 2.5: Illustration of the limit state transformation to the standard normal space.

In the standard normal space, the reliability index β is given by the distance between the origin and the design point $\boldsymbol{u}^*$, i.e., the point on the limit state hyperplane closest to the origin,

$$\beta = \|\boldsymbol{u}\| = \sqrt{\boldsymbol{u}^{*T} \cdot \boldsymbol{u}^*} \tag{2.26}$$

The vector that indicates the direction of the design point, called vector of direction cosines, $\boldsymbol{\alpha}$, is given by,

$$\boldsymbol{\alpha} = \frac{\nabla g(\boldsymbol{u}^*)}{\|\nabla g(\boldsymbol{u}^*)\|} \tag{2.27}$$

where $\nabla g = \{\partial g(\boldsymbol{u}^*)/\partial u_1, \ldots, \partial g(\boldsymbol{u}^*)/\partial u_n\}$ is the differential operator vector of g, evaluated at the design point $\boldsymbol{u}^*$.

In the case of linear limit state functions, the vector of direction cosines is invariant. Therefore, the reliability index can be obtained directly by solving the equation $g(\boldsymbol{u}^*) = 0$, in order to β, since the design point is given by,

$$\boldsymbol{u}^* = -\boldsymbol{\alpha} \cdot \beta \tag{2.28}$$

Non-linear limit states should be approximated by a first-order Taylor expansion about the design point $\boldsymbol{u}^*$. Since this point is initially unknown, the reliability index β is obtained by an iterative process, synthesized by Hasofer and Lind (1974) into the following algorithm:

1. Transformation of the random variables into independent standard normal variables, using equation 2.24. Therefore, the limit state function is also transformed into the standard space, $G(\boldsymbol{X}) \rightarrow g(\boldsymbol{u})$;
2. Choose an initial guess for the design point, $\boldsymbol{u}_0^*$;
3. Compute the reliability index, β_i, using equation 2.26;
4. Compute the vector of direction cosines, $\boldsymbol{\alpha}_i$, using equation 2.27;
5. Estimate a new point, $\boldsymbol{u}_i^*$, using equation 2.28.
6. Repeat steps 3 to 5 until convergence.

With this adaptation, the reliability index, β, becomes invariant under any reformulation of the limit state function.

2.5.2.4 First-order reliability method (FORM)

The first-order reliability method (FORM) is a generalization of the previous fundamentals to non-normal random variables. The major difficulty introduced is, therefore, to transform the original formulation, both variable and limit state function, into the standard space.

This method was translated into the following algorithm (Rackwitz and Fiessler 1978) for determining the design point $\boldsymbol{u}^*$:

1. Choose an initial guess for the design point in the original space, $\boldsymbol{x}_0^*$, which might be assumed as $\boldsymbol{\mu_x}$;

2. Transform the design point $\boldsymbol{x}_i^*$ into the independent standard normal space, $\boldsymbol{u}_i^*$, using:

   a) normal tail transformation (Ditlevsen 1981), if the random variables are independent;

   b) Rosenblatt transformation (Rosenblatt 1952), if the random variables are correlated and the joint probability distribution function, $F_{\boldsymbol{x}}(\boldsymbol{x})$, and its conditionals, $F_{x_i}(x_i|x_1,\cdots,x_{i-1})$, are known;

   c) Nataf transformation (Nataf 1962), if the random variables are correlated and only their marginal cumulative distribution functions $F_{x_n}(x_n)$ and the correlation matrix $\boldsymbol{P}$ are available;

   d) Hermite transformation, if the random variables are correlated and only their first two moments and the correlation matrix $\boldsymbol{P}$ are available;

3. Compute the reliability index, β_i, using equation 2.26;

4. Compute the vector of direction cosines, $\boldsymbol{\alpha}_i$, using equation 2.27. However, unlike the normal variable case, since $g(\boldsymbol{u})$ is not known explicitly, the components of ∇g are alternatively given by,

$$\nabla G(\boldsymbol{x}_i^*) = \boldsymbol{J}_i \cdot \nabla g(\boldsymbol{u}_i^*) \Leftrightarrow \nabla g(\boldsymbol{u}_i^*) = \boldsymbol{J}_i^{-1} \cdot \nabla G(\boldsymbol{x}_i^*) \tag{2.29}$$

   where $\boldsymbol{J}$ is the Jacobian matrix with elements $j_{nm} = \partial u_n / \partial x_m$.

5. Estimate a new point, $\boldsymbol{u}_{i+1}^*$,

$$\boldsymbol{u}_{i+1}^* = \boldsymbol{u}_i^* + \lambda_i \cdot \boldsymbol{d}_i \tag{2.30}$$

   where $\boldsymbol{d}_i$ is the search direction vector given by

$$\boldsymbol{d}_i = \left[\boldsymbol{\alpha}_i \cdot \boldsymbol{u}_i^* + G(\boldsymbol{u}_i^*) \cdot \left\|\nabla g(\boldsymbol{u}_i^*)\right\|^{-1}\right] \cdot \boldsymbol{\alpha}_i - \boldsymbol{u}_i^* \tag{2.31}$$

and λ_i is the step size determined through a line search method such that $f^{(1)}\left(\boldsymbol{u}_{i+1}^*\right) < f^{(1)}\left(\boldsymbol{u}_i^*\right)$, where $f^{(1)}\left(\boldsymbol{u}^*\right)$ is a nonnegative merit function given by,

$$f^{(1)}\left(\boldsymbol{u}^*\right) = \frac{\left\|\boldsymbol{u}^* - \boldsymbol{\alpha}\cdot\boldsymbol{u}^*\cdot\boldsymbol{\alpha}\right\|^2 + c_1\cdot G\left(\boldsymbol{u}^*\right)^2}{2} \tag{2.32}$$

where c_1 is a positive parameter.

6. Compute the design point, on the original space, by reverting the transformation carried out in step 2.

7. Repeat steps 2 to 6 until convergence of both β and $\boldsymbol{u}^*$.

Figure 2.6 shows the first-order approximation of the limit state function illustrated in Figure 2.5.

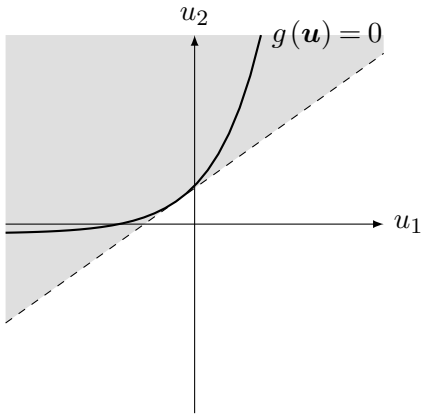

Figure 2.6: First-order approximation of the limit state function illustrated in Figure 2.5.

2.5.2.5 Second-order reliability methods (SORM)

The accuracy of FORM results decreases with the non-linearity of the limit state. To improve the estimation of the probability of failure in these cases, the second-order reliability methods (SORM) include information on the curvature of the limit state about the design point which is ignored in the FORM procedure.

Between many possible approximations of the failure domain, second-order (or quadratic) expansions of the limit state function were firstly studied by Fiessler *et al.* (1979) which used the statistical theory of quadratic forms to approximate the failure surface. A closed-form solution for the probability of failure, considering the typical parabolic approximation,

was given by Breitung (1984), using the theory of asymptotic approximations, such as,

$$p_f \approx \Phi(-\beta) \cdot \prod_{i=1}^{n-1} (1 + \beta \cdot \kappa_i)^{-1/2} \tag{2.33}$$

where β is the reliability index obtained in FORM, and κ_i is the i-th element of the vector $\boldsymbol{\kappa}$ of the curvature of the limit state function at the design point $\boldsymbol{u^*}$, given by the eigenvalues of the submatrix obtained by removing the last row and column of the following matrix,

$$\boldsymbol{A} = \frac{\boldsymbol{RDR}^T}{\sqrt{\left(\nabla g(\boldsymbol{u^*})\right)^T \cdot \nabla g(\boldsymbol{u^*})}} \tag{2.34}$$

where $\boldsymbol{D}$ is the Hessian (second-derivative) matrix of the limit state surface in the standard normal space evaluated at the design point, and $\boldsymbol{R}$ is the rotation matrix, which rotates the coordinate system $\boldsymbol{u}$ to a new system $\boldsymbol{u'}$ such that the last direction coincides with the vector of direction cosines, $\boldsymbol{\alpha}$, given by the Gram-Schmidt orthogonalization of the following matrix,

$$\boldsymbol{R_0} = \begin{bmatrix} 1 & 0 & \cdots & 0 \\ 0 & 1 & \cdots & 0 \\ \vdots & \vdots & \ddots & \vdots \\ \alpha_1 & \alpha_2 & \cdots & \alpha_n \end{bmatrix} \tag{2.35}$$

As equation 2.33 gives poorer results with increasing curvature of the limit states, alternative, but more complex, versions are available (Hohenbichler *et al.* 1987; Tvedt 1990).

Figure 2.7 shows the second-order approximation of the limit state function illustrated in Figure 2.5.

2.5.3 Simulation-based methods

2.5.3.1 General considerations

Simulation-based (or Monte Carlo) methods are numeric approaches that approximate an integral by the mathematical expectation of generated samples belonging to the integration domain.

In reliability analysis, these methods consist in re-writing the probability of failure

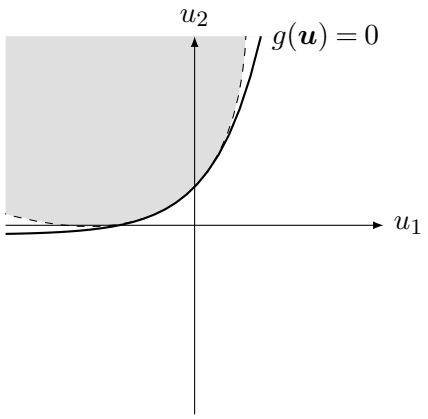

Figure 2.7: Second-order approximation of the limit state function illustrated in Figure 2.5.

(equation 2.19) as,

$$p_f = \int_{G(\boldsymbol{x})<0} f_X(\boldsymbol{x})\, d\boldsymbol{x} = \int_{R^n} I \cdot f_X(\boldsymbol{x})\, d\boldsymbol{x} \tag{2.36}$$

where I is an indicator function.

Based on an N-dimensional sample of I, the probability of failure is approximated by its mathematical expectation, i.e.,

$$p_f \approx E[I] = \sum_{i=1}^{N} I/N \tag{2.37}$$

The precision of the estimation can be evaluated through the sample variance of I, given by,

$$S^2[I] = \frac{E\left[I^2\right] - E[I]^2}{N-1} \tag{2.38}$$

The sample size needed depends on the accuracy required. A typical strategy followed is to stop the simulation procedure when a desired coefficient of variation of the estimation is achieved.

The efficiency of this method is strictly related with the sampling technique employed. The classic form of the Monte Carlo method, called crude Monte Carlo, is the simplest, although cumbersome, choice. It uses a direct (or random) sampling technique over the integration space. It generally requires a large amount of simulations and computational effort for typical safety problems in civil engineering. Consequently, variance reduction sampling techniques can be alternatively used. These techniques can be divided as those that do not use any previous information on the specific problem, such as, latin hypercube

(McKay *et al.* 1979) or directional (Bjerager 1988) sampling techniques and those that are based on the design point obtained by a previous FORM analysis, such as, importance (Melchers 1999), adaptive (Bucher 1988), conditional (Harbitz 1986) or line (Hohenbichler and Rackwitz 1988) sampling techniques. Combinations of techniques are also possible, such as, importance directional sampling (Ditlevsen *et al.* 1988), for instance.

Moreover, another variance reduction technique, named ring sampling, is proposed in this study aiming to improve the simulation efficiency in cases of low failure probability, when the design point cannot be previously obtained.

In the following sections the key concepts associated with these techniques are described.

2.5.3.2 Direct sampling (crude Monte Carlo method)

In the crude Monte Carlo method, the indicator function represents a failure counter, defined by,

$$I = \begin{cases} 1, \text{ if } G(\boldsymbol{x}) < 0 \\ 0, \text{ if } G(\boldsymbol{x}) > 0 \end{cases} \tag{2.39}$$

Realizations of I are obtained by generating N samples $\hat{\boldsymbol{x}}$ and testing the limit state function for failure ($G(\hat{\boldsymbol{x}}) < 0$) or non-failure ($G(\hat{\boldsymbol{x}}) > 0$).

For the generation of $\hat{\boldsymbol{x}}$, direct (or random) sampling technique is used individually for each random variable x_i. This technique consists in generating N uniformly distributed random values $\hat{z} = (\hat{z}_1, \cdots, \hat{z}_N)$, in the interval $[0,1]$, which are interpreted as probabilities assigned to the cumulative distribution function of x_i ($\hat{\boldsymbol{z}} = F_{x_i}(\hat{x}_i)$), and computing $\hat{x}_i$, using the inverse transformation method as,

$$\hat{x}_i = F_{x_i}^{-1}(\hat{\boldsymbol{z}}) \tag{2.40}$$

Figure 2.8 shows the outcome of the simulation procedure, using the direct sampling technique, considering the limit state function illustrated in Figure 2.5.

2.5.3.3 Latin hypercube sampling

Latin hypercube sampling technique ensures that all areas of the sample space are covered in the generation process. For that, the uniform sample space $[0,1]$ is divided in N strata of equal marginal probability $1/N$, sampling uniformly since from each stratum. This

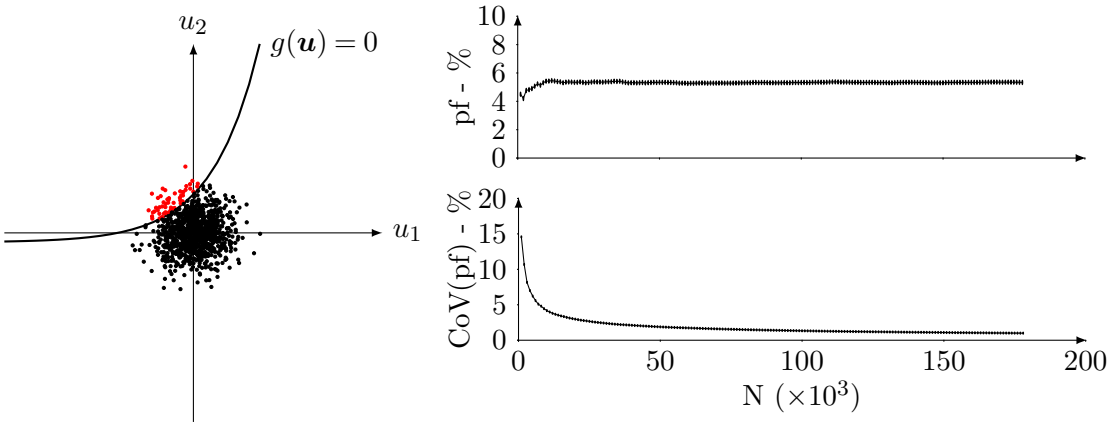

Figure 2.8: Simulation procedure, using the direct sampling technique, considering the limit state function illustrated in Figure 2.5.

technique is a n-dimensional extension of latin square (two-dimensional) sampling (Raj 1968).

Figure 2.9 compares samples obtained from direct and latin hypercube sampling techniques.

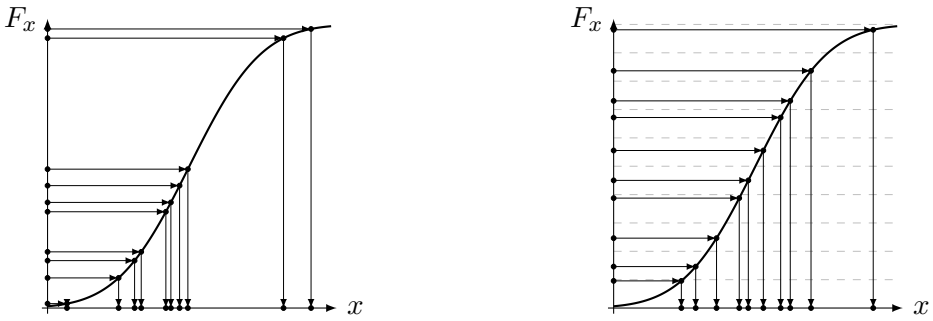

(a) Direct sampling

(b) Latin hypercube sampling

Figure 2.9: Comparison of the direct and latin hypercube sampling generation procedure.

Other sampling techniques, based on latin hypercube, such as, for instance, orthogonal array-based latin hypercube sampling (Tang 1993), are available.

2.5.3.4 Directional sampling

Directional sampling takes advantage of the rotational symmetry of the multinormal probability density. In the n-dimensional standard normal space, the probability content outside a hyper-spherical region with radius r is given by,

$$P\left[R \geq r\right] = 1 - \chi_n^2\left(r^2\right) \tag{2.41}$$

where χ^2_n is the chi-square distribution with n degrees of freedom.

Instead of sampling $\hat{\boldsymbol{x}}$, directions $\hat{\boldsymbol{\alpha}}$, from the origin of the standard normal space, are sampled and the conditioned probability of failure is quantified, given each sampled direction, using equation 2.41.

For that, the n-dimensional vector $\boldsymbol{u}$, which intersects the limit state function in the standard normal space ($g(\boldsymbol{u}) = 0$), is expressed as,

$$\boldsymbol{u} = r \cdot \boldsymbol{a} \tag{2.42}$$

where $\boldsymbol{a}$ is the directional unit vector, and r is the radius or the radial distance from the origin to the limit state function, which can be obtained using a line-search method.

Unlike the qualitative failure or non-failure outcome of the crude Monte Carlo method, the indicator function I is quantified as the conditional probability of failure given the direction defined by the unit vector $\boldsymbol{a}$ (Bjerager 1988), i.e.,

$$I = 1 - \chi^2_n\left(r^2\right) \tag{2.43}$$

where r is the distance from the origin to the limit state function in the direction defined by the unit vector $\boldsymbol{a}$.

Figure 2.10 shows the outcome of the simulation procedure, using the directional sampling technique, considering the limit state function illustrated in Figure 2.5.

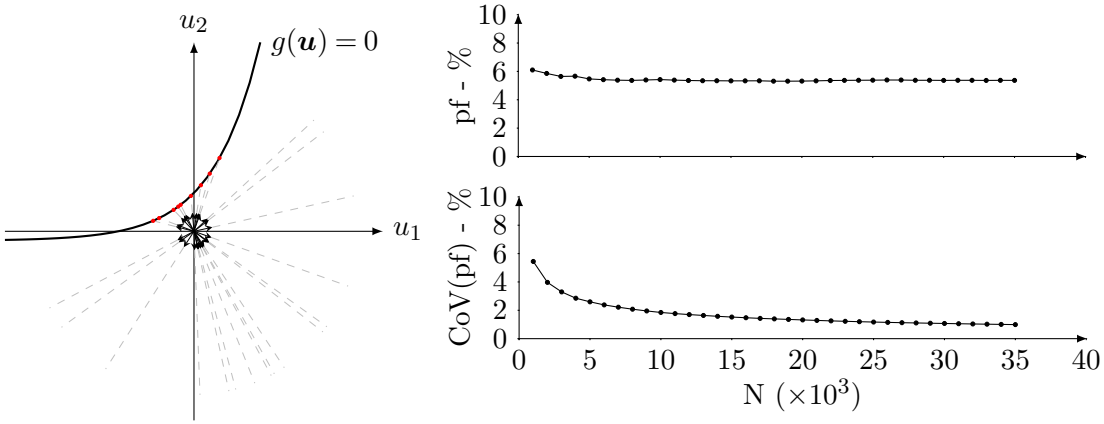

Figure 2.10: Simulation procedure, using the directional sampling technique, considering the limit state function illustrated in Figure 2.5.

This sampling technique is specially effective for small probabilities of failure, provided that n is not too large.

2.5.3.5 Importance sampling

The importance sampling technique consists in sampling, more frequently, the "important" (i.e. near-failure) regions. To deal with the biased estimation obtained from forcing the sampling points to fall into the "important" regions, each simulation is weighted by the likelihood ratio, i.e., the relation between the original probability density function, f_X, and the "importance sampling" probability density function, h_X. Therefore, the indicator function, in this technique, is given by,

$$I = \frac{f_X(\boldsymbol{x})}{h_X(\boldsymbol{x})} \cdot \begin{cases} 1, \text{ if } G(\boldsymbol{x}) < 0 \\ 0, \text{ if } G(\boldsymbol{x}) > 0 \end{cases} \tag{2.44}$$

The efficiency of the importance sampling estimate depends on the choice of h_X. Melchers (1999) suggests the use of the multinormal density function centred at the design point $\boldsymbol{x}^*$ with a diagonal variance-covariance matrix, $\boldsymbol{\sigma}$ ($h_X = \boldsymbol{\Phi}_n(\boldsymbol{x}|\boldsymbol{\mu} = \boldsymbol{x}^*, \Sigma)$), instead of just shift the original probability density function f_X to the design point.

2.5.3.6 Adaptive sampling

The adaptive sampling technique is an iterative Monte-Carlo simulation procedure, suggested by Bucher (1988), that uses the information from previous simulations to adapt the "importance sampling" probability density function h_X, which considerably reduces the variance of the estimation of the probability of failure.

The first and second moments of the "importance sampling" probability density function h_X are approximated by the sample mean and covariance of the samples, $\hat{\boldsymbol{x}}$, that have resulted in failure ($G(\hat{\boldsymbol{x}}) < 0$). Then, the conditional mean vector and covariance matrix are, respectively, given by,

$$\bar{\boldsymbol{x}}_{\boldsymbol{h}} = E\left[\hat{\boldsymbol{x}} | G(\hat{\boldsymbol{x}}) < 0\right] \tag{2.45a}$$

$$\bar{\boldsymbol{\sigma}}_{\boldsymbol{h}} = E\left[(\hat{\boldsymbol{x}} - \bar{\boldsymbol{x}}_{\boldsymbol{h}}) \cdot (\hat{\boldsymbol{x}} - \bar{\boldsymbol{x}}_{\boldsymbol{h}})^T | G(\hat{\boldsymbol{x}}) < 0\right] \tag{2.45b}$$

The initial run may be performed as standard importance sampling, if the design point $\bar{\boldsymbol{x}}_{\boldsymbol{h}} = \boldsymbol{x}^*$ from FORM analysis is known. If not, a starting procedure based on crude Monte Carlo method should be carried out in order to find an adequate starting point.

2.5.3.7 Conditional sampling

Considering the standard normal space, this technique, proposed by Harbitz (1986) and extensively detailed in Bernard and Fogli (1986), consists in excluding the β-sphere, i.e., the n-dimensional sphere with radius equal to β obtained in FORM analysis, from the sampling domain. Thus, the sampling domain is restricted to values outside the β-sphere, which has an "importance sampling" probability given by equation 2.41.

For sampling values outside the β-sphere, unit random directions $\hat{\boldsymbol{a}}$, uniformly distributed on the hypersphere, and chi-distributed random radius $\hat{r}$, conditioned to $r > \beta$, are generated. Since the product between an uniform and a chi distribution is a normal standard distribution, standard normal values outside the β-sphere are obtained using equation 2.42.

For generating chi-distributed random radius $\hat{r}$, conditioned to $r > \beta$, inverse transformation method can be used, considering that,

$$\chi_n^2\left(r^2 | r > \beta\right) = \frac{\chi_n^2\left(r^2\right) - \chi_n^2\left(\beta^2\right)}{1 - \chi_n^2\left(\beta^2\right)} \tag{2.46}$$

With this technique, the indicator function I is given by,

$$I = \left(1 - \chi_n^2\left(\beta^2\right)\right) \cdot \begin{cases} 1, \text{ if } G(\boldsymbol{x}) < 0 \\ 0, \text{ if } G(\boldsymbol{x}) > 0 \end{cases} \tag{2.47}$$

2.5.3.8 Line sampling

Line, or axis-orthogonal, sampling technique was proposed by Hohenbichler and Rackwitz (1988) to improve SORM estimates of the probability of failure, especially when asymptotic conditions are not verified, by sampling parallel to the direction defined by the vector of direction cosines.

Such as the SORM procedure to estimate the probability of failure (section 2.5.2.5), this technique is held in the standard normal space $\boldsymbol{u'}$, transformed from $\boldsymbol{u}$ such that the last direction coincides with the vector of direction cosines $\boldsymbol{\alpha}$, using the rotation matrix $\boldsymbol{R}$ obtained by the Gram-Schmidt orthogonalization of the matrix $\boldsymbol{R_0}$ given by equation 2.35, i.e.,

$$\boldsymbol{u'} = \boldsymbol{R} \cdot \boldsymbol{u} = \left\{\boldsymbol{u'_{n-1}}, \beta\right\} \tag{2.48}$$

where $\boldsymbol{u'_{n-1}}$ contains the $(n-1)$-dimensional subspace and β is the coordinate parallel to the vector of direction cosines.

This technique consists in generating samples $\hat{\boldsymbol{u}}'_{\boldsymbol{n-1}}$, belonging to the $\boldsymbol{\Phi}_{n-1}$ multinormal domain and find, by a line-search method, the distance $\hat{\beta}$ to the failure plane, i.e. the solution of $g(\boldsymbol{u}) = 0$ where $\boldsymbol{u}$ is given by reverting the transformation 2.48.

With this technique, the indicator function I is given by,

$$I = \Phi(-\beta) \cdot \tag{2.49}$$

The efficiency of this sampling technique, such as in the case of the directional sampling technique, is strictly related to the line-search method employed, since, for each simulation, the limit state function must be solved several times.

2.5.3.9 Ring sampling

A type of stratified directional technique, denoted ring sampling, is proposed in this study aiming at improving the simulation efficiency in cases of low failure probability, when the design point cannot be previously obtained, by spreading the sample points in the radial direction.

In this technique, the standard normal space shall be simplified in a space S defined by a hypersphere with radius equal to a large and finite r_{max} (usually the largest significant value according to the software used), and divided into m (m must be a factor of N) subsets or rings R_i, such that $S = \bigcup_{i=1}^{m} R_i$, defined internally by a hypersphere with radius $r_{in} = (i-1) \cdot r_{max}/m$ and externally by a hypersphere with radius $r_{out} = i \cdot r_{max}/m$.

Such as conditional sampling technique, for the ring R_i, unit random directions $\hat{\boldsymbol{a}}$, uniformly distributed on the hypersphere, and chi-distributed random radius $\hat{r}$, conditioned to $r > r_{in}$ and $r < r_{out}$, are generated.

For generating random radius $\hat{r}$, inverse transformation method can be used, considering that,

$$\chi_n\left(r^2 | r > r_{in}, r < r_{out}\right) = \frac{\chi_n\left(r^2\right) - \chi_n\left(r_{in}^2\right)}{\chi_n\left(r_{out}^2\right) - \chi_n\left(r_{in}^2\right)} \tag{2.50}$$

With this technique, for N realizations of the limit state function (N/m samples within

the i-th ring), the indicator function I is given by,

$$I = \left(\chi_n\left(r_{out}^2\right) - \chi_n\left(r_{in}^2\right)\right) \cdot m \cdot \begin{cases} 1, \text{ if } G(\boldsymbol{x}) < 0 \\ 0, \text{ if } G(\boldsymbol{x}) > 0 \end{cases} \tag{2.51}$$

The specific case $m = 1$ is equivalent to the direct sampling technique. The choice of m is dependent on the probability of failure and the non-linearity of the limit state function. The smaller the probability of failure to be computed and the stronger the non-linearity of the limit state function, the greater should m be.

Figure 2.11 shows the outcome of the simulation procedure, using the ring sampling technique, considering the limit state function illustrated in Figure 2.5.

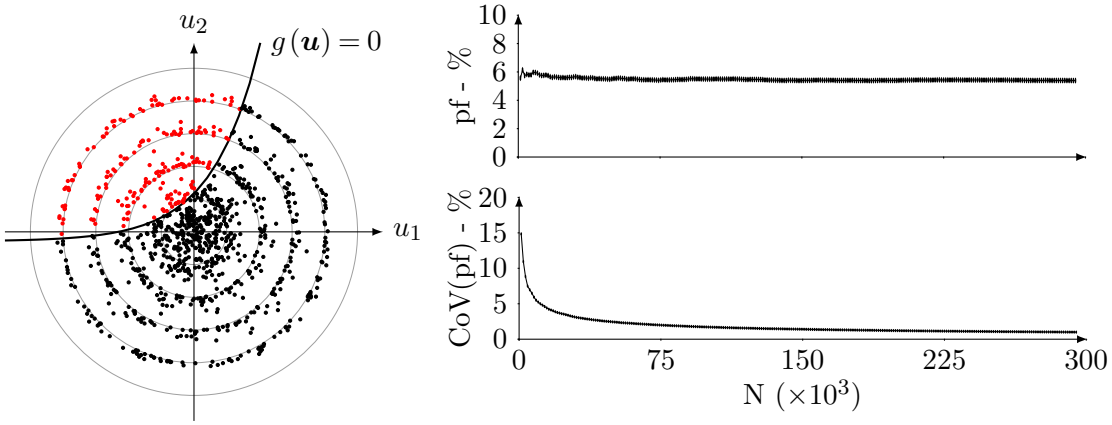

Figure 2.11: Simulation procedure, using the ring sampling technique, considering the limit state function illustrated in Figure 2.5.

2.6 Procedure for reliability-based design

2.6.1 General considerations

Structural design taking explicitly into account the sources of uncertainty is translated into an optimization problem, in which an objective function, often given by the total volume of structural materials or the cost of construction or manufacture (Melchers 1999), expressed in terms of design variables $\boldsymbol{\theta} = \{\theta_1, \cdots, \theta_n\}$, is minimized, providing that safety requirements are satisfied.

If the safety requirements are expressed by a target reliability index, the optimization problem is called reliability-based design optimization (RBDO), which, as opposite to deterministic design optimization (DDO), takes explicitly into account the uncertainties,

even though costs of failure are not included in the analysis such as in risk optimization (RO) (Melchers 1999).

In the RBDO, the solution of the minimization problem,

$$\boldsymbol{\theta}^* = \min_{\boldsymbol{\theta}} f(\boldsymbol{\theta}) \tag{2.52}$$

is subjected to the following reliability constraint,

$$\beta(\boldsymbol{\theta}) \geq \beta_T \tag{2.53}$$

where $\boldsymbol{\theta}^*$ is a vector with the optimum values of the design variables, $f(\boldsymbol{\theta})$ is an objective function, which can be a complex combination of several factors, given in terms of design variables $\boldsymbol{\theta}$, such as the cost of construction or manufacture (Melchers 1999), $\beta(\boldsymbol{\theta})$ is the reliability index and β_T is the target reliability index.

Since numerical solution of the minimization problem is often computationally expensive, Kiureghian *et al.* (1994) developed an extended version of the first-order Rackwitz-Fiessler algorithm (Rackwitz and Fiessler 1978), belonging to the class of inverse reliability problems, to determine one unknown design variable θ^*, usually a geometry parameter, for a given limit state function G, i.e.,

$$G(\boldsymbol{u}^*, \theta^*) = 0 \tag{2.54}$$

such that the prescribed target reliability index β_t is attained,

$$\beta(\theta^*) = \beta_T \tag{2.55}$$

This algorithm is based on a line-search method that iteratively approaches the optimal solution. Despite its accuracy, second-order algorithms are rarely used in inverse reliability analysis due to the cumbersome numerical computation of the Hessian matrix, although some faster approximate alternatives are available (Lim *et al.* 2014).

The algorithm, presented in the following section, can be used as an alternative to root-finding methods that would require repeated reliability analyses.

2.6.2 Solution algorithm

The algorithm proposed by Kiureghian *et al.* (1994) is developed in a similar way to the Rackwitz-Fiessler algorithm (Rackwitz and Fiessler 1978) presented in section 2.5.2.4.

After the selection of initial values of the design point $\boldsymbol{u}_0^*$ and the design variable θ_0^*, both are iteratively updated, until convergence, by,

$$\begin{pmatrix} \boldsymbol{u}_{i+1}^* \\ \theta_{i+1}^* \end{pmatrix} = \begin{pmatrix} \boldsymbol{u}_i^* \\ \theta_i^* \end{pmatrix} + \lambda_i \cdot \boldsymbol{d}_i \tag{2.56}$$

where the search direction vector $\boldsymbol{d}_i$ is given by,

$$\boldsymbol{d}_i = \begin{pmatrix} \beta_T \cdot \boldsymbol{\alpha}_i - \boldsymbol{u}_i^* \\ \dfrac{\nabla g\left(\boldsymbol{u}_i^*,\theta_i^*\right)\cdot\boldsymbol{u}_i^* - G\left(\boldsymbol{u}_i^*,\theta_i^*\right) + \beta_T \cdot \left\| \nabla g\left(\boldsymbol{u}_i^*,\theta_i^*\right) \right\|}{\partial G\left(\boldsymbol{u}_i^*,\theta_i^*\right)/\partial\theta} \end{pmatrix} \tag{2.57}$$

and the merit function, used to computed the step size λ_i, is given by,

$$f\left(\boldsymbol{u}^*,\theta^*\right) = f^{(1)}\left(\boldsymbol{u}^*,\theta^*\right) + f^{(2)}\left(\boldsymbol{u}^*,\theta^*\right) \tag{2.58}$$

where $f^{(1)}\left(\boldsymbol{u}^*,\theta\right)$ is similar to the equation 2.32, and $f^{(2)}\left(\boldsymbol{u}^*,\theta\right)$ is given by,

$$f^{(2)}\left(\boldsymbol{u}^*,\theta^*\right) = \frac{c_2 \cdot \left(\|\boldsymbol{u}^*\| - \beta_T\right)^2}{2} \tag{2.59}$$

where c_2 is a positive parameter.

2.7 Procedure for code calibration

2.7.1 General considerations

Standards community, has mentioned, often seeks for simple safety checking criteria, not requiring the performance of reliability analysis which, apart from its complexity, would depend on the engineer interpretation, based on specific conditions and a standardized code. Consequently, modern design codes are based on what is referred as the semi-probabilistic format of the structure safety evaluation which is considered as a consistent simplification of fully probabilistic methods (Vrouwenvelder 2008).

Moreover, aiming for simplicity and wide-coverage, making the design process easier

and invariant, codes usually classify structures and/or failure modes, according to the consequences of a potential failure, using the same reliability elements (partial safety factors, load reduction factors and modification factors). Although leading to less optimal structures, practical codes should have the smallest number of reliability elements that is consistent with reasonably uniform standards of reliability (Thoft-Christensen and Baker 1982).

Nonetheless, safety checking criteria will always have some degree of arbitrariness, due to limitations of semi-probabilistic design to account for the inherently probabilistic nature of structural safety problems, giving rise to fluctuations in the reliability index (Vrouwenvelder 1997). Code calibration shall then balance simplicity and optimality, ensuring a lower bound of reliability within the structure class.

Code calibration strategies usually adopt a combination of the following perspectives (Baravalle 2017):

1. Judgment, commonly considered when the reliability theory was not yet developed, which consists in modifying codes based on past experience;

2. Fitting which consists in calibrating the new code in order to achieve the same reliability levels as the old code;

3. Optimization which consists in calibrating the reliability elements to meet an optimal design concerning a certain code objective related to the risk acceptance criteria.

In the following section, the code optimization problem is detailed.

2.7.2 Optimization problem

2.7.2.1 General considerations

The procedure for the formulation of the code optimization problem is commonly translated into the following seven steps (Thoft-Christensen and Baker 1982; Ditlevsen and Madsen 1996; Gayton *et al.* 2004):

1. Definition of the structure class that the code will address, specifying types of structures, geographical domain of validity, failure modes, materials and geometric properties;

2. Definition of the code objective through the definition of an appropriate target value for the reliability index or the probability of failure. This decision is made either by a process of probabilistic calibration to an existing code or to a risk acceptance criteria;

3. Definition of the code format, which generally consists in the definition of the m random variables affected by partial safety factors γ_i $(i = 1, \cdots, m)$;

4. Selection of the N design situations, encompassing the typical failure modes and the differentiation between probabilistic descriptors of the random variables, which shall cover all domain of validity of the code, and the corresponding relative importance ω_j $(\sum_{j=1}^{N} w_j = 1)$ quantifying the importance of satisfying the code objective as well as possible;

5. Selection of a penalty function $M\left(\omega, \zeta\left(\boldsymbol{\gamma}\right) - \zeta_T\right)$, punishing the deviation of the code from the objective $\left(\zeta\left(\boldsymbol{\gamma}\right) - \zeta_T\right)$, where ζ is any degree-of-fit parameter such as the probability of failure or the reliability index. The simplest option is a quadratic penalty function, i.e.,

$$M\left(\omega, \zeta\left(\boldsymbol{\gamma}\right) - \zeta_T\right) = \omega \cdot \left(\zeta\left(\boldsymbol{\gamma}\right) - \zeta_T\right)^2 \tag{2.60}$$

   Since this function is symmetrical around ζ_T, equally penalizing under and over-designed structures, Lind (1977), based on economical measures of the deviations between the code and its objective, suggests the consideration of an asymmetrical penalty function given by,

$$M\left(\omega, \zeta\left(\boldsymbol{\gamma}\right) - \zeta_T\right) = \omega \cdot \left[k \cdot \left(\zeta\left(\boldsymbol{\gamma}\right) - \zeta_T\right) + e^{-k \cdot \left(\zeta(\boldsymbol{\gamma}) - \zeta_T\right)} - 1\right] \tag{2.61}$$

   where k is a positive curvature parameter (Ditlevsen and Madsen (1996) suggests $k \approx 4.35$). Figure 2.12 compares the shape of these penalty functions. Nonetheless, the final result is usually not very sensitive to the choice of penalty function (Thoft-Christensen and Baker 1982; Ditlevsen and Madsen 1996);

6. Determination of the best set of partial safety factors using an code optimization routine. In general, the code objective cannot be exactly achieved for all design situations. Thus, the search for the best set of partial safety factors is made by

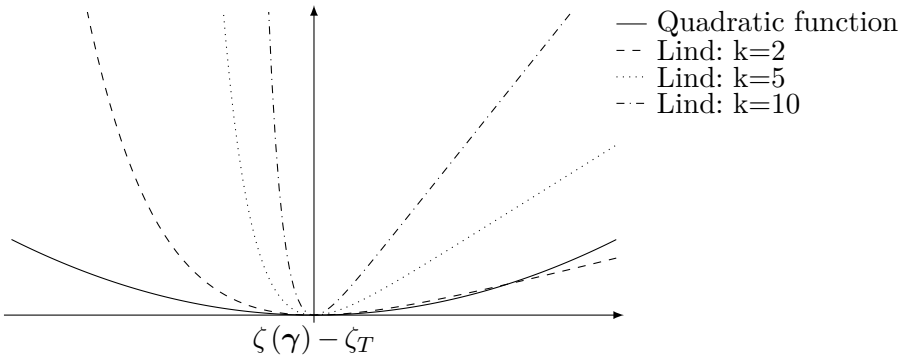

Figure 2.12: Shape of penalty functions.

minimizing the total expected losses Δ, i.e.,

$$\min_{\boldsymbol{\gamma}} \Delta(\boldsymbol{\gamma}) = \sum_{j=1}^{N} M\left(\omega_j, \zeta_j(\boldsymbol{\gamma}) - \zeta_T\right) \tag{2.62}$$

For the code optimization routine, two different approaches, detailed in the following sections, may be considered, namely:

- Global optimization method, which, although being time consuming as they require a large number of reliability analyses, solve directly the optimization procedure resulting in the best set of partial safety factors;
- Design-value (or approximate) methods, which are less time consuming leading to a set partial safety factors with a satisfactory precision.

7. Checking the code adequacy, by designing a set of test structures, using the set of partial safety factors obtained, and comparing the obtained ζ to the target value ζ_T, which may indicate the quality of the procedure.

2.7.2.2 Global optimization method

In the global optimization method, at the i-th iteration of the numerical minimization routine, the reliability analysis of structures designed for each of the N design situations, considering the partial safety factors $\boldsymbol{\gamma}$, must be performed. Figure 2.13 illustrates the corresponding optimization routine.

This method, which leads to the optimal set of partial safety factors, requires a large number of reliability analysis (as large as the number of design situations covered by

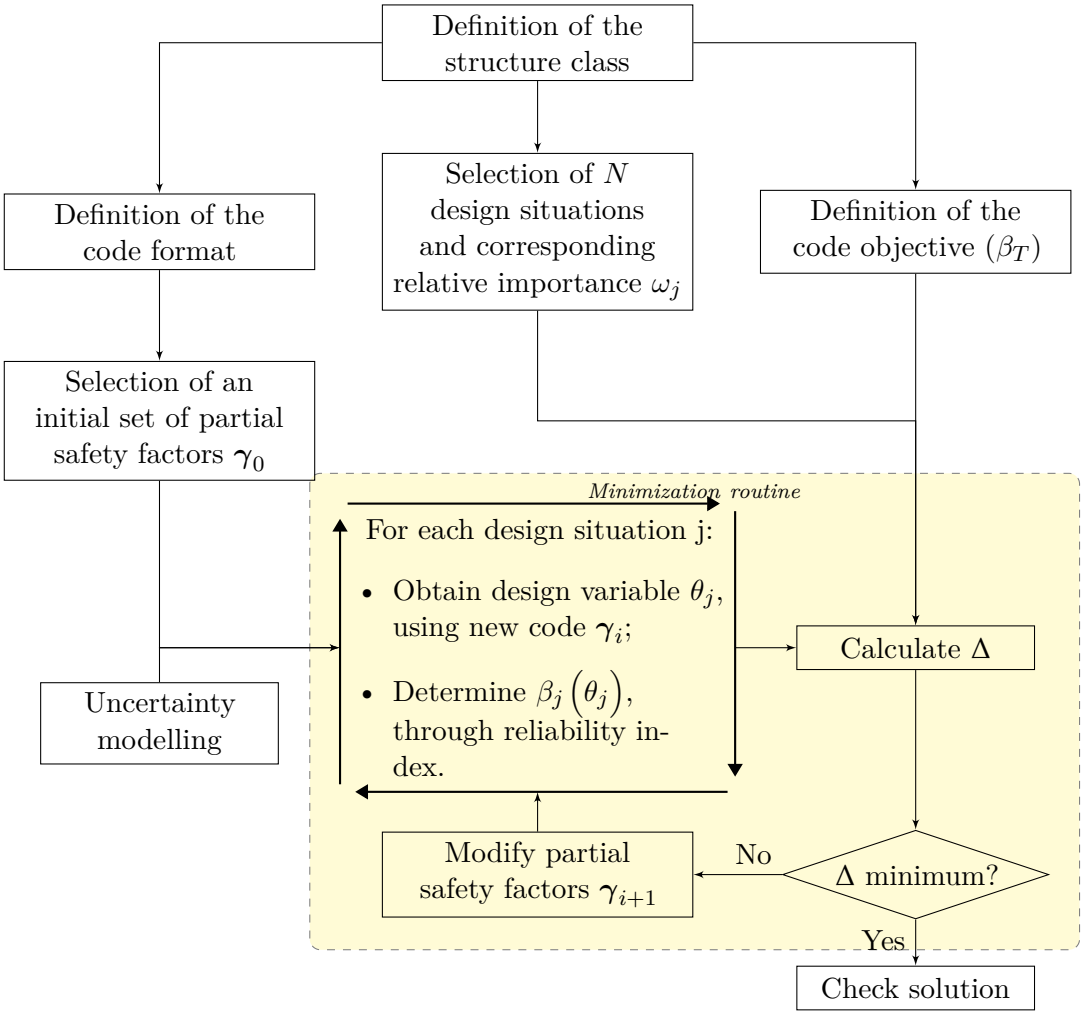

Figure 2.13: Flow chart of the code optimization routine considering the global optimization method.

the code), at each iteration, which can be very computer time consuming. Design-value methods (Ditlevsen and Madsen 1996) were developed to simplify this routine.

2.7.2.3 Design-value methods

The design-value methods to the optimization routine consist in avoiding the performance of reliability analyses at each iteration, by dividing the step 6 of the optimization problem into two substeps (Gayton *et al.* 2004): the design point search and the partial safety factor computation. Thus, the determination of the design variable, and the corresponding reliability index, for each design situation, can be move outside the optimization procedure, (Figure 2.14).

The design point search consists in obtaining the design point $\boldsymbol{u}_j^*$, and the corresponding

set of partial safety factors $\boldsymbol{\gamma}_j$ $(j = 1, \cdots, N)$, of each design situation considering structures designed according to the code objective through inverse reliability procedure.

The partial safety factor computation consists in obtaining a single set of partial safety factors $\boldsymbol{\gamma}$, which shall be representative for all design situations considered in the structure class. A simple approach is the consideration of the most conservative set of partial safety factors given by the maximum value of each partial safety factor $\gamma_i j$, i.e.,

$$\gamma_i = \max_j \gamma_{ij} \tag{2.63}$$

which, although leading to safety conditions for all structure class, is uneconomical. Other simple approach is the consideration of the weighted mean value of each partial safety factor,

$$\gamma_i = \sum_{j=1}^{N} \omega_j \cdot \gamma_{ij} \tag{2.64}$$

which may not be the optimal solution since the resulting deviations from the code were not assessed.

An improved method, based on a new and faster optimization problem, were suggested by Ditlevsen and Madsen (1996). The authors admit that there is a replacement vector $\boldsymbol{\delta}$, on the standard normal space, such that,

$$\beta_j \approx \beta_T \cdot \boldsymbol{\alpha}_j \cdot \boldsymbol{\delta} \tag{2.65}$$

where $\boldsymbol{\alpha}_j$ is obtained from the design points $\boldsymbol{u}_j^*$.

Theoretically, the replacement vector $\boldsymbol{\delta}$ indicates the direction of a design point $\boldsymbol{\delta} \cdot \beta_T$ common to all design situations. Since this point is unlikely to exist, all limit state functions are adjusted to contain that point, leading to variations of the reliability index, which shall be minimized, over the structure class.

The new optimization problem is re-written as,

$$\min_{\boldsymbol{\delta}} \Delta = \sum_{j=1}^{N} M\left(\omega_j, \beta_T \cdot \boldsymbol{\alpha}_j \cdot \boldsymbol{\delta} - \beta_T\right) \tag{2.66}$$

which is a numerical minimization problem that does not need the performance of reliability analyses. Figure 2.14 illustrates the optimization routine suggested by Ditlevsen and

Madsen (1996).

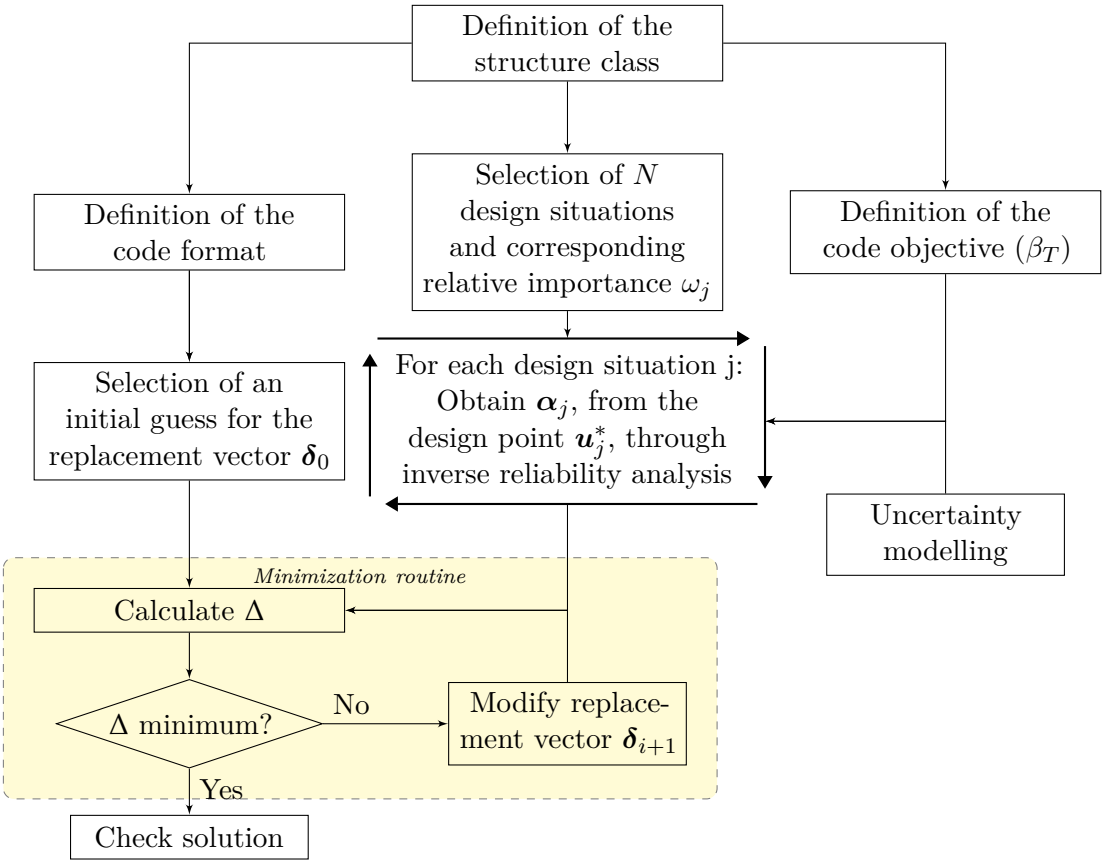

Figure 2.14: Flow chart of the code optimization routine considering the design-value method suggested by Ditlevsen and Madsen (1996).

However, Friis-Hansen and Sørensen (2002) highlighted that the minimization of Δ considering the assumption given by the equation 2.65, may lead to a $\boldsymbol{\delta}$ far outside the cluster of $\boldsymbol{\alpha}$. Moreover, even if the minimization is well-succeeded, the computation of the partial safety factors requires the transformation of $\boldsymbol{\delta}$ to the original variable space which may result in many sets of partial safety factors, since there are as many transformations as selected design situations (Gayton *et al.* 2004).

In this thesis, an alternative approach is used, based on the consideration of the design variable as degree-of-fit parameter ($\zeta = \theta$). Given that the optimum value of the design variable θ^* was computed through previous inverse reliability procedure, regarding a specific code objective (target reliability index), the deviations using the code may indicate its adequacy.

The minimization routine, which does not need the performance of reliability analyses,

is then expressed by,

$$\min_{\boldsymbol{\gamma}} \Delta(\boldsymbol{\gamma}) = \sum_{j=1}^{N} M\left(\omega_j, \theta_j(\boldsymbol{\gamma}) - \theta_j^*\right) \tag{2.67}$$

where the design variable θ_j, corresponding to the design situation j, is obtained by a line-search method. The set of partial safety factors given in equation 2.64 can be used as an initial guess and the set given in equation 2.63 can be used as an upper bound for the minimization routine.

However, gross errors may be introduced with this approach due to the expected non-linear relation between the reliability index β and the design variable θ. A small variation of the design variable θ may result into disproportional variation of the corresponding reliability index. In order to take that into account, it is proposed that the weights, ω_j, besides the relative importance of the design situation over the structure class, includes also some information regarding the effect of the variation of the design variable on the reliability index. Thus, in this approach, the weights are given by,

$$\omega_j = \frac{\omega_j^{(1)} \cdot \omega_j^{(2)}}{\sum \omega_j^{(1)} \cdot \omega_j^{(2)}} \tag{2.68}$$

where $\omega_j^{(1)}$ is the relative importance of the design situation j, as described in step 6 of the optimization problem, and $\omega_j^{(2)}$ is given by,

$$\omega_j^{(2)} = \frac{\partial \beta_j(\theta^*)}{\partial \theta} \approx \frac{\beta_j(\theta^* + \Delta_\theta) - \beta_T}{\Delta_\theta} \tag{2.69}$$

which can be approximate by the finite-difference formula. Therefore, more importance is given to the adequacy of the code to the design situations whose reliability index has shown more sensitiveness to variations in the design variable θ.

The computation of $\beta_j(\theta^* + \Delta_\theta)$ can be performed just after the inverse reliability procedure and before the minimization routine. This procedure is illustrated in Figure 2.15.

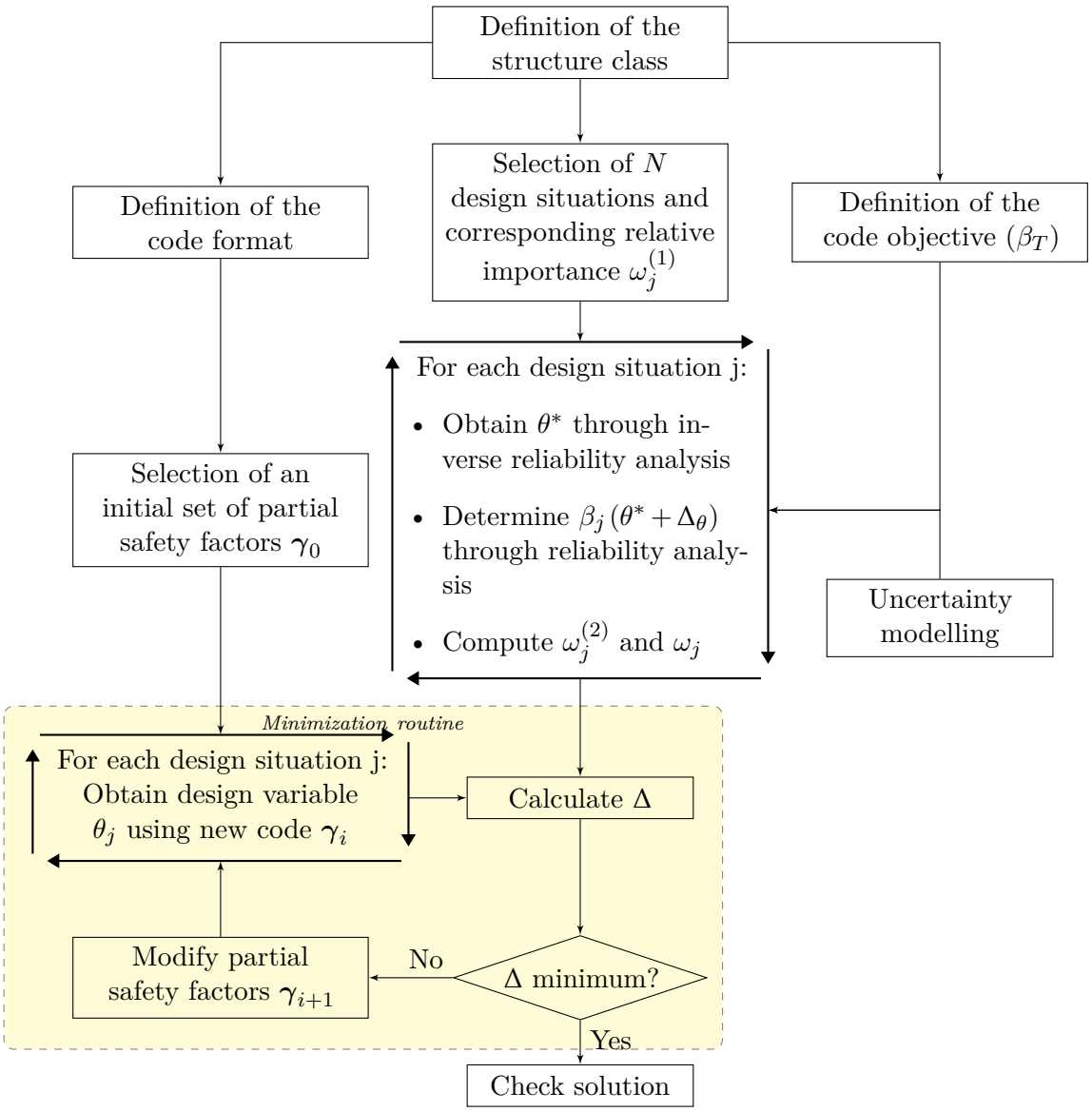

Figure 2.15: Flow chart of the code optimization routine considering the alternative design-value approach proposed.

CHAPTER 3

Safety of concrete gravity dams

3.1 General considerations on dams

Given their importance, dimensions, the problems that should be solved during design and construction, the influence on the environment and mainly the potential risks involving their operation, dams are one of the most significant engineering structures in general (Tanchev 2014).

Water-retention dams are single- or multiple-purpose structures, integrated in river water management projects, which intend to create storage reservoirs, raise the water level upstream or control the water level downstream (ICOLD 1990). The purposes for dam construction (water supply, irrigation, hydropower generation, navigation, flood control and recreation) determine the required volume of the reservoir and the structure height (APA 2001), defined as the overall distance between the lowest point of the foundation surface to the top of the dam (ICOLD 1998).

In the planning stage, the possible dam implantation sites, throughout the course of the river, are analyzed based on engineering, economical, political, social and environmental aspects. The decision should result in the selection of a site that provides the best conditions to ensure an optimal and safe exploitation of the water resources, according to the dam purposes, balancing costs of construction and maintenance.

Local hydrology dictates the reservoir water management policy, according to the dam purposes, given the water inflow into the hydrographic basin and the outlet works, designed

to discharge, in safe conditions, the water inflow from a possible but unlikely design flood, determined depending on the significance and size of the dam (Rissler 2001).

In general, three characteristic levels of water in the impounding reservoir are distinguished, namely: (i) the minimum operating level (MOL); (ii) the normal (or retention) water level (NWL), which provides the optimum operation conditions; and (iii) the flood (or maximum) water level (FWL), which is related to the design flood, often one meter below the crest. This discretization divides the reservoir into three parts (Tanchev 2014):

- Dead storage, below MOL, which is expected to become filled with silt and deposits during the service life and creates an area for fish during low levels;
- Live storage, between MOL and NWL, to be used during normal operation for water utilization purposes;
- Retention storage, between NWL and FWL, serving for retention of flood water, which shall be discharged, at a controlled or predicted rate, for safety reasons.

The structural solution, regarding the material and structural type, is not only conditioned on the topography but also on the hydraulic and mechanical characteristics of the foundation (Ramos 2004). While, generically, embankment dams are suitable for soft rock or soil foundations (APA 2001) or when the availability of proper construction materials, within a reasonable haul area, makes this solution economically more favorable, concrete dams require a rock mass foundation capable of withstanding reasonable stresses (Thomas 1976). The valley shape, defined by the ratio of the width at the crest level, W, to its depth below the crest level, H, may influence the choice of the structural type, generically divided into:

- Gravity dams (Figure 3.1a), which make use of their own weight to resist the external loads, are suitable solutions for wide valleys ($W/H > 6$), providing that the rock mass foundation is capable of facing stresses in the range of 3 to 4 MPa (Thomas 1976). Hollow gravity dams have some specific advantages. Arch-gravity dams also transmits part of the external loads to the abutments due to a curvature in plan;
- Arch dams (Figure 3.1b), which make use of an arch effect to transmit the external loads to the foundation through abutment banks, are suitable solutions for gorges ($W/H < 3$) and maybe narrow valleys ($3 < W/H < 6$), having been built in valleys

whose W/H ratio is up to 5 or more (Pedro 1999), providing the existence of rock abutments with capacity of facing stresses in the range of 7 to 10 MPa (Thomas 1976). Arch dams can be divided, according to their curvature, into single-curvature, curved only in plan, and double-curvature, curved in plan and in elevation;

- Buttress dams (Figure 3.1c), consisting in a water-tight flat or curved upstream wall supported by a series of triangular evenly-spaced buttresses, are suitable solutions for wide valleys in which gravity dams, due to their excessive volume, would become uneconomical solutions or when rock mass quality is heterogeneous throughout the implantation site (Ramos 2004), providing that buttresses rock mass foundation is capable of facing stresses in the range of 5 to 7 MPa (Thomas 1976). Multiple-arch, bulb head dams, among others, are some of the solutions considered as buttress dams (Thomas 1976).

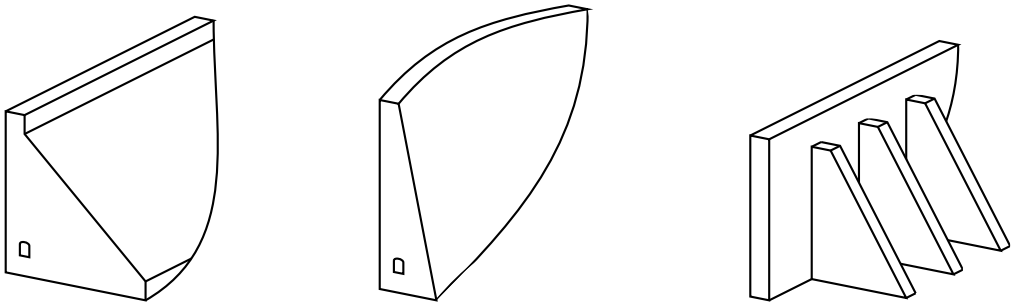

(a) Gravity dam. (b) Arch dam. (c) Buttress dam.

Figure 3.1: Types of concrete dams.

The practice regarding the dam safety analysis and control, at the design and operation stages, respectively, has been improved based on experience and guidance of the International Committee on Large Dams (ICOLD), which defines large dams, whose safety control is of major importance given their potential risks, as those which are (ICOLD 2011):

- at least 15 meters of height;
- between 5 to 15 meters of height, impounding more than 3 million cubic meters of water.

The Portuguese dam safety regulation (RSB 2018) classifies large dams according to the hazard associated to the dam operation and the potential risks, for which different

safety requirements and control measures are established. The hazard associated with the dam operation is characterized by a factor X, given by,

$$X = H^2 \cdot \sqrt{V} \tag{3.1}$$

where H is the dam height, in meters, and V is the reservoir volume, in cubic meters.

The potential risks are quantified according to the number of the permanent edifications (Y) and the existence of infrastructures, facilities and other important environmental assets in the downstream valley.

Table 3.1 presents the dam classification according to the Portuguese dam safety regulation (RSB 2018).

Table 3.1: Dam classification (RSB 2018)

Class	Dam operation hazard and potential risks
I	$X \geq 1000$ and $Y \geq 10$
II	$X < 1000$ and $Y \geq 10$; or $0 < Y < 10$; or existence of infrastructures, facilities and other important assets
III	Remaining cases

For the safety control of large dams, during the dam service life, monitoring equipment and outlet works, such as spillways and bottom outlet, must be used. Devices to measure strains, displacements, temperatures, uplift pressures, and the reservoir water level are commonly installed. Spillways, aiming to discharge the extra flood inflow, are divided in controlled and uncontrolled, whether outlet gates are installed or not, respectively. In some cases, related structures, such as the spillway channel and stilling basin may be necessary to discharge safely the overflow water into the river channel (Tanchev 2014). Bottom outlet, whose level of entrance is most often dictated by the dead storage, serves to lower the reservoir water level in extraordinary situations, such as for repair works or when the structural safety is threatened.

At the design stage, the goal is to define the structural characteristics of the dam (dimensions, materials and additional safety measures) that guarantee the structural safety, during the desired service life, under the expected most conditioning load combinations. Both load combinations and safety criteria are established in national or international regulations.

In the following sections, the structural safety of concrete gravity dams is analyzed. After a historical review on gravity dam design and construction, the constructive aspects and design principles, the acting loads and the framework of safety regulations and design codes of concrete gravity dams are presented. Lastly, the failure modes for typical gravity profiles are modeled by comparing analytical and numerical solutions of a representative, though generic, case study.

3.2 Historical background on dam design and construction

3.2.1 Developments until the 19th century

Although it is not clear when and where first water supply reservoirs were built, they are undoubtedly among the earliest structures devised by mankind, being closely linked to the rise and decline of civilizations (Jansen 1983).

The early dam builders created invariably simple embankment structures, easily erased by floods (Jansen 1988), such as the Sadd el-Kafara dam (Egypt), built somewhere between 2600 B.C. to 2900 B.C. and generally accepted as the oldest known dam of real significance, which breached after a short service period (Novak *et al.* 2007).

The Roman era brought understanding on engineering fundamentals and improved craftsmanship. The Romans built many dams of very durable mortared masonry (Jansen 1988), some of them, such as the Proserpina and Cornalba dams (Spain), from the 2nd century, are still in service. The Romans also adopted the arch principle in dam construction and the use of buttresses, such as in the Olisipo dam (Portugal), also from the 2nd century, which is believed to be the highest Roman dam with buttresses (Almeida 1969).

The masonry dams, which relied upon their weight for stability against sliding or overturning, being the predecessors of modern concrete gravity dams, were initially built based on rudimentary principles with both upstream and downstream faces sloped and the base thickness many times greater than the height (Thomas 1976).

3.2.2 Rational profile selection

Until the first half of the 19th century, dam design had been based on empirical methods and accumulated experience, which, although following the Roman legacy, resulted in a gradual but non-continuous decreasing of the quantities of masonry (Thomas 1976), leading to a more triangular section than trapezoidal. During that century, the masonry dam

construction made important advances after French dam engineers began to incorporate rational approaches into structural analysis, linking structural engineering to mathematical theory.

Sazilly (1853) advocated that, in order to ensure proper safety of dams: (i) the stresses sustained must not exceed a certain limit; and (ii) there must be no possibility of sliding in the dam-foundation interface or within the dam body. Given the difficulty on devising a designed formula containing both conditions, Sazilly (1853) stated that the dam shall be designed solely with reference to the stress criteria, since no masonry dam had failed by sliding, considering the two extreme load cases: (i) full reservoir, causing the maximum compressive stresses at the downstream face; and (ii) empty reservoir, causing the maximum compressive stresses at the upstream face in any horizontal section. Having established a limit value for the vertical stresses, Sazilly (1853) suggested an idealized profile, designated "profile of equal resistance", in which, due to economic requirements, the maximum vertical stress at both faces reach the limit for the two extreme load cases. After finding impossible to integrate the differential equations that determine analytically the form of the theoretical profile, Sazilly (1853) suggested a practical profile (Figure 3.2a) with horizontal layers and stepped slopes.

Delocre (1866), intending to obtain the best profile for masonry dams, demonstrated that a stepped profile involves considerable waste of materials while not resulting in a significant increase of safety. The proposed profile (Figure 3.2b), whose analytical formula was given, formed the basis for the design of the Furens dam (France), built in 1860-1866, and influenced the dams built subsequently.

Rankine (1872), although corroborating the former principles, argued that, since the downstream face are more sloped than the upstream face, the limit of the vertical stress for the first should be lower than for the latter, recommending, based on the analysis of existing masonry dams, a stress limit of 0.96 MPa and 0.75 MPa for the upstream and downstream faces, respectively. Rankine (1872) also pointed out that no tension must be allowed in the masonry, considering the possibility of water seepage since the dam is not an impermeable body, which is ensured since the line of pressures lies within the center-third of the profile. From these principles, Rankine (1872) suggested a profile (Figure 3.2c) with logarithmic curves for both faces, neglecting, by simplicity, the vertical component of the hydrostatic pressure on the upstream face.

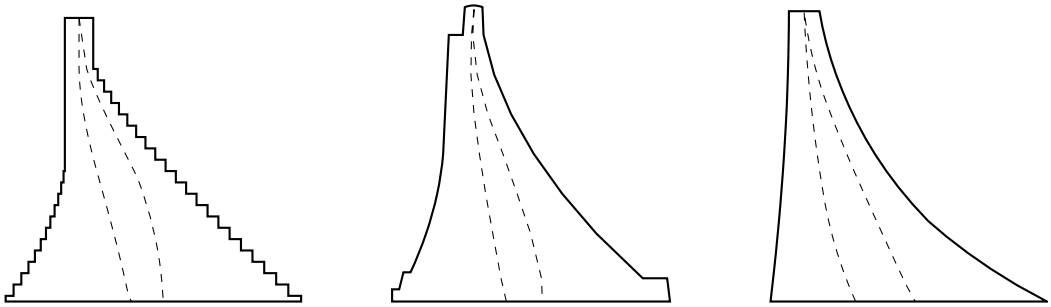

(a) Sazilly (1853) (b) Delocre (1866) (c) Rankine (1872)

Figure 3.2: Gravity profiles suggested in early studies (adapted from Wegmann (1908)).

3.2.3 The role of uplift pressures

While the center-third principle was generally accepted as ensuring for stability of moderately loaded gravity dams, engineers began to recognize the importance of uplift pressures (Jansen 1983), especially after some dam failures.

Uplift pressures were firstly considered in the design of Vyrnwy dam (Powys, Wales, UK), in 1882-1891. A drainage system consisting of a set of rock drains connected to a horizontal gallery with an outlet in the downstream face were built in order to reduce water-seeping pressures. Although this practice continued for the following 30 years (Thomas 1976), this subject remained overlooked, not being explicitly considered in stability calculations, until the Bouzey dam (France) failure, in 1895, due to cracking caused by tensile stresses of 0.2 MPa in the dam (Smith 1994).

Following this event, Lévy (1895) pointed out that the no-tension principle, in the upstream face, was not sufficient to prevent the water seepage through cracks that may occur by other processes, such as thermal loads, and the corresponding uplift pressures that may lead to the dam instabilization. Lévy (1895) stated that the compressive stress on each point of the upstream face must be equal or higher than the water pressure at that point and proved that this condition is equivalent to adopt a linear uplift distribution, varying from the reservoir water head at the upstream face to the tailwater head at the downstream face, for any horizontal joint of the dam, including the dam-foundation interface.

Since uplift pressures were recognized, a time of discussion on their intensity and acting area began. The evolution of masonry dams into cyclopean and mass concrete dams, due to technical and machinery innovations which led to a widespread and economical use of concrete (Chen 2015), also played an important role. Greater concern was placed on the water seepage through the dam-foundation interface, instead of dam body, where

waterproofing could not be ensured (Andrade 1982).

While becoming commonly accepted that the uplift pressures act over nearly the whole dam base, such as demonstrated in relevant studies (Terzaghi and Rendulic 1934; Leliavsky 1945) and confirmed by the analysis of first piezometric data (EPRI 1990), the intensity of the uplift pressures would depend on both the geological conditions of the foundation, specifically the strength, permeability and state of fracturing, and the seepage and uplift control measures undertaken, such as cutoff barriers, initially, and grout curtains and drains, later (EPRI 1990).

Casagrande (1961), after the failure of Malpasset dam (France) in 1959 which led to new studies on the hydromechanical behavior of the rock mass foundations (Londe 1987), confronted the settled practice of putting more effort into the construction of grout curtains, questioning their capacity on reducing the uplift pressures. Using the observed pressures in the foundation of Hiawassee dam (USA), Casagrande (1961) demonstrated that the uplift reduction is mainly caused by the drains whereas the grout curtain is ineffective for that purpose.

3.2.4 Modern challenges

Since the 1950s, the increase, in number and height, of dams accelerated around the world due to the demand of water supply and clean hydropower for exponentially growing cities (Chen 2015).

This period coincides with both the introduction of monitoring devices and techniques to monitor different control variables (Rocha *et al.* 1958) and the development of numerical methods, replacing the physical scaled models extensively used to study the dam behavior mainly under rupture conditions (Rocha 1965), and its application to structural analysis of concrete dams (Zienkiewicz 1947). Both monitoring and numerical methods for structural analysis allowed better understanding on structural behavior, the long-term behavior of materials, the hydromechanical behavior of the rock mass foundations and the dynamic response of dams, since the concern about the effects of earthquakes in the structural safety also increased as higher dams were built.

Nowadays, the development of roller-compacted concrete (RCC) dams reflects the concern of dam engineering community in searching for economical solutions (Bretas 2012). Economic reasons also motivate both the concern in maintenance and rehabilitation, as

operational dams become older, and the introduction of probabilistic principles into the decision-making process.

3.3 Constructive aspects and design principles of concrete gravity dams

3.3.1 General considerations

Until the beginning of the 20th century, masonry dams had been an economical solution to provide water supply, at a time when cement was scarce (Sims 1994). The evolution to concrete dams, due to the widespread manufacturing and use of Portland cement, as well as the technical and scientific developments in material and structural engineering, allowed the construction of higher dams.

The construction practice and the design solutions of modern concrete dams are influenced not only by economical reasons but also by the concrete behavior, as a structural material, and the durability and safety requirements. On one hand, the consequences of the use of concrete in such large structures, such as concrete gravity dams, and their effect on rock mass foundations, whose hydraulic and mechanical behavior is highly dependent on the existing discontinuities, have been reduced by adopting innovative construction techniques and additional waterproofing and strengthening measures, respectively. On the other hand, the mechanized concrete placement and formwork techniques have justified the adoption of the modern slender and straight cross-section profile (Novak *et al.* 2007), in which almost all recently built concrete gravity dams are configured (Chen 2015).

In the following sections, the main concerns, as well as the solutions usually adopted, for construction and design are detailed.

3.3.2 Constructive aspects

3.3.2.1 General considerations

Although the concrete dam construction follows a scheduling defined to optimize resources, some constructive solutions are employed to prevent the development of adverse effects that may compromise the structural safety. Therefore, both the construction of the concrete super-structure and the treatment carried out in the rock mass foundation intend to improve the performance of the reservoir-dam-foundation system during the service life.

Regarding the concrete super-structure, these solutions aim to minimize the consequences of restrained volume changes, namely the degradation of the stiffness, strength and durability of concrete dams, due to: i) external seasonal temperature variations, ii) internal temperature variations during the construction, and iii) expansive reactions.

Regarding the rock mass foundation, treatment measures, usually required to satisfy the requirements of stability, deformation and low permeability (Farinha 2010), aim to (ICOLD 1993):

- Improve its stiffness, ensuring homogeneity and integrity;
- Improve its strength, preventing sliding and uneven settlement;
- Improve its hydraulic behavior, reducing uplift and preventing piping;
- Extend its service life, preventing erosion and deterioration.

In the following sections, these issues are detailed.

3.3.2.2 Concrete super-structure

Due to their large dimensions, concrete dams are considered mass concrete structures, as measures to minimize cracking due to heat generation, from cement hydration, and attendant volume change (ACI 1996) are required.

Modern concrete dams are divided into independent monoliths, intersected by vertical transverse contraction joints, usually spaced about 15 meters apart, avoiding the cracking caused by high tension stresses during cooler seasons. However, since it is advantageous to derive extra strength from the three-dimensional shape of dams, which is even more relevant in narrow valleys (Herzog 1989), lateral teeth are built and grout is injected, after the dam has been naturally or artificially cooled, in the contraction joints, allowing the transmission of forces between adjacent monoliths. Thus, a concrete gravity dam acts as a horizontal beam and the joints as plastic hinges since they would open and redistribute the load (Thomas 1976). Waterstops are commonly used to prevent water leaks through contraction joints (Batista and Farinha 2011).

Each monolith is composed by concrete blocks, placed in batches of, at most, 2 meters of height (around 30 centimeters for roller-compacted concrete) or until 3 meters, if cooling coils, for an artificial cooling of blocks, are used (Batista and Farinha 2011). The corresponding lift joints are discontinuities which, if not carefully treated, may compromise

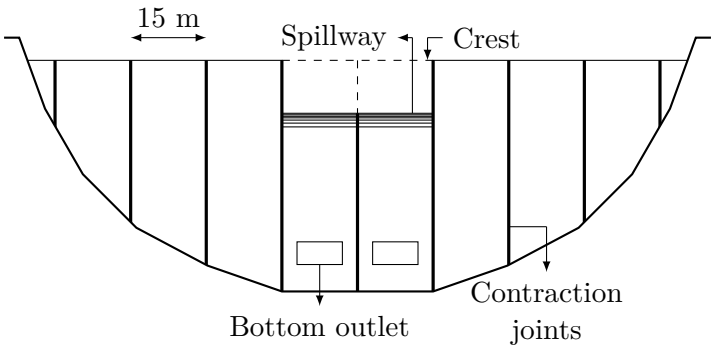

Figure 3.3: Elevation view of concrete gravity dams.

the stability of the blocks above and be a preferential path for water transfers with serious consequences regarding structural integrity.

This construction strategy aims at reducing the cracking risk due to heat dissipation during hardening of concrete, specially important at younger ages when temperature variations influence the development of mechanical properties. Otherwise, the resulting high temperature gradients could lead to stresses that could exceed the strength capacity (Serra 2017). This phenomena is enhanced by the addition of fly ash, which delays the development of the concrete strength.

Mass concrete applied to dams, which is used in the dam core, is produced with larger size aggregates, when compared with ordinary concrete, to reduce costs. Theoretically, larger maximum size of aggregate (MSA) lead to a reduction in cement required to achieve the desired quality and the rule should be use the larger MSA that is practical (ACI 2005). However, it was demonstrated (Higginson *et al.* 1963) that there is an optimal combination of the cement content and MSA to obtain the desired concrete strength (Figure 3.4).

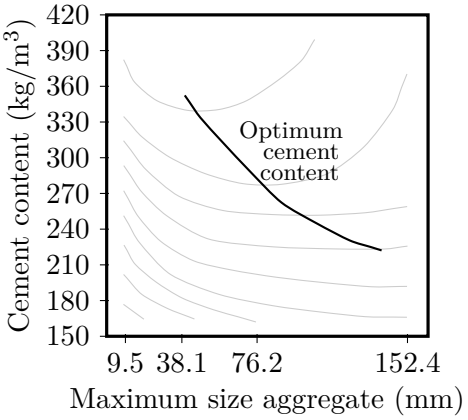

Figure 3.4: Effect of MSA on cement content (Higginson *et al.* 1963).

For modern dams, the cement content rarely exceeds 250 kg/m^3 (ICOLD 2008). To fulfill the workability requirement, the MSA commonly used is between 120 and 150 mm, for the dam core (ICOLD 2008). In reinforced zones (dam surfaces and galleries), smaller MSA has been used to both reduce the concrete permeability and accommodate reinforced bars.

Furthermore, some type of aggregates develops alkali-aggregate reactions (AAR), when in contact with cement, which can lead to an expansion effect in concrete. Since, due to their large dimensions, significant stresses and, consequently, cracking may result from the restrained volume change, cement is blended with pozzolans and/or fly ashes, reducing the AAR potential (ACI 2005) and the heat from hydration, without proportional strength decreasing (Coutinho and Gonçalves 1994).

3.3.2.3 Rock mass foundation

Concrete dams are generally founded on rock masses, which are fractured, heterogeneous and anisotropic media, due to the existence of non-planar discontinuities that govern its mechanical and hydraulic behavior (Muralha 1995).

Loads from the dam construction, reservoir filling and operation cause variations in the stress state of rock masses in a coupled hydromechanical process (Rutqvist and Stephansson 2003; Farinha 2010), since water flows, under pressure, through discontinuities causing deformations in fractured rock masses which lead, in turn, to changes in permeability and, consequently, in water flow.

The treatment usually required depends on both the type and dimensions of the structure and the foundation hydromechanical characteristics. Generally, these treatments are divided into:

- Consolidation grouting, which increases the shear strength and the stiffness of the uppermost strata of the rock mass foundation and seals some discontinuities close to the dam-foundation interface;
- Construction of a waterproof grout curtain, which creates a solid barrier reducing the seepage, composed by rarely more than one row of vertical or sub-vertical grout holes drilled from the drainage gallery close to the dam upstream face or from an upstream plinth, located at the dam heel;

- Construction of a drainage curtain, to reduce the uplift pressures, composed by, at least, one line of boreholes drilled downstream from the grout curtain.

Figure 3.5 illustrates the waterproofing and drainage systems, connected to the gallery.

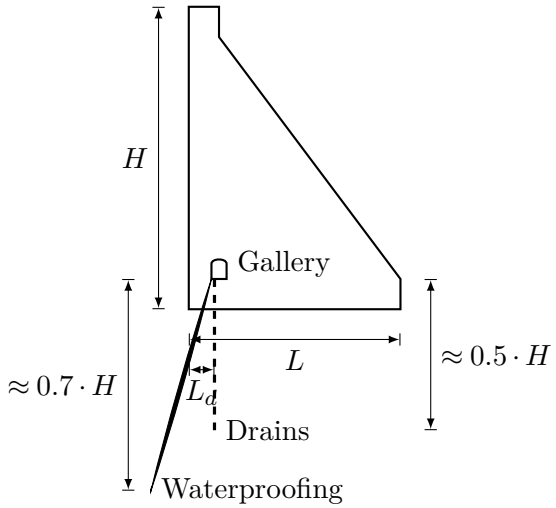

Figure 3.5: Waterproofing and drainage systems of the rock mass foundation.

The dam-foundation interface shall be treated in order to enhance the concrete-rock bond and improve its shear strength. In current day practice, foundation contacts are smoothed, by removing any rock outcrops, to minimize any geometrically induced stress concentrations and the exposed rock is cleaned with high-pressure water before concrete placements. Shaping of the foundation surface with teeth is also concerned, when the foundation consists of firm and sound rock, as a structural solution aimed at improving the joint with the foundation, as well as improving the resistance against sliding (Tanchev 2014).

3.3.3 Design principles

3.3.3.1 General considerations

Given the existence of transverse contraction joints, the safety analysis of concrete gravity dams is advantageously conducted based on two-dimensional simplifications, neglecting conservatively any three-dimensional effect, by considering the most conditioning monolith typically located on the riverbed.

The design of concrete gravity dams is based on the stability analysis of the cross-section profile, considering any rigid body mechanism. Although stresses shall not exceed

some admissible limits (Thomas 1976), the safety of concrete gravity dams is independent on the mechanical strength of the concrete, since sliding and overturning failures occur before a conditioning stress field is achieved (Chopra and Zhang 1991).

For that, any potential failure surface (Figure 3.6) shall be considered, namely: i) lift joints, ii) concrete-rock (dam-foundation) interface, and iii) rock mass discontinuities. Although they could attain some relevancy for large concrete dams, lift joints are not usually conditioning on the stability evaluation, since good construction strategy shall ensure adequate resistance properties.

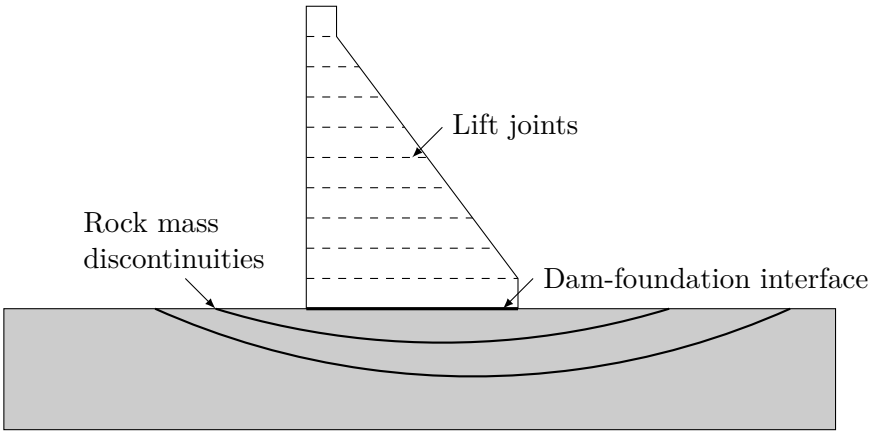

Figure 3.6: Potential failure surfaces of concrete gravity dams.

The design procedure starts with an initial definition of the cross-section geometry, which is progressively updated until the fulfillment of safety criteria. In addition, the stress analysis, especially in the dam-foundation interface, is of major importance since installed tensile strengths result in cracking from the dam heel and, consequently, in an increasing of the uplift pressures and reduction of the contact area.

In the following sections, the typical cross-section profile, the methods for stability analysis and the shear strength modeling are presented.

3.3.3.2 Cross-section profile

The cross-section profile of modern concrete gravity dams is approximately triangular, as suggested by Wegmann (1908) who proposed a thinner profile than those obtained in earlier studies (Figure 3.2), due to: i) the increased compressive stress limit considered; ii) the renunciation of the "equal resistance" rule, leading to a vertical upstream face; iii) the increased unit weight assumed.

In practice, the triangular cross-section is curved at the top to serve as spillway of an overflow section whose crest matches the NWL. The non-overflow section, which should be built when it is necessary to create a permanent access between the two margins and/or to support the outlet gates, requires a minimum width l_c at the top. Figure 3.7 shows the typical cross-section profile of modern concrete gravity dams.

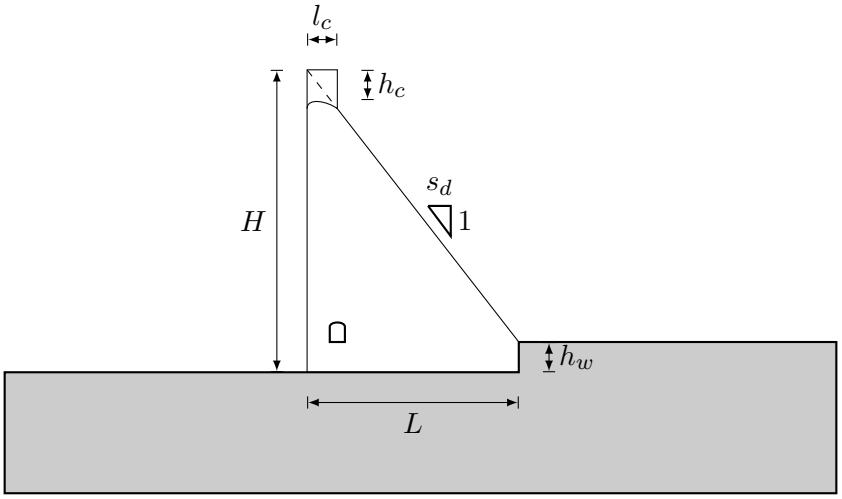

Figure 3.7: Practical cross-section profile of modern concrete gravity dams.

For economy, the upstream face is usually vertical. However, it may be flared or inclined, even if it leads to increased uplift pressures, to improve stability requirements (Chen 2015).

The downstream face slope is often considered as the design variable. To meet stability requirements, the slope is usually in the order of $0.7 \leq s_d \leq 0.8$, depending upon uplift assumptions (Corns *et al.* 1988). However, for higher dams with low density concrete or under seismic loading, $s_d = 0.8$ may not be necessarily appropriate (ICOLD 2000), and flatter slopes ($s_d > 0.8$) are needed.

The dam is usually keyed into the foundation, at a depth corresponding to 10% of the dam height (Pedro 2018), $h_w = 0.1H$, mobilizing a downstream passive resistance, which increases the safety of the profile.

Furthermore, in specific cases, in order to improve stability and make the structural solution viable, post-tensioned anchors have been used both in construction and rehabilitation (Brown 2015), although this solution is mostly adopted for rehabilitation purposes.

3.3.3.3 Stability analysis

Gravity dam stability analysis consists in verifying if the stabilizing loads can counterpoise the external loads.

A progressive methodology is normally adopted considering the limit equilibrium method (LEM) and beam theory, to compute stresses, before considering linear or nonlinear numerical analysis (Leclerc *et al.* 2003). The LEM is an analytical method that, considering any translational or rotational movement of rigid bodies, verifies the equilibrium of the structure. It is based on the computation of the total net force and its application point along any failure surface. Although considering the beam theory to compute stresses, this method does not take into account the relative deformability between the dam and the foundation, which may be an unsafe simplification (Bretas 2012).

In the LEM, the stability is represented by a safety (or stability) factor, having two interpretations (Chen 2015): i) the ultimate load to bring the structure to the limit of equilibrium, denoted as "over-load factor", suitable for overturning failure modes, and ii) the ratio between the ultimate strength and the mobilized strength, denoted as "strength reduction factor", suitable for sliding failure modes.

3.3.3.4 Shear strength modeling

The potential sliding surfaces are formed by two rough walls partially in contact (rock discontinuities) and partially bonded (concrete lift joints and concrete-rock interface) subjected to normal and shear stresses.

Their shear behavior usually experiences two stages: i) the pre-peak phase, when an increasing of the shear stress is followed by small shear deformation, and ii) the post-peak phase, characterized by a sharp softening toward a residual strength, after the asperities have been climbed (Figure 3.8a), due to a dilatancy phenomenon, or crushed (Figure 3.8b).

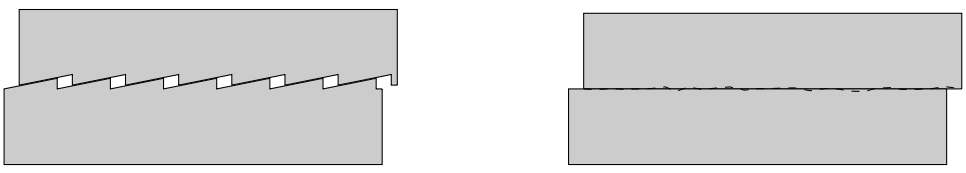

(a) Dilatancy mechanism (b) Crushing mechanism

Figure 3.8: Peak shear strength mobilization.

In reality, there is a coupled behavior, since the two mechanisms are not separated.

The dilatancy mechanism results in a decrease of the contact area and, consequently, in an increase of the stress in the contacts which eventually leads to punctual crushing. Therefore, the prominence of each mechanism depends on the normal load and local geometry (Plesha 1987). Figure 3.9 shows the non-linear transition between the two mechanisms.

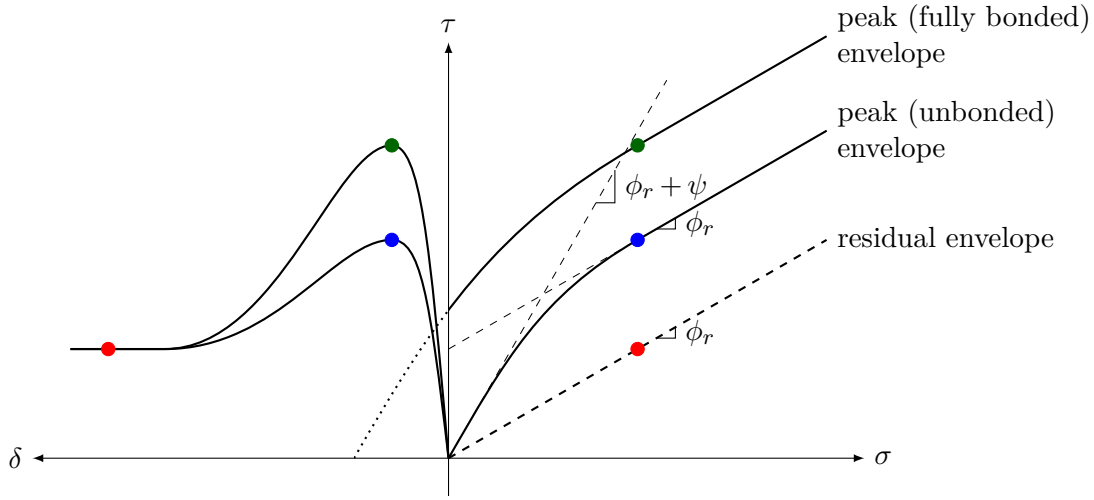

Figure 3.9: Typical shear behavior and failure envelope for interfaces.

In the range of low normal stresses beneath concrete dams (Westberg 2010), the failure envelope is remarkably non-linear. However, due to its simplicity, Mohr-Coulomb criterion is usually considered in stability analysis (Nicholson 1983) to model the shear strength. This criterion is formulated, for the peak strength, with increased friction angle (dilatancy) or the inclusion of a cohesive-like parameter (crushing), given, respectively, by,

$$\tau = \sigma \cdot \tan\left(\phi_b + \psi\right) \tag{3.2}$$

$$\tau = c_a + \sigma \cdot \tan\left(\phi_b\right) \tag{3.3}$$

where τ is the shear strength, σ is the normal stress, ϕ_r is the residual friction angle, ψ is the dilatancy angle (Patton 1966) and c_a is the apparent cohesion.

Furthermore, for concrete-rock interfaces and lift joints, the shear strength is also increased by the bond strength due to the binding properties of the concrete, resulting in extra tensile and cohesive strength. Since tests showed that these interfaces are partially bonded (Lo *et al.* 1991), the shear behavior is somewhere between the two extreme situations (fully bonded or unbonded), depending on the bonded area (Krounis *et al.* 2016).

For the residual strength, the Mohr-Coulomb criterion is given exclusively by the

friction component,

$$\tau = \sigma \cdot \tan(\phi_b) \tag{3.4}$$

3.4 Loads

3.4.1 General considerations

Loads acting on concrete dams can be distinguished between: i) static or dynamic loads, depending on whether the inertial effects are negligible or not, ii) direct or indirect loads, depending on whether resulting in surface and mass forces or in imposed displacements; iii) permanent, variable or accidental loads, depending on its probability of occurrence and variability; or iv) construction, reservoir filling or operation loads, depending on when they are applied.

For stability analysis, as the installed stress field is not conditioning, the loads considered in the design are: i) dead loads, ii) water loads, iii) ice loads, iv) silt loads and v) seismic loads. Thermal loads, as described below, do not influence the stability of gravity dams.

Figure 3.10 illustrates those loads.

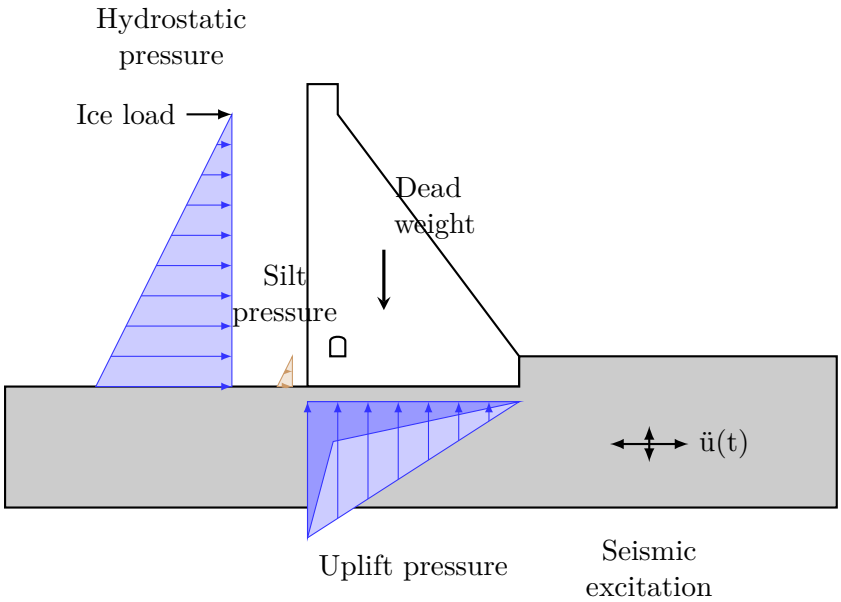

Figure 3.10: Loads for stability analysis of concrete gravity dams.

In the following sections the loads acting on concrete dams are detailed.

3.4.2 Dead loads

During dam construction, concrete placement introduces vertical mass forces in the structure, which can be approximately considered as a quasi-static loading. The resulted dead weight W, applied at the center of mass, is given by,

$$W = \rho_c \cdot g \cdot V = \gamma_c \cdot V \tag{3.5}$$

where ρ_c is the concrete density, g is the gravity acceleration, γ_c is the concrete unit (or specific) weight and V is the volume erected.

3.4.3 Water loads

3.4.3.1 General considerations

Water action on porous media originates both boundary forces and forces corresponding to the hydraulic gradient installed, from upstream to downstream, due to water seepage, inducing, in immersed zones of the dam and the rock mass foundation: i) hydrostatic pressures on the surfaces; and ii) water-seeping (or uplift) pressures in porous and discontinuous media.

Since the dam-foundation system may be assumed as impermeable with the exception of low permeability discontinuities through which water flows, the water loads usually considered in stability analysis are the hydrostatic pressures acting on dam faces and the uplift pressures acting in lift joints or opened cracks of the dam body, in the concrete-rock interface and in rock mass fractures.

3.4.3.2 Hydrostatic pressure

Water at rest exerts perpendicular hydrostatic pressure on the upstream and downstream dam faces, varying linearly with depth, as,

$$p_w(z) = \gamma_w \cdot z \tag{3.6}$$

where p_w is the hydrostatic pressure, γ_w is the water unit (or specific) weight and z is the depth from the free-surface.

The total hydrostatic force exerted in a horizontal layer, located at $z = y$, is given by its integration over y, i.e.,

$$I_w(y) = \int_0^y p_w(z)\, dz = \frac{1}{2} \cdot \gamma_w \cdot y^2 \tag{3.7}$$

applied at,

$$y_{I_w}(y) = \frac{1}{I_w(y)} \cdot \int_0^y z \cdot p_w(z)\, dz = \frac{2}{3} \cdot y \tag{3.8}$$

where $I_w(y)$ is the total hydrostatic force exerted on a horizontal layer located at $z = y$ and $y_{I_w}(y)$ is the corresponding application point.

3.4.3.3 Uplift pressure

After the dam construction, the reservoir filling install a hydraulic gradient, from upstream to downstream, causing the water seepage, under pressure, through the dam body and the rock mass foundation.

Water flows, preferentially, through discontinuities such as lift joints or cracks on the dam body, the dam-foundation interface and the rock mass foundation fractures. Therefore, the hydromechanical behavior of the dam-foundation set is only properly simulated by discontinuous models. Although the availability of numerical approaches, with increasing degree of complexity (Ruggeri 2004b), their use is limited as it is difficult to have a detailed knowledge of such discontinuities, specially those located at the rock mass foundation since in situ measurements can only be carried out at a limited number of points (Grenoble *et al.* 1995), and of their behavior under different loading conditions (Ruggeri 2004b).

Alternatively, equivalent continuum models, considering the dam body and foundation as porous media, are commonly used and can be particularly accurate for densely and evenly-spaced fractured rock mass foundation. Analytical solutions (Weaver 1932) for determining pressures in porous media were deduced by solving the Laplace's equation obtained from the Darcy's law (Darcy 1856) which admits a laminar flow, such as can be adequately considered for the foundation of concrete dams (Wittke 1990). The obtained pressure distribution, at the dam base, is approximately linear (Figure 3.11a) such as proposed by Lévy (1895), based on stability principles.

The effects of the construction of a perfect waterproofing curtain (Figure 3.11b), reaching different depths, were also studied (Weaver 1932), at a time when this practice was

believed to be sufficient to reduce or even eliminate uplift pressures.

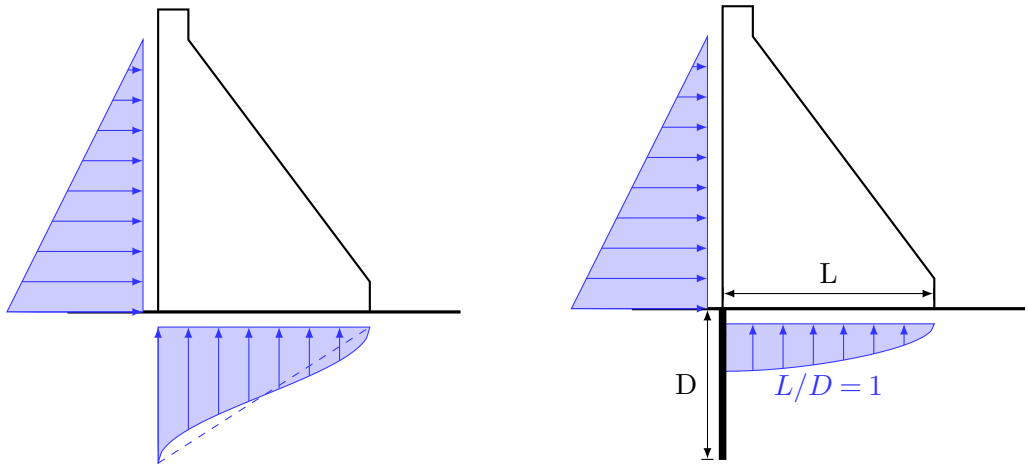

(a) Without waterproofing curtain (b) With a perfect waterproofing curtain

Figure 3.11: Hydraulic potential at the base of an impermeable dam founded on a porous foundation (Weaver 1932).

However, Casagrande (1961), after the analysis of the observed pressures in the foundation of the Hiawassee dam (USA), questioned the efficiency of the waterproof curtain, composed by a single row of grout holes, in reducing the uplift pressures. Based on reliable piezometric observations made at both sides of a single line of grout holes, Casagrande (1961) concluded that its efficiency was rarely greater than 30%, following the expression proposed by Dachler (1936) for the theoretical efficiency of imperfect cut-offs. Such efficiency could be attained, instead, with the construction of a line of drains located at one third of the distance between the dam heel and the dam toe, according to Brahtz (1936) who studied the theoretical uplift pressure reduction by a line of drains.

Furthermore, starting from a idealized model of a two-dimensional flow considering an impermeable dam founded on a finite, homogeneous, porous and isotropic media, with two vertical cracks at the dam heel and the dam toe, Casagrande (1961) approximate the solution of the piezometric surface, considering a horizontal laminar flow, given the existence of a vertical drainage system that reaches the impermeable zone.

Considering this theoretical model and the mentioned assumptions regarding the foundation properties, full reduction of the uplift pressures would be achieved by constructing a continuous trench. In practice, the drainage system, composed by a set of evenly-spaced boreholes, can only reduce partially the uplift pressures, originating the definition of an efficiency-related factor.

According to the Casagrande's solution, the efficiency of the drainage system is given

by the ratio between the average hydraulic head at the drainage line and the hydraulic gradient ($H_r - H_t$ or $H_r - H_g$ if the gallery is above the tailwater level) installed. Still used nowadays to design the drainage system (Mascarenhas 2005), this solution relates the drainage efficiency to the geometric characteristics of the drainage system (location, radius and spacing).

Depending on the regulatory specifications which define the required pressure reduction, the drains (Wyllie 1999) usually: i) have 0.076 mm of diameter; ii) are 1.5 to 5 m apart; iii) are preferably located at 10% of the dam base; and iv) reach a depth of 50%, at most, of the reservoir water head.

In the design phase, when no site information on the uplift pressure is available, a bi-linear pressure distribution (Figure 3.12a) is usually considered, to account for the pressure reduction by a drainage system drilled from the gallery, i.e.,

$$p_u(x) = \gamma_w \cdot \begin{cases} H_r - (H_r - H_d) \cdot \frac{x}{L_d} & , \text{ if } x \leq L_d \\ H_d - \Big(H_d - \max\{H_t, H_g\}\Big) \cdot \frac{x - L_d}{L - L_d} & , \text{ if } x > L_d \end{cases} \tag{3.9}$$

where H_r is the reservoir head, H_t is the tailwater head, H_g is the gallery level, L_d is the drainage system location, from the dam heel, and L is the dam base length. The average hydraulic head at the drainage line H_d is given by,

$$H_d = k_u \cdot \frac{L - L_d}{L} \cdot \Big(H_r - \max\{H_t, H_g\}\Big) \tag{3.10}$$

where k_u is an uplift factor, inversely proportional to the drainage effectiveness.

If there is no drainage system installed, or it become inoperative, linear pressure distribution (Figure 3.12b) with no uplift reduction is considered, i.e.,

$$p_u(x) = \gamma_w \cdot \left[H_r - (H_r - H_t) \cdot \frac{x}{L}\right] \tag{3.11}$$

The propagation of a crack from the upstream face may compromise the efficiency of the drainage system. The total reservoir pressure is considered along a crack, which can still be reduced if the crack length L_c is smaller than the drainage system location L_d, otherwise no drainage reduction is considered. For $L_c < L_d$, the uplift pressures (Figure

3.12c) are then given by,

$$p_u(x) = \gamma_w \cdot \begin{cases} H_r & , \text{ if } x \leq L_c \\ H_r - (H_r - H_d) \cdot \frac{x - L_c}{L_d - L_c} & , \text{ if } L_c \leq x \leq L_d \\ H_d - \left(H_d - \max\{H_t, H_g\}\right) \cdot \frac{x - L_d}{L - L_d} & , \text{ if } x > L_d \end{cases} \tag{3.12}$$

For $L_c \geq L_d$, the uplift pressures (Figure 3.12d) are then given by,

$$p_u(x) = \gamma_w \cdot \begin{cases} H_r & , \text{ if } x \leq L_c \\ H_r - (H_r - H_t) \cdot \frac{x - L_c}{L - L_c} & , \text{ if } x > L_c \end{cases} \tag{3.13}$$

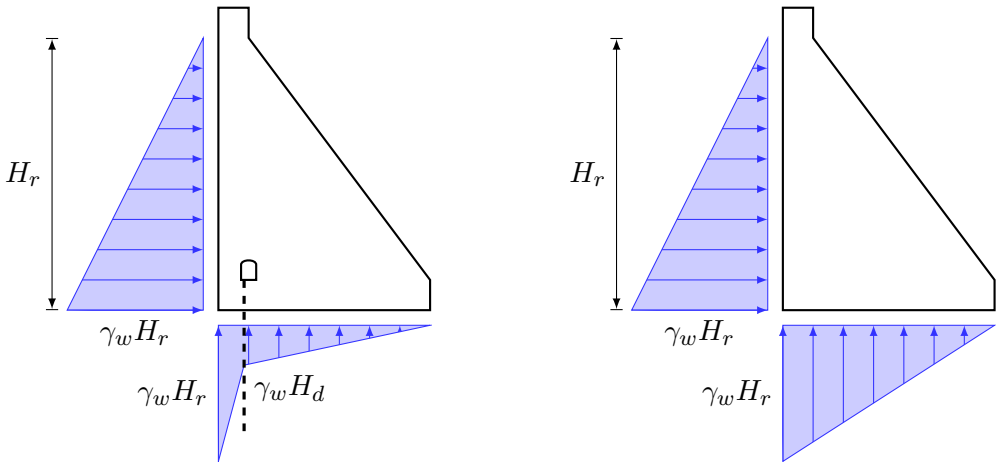

(a) With drainage system

(b) Without drainage system

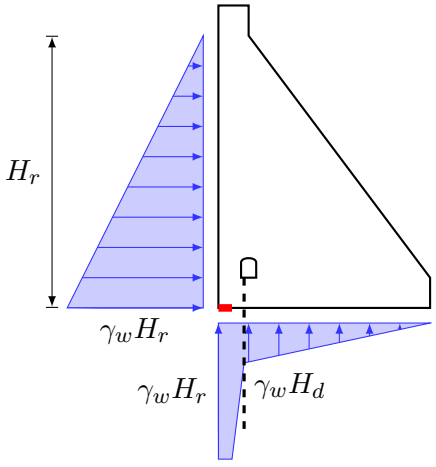

(c) With a crack propagated not beyond the drainage system

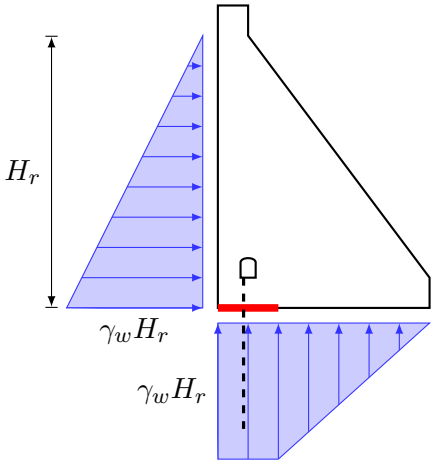

(d) With a crack propagated beyond the drainage system

Figure 3.12: Uplift pressure distribution considering in stability analysis.

The total uplift force exerted at the dam base, for instance, is given by its integration

over x, i.e.,

$$U = \int_0^L p_u(x)\, dx \tag{3.14}$$

applied at,

$$x_U = \frac{1}{U} \cdot \int_0^L x \cdot p_u(x)\, dx \tag{3.15}$$

3.4.4 Thermal loads

Concrete dams are under variable temperature conditions, resulting in expansion or shrinkage strains, which, due to restrained volume changes, causes both stresses and displacements. At a specific time, the thermal field of concrete dams are dependent on the fluctuations of the external temperature, structural and material properties and, as mentioned, the constructive techniques employed (Batista 1998).

As a spatial-time-dependent load, temperature development within concrete dams experiences three stages, as illustrated in Figure 3.13:

1. The exothermic stage, during concrete hardening when the highly exothermic chemical reaction between cement and water occurs, which induces an initial stress field into concrete dams whose consequences shall be minimized by adopting oriented constructive solutions and construction scheduling;

2. The transient stage, from the end of exothermic stage, when the concrete temperature is maximum, until reaching a steady-state thermal field, due to heat transfers with the environment;

3. The permanent stage, during normal operation conditions when the dam surfaces are exposed to seasonal temperature oscillations, which can be represented by overlapping harmonic functions with annual and daily periods (Teles 1985).

Thermal loads are usually not critical to the global safety of concrete gravity dams, since stability of rigid bodies are not influenced on the stress field installed because the resulting forces are self-balanced.

3.4.5 Ice loads

In cold regions, an ice layer formed near the reservoir free-surface exerts pressure on the upstream face of the dam, varying linearly over the ice thickness, due to (USBR 1976):

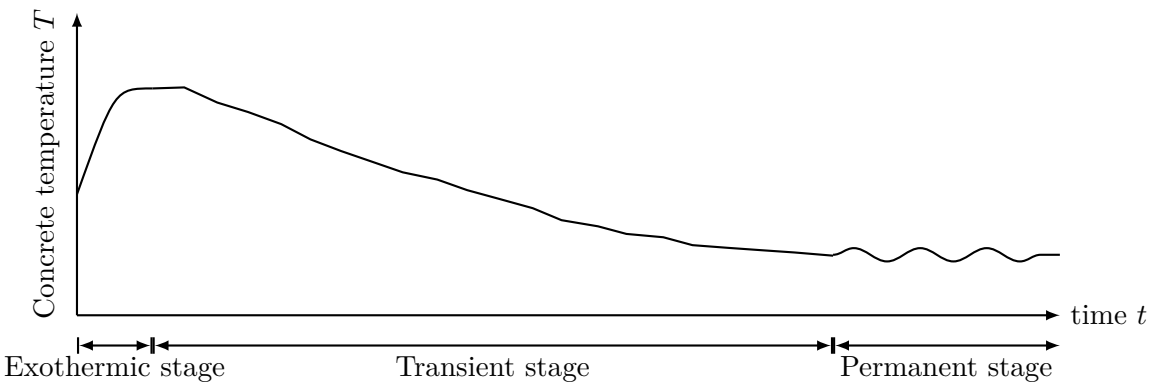

Figure 3.13: Temperature development process within concrete dams (adapted from Chen (2015)).

i) thermal expansion (static effect) of the ice layer, depending on the temperature rise, and its thickness, coefficient of expansion, elastic modulus and strength; and ii) wind drag (dynamic effect), depending on the size and shape of the exposed area, the roughness of the surface, and the direction and velocity of the wind.

Furthermore, freeze/thaw cycles of seepage water, due to restrained volume changes, play a significant role in degradation of concrete dams located in cold regions (Léger *et al.* 1995), which shall be considered in the prediction of their long-term behavior.

3.4.6 Silt loads

The water inflow drags fine materials which are deposited at the reservoir bed exerting perpendicular pressure against the dam upstream face.

The total silt force can be derived from the earth pressure at rest, such as,

$$I_s = \frac{1}{2} \cdot K_0 \cdot \gamma_s^{'} \cdot h_s^2 \tag{3.16}$$

where I_s is the total silt force, $\gamma_s^{'}$ is the silt (submerged) unit weight, h_s is the deposit height and K_0 is the coefficient of earth pressure at rest which, for a horizontal ground and cohesionless material, can be given by (Jaky 1948),

$$K_0 = 1 - \sin\phi_s \tag{3.17}$$

where ϕ_s is the internal friction angle of the silt deposit.

3.4.7 Seismic loads

3.4.7.1 General considerations

For complex structures, the earthquake effects on concrete dams can be accurately accessed using numerical models capable of simulating both the structure dynamic behavior and the seismic excitation, which implies the performance of nonlinear time-history analysis to achieve a realistic response of the reservoir-dam-foundation system (Bretas *et al.* 2014).

However, simpler methods, based on analytical seismic load models (Figure 3.14), are commonly used, mainly at the design phase, to evaluate the stability conditions of gravity profiles during seismic events, represented by response spectra.

The pseudo-static load model (Figure 3.14a) considers inertia forces, applied at the rigid body's centroid, as the product between mass and acceleration. This procedure disregards the amplification effect due to the high stiffness of the dam, as well as the dynamic nature of the load.

The pseudo-dynamic load model (Figure 3.14b) recognizes the dynamic amplification of the inertia forces along the dam height, using information from the earthquake design spectrum, even though the dynamic nature of the load is not considered since equivalent static loads are continuously applied.

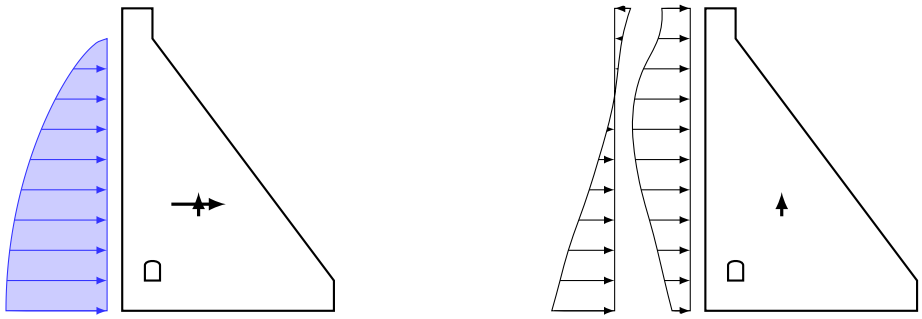

(a) Pseudo-static (b) Pseudo-dynamic

Figure 3.14: Analytical seismic load models.

In the following sections, the seismic action, as defined in the Eurocode 8 (EN1998 2004), and the corresponding specifications for Portugal are presented. Also, the pseudo-static and pseudo-dynamic seismic load models are detailed.

3.4.7.2 Seismic action defined according to the EN1998 (2004)

Regarding the structural design and safety evaluation, Eurocodes (EN1998 2004) uses response spectra for the representation of seismic actions. These are idealized curves that establish the minimum desired capacity (resistance) of structures according to the local seismology. Response spectra give the peak response (acceleration, velocity, displacement, etc) that a single degree-of-freedom oscillator must be designed to resist to, given its natural frequency or period.

Eurocode 8 (EN1998 2004) characterizes the (acceleration) elastic response spectrum S_e (Figure 3.15), according to,

$$S_e(T) = a_g \cdot S \cdot \begin{cases} 1 + T/T_B \cdot (\eta \cdot 2.5 - 1) & 0s \leq T \leq T_B \\ \eta \cdot 2.5 & T_B \leq T \leq T_C \\ \eta \cdot 2.5 \cdot T_C/T & T_C \leq T \leq T_D \\ \eta \cdot 2.5 \cdot \left(T_C \cdot T_D/T^2\right) & T_D \leq T \leq 4s \end{cases} \tag{3.18}$$

where T is the vibration period of a single degree-of-freedom linear system, S is the soil factor ($S = 1$ for type A or rock foundation), η is the damping correction coefficient ($\eta = 1$ for 5% viscous damping, usually considered for concrete structures), T_B, T_C and T_D are the limits of the period domain, characterizing the frequency content of the seismic action, defined by the national authorities.

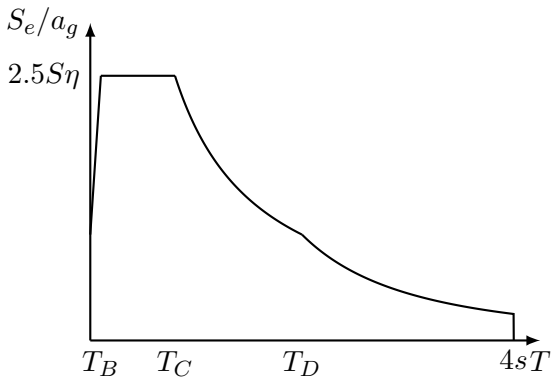

Figure 3.15: Elastic response spectrum according to the EN1998 (2004).

The design ground acceleration a_g, quantifying the intensity of the seismic action, are defined according to the local hazard, considering the subdivision of national territories into seismic zones, and the design return period, depending on the reliability requirements. It can be obtained, based on the reference peak ground acceleration a_{gr}, associated with

a return period of 475 years (corresponding to a probability of exceedance of 10% in 50 years, the service life considered for building structures), according to the following transformation function (EN1998 2004),

$$a_g\left(T_r\right) = a_{gr} \cdot \gamma_I\left(T_d\right) \tag{3.19}$$

where γ_I is the importance factor given by,

$$\gamma_I = \left(T_r/T_d\right)^{-1/k} \tag{3.20}$$

where $T_r = 475$ years is the reference return period and k is a seismicity-dependent parameter. The design return period T_d is related to the probability of exceedance p of a seismic action, during the service life t_L, by,

$$T_d = -\frac{t_L}{\ln\left(1-p\right)} \tag{3.21}$$

3.4.7.3 Seismic specifications for Portugal

The seismic specifications for the Portuguese territory can be found in the National appendix of the European Standards adopted (NP EN1998-1 2010).

Following the recommendation of the Eurocode 8 (EN1998 2004), for the Portuguese seismic characterization, two types of seismic action are distinguished: i) the seismic action type 1, modeling earthquakes with their epicenters located offshore; and ii) the seismic action type 2, referring to events with their epicenters located inland.

The parameters defining the elastic response spectra for each seismic action type are given in Table 3.2. The seismic zones for the mainland Portuguese territory are represented in Figure 3.16.

Table 3.2: Parameters that define the elastic response spectrum for rock foundations (NP EN1998-1 2010).

	Type 1	Type 2
T_B	0.10	0.10
T_C	0.60	0.25
T_D	2.00	2.00

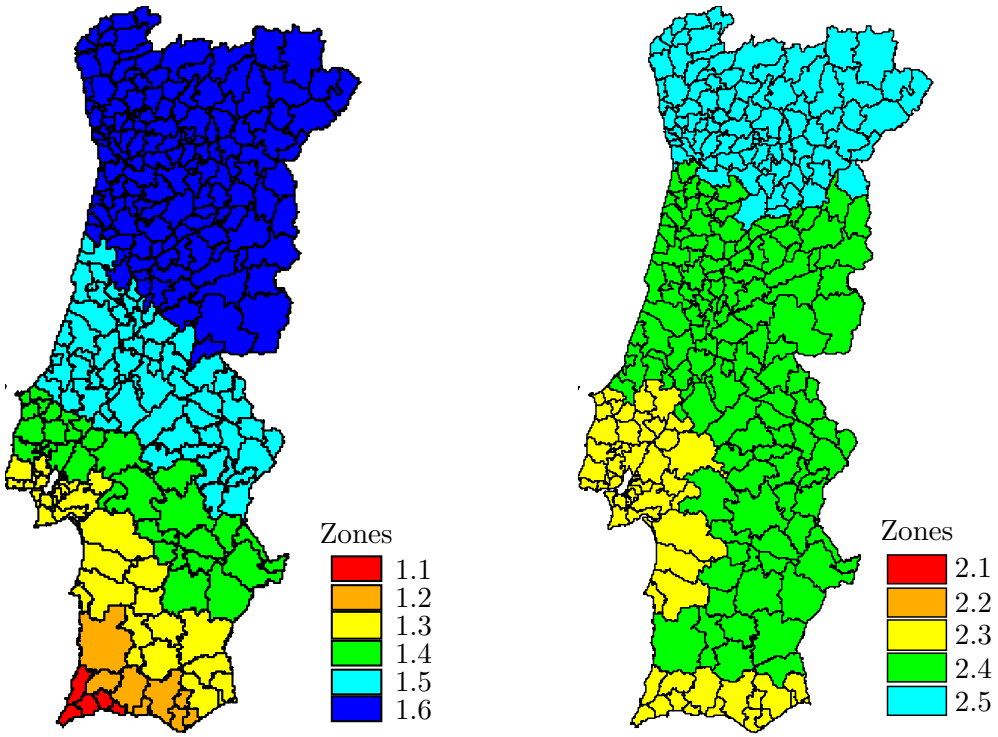

(a) Seismic type 1.

(b) Seismic type 2.

Figure 3.16: Seismic zones in mainland Portugal (NP EN1998-1 2010).

Table 3.3 shows the reference accelerations a_{gr}, established for the seismic zonation of the Portuguese territory. The design ground accelerations for other return periods can be obtained using the equation 3.19, considering $k = 1.5$ and $k = 2.5$ (NP EN1998-1 2010) for seismic actions type 1 and 2, respectively.

Table 3.3: Reference accelerations a_{gr} (m/s^2) for each seismic zone (NP EN1998-1 2010).

Zone	1	2	3	4	5	6
Type 1	2.50	2.00	1.50	1.00	0.60	0.35
Type 2	2.50	2.00	1.70	1.10	0.80	-

3.4.7.4 Pseudo-static load model

Equivalent static forces

The pseudo-static load model is a simplified load model that considers inertia forces as the product between mass and acceleration. Disregarding the amplification effect due to the flexibility of the dam, as well as the dynamic nature of the load, this approach assumes

a dam acceleration equals to the ground peak acceleration or, equivalently, a rigid body response.

This load model is particularly suitable for concrete gravity dams since, due to their high stiffness (then rigid-body formulation may not differ considerably from the real structural behavior), seismic actions generate mass-proportional inertia forces which play an important role in stability problems. Assuming that the structural response is due mainly to the fundamental vibration mode, in this procedure seismic equivalent static forces, F_s, are applied in the dam centroid according to the concept of seismic coefficient,

$$F_s = \alpha \cdot a_g \cdot V \cdot \rho_c \tag{3.22}$$

where α is the seismic coefficient, a_g is the seismic acceleration, V is the dam volume, ρ_c is the concrete density.

These inertia forces have a predominant horizontal component but also a vertical component which reduces the normal stress on sliding interfaces, when it is considered in the upper direction. Considering the combined effect of the horizontal and vertical components, the seismic coefficient α is very often taken as equal to 0.67 for the horizontal one and 0.20 for the vertical one (CFBR 2012) for the computation of the equivalent static forces.

Hydrodynamic pressure

The water-dam interaction has also significant influence on dam behavior during the earthquake. As opposite to the pseudo-dynamic load model which directly includes the effects of impounded water, the pseudo-static load model only deals with inertia forces, i.e. structural response to a seismic action. Therefore, in this approach, water-dam interaction must be considered through additional water pressure acting on the upstream dam face.

For that purpose, the theory of water pressure during earthquakes were presented by Westergaard (1933), and later corroborated using physical scaled models (Zangar 1952), considering the following assumptions: i) water incompressibility; ii) free water surface is at rest; iii) the reservoir is infinitely long; iv) the motion is horizontal; v) vertical upstream dam face; and vi) rigid dam.

The solution of this problem is expressed, for an arbitrary acceleration, a_g, in the form

of infinite Fourier series, i.e.,

$$p_{ws}(y) = a_g \cdot 8 \cdot H_r \cdot \sum_{i=1}^{\infty} \frac{(-1)^{i+1}}{[(2 \cdot i - 1) \cdot \pi]^2} \cdot \cos\left[\frac{(2 \cdot i - 1) \cdot y}{4 \cdot H_r}\right] \tag{3.23}$$

where p_{ws} is the water pressure and y is the vertical position ($y = 0$ defines the bottom of the reservoir, $y = H_r$ defines the water free surface).

The total force due to hydrodynamic pressure is given by the integration of this pressure over the height of the reservoir, i.e.,

$$I_{ws} = \int_0^{H_r} p_{ws}(y)\, dy \tag{3.24}$$

applied at,

$$y_{I_{ws}} = \frac{1}{I_{ws}} \cdot \int_0^{H_r} p_{ws}(y) \cdot y\, dy \tag{3.25}$$

3.4.7.5 Pseudo-dynamic load model

Chopra (1978) proposed a procedure for the elastic analysis for design and safety evaluation of concrete gravity dams, called pseudo-dynamic load model. This simplified analysis considers the contribution of the fundamental vibration mode, directly from the earthquake design spectrum, based on the response history analysis of finite-element idealizations of the dam monolith. Later, Fenves and Chopra (1986) extended this procedure to account for the effects of water-dam-foundation interactions and contributions of higher vibration modes through the "static correction" concept.

Contrary to the pseudo-static model, the pseudo-dynamic model recognizes the dynamic amplification of the inertia forces along the height of the dam, since the dam is no longer considered a rigid body, using information from the response spectrum. The dynamic amplification is considered only in the horizontal direction. For the vertical direction, equivalent static forces must still be considered. However, the non consideration of the oscillatory nature of the inertia forces is its main drawback, since the horizontal and vertical loads are continuously applied. Other disadvantage comes from the fact that this is an elastic response based model, and therefore it may not be suitable for seismic analysis in failure (non-elastic) conditions.

A detailed description of the pseudo-dynamic load model is presented in appendix A.

Considering only the fundamental vibration mode of the dam, the maximum effects of

the horizontal earthquake ground motion, including the effects of the impounded water, can be represented by equivalent lateral forces, f_1, acting on the dam, given by (Fenves and Chopra 1986),

$$f_1(y) = \frac{\tilde{L}_1}{\tilde{M}_1} \cdot \frac{S_a\left(\tilde{T}_1, \tilde{\xi}_1\right)}{g} \cdot \left[w(y) \cdot \phi(y) + g \cdot p\left(y, \tilde{T}_r\right)\right] \tag{3.26}$$

where $\tilde{M}_1$ and $\tilde{L}_1$ are the generalized mass and earthquake force coefficients given in equations A.7 and A.8, respectively, $S_a\left(\tilde{T}_1, \tilde{\xi}_1\right)$ is the pseudo-acceleration ordinate of the design spectrum evaluated at the vibration period $\tilde{T}_1$, which includes the influence of impounded water, and damping ratio $\tilde{\xi}_1$, given in equations A.4 and A.5, respectively, $w(y)$ is the weight of the dam per unit height, $\phi(y)$ is the horizontal component of the displacement in the fundamental vibration mode, obtained in Table A.4, and $p\left(y, \tilde{T}_r\right)$ is a function, obtained in Table A.5, representing the hydrodynamic pressure on the upstream face due to a harmonic acceleration of period $\tilde{T}_r$ which is the fundamental vibration period of the dam including the influence of the impounded water, given in equation A.2.

For higher vibration modes, with even smaller vibration periods, dam responds essentially as a rigid body with little dynamic amplification, leading to the "static correction" concept. The equivalent lateral earthquake forces, f_{sc}, associated with the higher vibration modes of dams, including the effects of the impounded water, are given by (Fenves and Chopra 1986),

$$f_{sc}(y) = \frac{a_g}{g} \cdot \left\{ w(y) \cdot \left[1 - \frac{L_1}{M_1} \cdot \phi(y)\right] + \left[g \cdot p_0(y) - \frac{B_1}{M_1} \cdot w(y) \cdot \phi(y)\right] \right\} \tag{3.27}$$

where $p_0(y)$ is a real-valued frequency-independent function, obtained in Table A.6, describing the hydrodynamic pressure on a rigid dam undergoing unit acceleration, with water compressibility neglected, both assumptions being consistent with the "static correction" concept, and B_1 provides a measure of the portion of $p_0(y)$ that acts in the fundamental vibration mode, given equation A.20.

Since the maximum effects of earthquake ground motion for the fundamental and higher vibration modes do not occur at the same time, Fenves and Chopra (1986) suggest their combination according to the square-root-of-the-sum-of-squares (SRSS) modal combination

rule. Therefore, the total force of the seismic pseudo-dynamic loads is obtained by,

$$F_s = \int_0^H \sqrt{f_1^2(y) + f_{sc}^2(y)}\, dy \tag{3.28}$$

applied at,

$$y_{F_s} = \frac{1}{F_s} \cdot \int_0^H y \cdot \sqrt{f_1^2(y) + f_{sc}^2(y)}\, dy \tag{3.29}$$

3.5 Design codes

3.5.1 General considerations

In spite of the general guidance provided by ICOLD, the design strategy, strongly influenced by local technical/scientific experience, vary considerably from country to country.

According to ICOLD orientations, to attain a satisfactory design, the structural solution should, together with the foundation and environment (ICOLD 1988):

- perform satisfactorily its function, without appreciable deterioration (limited permanent displacements and surface cracking and small changes in seepage), during the conditions expected normally to occur in the service life;
- not fail catastrophically during the most unlikely but possible conditions which may be imposed.

The major difficulty in formulating the design strategy lies in the definition of the conditions "expected normally to occur" and "unlikely but possible". While the interpretation of these terms is made by national authorities, based on the selection of load combinations according to their probability of simultaneous occurrence, ICOLD suggests the formulation of related design scenarios (ICOLD 1988), namely:

- Utilization scenarios, encompassing the credible combination of load conditions or events for which the selected design criteria will ensure the continuous satisfactory performance of the dam;
- Hazard scenarios, encompassing events resulting from combinations of load conditions or events which represent the limit of credibility and for which the selected design criteria will eliminate the risk of catastrophic damage.

In this formulation, an intrinsic distinction from the limit state philosophy is made, since, due to uncertainties, the fulfillment of performance requirements cannot be qualitatively measured and risks cannot be completely eliminated, such as mentioned in Chapter 2.

Although recognizing that the objective of specifying safety criteria based on partial safety factors could be accomplished, ICOLD (1988) refrained from following that design philosophy since: (i) much further study and discussion is needed to establish generally accepted values; and (ii) many parameters (such as those describing the constitutive properties of materials for instance) are not generally agreed upon and alternative specifications can often be used.

Therefore, in the Portuguese dam safety regulation (RSB 2018), as well as most other international guidelines (Ruggeri 2004a; ICOLD 2017), structural safety of concrete dams is still analyzed based on global safety factors, since it is supposed that the quantification of structural safety, in terms of probability, is difficult or even impossible.

However, in the last two decades, there has been a trend toward the adoption of the limit state philosophy and the probabilistic-based (China, France and Italy) or even risk-based (Spain) approaches to design of concrete dams. In China, standards for the reliability-based design of hydraulic structures (GB50199 1994) are used. In France, in order to harmonize the diversified practice regarding stability analysis of concrete gravity dams (Peyras *et al.* 2008), the guidelines for the justification of the stability of gravity dams (CFBR 2012) were published, considering a semi-probabilistic approach.

In these standards, the Eurocodes (EN1990 2002) formulation is followed: (i) design situations are classified according to its duration; (ii) combination of loads are grouped such that the sets of partial safety factors can be applied throughout the structure class; (iii) characteristic (strength properties and permanent loads) and representative (variable loads) values are related to the design situations; and (iv) limit state conditions and explicit safety criteria, based on the semi-probabilistic approach, are defined.

In the following sections, these subjects are addressed, comparing, when possible, the distinct interpretation of different national authorities.

3.5.2 Design situations

Design situations are sets of physical conditions representing the real phenomena occurring during a certain time interval. Design codes differentiate design situations according to its

frequency of occurrence. The design situations usually found in concrete dam design codes that follow the Eurocode terminology (GB50199 1994; CFBR 2012) are, generally:

- Permanent situations, corresponding to long duration conditions, usually same as the design service life;
- Temporary (or transient) situations, corresponding to construction or other temporary operating conditions that do not last long although are very likely to occur;
- Rare situations, corresponding to fairly likely conditions although not as likely as permanent situations;
- Exceptional situations, corresponding to fairly unlikely conditions;
- Accidental or extreme situations, corresponding to extreme and very unlikely conditions with serious consequences.

In other regulations, following the orientation of ICOLD, design scenarios are referred. As mentioned, these are divided into: (i) utilization, and (ii) hazard scenarios.

3.5.3 Load combinations

3.5.3.1 General considerations

Load combinations are derived in accordance with the differentiation of design situations.

The Chinese standards (GB50199 1994) distinguish the load combinations related to collapse limit states (basic or accident) from those related to serviceability limit states (short-term and long-term). The French guidelines (CFBR 2012) group load combinations in three categories: i) quasi-permanent, ii) rare, and iii) extreme combinations.

In most other regulations (Ruggeri 2004a), including the American standards (USBR 1976; USACE 1995; FERC 2002), distinction is made between three levels of load combinations, safeguarding that other cases may be considered if justified: i) usual, ii) non-usual, and iii) extreme combinations.

In Portugal (RSB 2018), reference is made to usual and extreme load combinations, derived, respectively, from:

1. Utilization scenarios, such as:

- during the construction, due to the construction process and the exothermic stage of temperature development;
- during the first filling, due to the static and thermal loads induced during the reservoir filling process;
- during the operation period, due the static (water, ice and silt), thermal and dynamic loads (operational basis earthquake - OBE).

2. Hazard scenarios, such as:

- during the design flood with high return period;
- during the maximum design earthquake (MDE).

In the following sections, the hazard scenarios are detailed, considering the terminology used in the French guidelines (CFBR 2012): i) extreme hydrostatic combination, and ii) accidental earthquake combination, respectively.

3.5.3.2 Extreme hydrostatic combination

The definition of the design flood is based on the inflow hydrograph, obtained through probabilistic methods considering the hydrologic properties of the region and the reservoir water volume-height curves, depending on the construction purpose and the outlet works.

The return periods for the computation of the design flood are defined according to the structure class (Table 3.1), such as shown in Table 3.4.

Table 3.4: Minimum return periods for the design flood (RSB 2018).

Height (m)	Return period (years)
$H \geq 100$	5000
$100 > H \geq 50$	2000
$50 > H \geq 15$	1000
$H < 15$	500

A dry freeboard (vertical distance between the FWL and the dam crest) of, at least, one meter is usually adopted.

3.5.3.3 Accidental earthquake combination

The definition of the maximum design earthquake (MDE), linked to the maximum credible earthquake (MCE), is based on engineer judgment since, in the current state of knowledge,

it is not possible to affirm decisively if deterministic or probabilistic approach should be used (ICOLD 1989).

In the deterministic definition of the MCE, its return period is meaningless since its occurrence depends on the geological environmental considered (ICOLD 1989). However, this is only possible through extended seismologic studies of the region, often complex and uncertain. In the design standards, ground motions associated with specific return periods are commonly adopted, although, for important structures, a deterministic quantification of the MCE may be considered.

The Eurocodes (EN1998 2004) define the design earthquake as the one that has a probability of exceedance of 10% during the structure service life. If considered for dam design, according to equation 3.21, this would result in a return period of 1000 years, since service life is often set at 100 years.

However, the Portuguese dam safety regulation (RSB 2018), recommends the quantification of the return period for the MDE as a function of a global seismic risk index i_R, given by,

$$i_R = i_1 + i_2 + i_3 \tag{3.30}$$

where i_1, i_2 and i_3 are partial indexes related to the reservoir capacity, the dam height and the potential risks, respectively. Their values are given in Table 3.5.

Table 3.5: Partial indexes for the computation of the global seismic risk index (RSB 2018).

Reservoir capacity		Dam height		Potential risks	
V (hm^3)	i_1	H (m)	i_2	Y	i_3
$V \geq 120$	6	$H \geq 50$	6	$Y \geq 400$ (class I)	32
$120 > V \geq 1$	4	$50 > H \geq 30$	4	$400 > Y \geq 10$ (class I)	28
$1 > V \geq 0.1$	2	$30 > H \geq 15$	2	$10 > Y \geq 1$ (class II)	16
$V < 0.1$	0	$H < 15$	0	$Y = 0$ (class II)	12
				$Y = 0$ (class III)	4

The return periods for the MDE are shown in Table 3.6.

3.5.4 Limit states

Limit states are states beyond which structures attained undesirable conditions. The distinction between ultimate and serviceability limit states are generally sufficient to attain the reliability requirements regarding the structural safety and functioning, respectively.

Table 3.6: Return periods for the quantification of the maximum design earthquake (RSB 2018).

i_R	Return period (years)
4 - 10	1000
12 - 20	2500
22 - 30	5000
32 - 44	10000/MCE

The French guidelines (CFBR 2012) and the Chinese standards (GB50199 1994) define: i) ultimate (or collapse) limit states, as those associated with loss of equilibrium or excessive stress, and ii) service limit states, as those related to the maintenance of regular operation conditions, such as the structural integrity (no-cracking requirement), drainage efficiency, discharge capacity, surveillance functionality, etc.

Similarly, the Portuguese dam safety regulation (RSB 2018), recommend that the structure shall: i) for hazard scenarios, not fail (loss of equilibrium or overstressing), considering residual material strengths; and ii) for utilization scenarios, have an elastic response, considering the drainage efficiency and peak material strengths.

3.5.5 Safety criteria

3.5.5.1 Chinese standards (GB50199 1994)

The Chinese standards (GB50199 1994) adopt safety criteria similar to the Eurocodes, given by,

$$\gamma_0 \cdot \psi \cdot S\left(\gamma_G \cdot G_k, \gamma_Q \cdot Q_k, a_k\right) \leq \frac{1}{\gamma_d} \cdot R\left(\frac{f_k}{\gamma_m}, a_k\right) \tag{3.31}$$

where S is the load effect function, R is the resistance function, γ_0 is the structure importance factor (1.1, 1.0, 0.9 for class I, II and III, respectively), ψ is the design situation factor (1.0, 0.95, 0.85 for permanent, temporary and accidental situations, respectively), γ_G and G_k are the partial safety factor and characteristic value, respectively, for permanent loads, γ_Q and Q_k are the partial safety factor and characteristic value, respectively, for variable loads, a_k is the characteristic value of geometric parameters, γ_m is the partial safety factor for material properties, and γ_d is the structural coefficient for collapse limit states.

Tables 3.7 and 3.8 shows the partial safety factors and structural coefficients for collapse

limit states, respectively.

Table 3.7: Partial safety factors (γ_G, γ_Q and γ_m) for collapse limit states (GB50199 1994).

Loads		
Self weight		1.0
Water loads	Hydrostatic pressure	1.0
	Uplift pressure	1.0
Silt pressure		1.2
Wave pressure		1.2
Material property		
Shear strength	Friction coefficient:	
	concrete-rock	1.3
	lift joints	1.3
	rock joints	1.4
	Cohesion:	
	concrete-rock	3.0
	lift joints	3.0
	rock joints	3.2
Concrete strength		1.5

Table 3.8: Structural coefficient (γ_d) for collapse limit states (GB50199 1994).

Failure mode	Combination	Structural coefficient
Sliding	Basic	1.2
	Accidental	1.2
Overstressing	Basic	1.8
	Accidental	1.8

3.5.5.2 French guidelines (CFBR 2012)

The French Guidelines (CFBR 2012) adopt a similar safety criteria. However, the partial safety factors are only applied to the material properties, such as,

$$\gamma_d \cdot S\left(G_k, Q_k, a_k\right) \leq R\left(\frac{f_k}{\gamma_m}, a_k\right) \tag{3.32}$$

where γ_d is the model coefficient depending on the load combination considered.

Tables 3.9 and 3.10 shows the partial safety factors and model coefficients for ultimate limit states, respectively.

Table 3.9: Partial safety factors (γ_m) for ultimate limit states (CFBR 2012).

	Quasi-permanent combination	Rare combination	Extreme combination
Friction coefficient:			
concrete-rock	1.5	1.2	1.0
lift joints	1.5	1.2	1.0
rock joints	1.5	1.2	1.0
Cohesion:			
concrete-rock	3.0	2.0	1.0
lift joints	3.0	2.0	1.0
rock joints	3.0	2.0	1.0
Concrete tensile strength:			
dam body	3.0	3.0	1.0
dam-foundation	3.0	3.0	1.0
Concrete compressive strength:			
dam body	3.0	2.0	1.0
dam-foundation	3.0	2.0	1.0

Table 3.10: Model coefficient (γ_d) for ultimate limit states (CFBR 2012).

Combination	Model coefficient
Quasi-permanent	1.0
Rare	1.0
Extreme	1.0

3.5.5.3 Portuguese dam safety regulation (RSB 2018)

The Portuguese dam safety regulation (RSB 2018) considers safety criteria derived from the allowable stress design philosophy, using strength reduction factors.

Regarding the loss of equilibrium, since the overturning mechanism does not depend on material strength properties, the strength reduction factors recommended refer to the sliding mechanism. The consideration of the Mohr-Coulomb failure criteria and peak shear

strengths (with cohesion), for utilization scenarios, and residual shear strengths (with no cohesion), for hazard scenarios, is recommended.

These recommendations can be translated into the following criteria,

$$\tau \leq \frac{c}{\lambda_c} + \frac{\sigma \cdot \tan(\phi)}{\lambda_{\tan(\phi)}} \tag{3.33}$$

where λ_c and $\lambda_{\tan(\phi)}$ are the strength reduction factors for the cohesion and friction coefficient, respectively.

Table 3.11 shows the strength reduction factors recommended.

Table 3.11: Strength reduction factors (λ_c and $\lambda_{\tan(\phi)}$) for the sliding mechanism (RSB 2018).

	Utilization scenarios	Hazard scenarios
Cohesion λ_c	3.0 - 5.0	-
Friction coefficient $\lambda_{\tan(\phi)}$	1.5 - 2.0	1.2 - 1.5

3.5.5.4 Other regulatory institutions

Although the regulatory framework have been changing in most countries since then (ICOLD 2017), Ruggeri (2004a) compile the regulatory rules, guidelines and common practice adopted in different countries for the safety assessment against sliding.

Such as in the Portuguese dam safety regulation (RSB 2018), strength reduction factors, applied separately to friction coefficient and cohesion, are considered in some cases (Table 3.12).

Table 3.12: Strength reduction factors λ in other countries (Ruggeri 2004a).

	Friction coefficient $\lambda_{\tan(\phi)}$	Cohesion λ_c
Spain	1.5	5
Switzerland	1.5	5
India	1.5	3.6 - 4.5

In other cases, reference is made to single global safety factors, given by the ratio between the total shear strength and sliding forces, i.e.,

$$\lambda = \frac{c + \sigma \cdot \tan(\phi)}{\tau} \tag{3.34}$$

where λ is the global safety factor.

Table 3.13 present the global safety factors, recommended in several countries/institutions, for the sliding stability along the dam-foundation interface (in some countries, different safety factors are recommended for other surfaces).

Table 3.13: Global safety factors λ in other countries (partially from Ruggeri (2004a)).

	Usual load combinations	Unusual load combinations	Extreme load combinations
Germany	1.2 - 1.5	1.2 - 1.3	1.2
Austria	1.5	1.2 - 1.35	1.1
Norway	1.5[a] 3[b] 2[c]	1.1[a] 2[b] 1.5[c]	1.1[a] 2[b] 1.5[c]
Canada	1.5[a] 3.0[b]	1.3[a] 2.0[b]	1.0[a] 1.3[b]
United Kingdom	3.0	2.0	1.0
USBR (1976)	3.0	2.0	1.0
FERC (2002)	2.0[d] 3.0[e]	1.25[d] 2.0[e]	1.0[d] 1.3[e]
USACE (1995)	2.0	1.7	1.3

[a] Residual strength (no cohesion).
[b] Peak strength (with no tests).
[c] Peak strength (with tests).
[d] Dams with low hazard potential.
[e] Dams with significant or high hazard potential.

3.6 Failure mode modeling

3.6.1 General considerations

In this work, intending to study the structural safety of concrete gravity dams regarding their global stability, the failure modes relating to pre-collapse equilibrium shall be identified. Since the performance of numerous reliability analyses will be required, the simpler rigid body formulation is followed.

The stress analysis at the dam base is not performed since the cohesion component of shear strength, only mobilized at the compressive zone, is not considering in failure situations (RSB 2018), corresponding to a limit analysis (Underwood and Dixon 1976).

Also the effects on the uplift distribution of an opened crack, in the dam base, are not considered.

Thus, the limit stability conditions for the typical unkeyed cross-sectional profile (Figure 3.17), for sliding and overturning, are, respectively, given by,

$$(\Sigma N) \cdot \tan(\phi_c) = \Sigma S \tag{3.35}$$

$$\Sigma M_{sta} = \Sigma M_{ins} \tag{3.36}$$

where ΣN and ΣS are the normal and shear net forces, respectively, and ΣM_{sta} and ΣM_{ins} are the stabilizing and instabilizing moments, respectively.

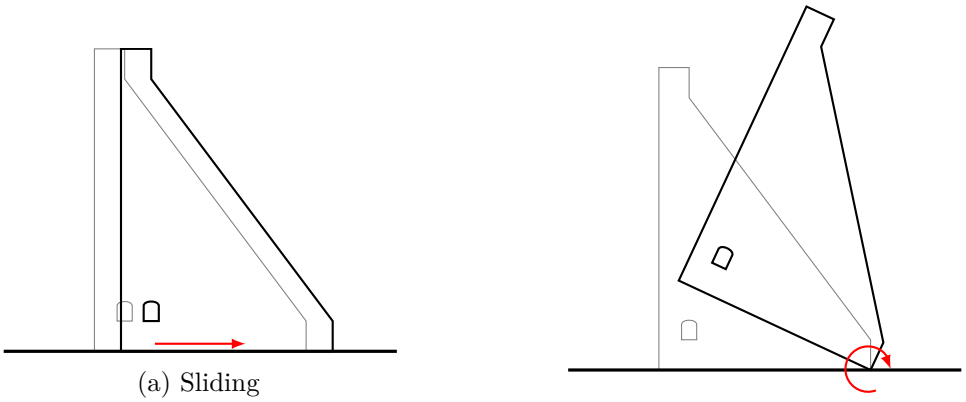

(a) Sliding

(b) Overturning

Figure 3.17: Failure modes for the traditional unkeyed profile.

However, as mentioned, concrete gravity dams are usually keyed into the foundation, mobilizing a passive wedge resistance, which may contribute crucially to the stability of the cross-section profile.

A downstream rock wedge, detached from the remain rock mass foundation, is considered to simulate this effect. Figure 3.18 shows the keyed profile.

Two stages of equilibrium are found: before and after complete interface plastification, when the profile tends to move.

Load incrementation after the plastification of the dam-foundation interface is compensated by a passive wedge resistance from the downstream rock wedge. The complete interface plastification is attained when the full shear strength is also mobilized in the rock wedge-foundation interface. The equilibrium conditions (Figure 3.19), corresponding

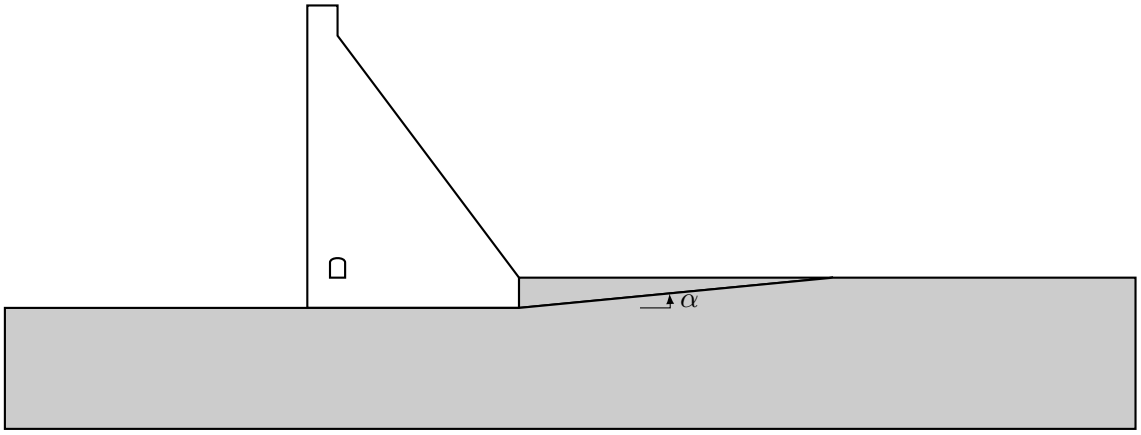

Figure 3.18: Simplified representation of a keyed profile.

to the small displacement approach, can be expressed by,

$$\sum F_{t,w} = 0 \tag{3.37}$$

where $F_{t,w}$ is total tangential force on the rock wedge-foundation interface.

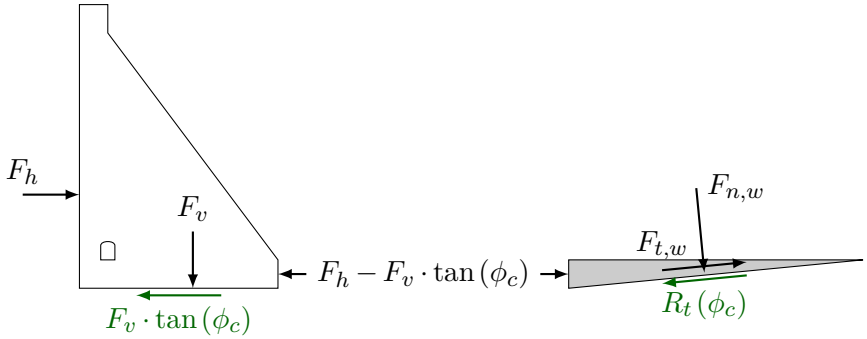

Figure 3.19: Free-body diagram in equilibrium conditions corresponding to the complete interface plastification.

After the complete interface plastification, unbalanced forces would cause the dam movement which is avoided because other stability configurations are achieved (large displacement approach), such as reported in experimental studies of physical models under static (Pina *et al.* 1994; Gomes *et al.* 1997) and dynamic loadings (Gomes 2005). Intuitively, four configurations or mechanisms (Figure 3.20), representing the pre-failure equilibrium, arise: failure mode 1) the gravity profile slides along the dam-foundation interface, pushing the downstream rock wedge; failure mode 2) the gravity profile and the downstream rock wedge slide together along the downstream rock slope; failure mode 3) the gravity profile rotates around its toe pushing the downstream rock wedge; and failure mode 4) the gravity

profile rotates over the downstream rock wedge. The occurrence of each failure mode would depend on the application point of the net force acting on the failure surfaces.

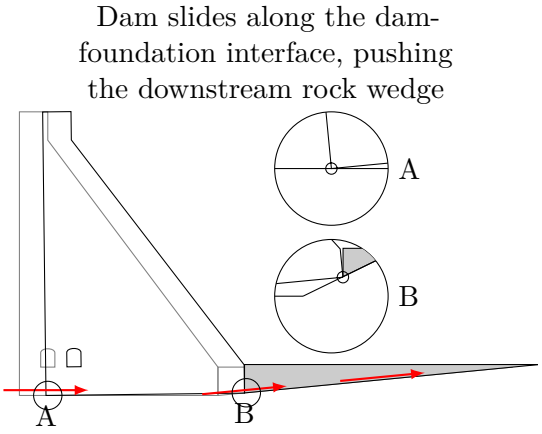

(a) Failure mode 1.

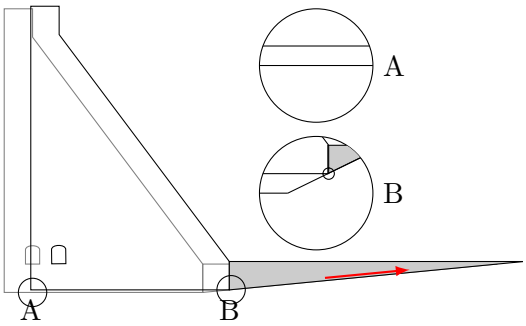

(b) Failure mode 2.

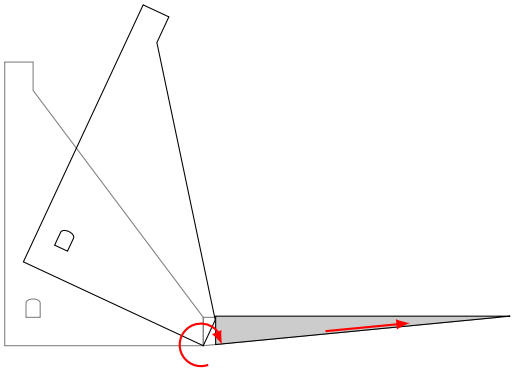

(c) Failure mode 3.

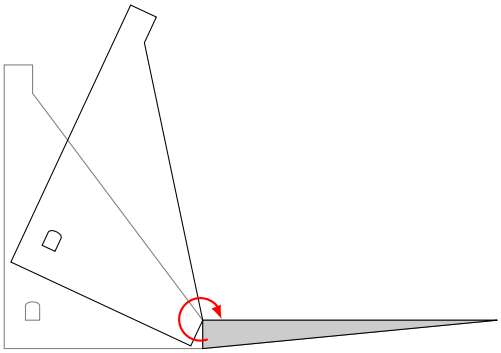

(d) Failure mode 4.

Figure 3.20: Ultimate failure modes of a keyed profile.

In the following sections, the validation of these failure mechanisms, using discrete-element models, is intended. For that, the analytical and numerical solutions for several load combinations, given in terms of the critical friction angle below which stability is not verified, are compared to justify the suitability of the analytical solution to model the pre-failure mechanisms.

The deduction of the failure mode equations are presented in the appendix B.

3.6.2 Analytical solution

3.6.2.1 Failure mode 1

Failure mode 1 is associated with the gravity profile sliding along the dam-foundation interface, pushing the downstream rock wedge. Figure 3.21 shows the free-body diagram of forces for the failure mode 1. This mechanism causes the rotation of the gravity profile around the instant center of rotation (icr) located at the intersection point between lines perpendicular to the movement of points A and B. This failure mode can occur if the direction of the net force intersects the dam-foundation (joint AB) interface.

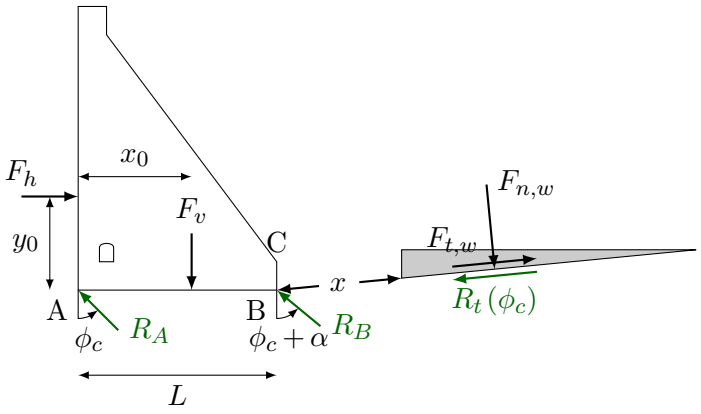

Figure 3.21: Free-body diagram of forces for the failure mode 1.

The critical friction coefficient $\tan\phi_c$ is given, in terms of the horizontal (F_h) and vertical (F_v) component, and the corresponding application point y_0 and x_0, respectively, of the net force acting on the dam body and the normal ($F_{n,w}$) and tangential ($F_{t,w}$) net forces acting on the downstream rock wedge, i.e.,

$$\tan\phi_c = S_1\left(F_v; x_0; F_h; y_0; F_{n,w}; F_{t,w}\right) \tag{3.38}$$

where S_1 is deduced in section B.1.

3.6.2.2 Failure mode 2

Failure mode 2 is associated with the gravity profile and the downstream rock wedge sliding together along the downstream rock slope. Figure 3.22 shows the free-body diagram of forces for the failure mode 2. This failure mode can occur if the direction of the net force intersects the dam-rock wedge (joint BC) interface, which is totally under compression.

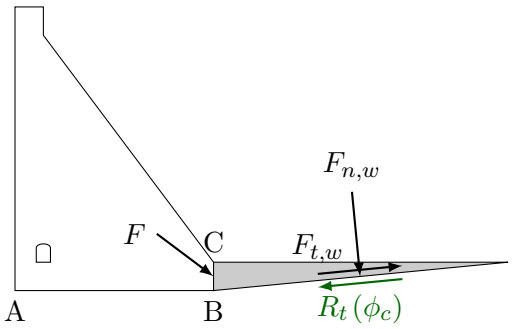

Figure 3.22: Free-body diagram of forces for the failure mode 2.

The critical friction coefficient $\tan\phi_c$ is given, in terms of the horizontal (F_h) and vertical (F_v) components of the net force acting on the dam body, F, and the normal ($F_{n,w}$) and tangential ($F_{t,w}$) net forces acting on the downstream rock wedge, i.e.,

$$\tan\phi_c = S_2\left(F_v; F_h; F_{n,w}; F_{t,w}\right) \tag{3.39}$$

where S_2 is deduced in section B.2.

3.6.2.3 Failure mode 3

Failure mode 3 is associated with the gravity profile rotating around its toe pushing the downstream rock wedge. Figure 3.23 shows the free-body diagram of forces for the failure mode 3. This failure mode can occur if the direction of the net force intersects the dam-rock wedge (joint BC) interface, which is not totally under compression.

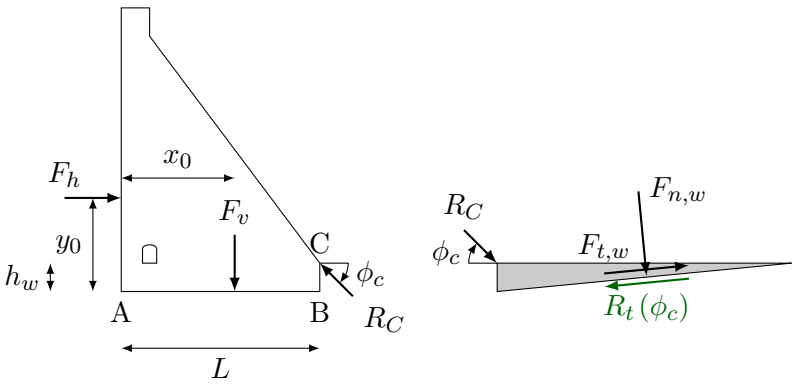

Figure 3.23: Free-body diagram of forces for the failure mode 3.

The critical friction coefficient $\tan\phi_c$ is given, in terms of the clockwise moment around the point B (M_b), due to the horizontal (F_h) and vertical (F_v) component, and the corresponding application point y_0 and x_0, respectively, of the net force acting on the dam

body, and the normal ($F_{n,w}$) and tangential ($F_{t,w}$) net forces acting on the downstream rock wedge, i.e.,

$$\tan\phi_c = S_3\left(F_v; x_0; F_h; y_0; F_{n,w}; F_{t,w}\right) \tag{3.40}$$

where S_3 is deduced in section B.3.

3.6.2.4 Failure mode 4

Failure mode 4 is associated with the dam rotating over the downstream rock wedge. This failure mode is independent on the friction angle and occurs if the net moment around C is positive.

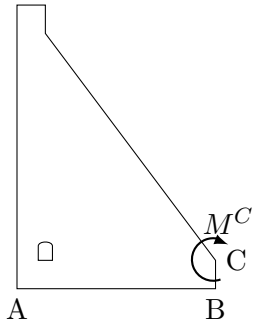

Figure 3.24: Free-body diagram of forces for the failure mode 4.

The limit equilibrium conditions are expressed by a null moment around the point C ($M_C = 0$), separating the stability conditions ($M_C < 0$) from non-stability conditions ($M_C > 0$).

3.6.3 Numerical solution

3.6.3.1 Case study

The case study used is a 100-meter high gravity profile, with downstream face slope of 0.75 and downstream rock wedge inclined at $\alpha = 5.5°$, considering several load cases, given by: i) three levels of the water in the reservoir ($H_r = 75$ m, $H_r = 85$ m and $H_r = 100$ m); ii) three values for the uplift factor ($k_u = 0$, $k_u = 0.4$ and $k_u = 0.8$); and iii) seismic ground accelerations from $a_g = 0$ m/s^2 to $a_g = 10$ m/s^2, with a step of 1 m/s^2.

3.6.3.2 DEM model

The rigid discrete-element model of the case study, considering the discrete-element method presented in the appendix C, of the case study is shown in Figure 3.25. The hydrostatic pressure is simulated through external forces applied on the nodes of the upstream face. For a specific seismic ground acceleration, the pseudo-static loads (see section 3.4.7.4) were considered. These loads are simulated by changing the gravity direction, since external loads cannot be applied directly on the rigid body centroid. Regarding the hydrodynamic pressure, the load caused by the reservoir-dam interaction during seismic motions was also simulating through external forces, quantified according to the Westergaard's theory (Westergaard 1933), and applied on the nodes of the upstream face. Finally, the uplift pressure was simulated through external forces applied on the nodes of the dam base.

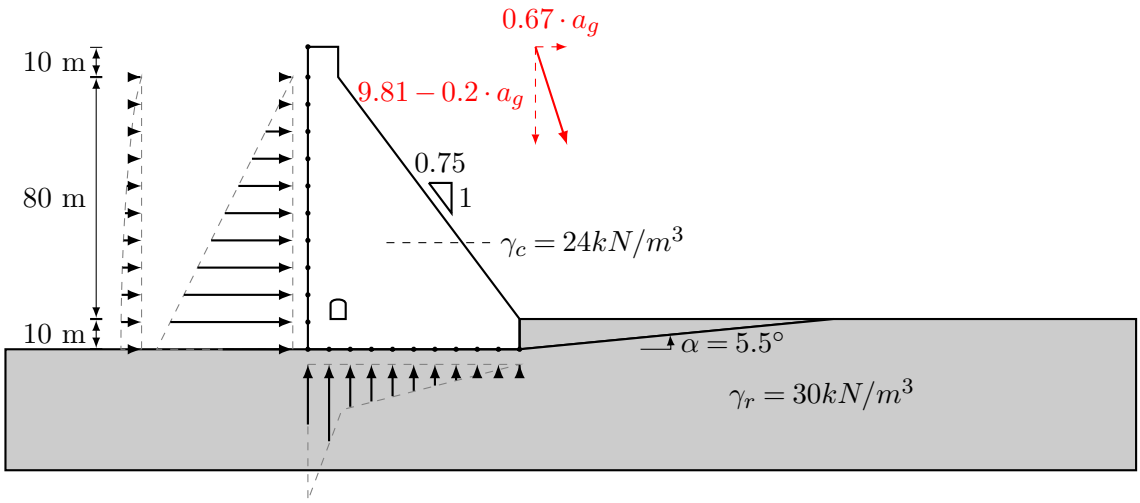

Figure 3.25: Schematic representation of the numeric model.

Strength reduction technique was used to obtain the critical friction angle. This technique consists in continually reduce the friction angle assigned to the joints since a safe value until failure, when the model does not converge to a static solution. In the following section, analytical and numeric solutions of the models tested are compared.

3.6.3.3 Relevant results

Figure 3.26 shows the results of the load cases tested. A comparison with the analytical solution is also made by plotting the solution of the equilibrium system of each failure modes described above against the numerical solution.

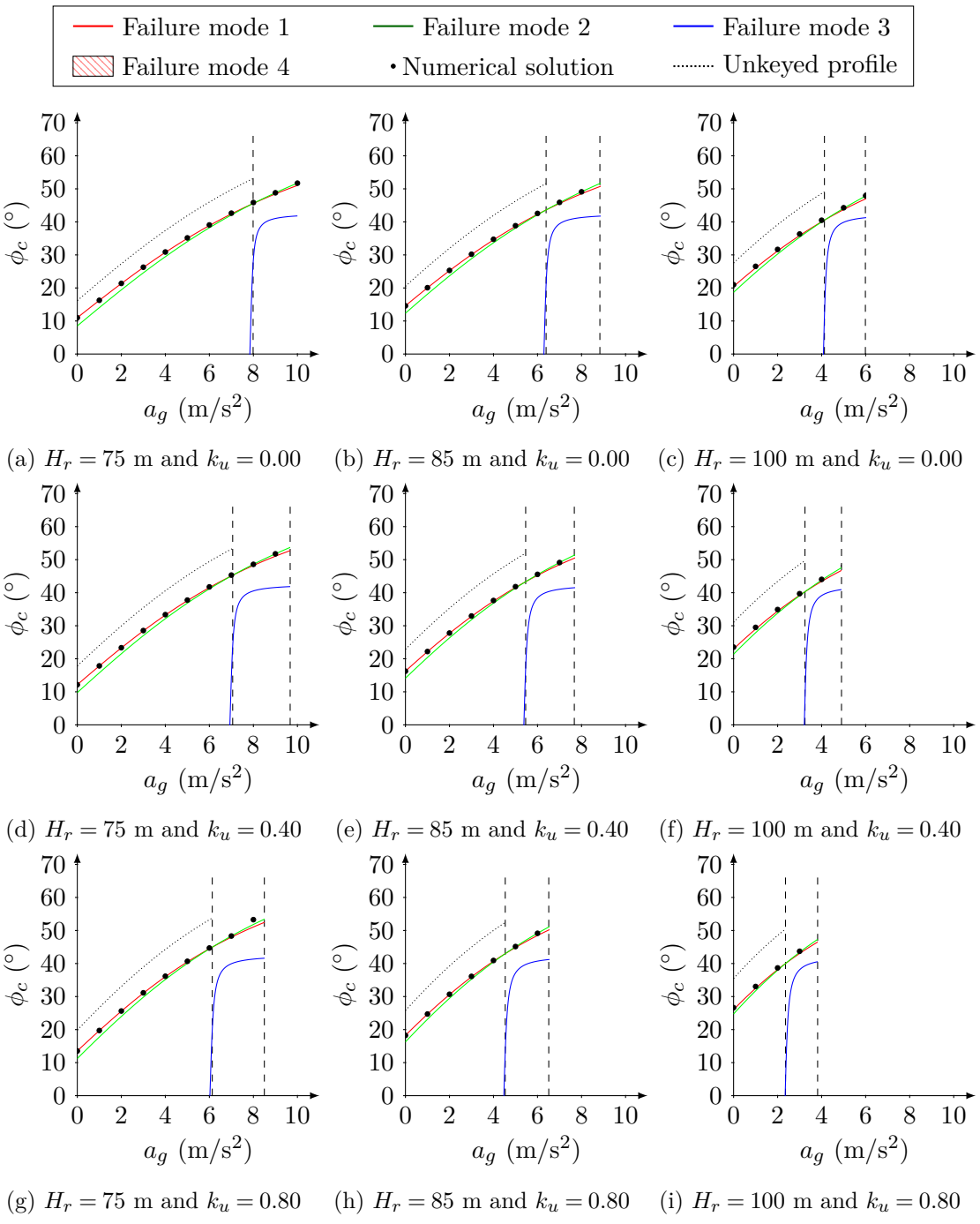

(a) $H_r = 75$ m and $k_u = 0.00$ (b) $H_r = 85$ m and $k_u = 0.00$ (c) $H_r = 100$ m and $k_u = 0.00$

(d) $H_r = 75$ m and $k_u = 0.40$ (e) $H_r = 85$ m and $k_u = 0.40$ (f) $H_r = 100$ m and $k_u = 0.40$

(g) $H_r = 75$ m and $k_u = 0.80$ (h) $H_r = 85$ m and $k_u = 0.80$ (i) $H_r = 100$ m and $k_u = 0.80$

Figure 3.26: Analytical and numerical solutions of the load cases tested.

The critical friction angle ϕ_c obtained for the rigid discrete-element model (black dots), using the strength reduction method, matches perfectly the analytical solution, given by the main failure mode. One can see that when the total moment at B becomes positive (from first vertical dashed line), failure mode 2 becomes the main failure mode while if the total moment at B is negative, failure mode 1 is the most relevant one. For this profile

geometry, failure mode 3 is not relevant for any load combination tested. For the failure mode 4, since it is not dependent on the friction angle, failure is verified for a seismic acceleration which leads to a positive total moment around C, represented by the second vertical dashed line.

CHAPTER 4

Uncertainty modeling

4.1 General considerations

Useful conclusions from reliability analysis cannot be obtained without proper modeling of the relevant sources of uncertainty. Regarding the structural safety analysis of concrete gravity dams, for ultimate limit states and stability failure modes, sources of uncertainty related to the loading conditions, material properties and model uncertainties, due to simplified mathematical formulations, shall be considered.

On one hand, the objective information available, either from the scientific literature or gathered data, shall be treated from a technical perspective in order to attain the most suitable models. On other hand, when such information is lacking, engineering judgment is the main tool to define conservative probabilistic models.

In this chapter, data from monitoring and quality control tests are used to derive probabilistic models for the water loads and the concrete mechanical properties, respectively. The quantification of other sources of physical uncertainties, such as the concrete density and concrete-rock interface shear strength, is based on the literature. The model uncertainty regarding the seismic load models is quantified by comparing the dynamic response and the analytical stability analysis of equivalent structures. While engineering judgment regulates all decisions, it becomes particularly relevant to define probabilistic models regarding other model uncertainties, such as the Mohr-Coulomb shear strength model and the rigid body stability formulation, that could not be alternatively quantified.

These tasks are detailed in the following sections.

4.2 Water loads

4.2.1 General considerations

Static water loads on dams are divided into: (i) hydrostatic pressures on the dam surfaces; and (ii) uplift pressures in emerged discontinuities. Apart from the water density, taken as deterministic, the total hydrostatic force (equation 3.7) is dependent on the reservoir water level, whereas the total uplift force (equation 3.14) is also dependent on the drainage effectiveness, quantified through the uplift factor k_u.

The derivation of probabilistic models for these random variables, from monitoring data, is detailed in the following sections.

4.2.2 Reservoir water level during normal operation conditions

4.2.2.1 General considerations

The reservoir water level varies over the year according to the water inflow and outflow, as a function of not only the environmental events but also of the dam exploitation management policy.

As mentioned, the dam construction purposes dictate that policy which intend to minimize both the current demand deficit and the costs of future water shortage, considering inter-year and intra-year models as a planning tool for long-term operation (You and Cai 2008b). Therefore, bearing in mind that dams are preferably multi-purpose structures, hedging rules (You and Cai 2008b) are established, given, for instance, that:

- in dams for flood control, during the rainy season, the water level shall be kept considerably below the NWL, such that the water inflow from a flood is partially or totally stored in the reservoir and later discharged, at a controlled rate, to downstream;
- in dams for water supply and irrigation, the reservoir water level shall be kept as close as possible to the NWL in order to ensure water supply in dry seasons;
- in dams for hydropower generation, the water shall be kept as close as possible to the NWL, to optimize energy production, embracing even pumping-storage equipment to pump discharged water up to the reservoir, especially during low demand periods.

Stochastic models for reservoir operation analysis (Labadie 2004), used to support rational operational decisions, could be considered for the uncertainty quantification regarding the reservoir water level. However, it is believed that the generalization of these models, combining inflow probability distribution, utility functions and delivery ratio (You and Cai 2008a), to general cases may be complex for the level of detail intended.

A low-cost alternative can be derived from data monitored in existent dams, which is used to derive statistical models (Pereira *et al.* 2016b; Pereira *et al.* 2018) suitable for: (i) the initial design and feasibility stages, and (ii) simplified routine safety assessment of existing structures.

For that, the annual history of the reservoir water level in existing large dams is considered as an observation of the effects of the environmental events and the dam exploitation policy on the reservoir water level. Afterwards, the sample of observations is used to infer about the properties of a representative probabilistic model.

In the following sections, after the analysis of the monitored data, regression models for the reservoir water level variation over the year are tested and, lastly, probability distributions, based on the geometrical properties of the dam and the reservoir, are derived from the results of the regression analysis.

4.2.2.2 Monitoring data analysis

Following the dam observation and inspection guidelines integrated in the Portuguese dam safety regulation (RSB 2018), the dam behavior monitoring provides useful information that can be used to identify unexpected events. Amongst other variables, the reservoir water level is periodically recorded. The measurements may be performed daily, weekly or monthly, using a limnimetric scale located at the reservoir, or continuously by automated monitoring systems. Accuracies of 0.1 m are usually obtained in both situations (Mata 2013).

The continuous monitoring of the reservoir water level in large dams shows a predictable distinction (APA 2001) between: (i) run-of-river, classified as "pure" if no reservoir storage capacity (less than two hours) is provided or "poundage" if little reservoir storage capacity (less than a week) is provided, and (ii) storage exploitation systems. While, for the first, the reservoir water level does not vary considerably (Figure 4.1a), for the latter, seasonal variations are evident (Figure 4.1b).

Therefore, meeting the recommendation of JCSS (2001) that larger populations shall

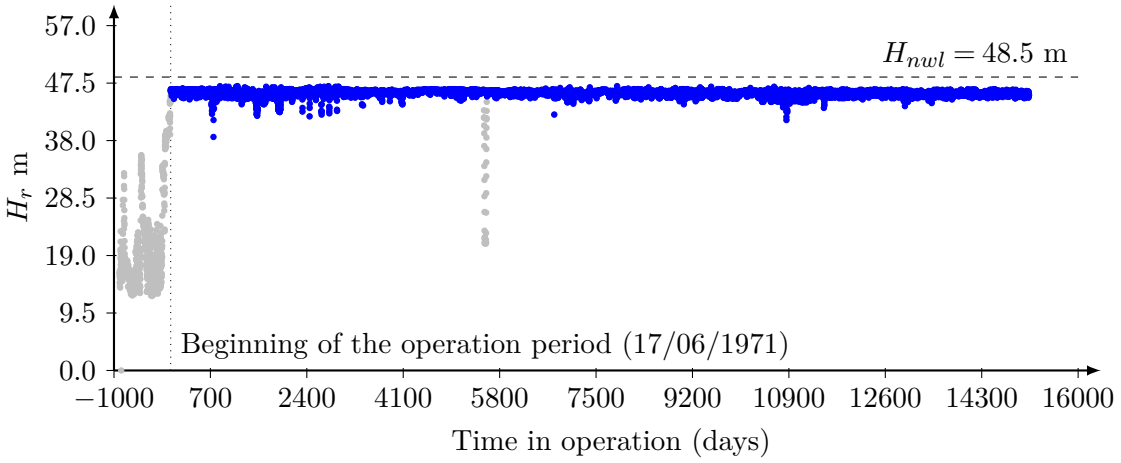

(a) Carrapatelo dam (run-of-river)

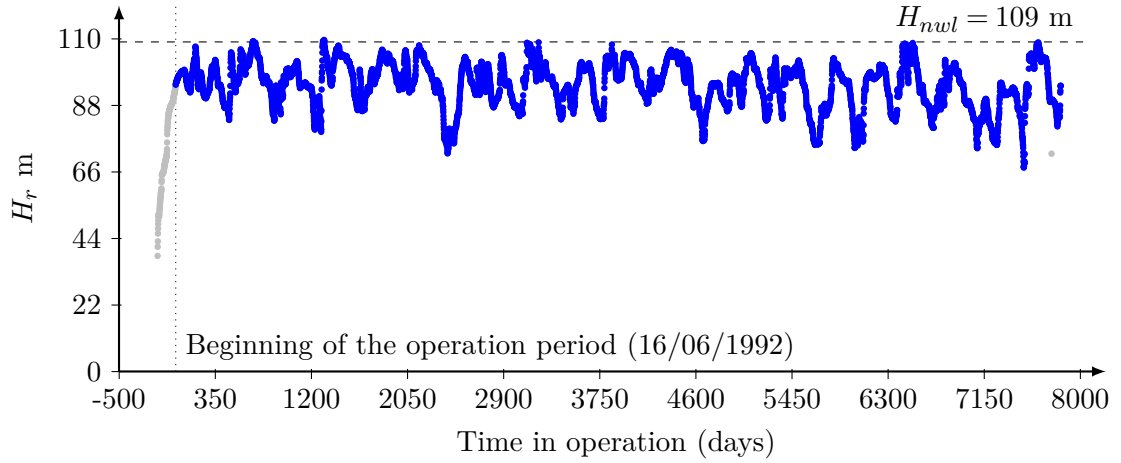

(b) Alto Lindoso dam (storage)

Figure 4.1: Reservoir water level history of two dams.

be divided into sub-populations, when clear behavior differences are noticed, in order to better study and distinguish variability within a population, data was divided into two data sets, corresponding to dams built for storage purposes and dams integrated in run-of-river projects.

Table 4.1 shows the relevant characteristics of the dams considered for the reservoir water level uncertainty modeling.

4.2.2.3 Regression model

The uncertainty model addressed in this section is intended to be considered throughout the wide range of large dams, which, as mentioned in Chapter 3, covers the dams higher than 15 meters, or between 5 to 15 m impounding more than 3 million cubic m of water (ICOLD 2011). Therefore, as data comes from different dams, the reservoir water level

Table 4.1: Main characteristics of the dams considered for the reservoir water level uncertainty modeling.

Dam	H (m)	H_{nwl} (m)	Year	Project type
Alqueva	96.00	94.00	2003	Storage
Alto Lindoso	110.00	109.00	1991	Storage
Alto Rabagão	94.10	94.00	1964	Storage
Belver	30.00	28.65	1952	Run-of-river
Bouçoais-Sonim	43.00	36.00	2004	Run-of-river
Cabril	132.00	129.00	1954	Storage
Caldeirão	39.00	33.90	1993	Storage
Carrapatelo	57.00	48.50	1972	Run-of-river
Castelo do Bode	115.00	111.70	1951	Storage
Catapereiro	37.50	34.90	1999	Storage
Crestuma-Lever	65.00	52.50	1985	Run-of-river
Ferradosa	33.40	31.00	2005	Storage
Fratel	48.00	35.00	1973	Run-of-river
Fronhas	62.00	56.10	1985	Storage
Olgas	34.50	30.25	2007	Storage
Pedrógão	43.00	33.70	2006	Storage
Penha Garcia	25.00	22.00	1979	Storage
Pocinho	49.00	35.50	1982	Run-of-river
Pretarouca	28.50	24.60	2007	Storage
Raiva	36.00	33.00	1981	Run-of-river
Ranhados	41.40	40.00	1986	Storage
Rebordelo	35.50	28.00	2005	Run-of-river
Régua	41.00	33.50	1973	Run-of-river
Touvedo	42.50	37.50	1993	Run-of-river
Valeira	48.00	40.00	1975	Run-of-river
Varosa	76.00	75.00	1976	Storage
Venda Nova	97.00	96.00	1951	Storage
Vilarinho das Furnas	94.00	93.50	1972	Storage

must be normalized to an unitary scale, given by the relation between the reservoir water level H_r and the dam height H, i.e.,

$$k_r = \frac{H_r}{H} \tag{4.1}$$

where k_r is the relative reservoir water level.

Considering that the environmental events that influences the water inflow may show a seasonal pattern, two models for the relative reservoir water level variation over the year are tested, namely:

- Model R1 which considers no explicit variation, i.e.,

$$k_r(t) = a_0 \tag{4.2}$$

  where t is the time of the year ($t = 0$ is the beginning of the year);

- Model R2 which considers a sinusoidal variation, i.e.,

$$k_r(t) = a_0 + a_1 \cdot \cos(t) + a_2 \cdot \sin(t) = a_0 + S_a \cdot \sin(t - \phi) \tag{4.3}$$

  where a_0, a_1 and a_2 are the unknown regression parameters and $S_a = \sqrt{a_1^2 + a_2^2}$ and $\phi = \arctan(a_1/a_2)$ are the corresponding semi-amplitude and phase, respectively.

These models shall be adjusted to each annual history of the relative reservoir water level of existing dams, by regression analysis, which estimates the conditional expectation of the dependent variable k_r, as a function of the independent variable t, and also the sample variance, characterizing the model residuals.

However, the traditional regression analysis based on the least-square method (LSM) cannot be used, since this model, representing a proportion, may violate its assumptions (Paolino 2001), specifically the multivariate normality and homoscedasticity. In those situations, generalized linear models (GLM), which allows for non-normal distributed residuals, must be considered (McCullagh and Nelder 1989).

A specific GLM, denoted as beta regression, has been proposed (Paolino 2001; Ferrari and Cribari-Neto 2004) for situations in which the dependent variable is measured continuously on the standard unit interval $]0,1[$. For that, a re-parametrization of the beta density function (see Table 2.1), in terms of the mean value $\mu = \alpha/(\alpha + \beta)$ and a precision parameter $\varphi = \alpha + \beta$, is recommended (Ferrari and Cribari-Neto 2004), such as,

$$f_Y(y|\mu,\varphi) = \frac{\Gamma(\varphi)}{\Gamma(\mu\varphi) \cdot \Gamma((1-\mu)\varphi)} \cdot y^{\mu\varphi-1} \cdot (1-y)^{(1-\mu)\varphi-1} \tag{4.4}$$

Thus, the expected value and variance of the dependent variable k_r, given in terms of the independent variable t, the unknown parameters $\boldsymbol{a}$ and the precision parameter φ, are,

respectively, given by,

$$E\left(k_r|t,\boldsymbol{a},\varphi\right)=\frac{\alpha}{\alpha+\beta}=\mu=g^{-1}\left(\boldsymbol{a}^T\cdot\boldsymbol{T}\right) \tag{4.5}$$

$$V\left(k_r|t,\boldsymbol{a},\varphi\right)=\frac{\alpha\beta}{\left(\alpha+\beta\right)^2\left(\alpha+\beta+1\right)}=\frac{\mu\cdot\left(1-\mu\right)}{1+\varphi} \tag{4.6}$$

where g is a strictly monotonic and twice differentiable link function that maps $]0,1[$ into the real line, $\boldsymbol{a}$ is the vector of unknown parameters ($\boldsymbol{a}=\{a_0\}$ for the model R1 or $\boldsymbol{a}=\{a_0,a_1,a_2\}$ for the model R2) and $\boldsymbol{T}$ is the vector of the independent variables ($\boldsymbol{T}=\{1\}$ for the model R1 or $\boldsymbol{T}=\{1,\cos\left(t\right),\sin\left(t\right)\}$ for the model R2).

Given the sample $\hat{\boldsymbol{y}}=\left\{\left(\hat{t}_1,\hat{k}_{r1}\right),\cdots,\left(\hat{t}_N,\hat{k}_{rN}\right)\right\}$ of the relative reservoir water level over a year, the unknown regression parameters $\boldsymbol{a}$ and the precision parameter φ, are estimated by maximizing the log-likelihood function, given by,

$$\log L\left(\boldsymbol{a},\varphi|\hat{\boldsymbol{y}}\right)=\sum_{i=1}^{N}\ln\left[f_Y\left(\hat{k}_{ri}|\mu\left(\boldsymbol{a},\hat{t}_i\right),\varphi\right)\right] \tag{4.7}$$

Figure 4.2 shows an example of the beta regression outcome, considering the link function given by the logit transformation,

$$g\left(x\right)=\ln\left(\frac{x}{1-x}\right) \tag{4.8}$$

whose inverse is given by,

$$g^{-1}\left(x\right)=\frac{e^x}{1+e^x} \tag{4.9}$$

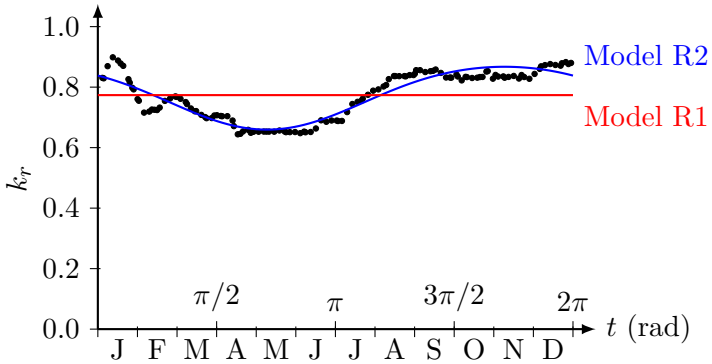

Figure 4.2: Example of the beta regression outcome, considering the reservoir water level monitored during 2011 in the Venda Nova dam.

4.2.2.4 Uncertainty model

The regression models presented above were adjusted to the annual history of the relative reservoir water level, considering each operation year of 28 large concrete dams (Table 4.1), providing 670 observations of the regression model parameters $\boldsymbol{a}$ and the precision φ, where 374 comes from storage dams and 296 from run-of-river dams.

Since the NWL, whose relation to the dam height (k_{nwl}=H_{nwl}/H) is different for each dam, defines the optimum operation conditions, the regression models must be transformed to other values of k_{nwl} in order to serve as predictive models in a generic case. Thus, for a generic k_{nwl}, the mean and variance of k_r, in terms of the independent variable t and of each observation j of the regression parameters $\hat{\boldsymbol{a}}_j$ and the precision parameter $\hat{\varphi}_j$, are, respectively, given by,

$$E\left(k_r\left(k_{nwl}\right)|t,\hat{\boldsymbol{a}}_j,\hat{\varphi}_j\right)=g^{-1}\left(\hat{\boldsymbol{a}}_j^T\cdot\boldsymbol{T}\cdot\frac{g\left(k_{nwl}\right)}{g\left(k_{nwl,j}\right)}\right) \tag{4.10}$$

$$V\left(k_r\left(k_{nwl}\right)|t,\hat{\boldsymbol{a}}_j,\hat{\varphi}_j\right)=\frac{E\left(k_r\left(k_{nwl}\right)|t,\hat{\boldsymbol{a}}_j,\hat{\varphi}_j\right)\cdot\left(1-E\left(k_r\left(k_{nwl}\right)|t,\hat{\boldsymbol{a}}_j,\hat{\varphi}_j\right)\right)}{1+\hat{\varphi}_j} \tag{4.11}$$

The deduction of absolute (unconditional) values of the expected value and variance of the relative reservoir water level k_r, as functions of k_{nwl}, is performed in two steps, using, respectively, the law of total expectation (Blitzstein and Hwang 2004),

$$E\left(Y_1\right)=E\left(E\left(Y_1|Y_2\right)\right) \tag{4.12}$$

and the law of total variance (Blitzstein and Hwang 2004),

$$V\left(Y_1\right)=V\left(E\left(Y_1|Y_2\right)\right)+E\left(V\left(Y_1|Y_2\right)\right) \tag{4.13}$$

where Y_1 and Y_2 are two random variables of the same probability space. The components $V\left(E\left(Y_1|Y_2\right)\right)$ and $E\left(V\left(Y_1|Y_2\right)\right)$ are commonly denoted as "explained" and "unexplained" components, respectively, of the variance.

In the first step, for each observation j of the regression parameters $\hat{\boldsymbol{a}}_j$ and the precision parameter $\hat{\varphi}_j$, the total annual mean of k_r, considering advantageously time t varying

between 0 and 2π, is given by,

$$\begin{aligned} E\left(k_r\left(k_{nwl}\right)|\hat{\boldsymbol{a}}_j,\hat{\varphi}_j\right) &= E\left[E\left(k_r\left(k_{nwl}\right)|t,\hat{\boldsymbol{a}}_j,\hat{\varphi}_j\right)\right] \\ &= \frac{1}{2\pi}\int_{t=0}^{2\pi} E\left(k_r\left(k_{nwl}\right)|t,\hat{\boldsymbol{a}}_j,\hat{\varphi}_j\right)\,\partial t \end{aligned} \tag{4.14}$$

and the total annual variance is given by,

$$\begin{aligned} V\left(k_r\left(k_{nwl}\right)|\hat{\boldsymbol{a}}_j,\hat{\varphi}_j\right) &= V\left[E\left(k_r\left(k_{nwl}\right)|t,\hat{\boldsymbol{a}}_j,\hat{\varphi}_j\right)\right] + E\left[V\left(k_r\left(k_{nwl}\right)|t,\hat{\boldsymbol{a}}_j,\hat{\varphi}_j\right)\right] \\ &= E\left[E\left(k_r\left(k_{nwl}\right)|t,\hat{\boldsymbol{a}}_j,\hat{\varphi}_j\right)^2\right] - E\left(k_r\left(k_{nwl}\right)|\hat{\boldsymbol{a}}_j,\hat{\varphi}_j\right)^2 + \\ &\quad E\left[V\left(k_r\left(k_{nwl}\right)|t,\hat{\boldsymbol{a}}_j,\hat{\varphi}_j\right)\right] \\ &= \frac{1}{2\pi}\int_{t=0}^{2\pi} E\left(k_r\left(k_{nwl}\right)|t,\hat{\boldsymbol{a}}_j,\hat{\varphi}_j\right)^2\,\partial t - \\ &\quad \left(\frac{1}{2\pi}\int_{t=0}^{2\pi} E\left(k_r\left(k_{nwl}\right)|t,\hat{\boldsymbol{a}}_j,\hat{\varphi}_j\right)\,\partial t\right)^2 + \\ &\quad \frac{1}{2\pi}\int_{t=0}^{2\pi} V\left(k_r\left(k_{nwl}\right)|t,\hat{\boldsymbol{a}}_j,\hat{\varphi}_j\right)\,\partial t \end{aligned} \tag{4.15}$$

In the second step, the absolute expected value of k_r, is inferred from the finite sample of N observations (N=374 for storage dams and N=296 for run-of-river dams) of the regression parameters $\hat{\boldsymbol{a}}_j$ and the precision parameter $\hat{\varphi}_j$, such as,

$$E\left(k_r\left(k_{nwl}\right)\right) = E\left[E\left(k_r\left(k_{nwl}\right)|\hat{\boldsymbol{a}}_j,\hat{\varphi}_j\right)\right] = \frac{1}{N}\sum_{j=1}^{N} E\left(k_r\left(k_{nwl}\right)|\hat{\boldsymbol{a}}_j,\hat{\varphi}_j\right) \tag{4.16}$$

The absolute variance, computed similarly, is given by,

$$\begin{aligned} V\left(k_r\left(k_{nwl}\right)\right) &= V\left[E\left(k_r\left(k_{nwl}\right)|\hat{\boldsymbol{a}}_j,\hat{\varphi}_j\right)\right] + E\left[V\left(k_r\left(k_{nwl}\right)|\hat{\boldsymbol{a}}_j,\hat{\varphi}_j\right)\right] \\ &= E\left[E\left(k_r\left(k_{nwl}\right)|\hat{\boldsymbol{a}}_j,\hat{\varphi}_j\right)^2\right] - E\left(k_r\left(k_{nwl}\right)\right)^2 + \\ &\quad E\left[V\left(k_r\left(k_{nwl}\right)|\hat{\boldsymbol{a}}_j,\hat{\varphi}_j\right)\right] \\ &= \frac{1}{N}\sum_{j=1}^{N} E\left(k_r\left(k_{nwl}\right)|\hat{\boldsymbol{a}}_j,\hat{\varphi}_j\right)^2 - \left(\frac{1}{N}\sum_{j=1}^{N} E\left(k_r\left(k_{nwl}\right)|\hat{\boldsymbol{a}}_j,\hat{\varphi}_j\right)\right)^2 + \\ &\quad \frac{1}{N}\sum_{j=1}^{N} V\left(k_r\left(k_{nwl}\right)|\hat{\boldsymbol{a}}_j,\hat{\varphi}_j\right) \end{aligned} \tag{4.17}$$

Figure 4.3 shows the moments (expected value and variance) of the relative reservoir

water level k_r, as functions of k_{nwl}, comparing the model R1 and R2.

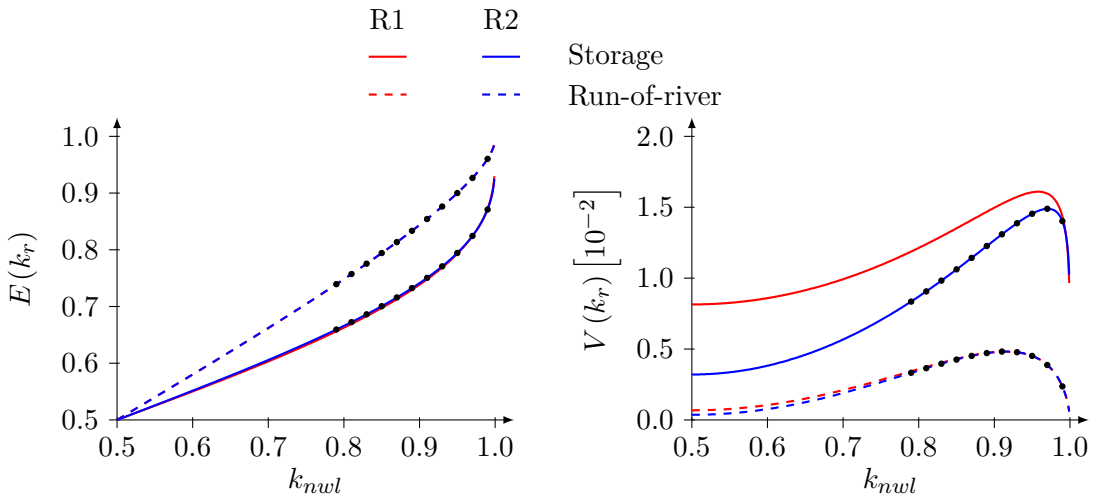

(a) Expected value (b) Variance

Figure 4.3: Distribution moments of k_r, as functions of k_{nwl}.

As insignificant seasonal variation is verified for run-of-river dams (blue line), similar accuracy (variance) were obtained from models R1 (dashed line) and R2 (solid line). On the other hand, model R2 is more accurate than model R1 for storage dams (red line), since a significant portion of the reservoir water level variation over the year is explained by the seasonal pattern.

Table 4.2 lists the beta distribution moments of the relative reservoir water level k_r, considering a seasonal pattern described by the model R2, since this model results in lower variance, for different values of k_{nwl}.

4.2.3 Uplift pressure

4.2.3.1 General considerations

The hydromechanical behavior of rock mass foundations depends on the spatial variation of their properties, which, due to the complex discontinuous structure, is difficult to describe in detail even after extensive field investigations. The simplification of their behavior by means of equivalent continuum idealizations may result in erroneous predictions of the uplift pressure distribution under concrete dams, specially relevant for the stability analysis of the most conditioning dam monoliths.

The uplift pressure in rock mass foundations, possibly exhibiting high spatial variations

Table 4.2: Beta distribution moments for the relative reservoir water level k_r, considering the model R2.

k_{nwl}	Storage		Run-of-river	
	E	V	E	V
0.79	0.66	0.0084	0.74	0.0033
0.81	0.67	0.0091	0.76	0.0037
0.83	0.69	0.0098	0.78	0.0040
0.85	0.70	0.0106	0.79	0.0043
0.87	0.72	0.0114	0.81	0.0045
0.89	0.73	0.0123	0.83	0.0047
0.91	0.75	0.0131	0.85	0.0048
0.93	0.77	0.0139	0.88	0.0048
0.95	0.79	0.0145	0.90	0.0045
0.97	0.82	0.0149	0.93	0.0039
0.99	0.87	0.0140	0.96	0.0024

(Ruggeri 2004b), are not only influenced by the geologic features, such as the geologic structure, the rock type and the joint pattern (EPRI 1990), but also by the joint permeability, mainly characterized by the filling, roughness and specially the joint aperture (EPRI 1992). According to the Darcy's law (Darcy 1856), the uplift linear distribution is observed in joints with constant aperture. For a tapered joint, the rate of pressure reduction increases, whereas, for widening joints, the rate of pressure reduction decreases so that it becomes parabolic rather than linear. Figure 4.4 illustrates the influence of the joint aperture on the uplift pressure distribution.

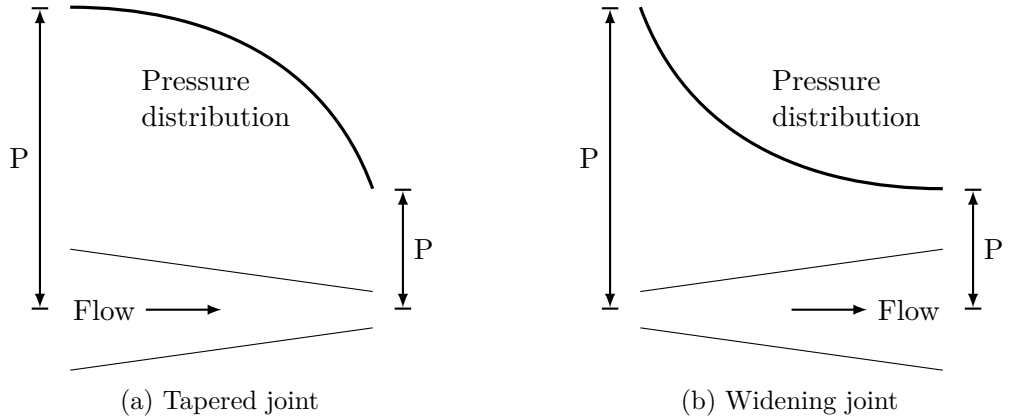

(a) Tapered joint (b) Widening joint

Figure 4.4: Influence of joint aperture on uplift distribution (EPRI 1992).

Changes in the stress field of the rock mass foundations, due to loads on dams, cause

variations in the uplift pressure distribution in joints, where most of the deformation occurs. These phenomena are due to:

- the reservoir water level variations, which cause the dam rotation and the opening/-closing of joints, resulting in a non-linear relation with the uplift pressure (Grenoble *et al.* 1995; Ruggeri 2004b);
- cyclic thermal variations, which cause volumetric variations and changes on the hydraulic conductivity and on the kinematic viscosity of water (Guiducini and Andrade 1988; Kalkani 1992).

In the few cases in which the pressures were recorded during a seismic action (FERC 2002), small or no changes in the uplift pressures were observed. This is commonly justified by the short duration of the seismic action.

The effectiveness of the drainage system, designed according to the equivalent continuum approach, may vary under a dam monolith since it is not expected that the drains can intersect all relevant joints. In fact, a distinction between regular and unfavorable geologic conditions of the rock mass foundation is already made in the French guidelines (CFBR 2012) which recommend the uplift lowering coefficient (equivalent to k_u) presented in Table 4.3. Also a time-dependent variation is possible due to drain clogging. This justifies the wide variation of piezometric recordings in several Portuguese large concrete dams.

Table 4.3: Recommended uplift reduction coefficient in the French guidelines (CFBR 2012).

Foundation	k_u
Regular geology	0.33 - 0.50
Unfavorable geology	>0.50
No drainage	1.00

For the uncertainty quantification of the uplift pressures, considering the uplift factor k_u as a random variable, gathered data corresponding to monitored pressures are used. Altarejos (2009) also proceeded this way, whereas Westberg (2009a) and Westberg (2009b) followed a geostatistical approach testing different statistical descriptors of the spatial variation and correlation of the foundation permeability.

In the following sections, after the analysis of the monitored data, the uncertainty quantification of the uplift factor, based on the parametric inference of beta mixtures, is presented, followed by the derivation of probability distributions from the previous results

and the introduction of the bi-linear model uncertainty, such as presented in Pereira *et al.* (2016a).

4.2.3.2 Monitoring data analysis

The uplift pressures are measured using piezometers, usually installed in sealed boreholes, drilled downstream from both grout and drainage systems. Generally, one piezometer is installed per dam monolith. For this reason, the piezometric recordings provide only localized information.

Multi-chamber piezometers, crossing different major discontinuities, allow the measurement of the water pressures in specific sections. However, in Portugal, the majority of the piezometers installed in the concrete dam foundations has a single chamber, providing therefore only the average pressure from the water inflow and outflow over their length.

Rarely, more than one piezometer, forming an upstream-downstream network, is installed within a specific cross-section. Often, piezometers are not aligned with drains, being installed in an intermediate zone.

For the uncertainty quantification of the uplift pressures, data monitored in 148 piezometers, from 15 Portuguese large concrete dams of the gravity and thick arch types, is used. Only the piezometers installed in higher dam monoliths are considered, since negligible uplift pressures, exceeding the reservoir water level, may be observed near the abutments (EPRI 1992). Table 4.4 shows the relevant characteristics of the dams considered for the uplift factor uncertainty modeling, namely the maximum height (H), the year of completion and the number of piezometers (N_{pz}) considered.

Since the piezometric line is located downstream from the line of drains (Figure 4.5), recorded pressures shall be extrapolated to the drainage line allowing their utilization for uplift factor uncertainty modeling. The extrapolation is given by,

$$H_d = (H_p - H_d) \cdot \frac{L - L_d}{L - L_p} + H_t \tag{4.18}$$

where H_d and H_p are the hydraulic heads at the drainage and piezometric lines and L_d and L_p are the respectively distance, from the dam heel.

As an example, Figure 4.6 shows the pressure head history of Alto Lindoso dam, extrapolated to the drainage line from the recordings of the piezometer "P10/11", and the corresponding history of the uplift factor k_u, computed using the equation 3.10.

Table 4.4: Main characteristics of the dams considered for the uplift factor uncertainty modeling.

Dam	$H(m)$	Year	N_{pz}
Alqueva	96.00	2003	19
Alto Lindoso	110.00	1991	15
Alto Rabagão	94.10	1964	7
Bouçoais-Sonim	43.00	2004	3
Cabril	132.00	1954	9
Castelo do Bode	115.00	1951	7
Ferradosa	33.40	2005	2
Fronhas	62.00	1985	10
Pedrógão	43.00	2006	12
Penha Garcia	25.00	1979	10
Pretarouca	28.50	2007	1
Raiva	36.00	1981	13
Rebordelo	35.50	2005	1
Varosa	76.00	1976	26
Vilarinho das Furnas	94.00	1972	13
Total			148

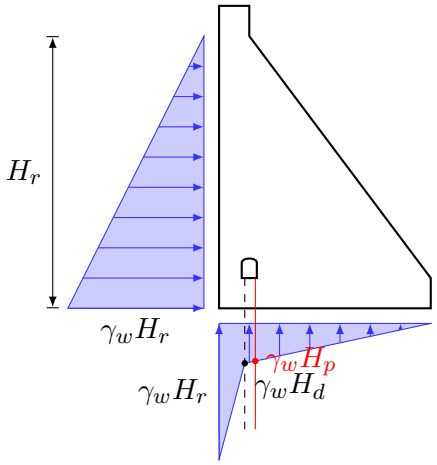

Figure 4.5: Extrapolation of the piezometric readings to the drainage line.

In this case, the uplift factor k_u presents a non-linear relation with the reservoir water level and a time evolution probably due to loss of drainage effectiveness.

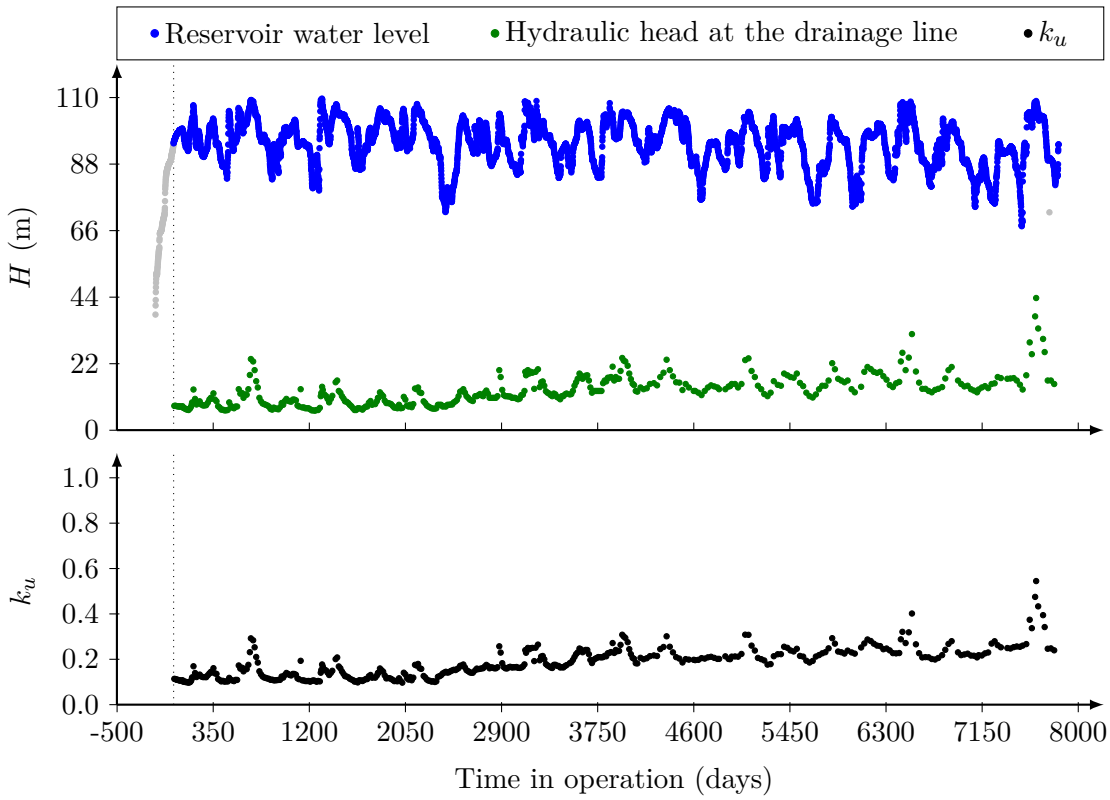

Figure 4.6: Pressure head history of Alto Lindoso dam, extrapolated to the drainage line from the recordings of the piezometer "P10/11".

4.2.3.3 Parametric inference of beta mixtures

Each history of the uplift factor k_u is interpreted as punctual and independent information regarding the drainage system effectiveness over the dam operation period, since uplift pressure distribution beneath dams are site-specific and may even vary considerably across a given site (EPRI 1990) since they depend on the water flow paths within the rock mass (Farinha 2010).

Before the utilization of automated monitoring systems which collect data continuously, the manual measurements of the uplift pressure were performed weekly or biweekly. In order to achieve a fair representation of the uplift pressures, since the frequency of data collection varies from dam to dam, only the average uplift pressure recorded in each piezometer, during a specific time-interval, is considered.

Thus, the data recorded from different piezometers were organized in time intervals two weeks long, resulting in a collection of samples, each one associated with a time interval, that can be analyzed separately. A shorter time-interval could reduce significantly the sample dimension and a much larger time-period could ignore some relevant time-variations.

For each sample of the average biweekly uplift pressures, a mixture of two beta distributions were adjusted. On one hand, the uplift factor k_u must be modeled by a continuous probability distribution defined on the unit interval, and, on the other hand, information about the foundation properties, which could be used to distinguish between data recorded in zones with regular or unfavorable geologic conditions (CFBR 2012), is not available.

The adjustment of a mixture of two beta distributions was made by the MLE method, given that the likelihood function of a sample $\hat{\boldsymbol{x}}$ composed by n independent occurrences of a mixture of two beta variables is given by (Casaca and Pereira 2017),

$$L\left(\boldsymbol{\Theta},\boldsymbol{\Omega}|\hat{\boldsymbol{x}}\right) = \prod_{l=1}^{n}\sum_{j=1}^{2}\omega_j \cdot f_X\left(\hat{x}_l|\alpha_j,\beta_j\right) \tag{4.19}$$

where $\boldsymbol{\Theta} = \{\alpha_1,\beta_1,\alpha_2,\beta_2\}$ and $\boldsymbol{\Omega} = \{\omega_1,\omega_2\}$ are the unknown beta distribution parameters and weights, respectively, of the variables in the mixture. Figure 4.7 shows, as an example, the outcome of the beta mixture adjustment to the sample from the 3$^{\text{th}}$ time-interval.

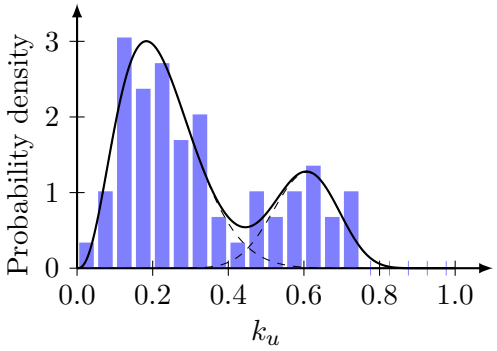

Figure 4.7: Adjustment of a mixture of two beta distributions to the sample from the 3$^{\text{th}}$ interval.

4.2.3.4 Uncertainty model

The procedure for the parametric inference of the mixture of two beta distributions presented in the last section was repeated for the samples corresponding to the majority of the time intervals considered, namely those whose sample size is greater than 30 observations in order to avoid relevant statistical uncertainty. Figure 4.8 synthesizes the results.

From the results of the parametric inference, considering the distribution parameters of each beta distribution as observations associated with foundations with regular and unfavorable geologic conditions, the absolute expected value of the uplift factor k_u is given

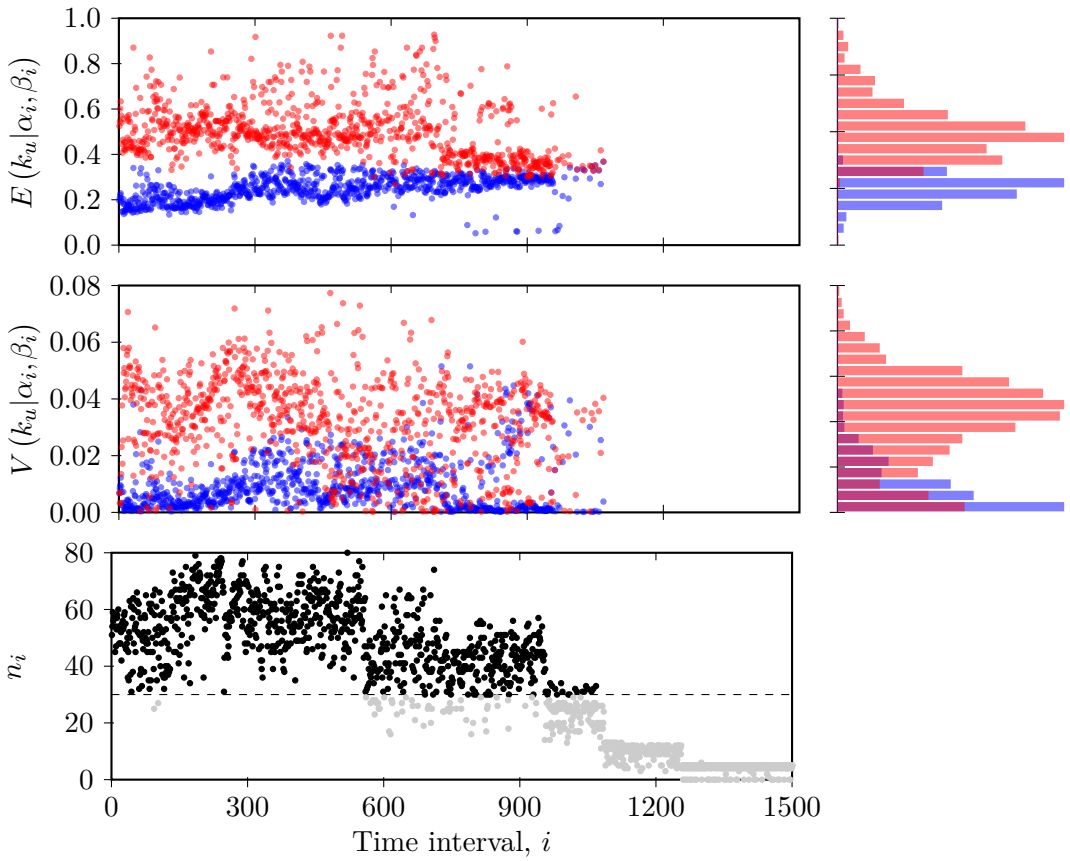

Figure 4.8: Results of parametric inference of beta mixtures to the time intervals considered.

by,

$$E\,(k_u) = E\left(E\,(k_u|\alpha_i,\beta_i)\right) = \frac{1}{N}\sum_{i=1}^{N} E\,(k_u|\alpha_i,\beta_i) \tag{4.20}$$

where N is the number of time intervals. The absolute variance is then given by,

$$\begin{aligned} V\,(k_u) &= V\left(E\,(k_u|\alpha_i,\beta_i)\right) + E\left(V\,(k_u|\alpha_i,\beta_i)\right) \\ &= \frac{1}{N}\sum_{i=1}^{N}\left(E\,(k_u|\alpha_i,\beta_i) - E\,(k_u)\right)^2 + \frac{1}{N}\sum_{i=1}^{N} V\,(k_u|\alpha_i,\beta_i) \end{aligned} \tag{4.21}$$

Table 4.5 presents the beta distributions moments of the uplift factor k_u, considering the first beta distribution as related to foundations with regular geology and the second beta distribution as related to foundations with unfavorable geology.

4.2.3.5 Model uncertainty

As mentioned above, when analyzing the rock mass hydrodynamic behavior from a discontinuum approach, non-linear uplift pressure distribution can be observed in joints. The

Table 4.5: Beta distribution moments for the uplift factor k_u.

Foundation	Expected value	Variance
Regular geology	0.25	0.012
Unfavorable geology	0.48	0.042

overall effect of the spatial variation of the foundation permeability on the stability of a dam monolith was studied in Westberg (2009a) and Westberg (2009b), considering a geo-statistical approach, which concluded that even for effective drainage, high uplift pressures can be obtained if the hydraulic conductivity field is unfavorable.

The probabilistic model-code for concrete dams (Westberg and Johansson 2016), based on the conclusions of these studies, recommends uncertainty models for: i) the cases in which the drainage effectiveness can be assured; and ii) the remain cases in which uplift reduction shall not be considered. The latter, representing the deviations from the linear uplift distribution, is here considered as an uncertainty model, affecting the uplift net force U (equation 3.14), which follows a normal distribution with mean value of 1.00 and standard deviation of 0.05.

4.3 Material properties

4.3.1 Concrete density

The uncertainty on the magnitude of dead loads, whose probability of occurrence is approximately one and their variation with time is negligible (permanent loads), is generally small in comparison with other types of loads (JCSS 2001).

However, for some problems, such as the static equilibrium, the variability of the weight within a structural element, due to uncertain material density and its dimensions, may be important.

For ordinary concrete without reinforcement and with stable moisture content, the JCSS (2001) recommends that its density ρ_c follows a normal distribution with mean value of 2400 kg/m^3 and coefficient of variation of 0.04 which shall be affected by a reduction factor of 0.85 to account for the decreased variability in large structures.

Regarding the structural dimensions, although indicating deviations of few centimeters, JCSS (2001) indicates that the variability of the geometrical parameters can be neglected in comparison with the variability of loads and material properties.

4.3.2 Concrete mechanical properties

4.3.2.1 General considerations

Due to its performance requirements, mass concrete used in concrete dams usually has a lower cement content, which has even been blended with pozzolans and/or fly ashes up to 50% (Serra *et al.* 2016), and larger coarse aggregates, leading to different mechanical properties that develop slower than the ordinary concrete.

Considering that the concrete mechanical properties shall be quantified taking its variation into account (ICOLD 2008), information from former structures becomes relevant. Furthermore, the concrete prescription procedure usually requires extensive laboratory studies within a detailed quality control program. Given the difficulty in testing concrete composed by such large coarse aggregates, concrete quality control and characterization are mostly based on results from tests on wet-screened concrete, obtained from the full-mixed mass concrete by removing aggregates larger than 38 mm. Since the composition of this concrete significantly differs from the original mix, correlations must still be determined (USBR 1981; ICOLD 2008; Serra *et al.* 2016), by comparison to larger specimens, with the minimum dimension of, at least, three times the MSA, of full-mixed concrete tested in large capacity rigid presses.

Besides the difference in composition between wet-screened and full-mixed concrete, the prediction of dam concrete mechanical properties from tests on small-sized specimens at the reference age, denoted as potential properties (Gonçalves 1999), cannot be made without considering other differences between "in situ" and laboratory conditions, namely the failure mechanism according to the specimen geometry (Mier and Nooru-Mohamed 1990) and scale effects (Kim *et al.* 1999).

Furthermore, since concrete dams are separated into independent monoliths composed by concrete blocks, dam faces have frequently showed, at the beginning of the dam operation, some degree of spatial heterogeneity characterized by imperfect links between batches through which small permanent water transfers occur. The lack of homogeneity, associated not only with inappropriate transport, placing, vibration and/or hardening conditions, but also to careless treatment of joints, should also be accounted in the estimation of the real structural properties from the potential properties.

In the following sections, models for the estimation of potential properties (Pereira *et al.* 2016c), as a function of the prescribed characteristic compressive strength, and structural

properties (Pereira *et al.* 2016d) are proposed, based on the analysis of the results of several laboratory tests, carried out in specimens from the concrete of Baixo Sabor, Pedrógão and Ribeiradio dams.

4.3.2.2 Potential properties

General considerations

Potential properties of dam concrete are obtained from small-sized specimens tested, in normalized conditions, at the reference age. Since, due to construction scheduling, the results of tests at the strength characteristic age (90 or 180 days) are not available before concrete placing, the desired characteristic strength is usually targeted at 28 days (ICOLD 2008), although earlier tests are carried out for quality control.

Mostly, tests are performed in wet-screened concrete specimens of standard geometry and size (NP EN206-1 2007), typically cubes and cylinders of 150 mm, even though few full-mixed concrete cylindric specimens, with larger dimensions, are also tested for validation purposes.

Apart from the compressive strength, the Young's modulus and tensile strength are also estimated in laboratory tests. Naturally, these properties are related to the compressive strength, usually by exponential laws (EN1992 2004; ACI 2005; FIB 2010). While Young's modulus are estimated from the early specimen response in strength tests, tensile strength is commonly obtained by (ICOLD 2008): i) direct (pure) tensile test; ii) splitting tensile (Brazilian) test; or iii) flexural tensile (modulus of rupture) test.

The test that simulates the real loading conditions in dams depends on the anticipated mode of failure. While the flexural strength can be directly used in numerical analysis of dams (Raphael 1984), splitting tests are the easiest to handle and more reliable estimation of the tensile strength can be accomplished by performing large number of tests (ICOLD 2008). However, on a localized level, typical cracking due to static loading follows the laboratory condition of direct tensile strength.

Being indirect measures of the potential mechanical properties, the results of laboratory tests shall be transformed, due to the geometry and scale effects, taking into account the corresponding transformation errors. At the end, the predictive models for Young's modulus and tensile strength, as a function of the compressive strength, are obtained by weighted linear regression, ensuring that the results which have lower propagated error have more

preponderance, which is commonly given by,

$$\left(\boldsymbol{X}'\boldsymbol{W}\boldsymbol{X}\right)^{-1}\boldsymbol{X}'\boldsymbol{W}\boldsymbol{Y}=\hat{\boldsymbol{\beta}} \tag{4.22}$$

where $\boldsymbol{X}$ and $\boldsymbol{Y}$ are the vectors of the independent and dependent variables, respectively, $\boldsymbol{W}$ is the corresponding diagonal matrix containing the weights, defined as the reciprocal of the variance (error) of an observation ($\omega_i = 1/\sigma_i^2$), and $\hat{\boldsymbol{\beta}}$ is the vector of the estimators of the unknown regression parameters.

For instance, the compressive strength shall be consecutively transformed:

1. Firstly, into the equivalent strength of cylindric specimens of standard dimensions (cylinders with h=300 mm and Φ=150 mm, $f_{c,y150}$, for the wet-screened concrete or with h=900 mm and Φ=450 mm, $f_{c,y450}$, for the full-mixed concrete). The expected value and variance of the model that transforms the strength obtained in cubic specimens of wet-screened concrete $f_{c,c150}$ (Figure 4.9), can be, respectively, given by,

$$E\left(f_{c,y150}|f_{c,c150}\right)=0.80\cdot f_{c,c150} \tag{4.23}$$

$$V\left(f_{c,y150}|f_{c,c150}\right)=3.38^2 \tag{4.24}$$

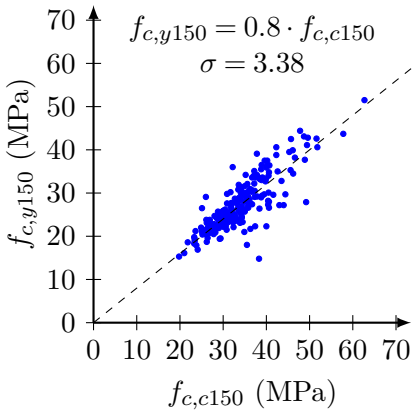

Figure 4.9: Transformation model from standard cubes to standard cylinders.

2. Secondly, into the potential strength f_c by removing the scale effects. Kim *et al.* (1999) proposes an expression for the estimation of the strength, in terms of the dimensions of cylindric specimens, concluding that the potential strength tends to 80% of the laboratory reference strength, $f_{c0} = f_{c,y150}$. Moreover, Kim *et al.* (1999)

states that, since the strength of the concrete is mostly dependent on the cement content, the effect of the MSA is negligible within the practical range of size. Thus, the expected value of the transformation model proposed (Figure 4.10a), can be given, independently of the MSA, by,

$$E\left(f_c\left(h,\Phi\right)|f_c\left(h_i,\Phi_i\right)\right)=\frac{0.8\cdot\left(1-X\left(h,\Phi\right)\right)+X\left(h,\Phi\right)}{0.8\cdot\left(1-X\left(h_i,\Phi_i\right)\right)+X\left(h_i,\Phi_i\right)}\cdot f_c\left(h_i,\Phi_i\right) \tag{4.25}$$

where h and Φ are the specimen height and diameter ($h/\Phi=\infty$ to potential structural properties), in millimeters, h_i and Φ_i are the height and diameter of the specimen i and X is given by,

$$X\left(h,\Phi\right)=\frac{2}{\sqrt{1+\left(h-\Phi\right)/50}} \tag{4.26}$$

The variation can be estimated by comparing the compressive strength measured in full-mixed concrete specimens $f_{c,y450}$, to the calculated from wet-screened concrete specimens $f_{c0}=f_{c,y150}$, shown in Figure 4.10b. The variation can then be given by,

$$V\left(f_c\left(h,\Phi\right)|f_c\left(h_i,\Phi_i\right)\right)=5.22^2 \tag{4.27}$$

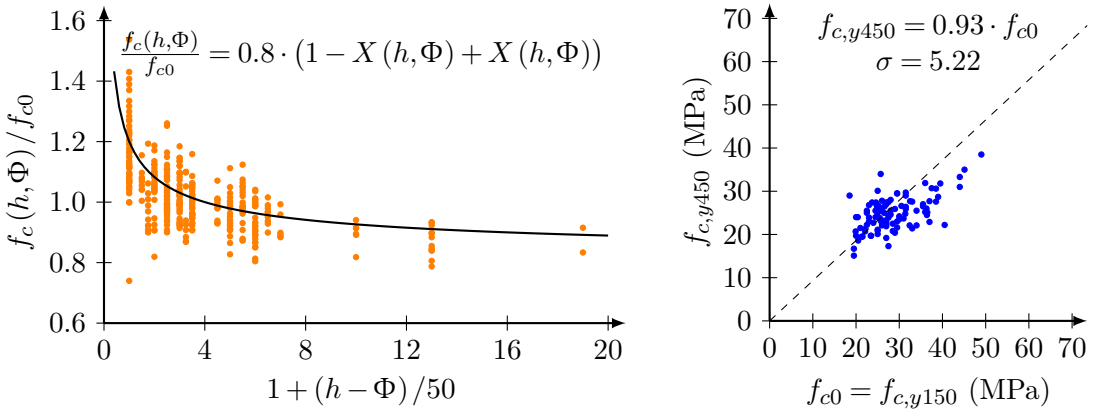

(a) Size effects (Kim *et al.* 1999)

(b) Laboratory tests

Figure 4.10: Transformation model from cylindric compressive strength to the potential compressive strength.

The transformation models, obtained preferentially from the available results, shall allow the estimation of the mechanical properties, from the results on laboratory tests,

and the associated model uncertainty.

Young's modulus

The Young's modulus, being estimated from the early specimen response in strength tests, does not depend on the failure mechanism and, consequently, on the specimen geometry and loading conditions. Although the concrete deformability is mostly dependent on the aggregates, the modeling of the effect of wet-screening (Serra *et al.* 2016) is complex for the detail required. By simplicity, it is considered that the concrete Young's modulus does not depend on neither the specimen dimensions nor its composition and can be estimated directly from the strength obtained in flexural tensile, splitting tensile or compression tests.

On the other hand, when predicting the Young's modulus based on the concrete compressive strength, the compressive strength must be transformed, according to the models presented. Figure 4.11 illustrates the procedure to obtain prediction models for the Young's modulus.

Although exponential laws are usually considered for the relation between compressive strength and other mechanical properties, in the range of values available, linear relations are not inappropriate. Thus, from the weighted least square regression, the expected value and variance of the Young's modulus E_c are, respectively, given by,

$$E\left(E_c|f_c\right) = 19.37 + 0.39 \cdot f_c \tag{4.28}$$

$$V\left(E_c|f_c\right) = 18.71^2 \tag{4.29}$$

The absolute (unconditional) expected value and variance of the Young's modulus are, respectively, given by,

$$E\left(E_c\right) = E\left(E\left(E_c|f_c\right)\right) = E\left(19.37 + 0.39 \cdot f_c\right) = 19.37 + 0.39 \cdot E\left(f_c\right) \tag{4.30}$$

$$\begin{aligned} V\left(E_c\right) &= V\left(E\left(E_c|f_c\right)\right) + E\left(V\left(E_c|f_c\right)\right) = V\left(19.37 + 0.39 \cdot f_c\right) + V\left(E_c|f_c\right) \\ &= 0.39^2 \cdot V\left(f_c\right) + 18.71^2 \end{aligned} \tag{4.31}$$

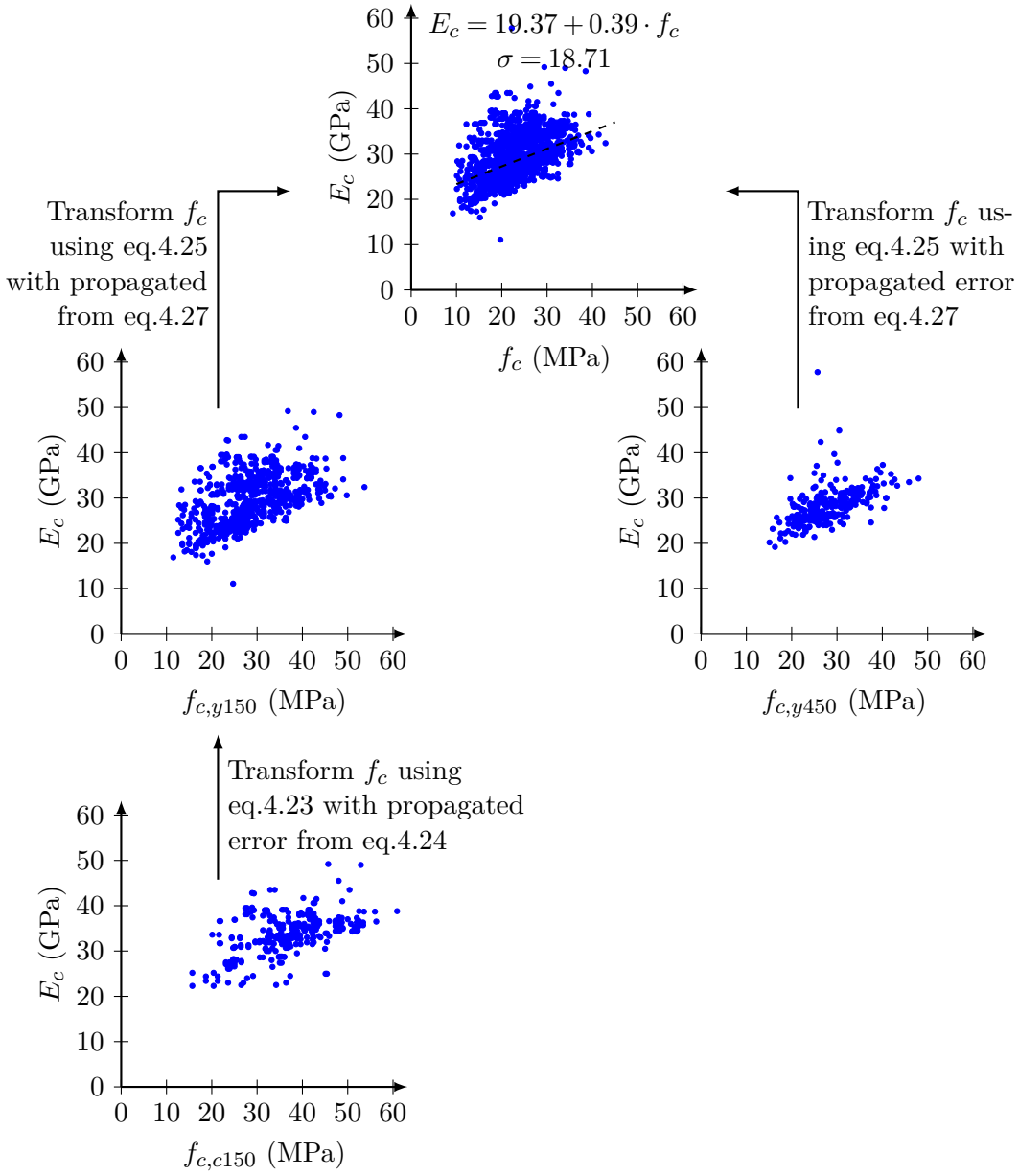

Figure 4.11: Illustrative scheme from data treatment to Young's modulus regression model.

Tensile strength

The tensile strength is obtained directly from direct tensile tests on cylindric specimens or, indirectly, from splitting or flexural tests on cylinders or prisms, respectively. Therefore, results from laboratory tests must be consecutively transformed:

1. Firstly, into the equivalent direct strength of cylindric specimens of standard dimensions and geometry (cylinders with h=300 mm and Φ=150 mm, $f_{t,y150}$, for the wet-screened concrete or with h=900 mm and Φ=450 mm, $f_{t,y450}$, for the full-mixed

concrete). From the flexural strength f_f, obtained in prismatic specimens, the direct tensile strength can be estimated by (Coutinho and Gonçalves 1994),

$$E\left(f_t|f_f\left(h\right)\right) = \frac{0.06 \cdot h^{0.7}}{1 + 0.06 \cdot h^{0.7}} \cdot f_f\left(h\right) \tag{4.32}$$

with a coefficient of variation of 6%, i.e.,

$$V\left(f_t|f_f\left(h\right)\right) = \left(0.06 \cdot \frac{0.06 \cdot h^{0.7}}{1 + 0.06 \cdot h^{0.7}} \cdot f_f\left(h\right)\right)^2 \tag{4.33}$$

where h is the height of the prisms, in mm.

From the splitting strength, f_s, the direct tensile strength can be estimated by (Coutinho and Gonçalves 1994),

$$E\left(f_t|f_s\right) = f_s \tag{4.34}$$

with a coefficient of variation of 5%, i.e.,

$$V\left(f_t|f_s\left(h\right)\right) = \left(0.05 \cdot f_s\right)^2 \tag{4.35}$$

2. Secondly, into the potential tensile strength f_t by removing the scale effects. Similarly to the compressive strength, the relation proposed by Kim *et al.* (1999), given in equation 4.25, can be used to remove the scale effects of the tensile strength obtained in cylindric specimens (4.12a). The variation, can be estimated by comparing the tensile strength measured in full-mixed concrete specimens, $f_{t,y450}$, to the calculated from wet-screened concrete specimens, $f_{t0} = f_{t,y150}$, shown in Figure 4.12b. The variation can then be given by,

$$V\left(f_t\left(h,\Phi\right)|f_t\left(h_i,\Phi_i\right)\right) = 0.46^2 \tag{4.36}$$

Figure 4.13 illustrates the procedure to obtain the prediction model for the tensile strength.

From the weighted least square regression, the expected value of the tensile strength

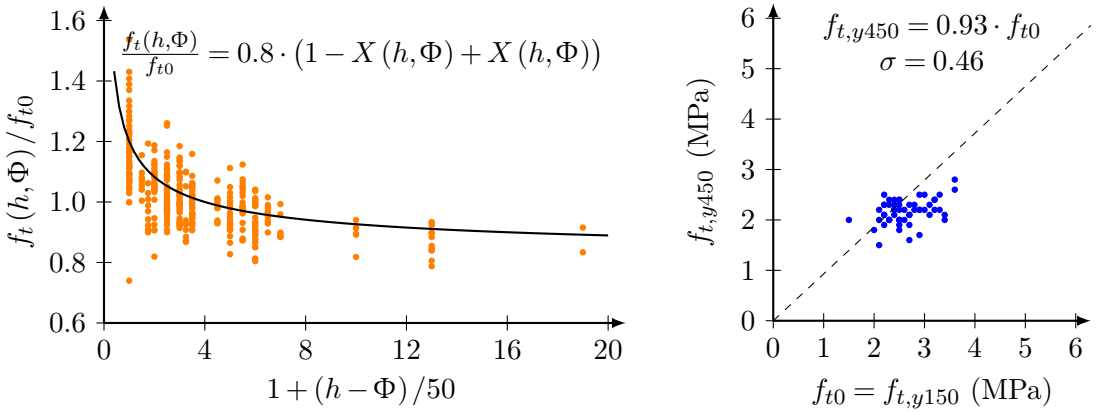

(a) Size effects (Kim *et al.* 1999)

(b) Laboratory tests

Figure 4.12: Transformation model from cylindric tensile strength to the potential tensile strength.

f_t is given by,

$$E(f_t|f_c) = 0.10 \cdot f_c \tag{4.37}$$

Given the increasing residuals as the compressive strength increases, the model error (through variance) is advantageously given by a coefficient of variation which was found to be approximately 25%. Therefore, the variance of the tensile strength f_t is given by

$$V(f_t|f_c) = (0.25 \cdot 0.10 \cdot f_c)^2 \tag{4.38}$$

The absolute (unconditional) expected value and variance of the Young's modulus are, respectively, given by,

$$E(f_t) = E\left(E(f_t|f_c)\right) = E(0.10 \cdot f_c) = 0.10 \cdot E(f_c) \tag{4.39}$$

$$\begin{aligned} V(f_t) &= V\left(E(f_t|f_c)\right) + E\left(V(f_t|f_c)\right) = V(0.10 \cdot f_c) + V(f_t|f_c) \\ &= 0.10^2 \cdot V(f_c) + 0.25^2 \cdot E\left(f_c^2\right) = \left(0.10^2 + 0.25^2\right) \cdot V(f_c) + 0.25^2 \cdot E(f_c)^2 \end{aligned} \tag{4.40}$$

4.3.2.3 Structural properties

The concrete placing and hardening conditions are influenced by different factors, namely the formwork preparation, the cleaning of the joints, the construction scheduling process, the utilization of cooling coils and the heat generation from cement hydration. From the visual inspection of the conditions of the dam downstream face and gallery, where the

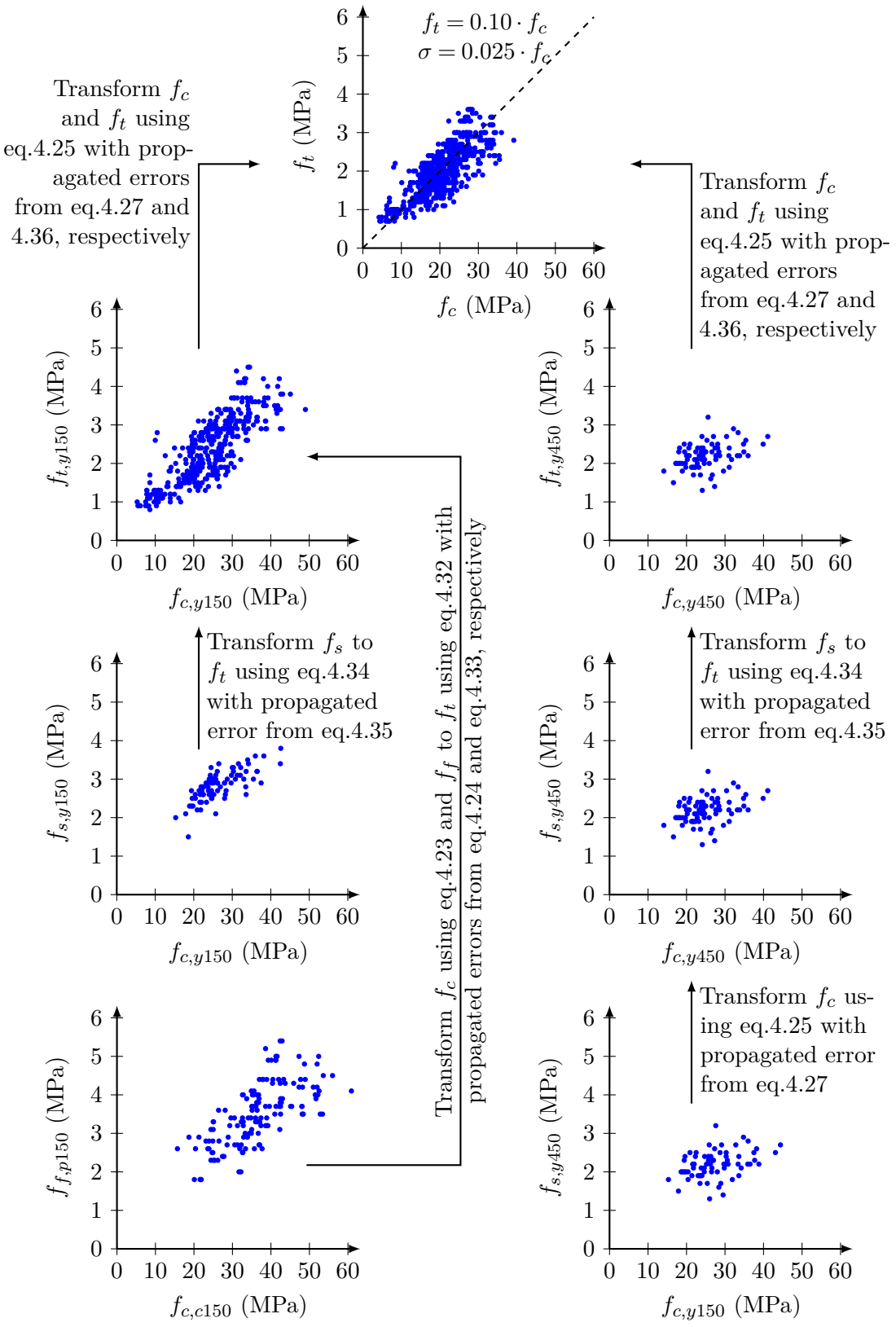

Figure 4.13: Illustrative scheme from data treatment to tensile strength regression model.

effects of most construction defects are visible, the construction quality can be roughly estimated. These conditions usually vary from a compact and homogeneous aspect to severely altered aspect associated with water transfers.

In view of these circumstances, an empirical classification of the construction quality, from the visual inspection, is proposed. Table 4.6 presents the referred classification, in terms of structural acceptability.

Table 4.6: Concrete conditions from visual inspection and corresponding classification in terms of structural acceptability.

Concrete condition	Classification
Homogeneous, the link between batches is perfect, the concrete joints are imperceptible	Excellent
Almost homogeneous, there are a small number of poor links between batches through which small water transfers plugged	Very good
Almost homogeneous, there are some poor links between batches, including a reduced subset through which small permanent water transfers were observed	Good
Less homogeneous, there are a significant number of poor links between batches, including a high percentage (up to 5%) through which small permanent water transfers were observed	Satisfactory

The characterization of the concrete mechanical properties, during the dam operation, can be made: i) directly, through laboratory tests on samples cut from the dam (strength and deformability); or ii) indirectly, through ultra-sound and forced vibration tests (only deformability).

While, given the structural dimensions, the number of samples cut from the dam is usually small, ultra-sound and forced vibration tests can provide valuable information regarding the global deformability of the structure.

The quantification of the construction quality factor γ_{cq}, representing the overall integrity conditions of the structure, can be initially made by comparing the average potential Young's modulus (E_p), obtained in laboratory tests, to the average one considered in structural modeling (E_m) in order to interpret properly the observed behavior during the reservoir filling and first operation period. The cases in which both results are available (Catapereiro, Pedrógão, Pretarouca, Baixo Sabor and Ribeiradio dams), are presented in Table 4.7.

Besides the small number of dams with available results, three extreme cases are included in this group, specifically the Ribeiradio dam with excellent construction quality,

Table 4.7: Comparison between the average potential Young's modulus and the one considered in structural modeling.

Dam	E_p (GPa)	E_m (GPa)	E_m/E_p
Baixo Sabor	28	27	0.96
Catapereiro	33	28	0.85
Pedrógão	29	25	0.86
Pretarouca	33	30	0.91
Ribeiradio	29	28	0.97

and Catapereiro and Pedrógão dams in which the construction quality is satisfactory. For the first, there are a significant number of construction joints that have a poor link between batches. The second is the first RCC dam built in Portugal.

Given the reduced information available, the quantification of the construction quality factor can be alternatively made by assigning values according to the visual conditions of several dams. These values were limited between 0.85 and 1.00. The proposal for the compressive, tensile and shear strength reduction, the corresponding construction quality coefficient according to the classification made in terms of structural acceptability, and the number of dams assigned, is presented in Table 4.8.

Table 4.8: Strength reduction and construction quality factor in terms of the structural classification.

Classification	Dams	Strength reduction			γ_{cq}
		Compressive	Shear	Tension	
Excellent	16	1.00	1.00	1.00	1.00
Very good	28	1.00	0.95	0.90	0.95
Good	8	1.00	0.90	0.80	0.90
Satisfactory	1	1.00	0.85	0.70	0.85

The values proposed for the strength reduction, which shall be understood as a portion of the strength of a concrete in good conditions, are based on the practical experience of the Materials Department of LNEC from the tests performed on cores drilled from concrete lift joints of existent dams (LNEC 2007; LNEC 2014). Thus, since the structural acceptability criteria are fulfilled, it is considered that:

- The compressive strength is not affected;
- Due to imperfect links between batches, the tensile strength may be reduced up to

70% of a concrete in good conditions;

- Since it is less affected by imperfect links between batches, the shear strength may be reduced up to 85% of a concrete in good conditions, corresponding to an average value between the compressive and tensile strengths.

Since the dam structural failure often occurs by shear and the dam design aims at eliminating the tensile stresses, the construction quality coefficients proposed are identical to the shear strength reduction.

Based on the classification of 53 Portuguese large concrete dams, for the construction quality factor γ_{cq}, which shall multiply any potential mechanical property, a normal distribution with mean value of 0.959 and standard deviation of 0.037 truncated at 0.85 (worse cases may not ensure safe operation conditions and need repair works before the dam entry into operation) and 1.00 (optimal concrete condition), is proposed.

4.3.3 Concrete-rock interface shear strength

According to the Portuguese dam safety regulation (RSB 2018), for failure scenarios, residual values of the friction component and zero cohesion shall be considered, based on the simplification proposed by Underwood and Dixon (1976).

To generalize the shear strength parameters of the concrete-rock interface, the Chinese standards (GB50199 1994) indicate standard values, based on testing results of similar projects, that could be adopted for the dam design. The approach behind these standard values is to cover all realistic situations regarding the shear strength capacity of the concrete-rock interface, in a conservative point of view. The mean value (μ) and the coefficient of variation (σ/μ) of the friction coefficient, grouped into three rock mass classes associated with the rock mass properties, such as the uniaxial compressive strength R_b, the p-wave velocity v_p and the Young's modulus E_r, are shown in Table 4.9.

Considering that the mean value (μ) of the friction coefficient follows an uniform distribution, since no further information is proposed (GB50199 1994), within the range of values recommended for each rock mass class, the expected value and variance of the friction coefficient, using the law of total expectation (equation 4.12) and the law of total variance (equation 4.13), are, respectively, given by,

$$E\left(\tan\phi\right) = E\Big(E\left(\tan\phi|\mu\right)\Big) = E\left(\mu\right) \tag{4.41}$$

Table 4.9: Standard values of the friction coefficient of concrete-rock interface according to the Chinese standards (GB50199 1994).

Rock mass class	Rock mass properties	Variation range of rock mass mechanical properties	Shear strength parameter ($\tan\phi$)	
			μ	σ/μ
I	Dense and sound rock mass. Distance between cracks > 1.0 m. (e.g., magnetic, volcanic, abysmal and massive thick layer sedimentary rock).	$R_b > 100$ MPa $v_p > 5000$ m/s $E_r > 20$ GPa	$1.30 - 1.50$	20%
II	Sound and weakly weathered massive rock. Distance between cracks $0.5 - 1.0$ m. The rock mass is stable except in few local areas (e.g., thick-layer sandstone, conglomerate, limestone without resorption, dolomite, quartzite, pyroclastic, rock).	$60 < R_b < 100$ MPa $4000 < v_p < 5000$ m/s $10 < E_r < 20$ GPa	$1.10 - 1.30$	20%
III	Medium-sound and weakly weathered massive rock, poor completeness and cyclopean structure. Distance between cracks $0.3 - 0.5$ m.	$30 < R_b < 60$ MPa $3000 < v_p < 4000$ m/s $5 < E_r < 10$ GPa	$0.90 - 1.10$	20%

$$\begin{aligned} V(\tan\phi) &= V\left(E(\tan\phi|\mu)\right) + E\left(V(\tan\phi|\mu)\right) = V(\mu) + E\left(0.2^2 \cdot \mu^2\right) \\ &= V(\mu) + 0.2^2 \cdot E\left(\mu^2\right) = V(\mu) + 0.2^2 \cdot \left(V(\mu) + E(\mu)^2\right) \end{aligned} \tag{4.42}$$

where, from Table 2.1, $E(\mu)$ and $V(\mu)$ are, respectively, given by,

$$E(\mu) = \frac{a+b}{2} \tag{4.43}$$

$$V(\mu) = \frac{(b-a)^2}{12} \tag{4.44}$$

where a and b are the lower and upper limits of the uniform distribution, respectively.

Table 4.10 synthesizes the probability distribution properties for the residual friction coefficient, considering a lognormal distribution, as recommended in the Eurocodes (EN1990 2002) for material physical properties.

Table 4.10: Distribution properties for the residual friction coefficient $\tan\phi$.

Rock mass class	Distribution	E	V
I	Lognormal	1.40	0.082
II	Lognormal	1.20	0.061
III	Lognormal	1.00	0.043

4.4 Model uncertainties

4.4.1 General considerations

The consideration of models, given in terms of random variables, contains inaccuracies due to the simplification inherent in their mathematical formulation, that shall be considered in reliability analysis.

In the following sections, the uncertainties introduced by the seismic load models, the Mohr-Coulomb shear criteria and the rigid body formulation of the stability problem are addressed.

4.4.2 Seismic load models

4.4.2.1 General considerations

The consideration of either the pseudo-static or the pseudo-dynamic (Fenves and Chopra 1986) seismic load models for the stability analysis results in approximations of the real structure response, which can only be alternatively assessed using numerical models capable of simulating both the structure dynamic behavior and the seismic excitation.

Since information on those approximations is lacking, simple numerical models can be used to compare the analytical solution of the stability problem considering either the pseudo-static or the pseudo-dynamic seismic load models and the seismic response of the corresponding numerical models varying, on one hand, the seismic loading according to the response spectrum of each seismic type and zone, and, on the other hand, the geometrical characteristics and other loading conditions of the structure.

In the following sections, the time-history loading and the numerical models are presented. Lastly, the relevant results are analyzed and the model uncertainty is quantified.

4.4.2.2 Time-history loading

For analyzing the variability of the seismic loading, accelerograms, describing the ground acceleration over time, are considered to represent the seismic excitation, since the structural non-linear behavior can only be estimated through time-history analysis. Artificial accelerograms can be generated according to the characteristics expected for the local seismology. Thus, the variation of the seismic loading is taken from 10 artificial accelerograms (Carvalho 2007), generated in consistency with the Lisbon seismology. As for rock (type A) foundations, the unitary acceleration response spectrum does not vary with the seismic zone (the soil coefficient S is independent of the ground acceleration), the accelerograms can just be scaled to represent the remain seismic zones. The unitary accelerograms are shown in Figures 4.14 and 4.15, for seismic action type 1 and 2, respectively.

To verify its suitability according to the seismic zonation, the response spectra of the artificial accelerograms were compared to the regulatory spectrum (Figure 3.15). Figure 4.16 shows the adequability of the response spectra, obtained through the Duhamel's integral, which represent the response of single degree-of-freedom oscillators to time-varying excitations.

The accelerograms fulfill the regulatory rules (EN1998 2004), since the mean of the spectral response acceleration (gray line): i) is not smaller, at zero period, than the value of $a_g \cdot S$; and ii) is not smaller than 90% of the corresponding value of the response spectrum (black dashed line), in the range of periods between $0.2 \cdot T_1$ and $2.0 \cdot T_1$, where T_1 is the fundamental period of the structure in the direction where the accelerogram will be applied.

4.4.2.3 Numerical models

Discrete-element models (appendix C), with flexible block for the dam and rigid blocks for the foundation, of a 100 meter high gravity profile were analyzed for 100 combinations of geometry, loads and material properties, varying randomly: i) the downstream face slope (s_d) between 0.75 and 1.00; ii) the reservoir water level (H_r) between 50% and 100% of the dam height; iii) the uplift factor (k_u) between 0.10 and 0.70; and iv) the concrete Young's modulus (E_c) between the discrete values in which pseudo-dynamic analysis is set: 6.9, 13.8, 17.3, 20.7, 24.1, 27.6, 31.0 and 34.5 GPa.

The dynamic loads, due to seismic actions, are given by velocity histories applied to

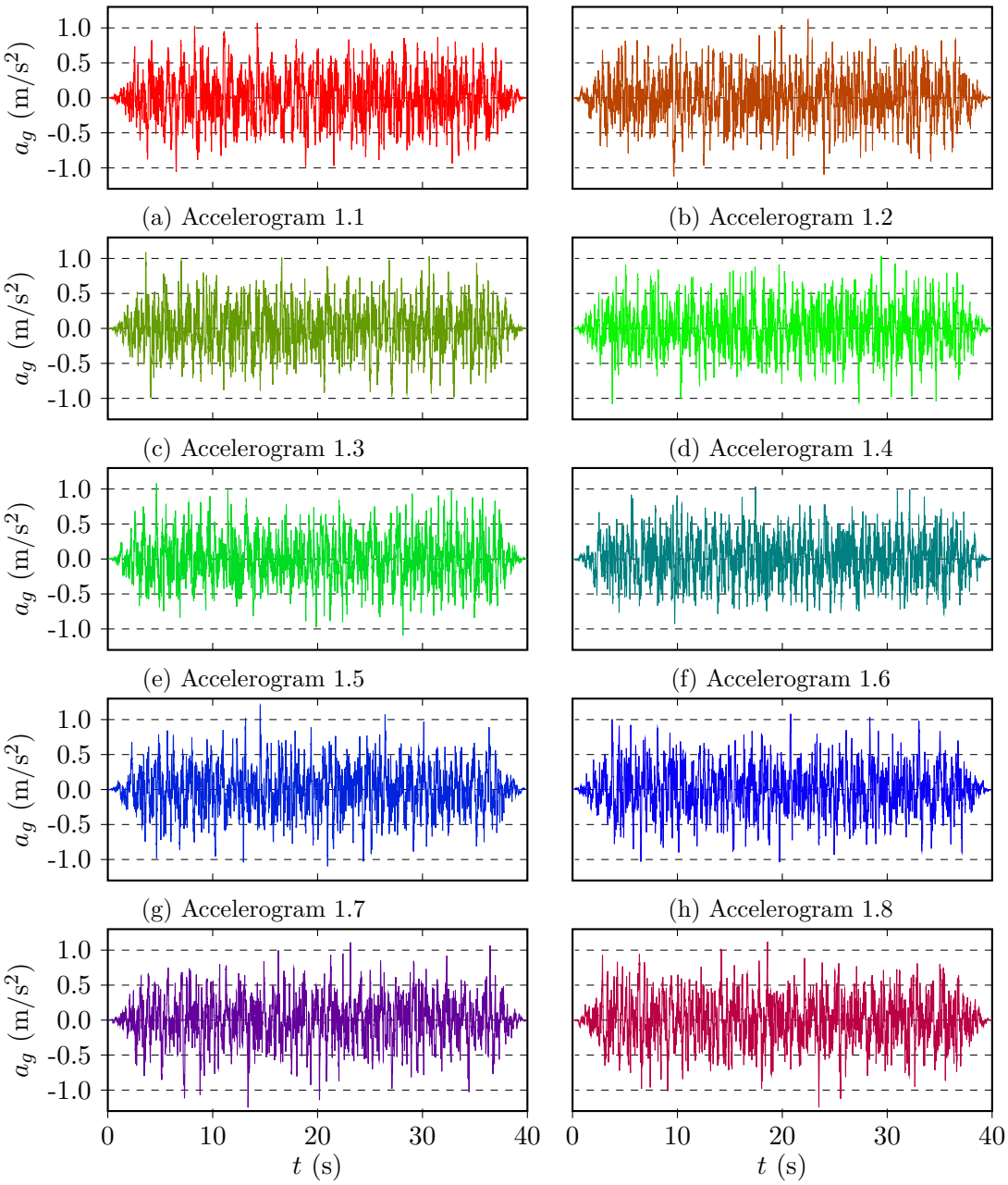

(a) Accelerogram 1.1

(b) Accelerogram 1.2

(c) Accelerogram 1.3

(d) Accelerogram 1.4

(e) Accelerogram 1.5

(f) Accelerogram 1.6

(g) Accelerogram 1.7

(h) Accelerogram 1.8

(i) Accelerogram 1.9

(j) Accelerogram 1.10

Figure 4.14: Artificial (unitary) accelerograms for seismic action type 1.

the rock foundation block, obtained by numerical integration of the accelerograms. For different seismic zones, the unitary accelerograms (Figures 4.14 and 4.15) were directly scaled, according to the respective design acceleration, given in Table 3.3. For the vertical component, velocity histories corresponding to 30% of the horizontal ones were also applied.

For the inclusion of the dynamic dam-reservoir interaction, a simplified representation of the reservoir by an elastic block with very low shear modulus can be used (Lemos

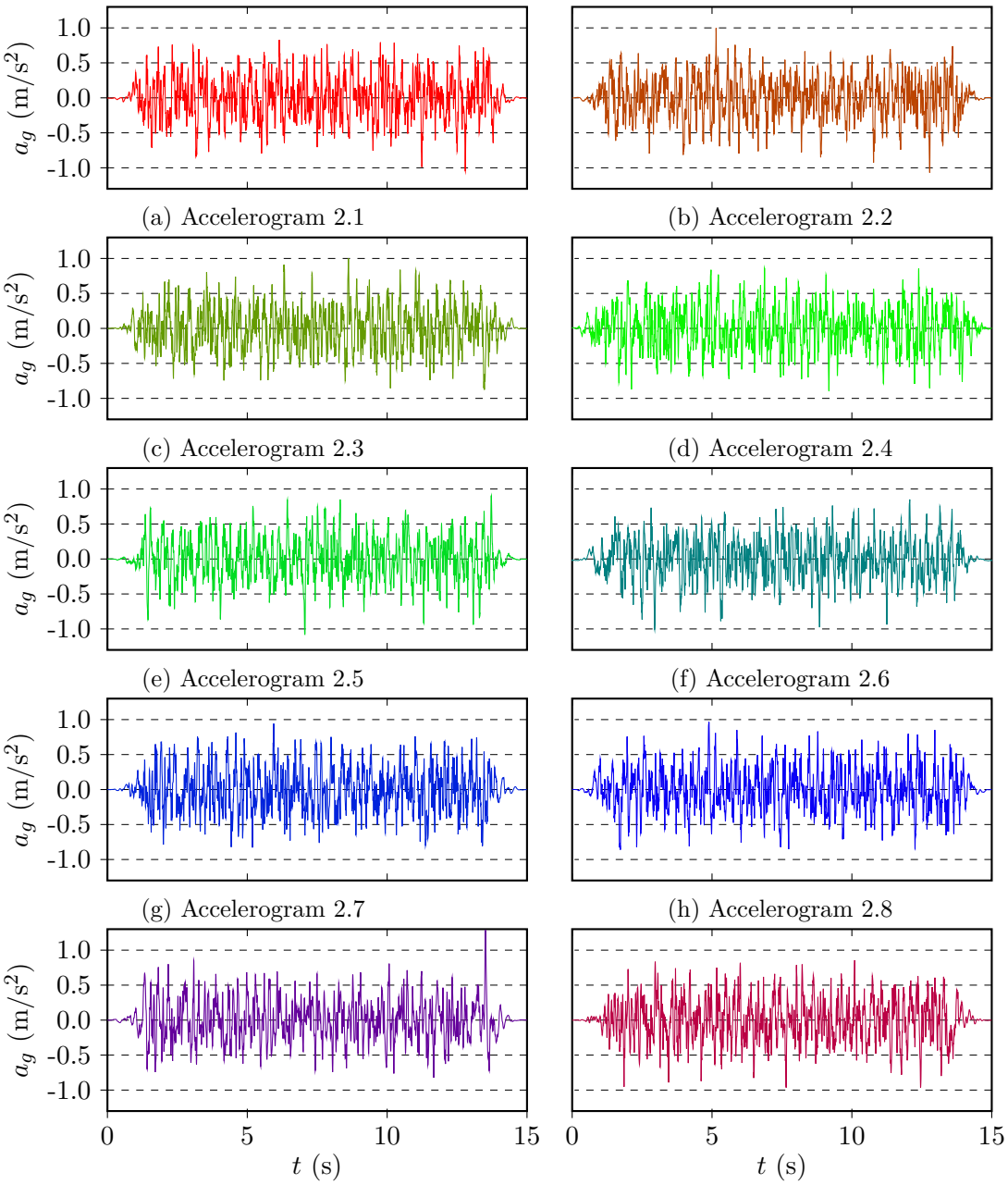

(a) Accelerogram 2.1

(b) Accelerogram 2.2

(c) Accelerogram 2.3

(d) Accelerogram 2.4

(e) Accelerogram 2.5

(f) Accelerogram 2.6

(g) Accelerogram 2.7

(h) Accelerogram 2.8

(i) Accelerogram 2.9

(j) Accelerogram 2.10

Figure 4.15: Artificial (unitary) accelerograms for seismic action type 2.

1987), allowing the separation of the fluid from the dam face, and quiet boundaries can be attached to the far end of the reservoir. However, in many practical applications, an approximate representation of the reservoir effects by means of the added mass concept, based on Westergaard's theory (Westergaard 1933), is sufficient. Thus, extra masses are added to the gridpoints on the dam upstream face, quantified according to the solution for the dynamic forces that an incompressible fluid exerts on a moving vertical wall.

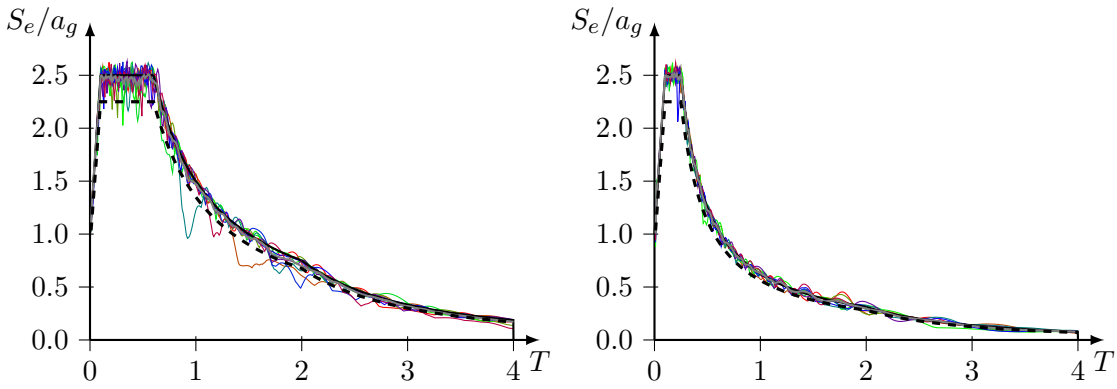

(a) Seismic action type 1.

(b) Seismic action type 2.

Figure 4.16: Response spectrum, obtained from the accelerograms, and regulatory spectrum according to the NP EN1998-1 (2010).

A schematic representation of the discrete-element model is shown in Figure 4.17.

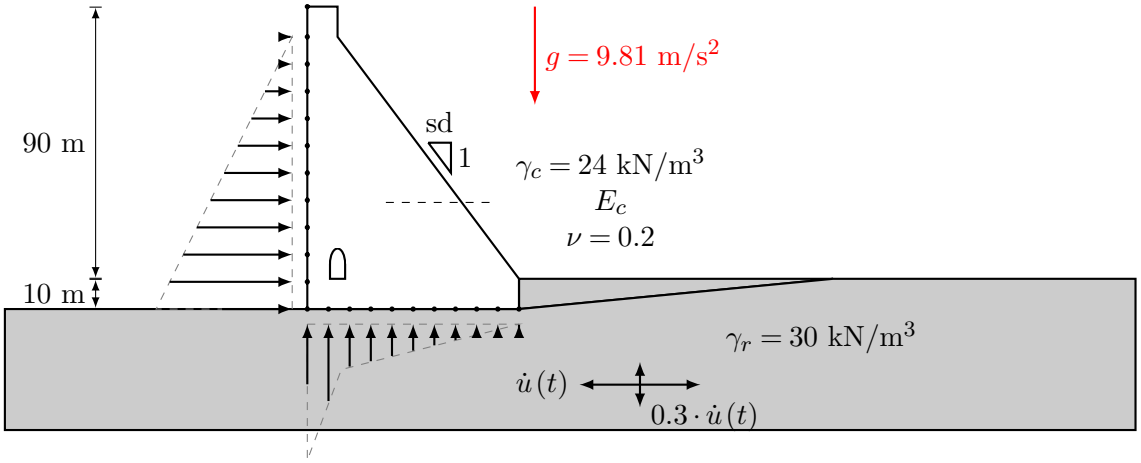

Figure 4.17: Schematic representation of the numerical models analyzed.

Each dynamic analysis, using the UDEC software (Itasca 2011) and considering a Rayleigh damping of 5%, took approximately 5 minutes, for seismic actions type 1, and 2 minutes, for seismic actions type 2, since 40-seconds and 15-seconds accelerograms, respectively, were used.

The desired numerical solution is obtained using a root-finding procedure, based on the Brent's method (section D.3.7 of the appendix D), which, varying judiciously the friction angle, finds the value resulting in a residual displacement of the dam heel (d_t) of 38 mm, since it is considered that residual displacements beyond half diameter of the drains would represent the disruption of the drainage system, leading to structural failure caused by excessive uplift pressures installed. For each seismic zone, this procedure was repeated for

1000 cases (100 combinations of geometry and loads for each of 10 velocity histories).

The root-finding procedure was not always successful since, in some cases, the wide initial interval for the friction angle did not lead to opposite sign roots. This was more prominent for seismic zones with higher ground acceleration since two undesired phenomena may occur more frequently: i) overturning; or ii) rocking, which does not allow the convergence of the procedure based on the residual displacement of the dam heel. Those cases were disregarded. Table 4.11 shows the number of successful root-finding procedures used later as observations for the uncertainty quantification.

Table 4.11: Number of successful root-finding procedures.

Seismic	Seismic type	
zone	1	2
1	296	654
2	458	759
3	704	858
4	892	947
5	935	954
6	942	-

As an example, Figure 4.18 shows the displacement history during the dynamic analysis, considering the Accelerogram 1.5 for the seismic zone 1.3 ($a_g = 2.46$ (m/s^2) for a return period of 1000 years), of a model characterized by: i) downstream face slope of 1.00; ii) reservoir water level at 96% of the dam height; iii) uplift factor of 0.42; iv) concrete Young's modulus of 27.6 GPa; and v) friction angle of 33.7°, which results in a residual displacement of 38 mm, approximately.

4.4.2.4 Results analysis and uncertainty quantification

As referred in section 2.3.4, the model uncertainties, which shall be considered as random variables to account for the neglected information in the simplified formulation, can be given by the relation between the real and the empirical model.

In this case, it is considered that each observation of the model uncertainty θ_e is obtained by solving the following equality, for each case,

$$\phi_c^a\left(\theta_e \cdot a_g\right) = \phi_c^n\left(a_g\right) \tag{4.45}$$

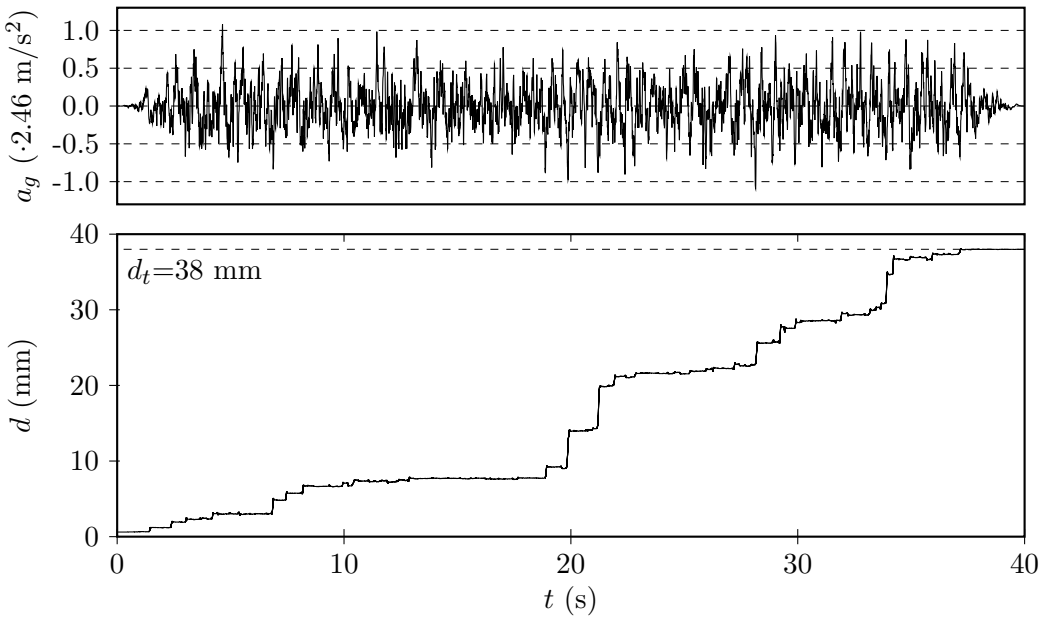

Figure 4.18: Example of the displacement history obtained for a load case which resulted in a residual displacement of 38 mm.

where $\phi_c^a(\theta_e \cdot a_g)$ is the analytical solution of the stability problem, given by the conditioning sliding failure mode (from equations 3.38, 3.39 or 3.40), considering a ground acceleration a_g multiplied by the model uncertainty θ_e, and ϕ_c^n is the corresponding numerical solution, considering an unitary accelerogram scaled to a_g.

Figures 4.19 and 4.20 show the histograms of the model uncertainty, θ_e, for each seismic zone, considering the pseudo-static and the pseudo-dynamic seismic load models, respectively.

For the samples $\hat{\boldsymbol{x}}$ obtained for each seismic zone, considering either load models, two non-negative probability distributions (lognormal and Weibull) were adjusted by the MLE method and compared. The best distribution to model this variable is the one resulting in the highest likelihood (equations 2.4 or 2.5). Naturally, in left-skewed samples the lognormal distribution fits better, whereas, in right-skewed samples, the Weibull distribution fits better. Table 4.12 presents the estimated distribution moments.

The following aspects are concluded from these results:

- As expected, greater peak accelerations lead to greater standard deviation of the model uncertainties;
- Pseudo-dynamic seismic load model results, in average, in an overestimation, for seismic actions type 1, and a good approximation of the analytical solution, for

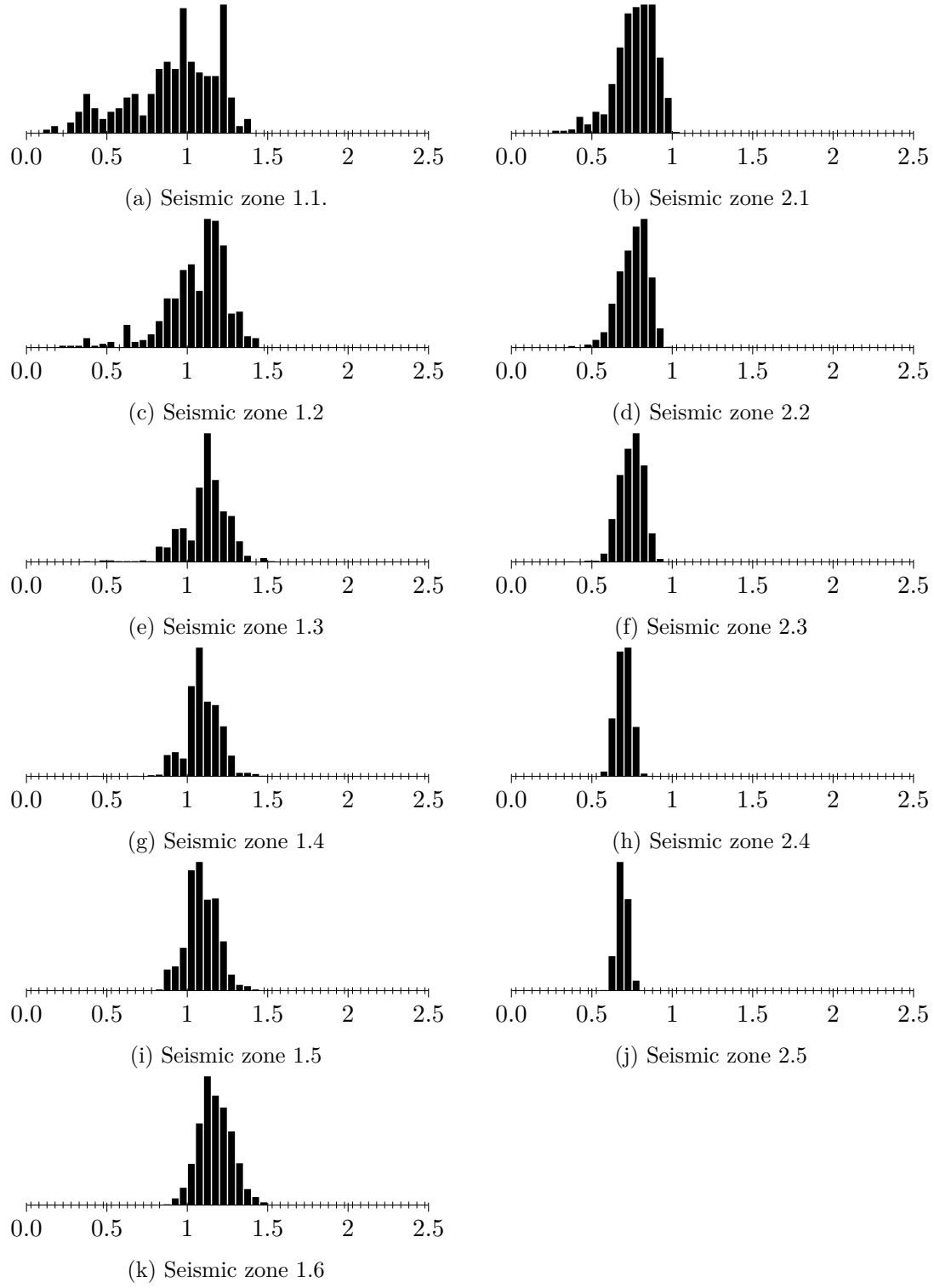

(a) Seismic zone 1.1.

(b) Seismic zone 2.1

(c) Seismic zone 1.2

(d) Seismic zone 2.2

(e) Seismic zone 1.3

(f) Seismic zone 2.3

(g) Seismic zone 1.4

(h) Seismic zone 2.4

(i) Seismic zone 1.5

(j) Seismic zone 2.5

(k) Seismic zone 1.6

Figure 4.19: Histograms of the model uncertainty variable, θ_e, considering the pseudo-static seismic load model.

seismic actions type 2;

- Pseudo-static seismic load model results, in average, in a good approximation for

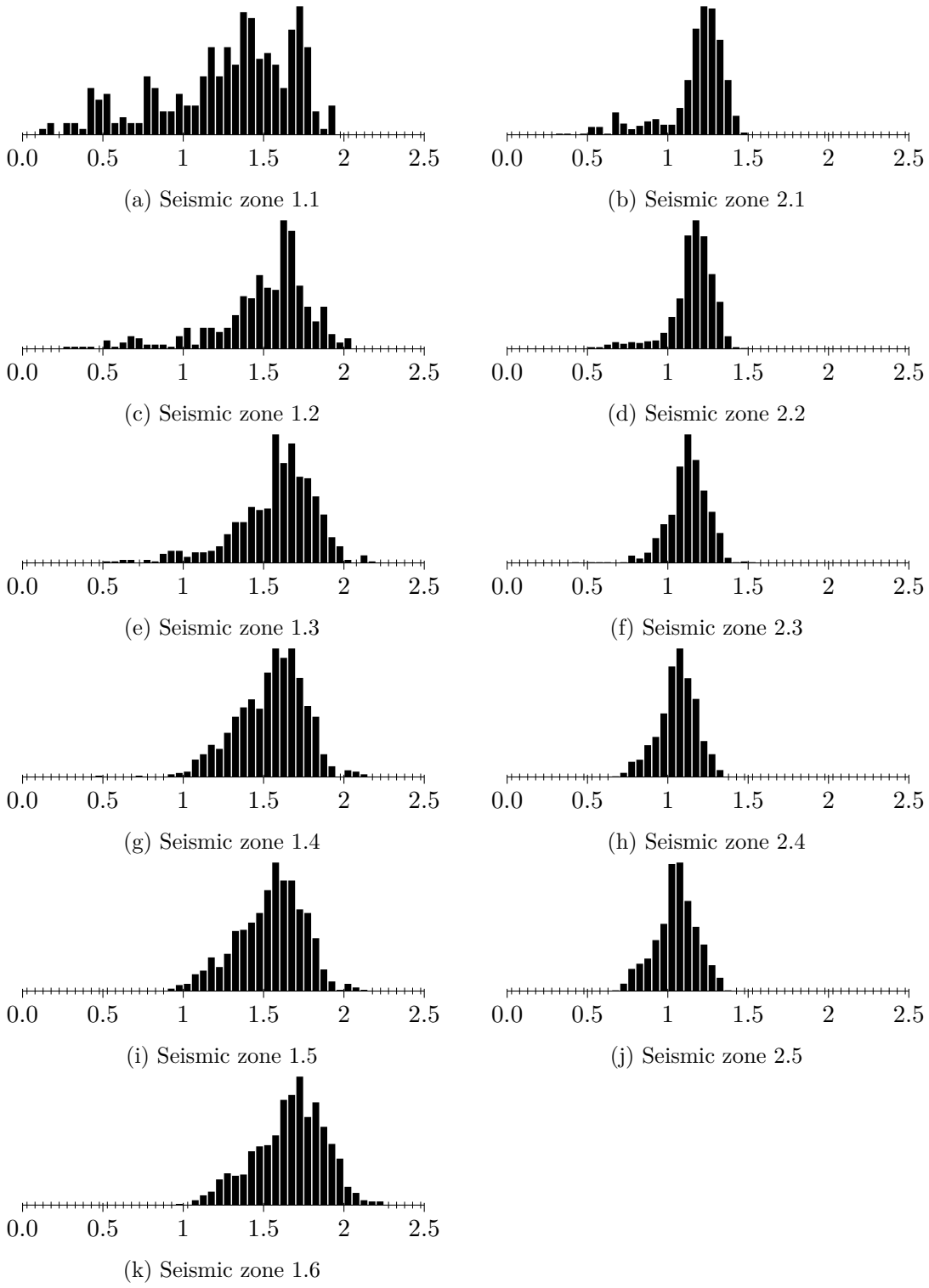

(a) Seismic zone 1.1

(b) Seismic zone 2.1

(c) Seismic zone 1.2

(d) Seismic zone 2.2

(e) Seismic zone 1.3

(f) Seismic zone 2.3

(g) Seismic zone 1.4

(h) Seismic zone 2.4

(i) Seismic zone 1.5

(j) Seismic zone 2.5

(k) Seismic zone 1.6

Figure 4.20: Histograms of the model uncertainty variable, θ_e, considering the pseudo-dynamic seismic load model.

seismic actions type 1, and an underestimation of the analytical solution for seismic actions type 2;

Table 4.12: Distribution moments of the model uncertainty associated with the pseudo-static and pseudo-dynamic load models.

Seismic zone	Pseuto-static model				Pseudo-dynamic model			
	E	V	Log-likelihood		E	V	Log-likelihood	
			LN	W			LN	W
1.1	0.91	0.0677	-100.55	**-36.75**	1.27	0.1519	-231.18	**-158.66**
1.2	1.06	0.0328	-13.51	**117.04**	1.50	0.0765	-233.07	**-86.48**
1.3	1.11	0.0201	305.05	**405.98**	1.57	0.0569	-130.07	**8.69**
1.4	1.09	0.0123	**701.32**	696.69	1.54	0.0467	61.59	**135.34**
1.5	1.09	0.0099	**837.87**	781.21	1.54	0.0452	106.50	**158.79**
1.6	1.17	0.0103	**825.16**	763.32	1.66	0.0500	59.80	**111.18**
2.1	0.77	0.0146	341.59	**452.41**	1.18	0.0257	0.76	**222.76**
2.2	0.76	0.0082	709.00	**771.72**	1.15	0.0159	309.08	**496.71**
2.3	0.74	0.0059	993.86	**1030.41**	1.12	0.0165	515.54	**596.81**
2.4	0.70	0.0022	**1562.40**	1536.54	1.06	0.0151	654.75	**692.77**
2.5	0.69	0.0012	**1851.83**	1806.08	1.05	0.0182	586.97	**609.07**

- For seismic actions type 2, both analytical models show lower standard deviation than for seismic actions type 1;
- Pseudo-static load model has lower standard deviation than pseudo-dynamic load model, for all seismic zones.

Unexpectedly, the pseudo-dynamic load model presents a greater bias (or standard deviation) than the simpler pseudo-static load model. This is probably due to the inadequacy of the first to model the seismic loads for large displacement analysis, as it was developed for the elastic (and therefore non-limit) analysis.

The load duration also plays, apparently, an important role in the precision of the stability solution using analytical seismic load models. Actually, the cumulative displacement is developed by small increments due to the instantaneous acceleration exceeding the critical acceleration. As the duration of seismic action increases, the number of acceleration peaks that exceed the critical acceleration will probably increase, leading to a greater residual displacement. Thus, even for the same peak acceleration, longer dynamic excitations result in greater residual displacement.

4.4.3 Mohr-Coulomb shear strength model

Although the shear envelope is recognizedly non-linear (Nicholson 1983), the linear Mohr-Coulomb failure criteria is a simple model usually considered in stability analysis problems. Regarding the uncertainty related to this assumption, Krounis *et al.* (2015) proposed bias up to 40% of the mean strength due particularly to the spatial variation of the cohesion. On the other hand, JCSS (2001) proposed the consideration of a lognormal distribution with mean value of 1.4 and standard deviation of 0.25 for the model uncertainties associated with shear capacity of concrete.

However, the residual strength assumption justifies the consideration of smoother variations in strength, since the residual shear envelope shall not differ considerably from a linear failure criteria. In this work, significantly lower bias is assumed, considering that in average, the linear Mohr-Coulomb criteria models the strength on the interface. Therefore, a model uncertainty θ_S affecting the mobilized friction coefficient, given by a lognormal distribution with mean value of 1.0 and standard deviation of 0.10, is considered.

4.4.4 Rigid body stability model

The analytical calculation of the necessary friction coefficient, as a function of loads and the geometry, requires a rigid body formulation which allows the solution of the static equilibrium. Although the existent discontinuities govern the movement during structural failure, the required rigid body assumption neglects some aspects, namely: (i) crushing that may occur in stress concentrated zones (interbody contacts); or (ii) structural deformations.

On one hand, given the high stresses installed in contact points A and B (for the failure mode 1) or B and C (for the failure mode 3), concrete crushing is expected to occur leading to a transition from vertex-edge to edge-edge contacts. One other hand, deformations in the concrete and rock mass would also change the pre-failure equilibrium configuration, affecting the suitability of the critical friction coefficient computed from the rigid body formulation.

Since no information regarding the rigid body model uncertainty is available, the introduction of subjectivity in the estimation of related probabilistic properties is inevitable. So, avoiding the over dependency between the estimated probability of failure and imponderable variables, a model uncertainty affecting the computed critical friction coefficient ($\tan\phi_c$), θ_S, given by a lognormal distribution with mean value of 1.0 and small standard

deviation of 0.03, is considered.

4.5 Final considerations

The uncertainty modeling is a central task for the reliability- and risk-based approach to structural safety analysis. As the estimation of the probability of failure, through reliability methods, is highly sensitive to the probabilistic distributions used, uncertainty modeling shall carefully combine data available (objective information) and physical arguments, experience and judgment (subjective information).

In this chapter, data from monitoring and quality control tests were used to derive probabilistic models for the water loads and the concrete mechanical properties, respectively. The quantification of other sources of physical uncertainties, such as the concrete density and concrete-rock interface shear strength, was based on the literature. The model uncertainty regarding the seismic load models was quantified by comparing the dynamic response and the analytical stability analysis of equivalent structures. While engineering judgment regulates all decisions, it became particularly relevant to define probabilistic models regarding other model uncertainties, such as the Mohr-Coulomb shear strength model and the rigid body stability formulation, that could not be alternatively quantified.

The advances made allowed the quantification of the relevant sources of uncertainty involved in the concrete dam safety which will enable, in the following chapters, both the studies on the reliability-based design and the code calibration for ultimate limit states.

CHAPTER 5

Reliability-based design for concrete gravity dams

5.1 General considerations

The decision upon the construction of concrete dams shall balance the expected profits coming from the exploitation of the water resources against the costs of conceiving a structural solution that fulfills the performance requirements, regarding the structural safety, functionality and durability.

In the design phase, the choice for concrete gravity dams, to the detriment of other types of structures, shall lead to engineering and/or economical advantages, ideally justified in a risk-based approach minimizing the expected life-cycle costs (Ang and Leon 1997) as a function of the underlying risk. However, as this approach is highly influenced by the interpretation of the practitioner, standards often establish deterministic criteria, representing the performance requirements, which shall accommodate a safety margin to account for the inherent uncertainties of the problem, as well as, the severity of the consequences of a structural failure.

Regarding the safety requirements in particular, the Portuguese dam safety regulation (RSB 2018) simplifies the time-variant safety problem by considering that the ultimate structural capacity, characterized by the residual strength, shall guarantee the structural safety under the most conditioning foreseeable load conditions arising during the intended

service life of the structure, namely those derived from the occurrence of the design flood and the design earthquake.

In the standards-based approach, the required structural characteristics of a concrete gravity dam are then obtained by a DDO procedure, considering the local constraints, namely with regard to the local hydrology, the hydraulic and mechanical characteristics of the rock mass foundation and the local seismic hazard. Although safety factors shall implicitly account for the reservations about the predicted structural capacity, the severity of the consequences of a possible structural failure and the magnitude of loads, the trade-off between safety and economy is thus only addressed subjectively (Beck and Gomes 2012), since structural characteristics obtained by a DDO procedure: (i) grossly neglects the effects of the sources of uncertainties on structural safety, and (ii) may not be optimal due to the deviations of the reliability levels throughout a class of structures.

In face of unavoidable uncertainties, optimum structural solutions can alternatively be obtained by a RBDO procedure, where the safety requirements, given by a target reliability index or a target probability of failure derived from risk acceptance criteria, are introduced as optimization constraints. Thus, an objective function $f(\boldsymbol{\theta})$, such as the cost of construction or manufacture (Melchers 1999) given in terms of design variables $\boldsymbol{\theta}$, is minimized providing that safety requirements are fulfilled.

The benefits from this procedure, upon decision-making, depends on the ability to: (i) define the boundary conditions between the occurrence of consequences and their avoidance (failure modes); (ii) simulate either analytically or numerically the structural response in those conditions (limit states); (iii) quantify properly the relevant sources of uncertainty; and (iv) define target reliability index reflecting realistically the severity of the consequences of failure and the risk acceptance criteria. However, doubts on the effects of the simplifications required regarding the structural behavior of concrete dams, strongly influenced by roughly known foundation characteristics, on the estimation of the real probability of failure have refrained the dam engineering community of adopting definitely a probabilistic-based approach. The successful works (e.g. Altarejos 2009; Westberg 2010), either on an academic or practical levels, were limited to concrete gravity dams with well defined failure conditions, whose structural analysis can be conducted based on bi-dimensional rigid models, enabling the definition of analytical limit states since structural stability is often the conditioning failure mode.

Therefore, the advances made in this thesis, regarding the failure mode and uncertainty

modeling, encourage the application of probabilistic principles to the design of theoretical concrete gravity dams, through RBDO procedure, based on similar simplifications regarding the structural behavior, namely: (i) the pre-selection of a failure surface (dam-foundation interface); (ii) equivalent rigid body behavior; and (iii) residual shear strength, given only by the frictional component, corresponding to a limit analysis valid for ultimate limit states.

Accordingly, since structural safety of concrete gravity dams depends mostly on their geometry, the objective function $f(\boldsymbol{\theta})$ to be minimized in the RBDO procedure shall expectedly be proportional to the geometric characteristics (upstream and downstream face slopes or the keyed depth). Given that the upstream face slope shall not differ considerably from a vertical surface (Chen 2015) and the keying works may be usually more expensive than increasing the material volume, the downstream face slope is considered, in this study, the only design variable $\theta = s_d$. Therefore, the RBDO procedure is simplified into an inverse reliability problem, whose solution algorithm, based on FORM principles, was detailed in section 2.6.2, in which the minimum design variable θ^* that fulfills the reliability requirements β_{Ti} for each failure mode i is sought, i.e.,

$$\beta_i(\theta^*) = \beta_{Ti} \tag{5.1}$$

Since the structural solution shall ensure adequate levels of safety for the two different load events that may plausibly compromise its safety, namely the flood and earthquake load events, the geometric characteristics of the concrete gravity dam shall meet the safety requirements for both, being naturally given by the most demanding case. Therefore, to cover all range of possibilities regarding the loading conditions, the inverse reliability procedure is applied, for a specific load event, considering separately each limit state, and repeated to each design situation, within the calculation sequence illustrated in Figure 5.1.

In the following sections, the required information of the case study, namely the geometrical properties of the theoretical profile, the load effects on the structure, the limit states, the random variables and the reliability requirements, is presented. After that, the inverse reliability procedure is applied to the design situations derived from the flood and seismic load events. At the end, some final considerations regarding the most conditioning failure modes and load events are made based on the results presented.

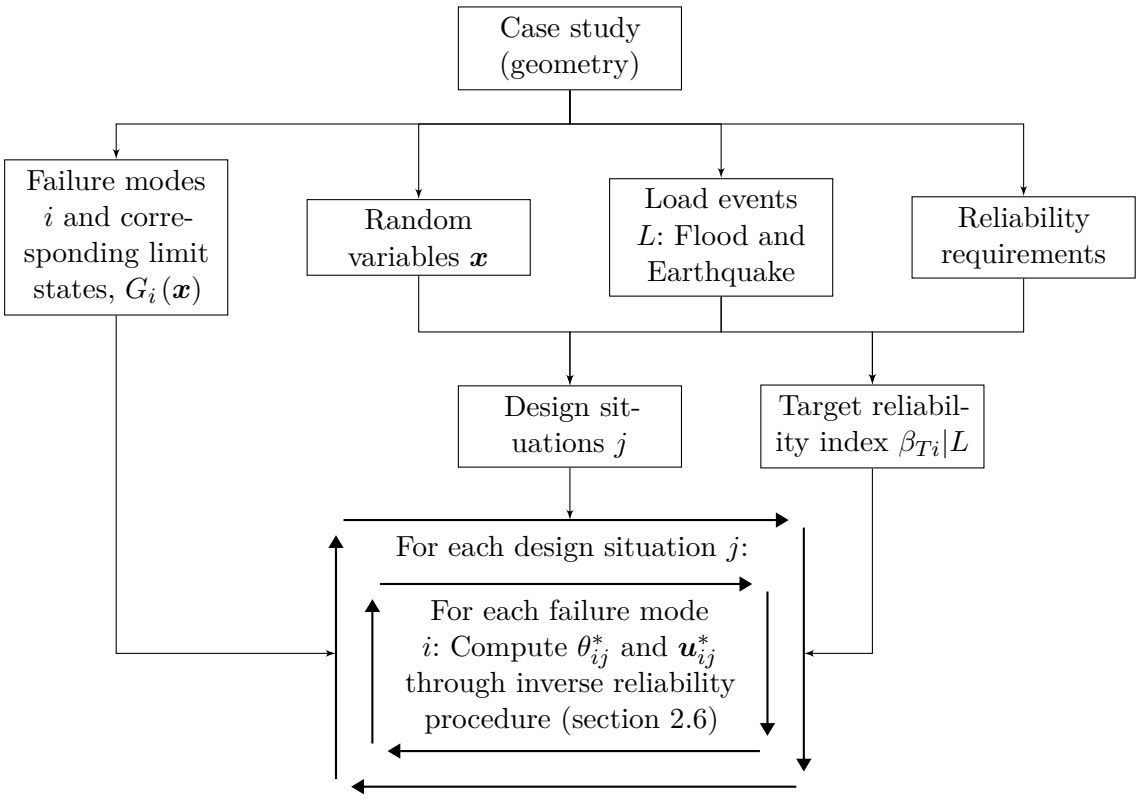

Figure 5.1: Calculation sequence for the reliability-based design considering each design situation.

5.2 Case study

5.2.1 Geometric characteristics

The case study considered is a theoretical gravity monolith with 100 meter of height, keyed into the foundation at a depth corresponding to 10% of its height ($h_w = 10$ m), such as practiced in the dam construction in Portugal (Pedro 2018).

The stability analysis of the simplified two-dimensional profile is performed analytically considering the failure modes detailed in section 3.6. For that, a downstream rock wedge, detached from the remain rock mass foundation, must be considered.

Tests on the influence of the downstream rock wedge slope (α) on the structural capacity were performed by varying the loading conditions, the downstream face slope and the downstream rock wedge slope. The most conditioning rock wedge slope, which result in the loss of equilibrium for a larger critical friction angle (ϕ_c), varies between $\alpha = 4°$ and $\alpha = 7°$, with an average value of $\alpha = 5.5°$, depending on the loading conditions and the downstream face slope. Note that, if the equilibrium conditions at the complete

interface plastification (Figure 3.19), corresponding to the small displacement approach, were considered, the most conditioning rock wedge slope would vary between $\alpha = 25°$ and $\alpha = 40°$, validating the suggested ($\alpha = 45° - \phi/2$) in the CADAM software (Leclerc *et al.* 2001) for the stability analysis of gravity dams.

Therefore, in the case study considered, a downstream rock wedge inclined at $\alpha = 5.5°$ is assumed. Figure 5.2 shows the geometry of the case study.

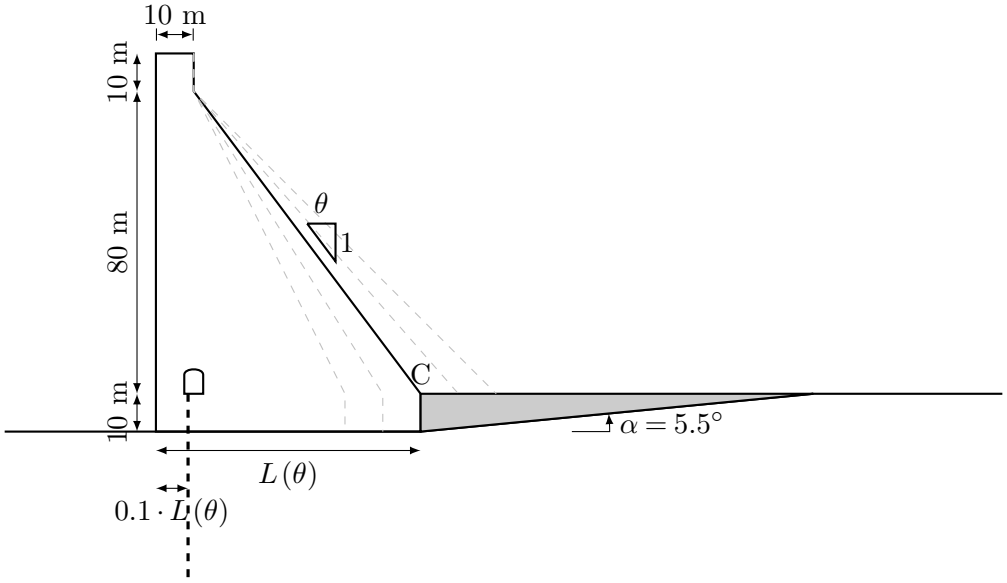

Figure 5.2: Geometry of the case study.

5.2.2 Random variables

The relevant sources of uncertainty in engineering problems are considered, in time- and space-invariant problems, as random variables, modeled by distribution functions which assign probabilities to a range of values of a specific quantity.

The sources of uncertainty, involved in the structural safety of concrete gravity dams, were quantified in chapter 4, combining objective and subjective perspectives, using, in addition to the elements found in the literature, data from monitoring of the concrete dam behavior during the construction, first filling and operation periods. The random variables considered in the inverse reliability procedure, namely in regard to loads, material properties and model uncertainties, are associated with:

- Uncertainty on the reservoir water level, in normal operation conditions, is modeled by a beta distributed random variable k_r, quantifying the water level in relation to the

dam height (equation 4.1). Since the probability distribution of k_r depends on both the relative normal water level k_{nwl} and the project exploitation type, as observed in the monitoring data analysis presented in section 4.2.2.2, several theoretical cases characterized by different values of k_{nwl} (from 0.79 to 0.99 with a step of 0.02) were considered for both groups, namely "Group L1" for storage dams and "Group L2" for run-of-river dams. The distribution moments, obtained through equations 4.16 and 4.17, were shown in Table 4.2;

- Uncertainty on the uplift pressures is modeled by a beta distributed random variable k_u, quantifying the uplift pressures at the drainage line, which, based on the distinction made in the French guidelines (CFBR 2012), were divided into two groups, namely "Group U1" for regular geology foundation and "Group U2" for unfavorable geology foundation;

- Uncertainty due to the consideration of the linear or bi-linear uplift model is modeled by a normal distributed random variable θ_u that shall multiply the uplift factor k_u;

- Uncertainty on the structure weight is taken into account by considering the concrete density modeled by a normal distributed random variable ρ_c;

- Uncertainty on the dam-foundation shear strength is taken into account by considering the friction coefficient modeled by a lognormal distributed random variable $\tan\phi$, which, based on the recommendations of the Chinese standars (GB50199 1994), were divided into three groups, namely "Group S1" for rock mass class I, "Group S2" for rock mass class II and "Group S3" for rock mass class III;

- Uncertainty due to the consideration of the linear Mohr-Coulomb failure criteria is modeled by a lognormal distributed random variable θ_R, which shall multiply the friction coefficient $\tan\phi$;

- Uncertainty introduced by the rigid body formulation is modeled by a lognormal distributed random variable θ_S, which shall multiply the critical friction coefficient $\tan_{\phi_c}$ obtained by solving the systems of equations 3.38, 3.39 and 3.40, for the failure modes 1, 2 and 3, respectively;

- Uncertainty associated with the consideration of the pseudo-static seismic load model is modeled by a random variable θ_e, whose moments were listed in Table 4.12

according to the seismic type and zone, which shall multiply the seismic acceleration a_g.

The distribution properties of the random variables are synthesized in Table 5.1.

Table 5.1: Distribution properties of the random variables.

Random variable	Group	Distribution	Mean value	Variance
Relative reservoir water level, k_r	L1 L2	Beta	see Table 4.2	
Uplift factor, k_u	U1	Beta	0.25	0.012
	U2		0.48	0.042
Uplift model uncertainty, θ_u		Lognormal	1.00	0.05^2
Concrete density, ρ_c (kg/m^3)		Normal	2400	81.6^2
Friction coefficient, $\tan\phi$	S1	Lognormal	1.40	0.082
	S2		1.20	0.061
	S3		1.00	0.043
Mohr-Coulomb shear strength model uncertainty, θ_R		Lognormal	1.00	0.10^2
Model uncertainty due to the rigid body formulation, θ_S		Lognormal	1.00	0.03^2
Seismic load model uncertainty, θ_e		see Table 4.12		

5.2.3 Ultimate limit states

As mentioned, limit states, defining the boundary between desired (non-failure conditions) and undesired (failure conditions) structural response, are generally divided into ultimate limit states, concerning partial or global structural collapse, and serviceability limit states, concerning the functionality, durability and aesthetics of the structure.

In this study, ultimate limit states involving the loss of structural equilibrium are considered. Since most engineering problems can be reduced to a comparison between solicitation S and structural capacity R, these limit states, derived from the failure modes 1 to 4 presented in section 3.6, are expressed, in terms of the random variables $\boldsymbol{x} = \{ k_r, k_u, \theta_u, \rho_c, \tan\phi, \theta_e, \theta_R, \theta_S\}$ and the design variable θ, respectively, by,

$$G_1(\boldsymbol{x},\theta) = \tan\phi \cdot \theta_R - S_1 [\, F_v(k_u \cdot \theta_u, \rho_c, \theta_e, \theta), x_0(k_u \cdot \theta_u, \rho_c, \theta_e, \theta), F_h(k_r, \theta_e, \theta), y_0(k_r, \theta_e, \theta), F_{n,w}(\theta_e), F_{t,w}(\theta_e)] \cdot \theta_S \tag{5.2}$$

$$G_2(\boldsymbol{x},\theta) = \tan\phi\cdot\theta_R - S_2\left[F_v\left(k_u\cdot\theta_u,\rho_c,\theta_e,\theta\right),F_h\left(k_r,\theta_e,\theta\right),\right.$$
$$\left.F_{n,w}\left(\theta_e\right),F_{t,w}\left(\theta_e\right)\right]\cdot\theta_S \tag{5.3}$$

$$G_3(\boldsymbol{x},\theta) = \tan\phi\cdot\theta_R - S_3\left[F_v\left(k_u\cdot\theta_u,\rho_c,\theta_e,\theta\right),x_0\left(k_u\cdot\theta_u,\rho_c,\theta_e,\theta\right),F_h\left(k_r,\theta_e,\theta\right),\right.$$
$$\left.y_0\left(k_r,\theta_e,\theta\right),F_{n,w}\left(\theta_e\right),F_{t,w}\left(\theta_e\right)\right]\cdot\theta_S \tag{5.4}$$

$$G_4(\boldsymbol{x},\theta) = -M_C\left(k_u\cdot\theta_u,k_r,\rho_c,\theta_e,\theta\right) \tag{5.5}$$

where S_1, S_2 and S_3 are the critical (or minimum necessary) friction coefficient, below which failure occurs, obtained in equations 3.38, 3.39 and 3.40, respectively, and:

- F_v is the vertical net force, acting on the dam body, given by,

$$F_v\left(k_u\cdot\theta_u,\rho_c,\theta_e,\theta\right) = W\left(\rho_c,\theta\right) - U\left(k_u\cdot\theta_u,\theta\right) - F_{s,v}\left(\theta_e,\theta\right) \tag{5.6}$$

  where W is the structure weight, given in equation 3.5, U is the total uplift force, given in equation 3.14 and $F_{s,v}$ is the vertical component of the inertia forces due to seismic action;

- x_0 is the point of application of the total vertical net force F_v, given by,

$$x_0\left(k_u\cdot\theta_u,\rho_c,\theta_e,\theta\right) = \frac{\left[W\left(\rho_c,\theta\right) - F_{s,v}\left(\theta_e,\theta\right)\right]\cdot x_W\left(\theta\right) - U\left(k_u\cdot\theta_u,\theta\right)\cdot x_U\left(\theta\right)}{F_v\left(k_u\cdot\theta_u,\rho_c,\theta_e,\theta\right)} \tag{5.7}$$

  where x_W is the x-coordinate of the centroid of the dam structure and x_U is the application point of the total uplift force, given in equation 3.15.

- F_h is the horizontal net force, acting on the dam body, given by,

$$F_h\left(k_r,\theta_e\right) = I_w\left(k_r\right) + \sum_i F_{s,h,i}\left(\theta_e,\theta\right) \tag{5.8}$$

  where I_w is the total hydrostatic force, given in equation 3.7, and $F_{s,h}$ is the horizontal component of the inertia forces due to seismic action, given: (i) for the pseudo-static seismic load model, by both the equivalent static forces (equation 3.22) and the hydrodynamic forces (equation 3.24); or (ii) for the pseudo-dynamic seismic load model, by pseudo-dynamic equivalent lateral forces (equation 3.28);

- y_0 is the point of application of the total horizontal net force F_h, given by,

$$y_0\left(k_r,\theta_e,\theta\right)=\frac{I_w\left(k_r\right)\cdot y_{I_w}\left(k_r\right)-\sum_i F_{s,h,i}\left(\theta_e,\theta\right)\cdot y_{F_s,i}\left(\theta\right)}{F_h\left(k_r,\theta_e\right)} \tag{5.9}$$

  where y_{I_w} is the application point of the total hydrostatic force, given in equation 3.8, and y_{F_s} is the application point of the horizontal component of the inertia forces due to seismic action, given: (i) for the pseudo-static seismic load model, by the y-coordinate of the centroid of the dam structure (y_W), for the equivalent static forces, and by $y_{I_{ws}}$ (equation 3.25), for the total hydrodynamic forces; or (ii) for the pseudo-dynamic seismic load model, by equation 3.29;

- M_C is the clockwise moment around the point C, given by,

$$\begin{aligned}M_C\left(k_u\cdot\theta_u,k_r,\rho_c,\theta_e\right)=&F_h\left(k_r,\theta_e\right)\cdot\left[y_0\left(k_r,\theta_e,\theta\right)-h_w\right]-\\&F_v\left(k_u\cdot\theta_u,\rho_c,\theta_e,\theta\right)\cdot\left[L\left(\theta\right)-x_0\left(k_u\cdot\theta_u,\rho_c,\theta_e,\theta\right)\right]\end{aligned} \tag{5.10}$$

- $F_{n,w}$ is the normal net force due to the downstream rock wedge, given by,

$$F_{n,w}\left(\theta_e\right)=\left[W_w-F_{s,v,w}\left(\theta_e\right)\right]\cdot\cos\alpha+F_{s,h,w}\cdot\sin\alpha \tag{5.11}$$

  where W_w is the weight of the downstream rock wedge and $F_{s,v,w}$ and $F_{s,h,w}$ are the vertical and horizontal components of the pseudo-static seismic forces acting on the downstream rock wedge.

- $F_{t,w}$ is the tangential net force due to the downstream rock wedge, given by,

$$F_{h,w}\left(\theta_e\right)=\left[W_w-F_{s,v,w}\left(\theta_e\right)\right]\cdot\sin\alpha-F_{s,h,w}\cdot\cos\alpha \tag{5.12}$$

5.2.4 Safety or reliability requirements

Although large dams often fall into the highest consequence class (Schneider 1997), Westberg (2010) concluded that the consequences of structural failure are naturally dependent on the dam height, acknowledging the suitability of the reliability differentiation principle, such as followed in the Eurocodes (EN1990 2002). In this study, three different values for the target probability of failure, p_{ft}, are tested, namely $1/10^8$, $1/10^7$ and $1/10^6$.

Since the probabilistic analysis of the structural response under non-permanent load events, would result in an estimation of the probability of failure conditioned to the occurrence of such event, a conditional value for the target probability of failure shall be considered in the inverse reliability procedure, based on the definition of conditional probability, expressed as,

$$p(A) = p(A|B) \cdot p(B) \tag{5.13}$$

where A and B are two random variables of the same probability space.

Therefore, the probability of failure targeted in the inverse reliability procedure, given the occurrence of a load event E is given by,

$$p_{ft}|E = p\Big(G(\boldsymbol{x}^*, \theta^*) < 0, |E\Big) = \frac{p\big(G(\boldsymbol{x}^*, \theta^*) < 0\big)}{p(E)} \tag{5.14}$$

or, equivalently, the target reliability index,

$$\beta_t|E = -\Phi\Big(p_{ft}|E\Big)^{-1} \tag{5.15}$$

where $p\big(G(\boldsymbol{x}^*, \theta^*) < 0\big)$ is the total probability of failure, $p(E)$ is the probability of occurrence of a load event E and $p\big(G(\boldsymbol{x}^*, \theta^*) < 0, |E\big)$ is the probability of failure given the occurrence of such event, computed through reliability analysis.

5.3 Extreme hydrological combination (flood load event)

5.3.1 General considerations

The loading conditions for the extreme hydrological combination are obtained by overlapping the operational loads to the water loads due to the occurrence of the design flood (RSB 2018), whose return period, depending on the dam height, is presented in Table 3.4. For a 100 meter high dam, the minimum return period considered is 5000 years (annual probability of occurrence of 0.0002).

The reservoir water level for the design flood, obtained through probabilistic methods considering the hydrologic properties of the region and the reservoir water volume-height curves, is typically located one meter below the dam crest, considering the dry freeboard usually adopted. Since safety analysis conditioned to the occurrence of such event is intended, the reservoir water level for the extreme hydrological combination, is considered

as a deterministic variable defined, for a 100 meter high dam, by a relative reservoir water level of $k_r = 0.99$. By simplicity, the load effects of the downstream water level are not considered.

In order to cover all possible scenarios, regarding the foundation hydraulic and mechanical properties, the groups of random variables were combined into 6 design situations F1 to F6, synthesized in Table 5.2.

Table 5.2: Design situations for the extreme hydrostatic load combination.

Design	k_u		$\tan\phi$		
situation	U1	U2	S1	S2	S3
F1	✓		✓		
F2		✓	✓		
F3	✓			✓	
F4		✓		✓	
F5	✓				✓
F6		✓			✓

Moreover, given the target values for the total probability of failure assumed above and the return period of the design flood considered, the target conditional probabilities of failure for the flood load event are presented in Table 5.3.

Table 5.3: Target probabilities of failure (and reliability indexes) conditioned to the occurrence of the design flood with a return period of 5000 years.

p_{ft}	$p_{ft}\|E$ ($\beta_T\|E$)
10^{-8}	$5 \cdot 10^{-5}$ (3.89)
10^{-7}	$5 \cdot 10^{-4}$ (3.29)
10^{-6}	$5 \cdot 10^{-3}$ (2.58)

5.3.2 Inverse reliability results

5.3.2.1 General considerations

The inverse reliability procedure starts with the selection of an initial value for the design variable θ and the design point $\boldsymbol{x}$. Since the convergence of the procedure is sensitive to the initial conditions selected, the procedure was restarted with different assumptions when convergence was not achieved. Mostly, the selection of a small value for the downstream

face slope ($\theta_0 = 0.30$) and a design point given by the mean values of the random variables was successful.

The main results of the procedures (first and last iterations) considering different target reliability indexes, for the listed design situations, are presented in the following sections.

5.3.2.2 Design situation F1

Table 5.4 to 5.7 show the relevant results of the inverse reliability procedure, considering the limit states derived from failure modes 1 to 4, respectively, for the design situation F1.

Table 5.4: Inverse reliability results, considering the limit state derived from failure mode 1, for the design situation F1.

	i	k_u	θ_u	ρ_c (kg/m^3)	$\tan\phi$	θ_R	θ_S	θ	$G_1(\boldsymbol{x},\theta)$	β
	0	0.25	1.00	2400.00	1.40	1.00	1.00	0.30	0.80	-
$\beta_t = 3.89$	6	0.30	1.00	2360.35	0.69	0.84	1.01	**0.38**	0	3.89
$\beta_t = 3.29$	6	0.28	1.00	2371.92	0.76	0.86	1.01	**0.21**	0	3.29
$\beta_t = 2.58$	-	-	-	-	-	-	-	-	-	-

Table 5.5: Inverse reliability results, considering the limit state derived from failure mode 2, for the design situation F1.

	i	k_u	θ_u	ρ_c (kg/m^3)	$\tan\phi$	θ_R	θ_S	θ	$G_2(\boldsymbol{x},\theta)$	β
	0	0.25	1.00	2400.00	1.40	1.00	1.00	0.30	0.76	-
$\beta_t = 3.89$	6	0.32	1.00	2354.10	0.69	0.84	1.01	**0.40**	0	3.89
$\beta_t = 3.29$	7	0.29	1.00	2364.07	0.77	0.86	1.01	**0.30**	0	3.29
$\beta_t = 2.58$	6	0.27	1.00	2374.63	0.87	0.89	1.01	**0.18**	0	2.58

Table 5.6: Inverse reliability results, considering the limit state derived from failure mode 3, for the design situation F1.

	i	k_u	θ_u	ρ_c (kg/m^3)	$\tan\phi$	θ_R	θ_S	θ	$G_3(\boldsymbol{x},\theta)$	β
	0	0.25	1.00	2400.00	1.40	1.00	1.00	0.30	0.61	-
$\beta_t = 3.89$	14	0.44	1.01	2297.66	0.75	0.86	1.01	**0.42**	0	3.89
$\beta_t = 3.29$	11	0.34	1.01	2339.34	0.79	0.87	1.01	**0.39**	0	3.29
$\beta_t = 2.58$	7	0.26	1.00	2385.48	0.87	0.89	1.01	**0.33**	0	2.58

Table 5.7: Inverse reliability results, considering the limit state derived from failure mode 4, for the design situation F1.

	i	k_u	θ_u	ρ_c (kg/m^3)	$\tan\phi$	θ_R	θ_S	θ	$G_4(\boldsymbol{x},\theta)$	β
	0	0.25	1.00	2400.00	-	-	-	0.30	-127779.28	-
$\beta_t = 3.89$	9	0.62	1.03	2196.81	-	-	-	**0.40**	0	3.89
$\beta_t = 3.29$	10	0.57	1.03	2230.58	-	-	-	**0.39**	0	3.29
$\beta_t = 2.58$	6	0.50	1.02	2268.05	-	-	-	**0.37**	0	2.58

5.3.2.3 Design situation F2

Table 5.8 to 5.11 show the relevant results of the inverse reliability procedure, considering the limit states derived from failure modes 1 to 4, respectively, for the design situation F2.

Table 5.8: Inverse reliability results, considering the limit state derived from failure mode 1, for the design situation F2.

	i	k_u	θ_u	ρ_c (kg/m^3)	$\tan\phi$	θ_R	θ_S	θ	$G_1(\boldsymbol{x},\theta)$	β
	0	0.48	1.00	2400.00	1.40	1.00	1.00	0.50	0.86	-
$\beta_t = 3.89$	7	0.71	1.01	2354.22	0.70	0.85	1.01	**0.50**	0	3.89
$\beta_t = 3.29$	7	0.65	1.01	2367.30	0.77	0.87	1.01	**0.31**	0	3.29
$\beta_t = 2.58$	-	-	-	-	-	-	-	-	-	-

Table 5.9: Inverse reliability results, considering the limit state derived from failure mode 2, for the design situation F2.

	i	k_u	θ_u	ρ_c (kg/m^3)	$\tan\phi$	θ_R	θ_S	θ	$G_2(\boldsymbol{x},\theta)$	β
	0	0.48	1.00	2400.00	1.40	1.00	1.00	0.30	0.73	-
$\beta_t = 3.89$	6	0.73	1.01	2348.14	0.71	0.85	1.01	**0.50**	0	3.89
$\beta_t = 3.29$	6	0.68	1.01	2360.12	0.78	0.87	1.01	**0.37**	0	3.29
$\beta_t = 2.58$	6	0.62	1.00	2372.36	0.88	0.89	1.01	**0.23**	0	2.58

Table 5.10: Inverse reliability results, considering the limit state derived from failure mode 3, for the design situation F2.

	i	k_u	θ_u	ρ_c (kg/m^3)	$\tan\phi$	θ_R	θ_S	θ	$G_3(\boldsymbol{x},\theta)$	β
	0	0.48	1.00	2400.00	1.40	1.00	1.00	0.30	0.60	-
$\beta_t = 3.89$	26	0.83	1.02	2298.61	0.77	0.86	1.01	**0.47**	0	3.89
$\beta_t = 3.29$	16	0.74	1.01	2343.34	0.80	0.87	1.01	**0.43**	0	3.29
$\beta_t = 2.58$	8	0.56	1.00	2384.99	0.87	0.89	1.01	**0.36**	0	2.58

Table 5.11: Inverse reliability results, considering the limit state derived from failure mode 4, for the design situation F2.

	i	k_u	θ_u	ρ_c (kg/m^3)	$\tan\phi$	θ_R	θ_S	θ	$G_4(\boldsymbol{x},\theta)$	β
	0	0.48	1.00	2400.00	-	-	-	0.30	-200446.15	-
$\beta_t = 3.89$	22	0.92	1.06	2171.24	-	-	-	**0.46**	0	3.89
$\beta_t = 3.29$	79	0.90	1.04	2217.31	-	-	-	**0.44**	0	3.29
$\beta_t = 2.58$	24	0.86	1.03	2269.98	-	-	-	**0.42**	0	2.58

5.3.2.4 Design situation F3

Table 5.12 to 5.15 show the relevant results of the inverse reliability procedure, considering the limit states derived from failure modes 1 to 4, respectively, for the design situation F3.

Table 5.12: Inverse reliability results, considering the limit state derived from failure mode 1, for the design situation F3.

	i	k_u	θ_u	ρ_c (kg/m^3)	$\tan\phi$	θ_R	θ_S	θ	$G_1(\boldsymbol{x},\theta)$	β
	0	0.25	1.00	2400.00	1.20	1.00	1.00	0.30	0.60	-
$\beta_t = 3.89$	7	0.32	1.00	2356.04	0.59	0.84	1.01	**0.57**	0	3.89
$\beta_t = 3.29$	7	0.29	1.00	2366.23	0.65	0.86	1.01	**0.41**	0	3.29
$\beta_t = 2.58$	7	0.27	1.00	2378.49	0.74	0.89	1.01	**0.21**	0	2.58

Table 5.13: Inverse reliability results, considering the limit state derived from failure mode 2, for the design situation F3.

	i	k_u	θ_u	ρ_c (kg/m^3)	$\tan\phi$	θ_R	θ_S	θ	$G_2(\boldsymbol{x},\theta)$	β
	0	0.25	1.00	2400.00	1.20	1.00	1.00	0.30	0.56	-
$\beta_t = 3.89$	6	0.33	1.00	2350.79	0.59	0.84	1.01	**0.54**	0	3.89
$\beta_t = 3.29$	6	0.30	1.00	2361.22	0.66	0.87	1.01	**0.42**	0	3.29
$\beta_t = 2.58$	6	0.28	1.00	2372.28	0.74	0.89	1.01	**0.29**	0	2.58

Table 5.14: Inverse reliability results, considering the limit state derived from failure mode 3, for the design situation F3.

	i	k_u	θ_u	ρ_c (kg/m^3)	$\tan\phi$	θ_R	θ_S	θ	$G_3(\boldsymbol{x},\theta)$	β
	0	0.25	1.00	2400.00	1.20	1.00	1.00	0.30	0.41	-
$\beta_t = 3.89$	18	0.50	1.02	2269.27	0.69	0.88	1.01	**0.44**	0	3.89
$\beta_t = 3.29$	11	0.42	1.01	2306.27	0.72	0.88	1.01	**0.42**	0	3.29
$\beta_t = 2.58$	9	0.32	1.00	2351.70	0.76	0.90	1.01	**0.39**	0	2.58

Table 5.15: Inverse reliability results, considering the limit state derived from failure mode 4, for the design situation F3.

	i	k_u	θ_u	ρ_c (kg/m^3)	$\tan\phi$	θ_R	θ_S	θ	$G_4(\boldsymbol{x},\theta)$	β
	0	0.25	1.00	2400.00	-	-	-	0.30	-127779.28	-
$\beta_t = 3.89$	9	0.62	1.03	2196.81	-	-	-	**0.40**	0	3.89
$\beta_t = 3.29$	10	0.57	1.03	2230.58	-	-	-	**0.39**	0	3.29
$\beta_t = 2.58$	6	0.50	1.02	2268.05	-	-	-	**0.37**	0	2.58

5.3.2.5 Design situation F4

Table 5.16 to 5.19 show the relevant results of the inverse reliability procedure, considering the limit states derived from failure modes 1 to 4, respectively, for the design situation F4.

Table 5.16: Inverse reliability results, considering the limit state derived from failure mode 1, for the design situation F4.

	i	k_u	θ_u	ρ_c (kg/m^3)	$\tan\phi$	θ_R	θ_S	θ	$G_1(\boldsymbol{x},\theta)$	β
	0	0.48	1.00	2400.00	1.20	1.00	1.00	0.30	0.57	-
$\beta_t = 3.89$	7	0.73	1.01	2349.30	0.61	0.85	1.01	**0.71**	0	3.89
$\beta_t = 3.29$	7	0.68	1.01	2361.53	0.67	0.87	1.01	**0.51**	0	3.29
$\beta_t = 2.58$	6	0.61	1.00	2375.19	0.75	0.89	1.01	**0.29**	0	2.58

Table 5.17: Inverse reliability results, considering the limit state derived from failure mode 2, for the design situation F4.

	i	k_u	θ_u	ρ_c (kg/m^3)	$\tan\phi$	θ_R	θ_S	θ	$G_2(\boldsymbol{x},\theta)$	β
	0	0.48	1.00	2400.00	1.20	1.00	1.00	0.30	0.53	-
$\beta_t = 3.89$	6	0.75	1.01	2344.06	0.61	0.85	1.01	**0.66**	0	3.89
$\beta_t = 3.29$	6	0.70	1.01	2356.68	0.67	0.87	1.01	**0.51**	0	3.29
$\beta_t = 2.58$	6	0.64	1.01	2369.62	0.75	0.89	1.01	**0.35**	0	2.58

Table 5.18: Inverse reliability results, considering the limit state derived from failure mode 3, for the design situation F4.

	i	k_u	θ_u	ρ_c (kg/m^3)	$\tan\phi$	θ_R	θ_S	θ	$G_3(\boldsymbol{x},\theta)$	β
	0	0.48	1.00	2400.00	1.20	1.00	1.00	0.30	0.40	-
$\beta_t = 3.89$	36	0.87	1.03	2263.58	0.70	0.88	1.01	**0.50**	0	3.89
$\beta_t = 3.29$	26	0.81	1.02	2309.69	0.73	0.89	1.01	**0.47**	0	3.29
$\beta_t = 2.58$	68	0.70	1.01	2355.63	0.77	0.90	1.01	**0.43**	0	2.58

Table 5.19: Inverse reliability results, considering the limit state derived from failure mode 4, for the design situation F4.

	i	k_u	θ_u	ρ_c (kg/m^3)	$\tan\phi$	θ_R	θ_S	θ	$G_4(\boldsymbol{x},\theta)$	β
	0	0.48	1.00	2400.00	-	-	-	0.30	-200446.15	-
$\beta_t = 3.89$	22	0.92	1.06	2171.24	-	-	-	**0.46**	0	3.89
$\beta_t = 3.29$	79	0.90	1.04	2217.31	-	-	-	**0.44**	0	3.29
$\beta_t = 2.58$	24	0.86	1.03	2269.98	-	-	-	**0.42**	0	2.58

5.3.2.6 Design situation F5

Table 5.20 to 5.23 show the relevant results of the inverse reliability procedure, considering the limit states derived from failure modes 1 to 4, respectively, for the design situation F5.

Table 5.20: Inverse reliability results, considering the limit state derived from failure mode 1, for the design situation F5.

	i	k_u	θ_u	ρ_c (kg/m^3)	$\tan\phi$	θ_R	θ_S	θ	$G_1(\boldsymbol{x},\theta)$	β
	0	0.25	1.00	2400.00	1.00	1.00	1.00	0.30	0.40	-
$\beta_t = 3.89$	6	0.33	1.00	2352.48	0.49	0.85	1.01	**0.81**	0	3.89
$\beta_t = 3.29$	6	0.30	1.00	2362.43	0.54	0.87	1.01	**0.63**	0	3.29
$\beta_t = 2.58$	6	0.28	1.00	2373.50	0.61	0.89	1.01	**0.43**	0	2.58

Table 5.21: Inverse reliability results, considering the limit state derived from failure mode 2, for the design situation F5.

	i	k_u	θ_u	ρ_c (kg/m^3)	$\tan\phi$	θ_R	θ_S	θ	$G_2(\boldsymbol{x},\theta)$	β
	0	0.25	1.00	2400.00	1.00	1.00	1.00	0.30	0.36	-
$\beta_t = 3.89$	6	0.34	1.01	2347.09	0.49	0.85	1.01	**0.72**	0	3.89
$\beta_t = 3.29$	6	0.31	1.00	2358.09	0.54	0.87	1.01	**0.58**	0	3.29
$\beta_t = 2.58$	5	0.29	1.00	2369.78	0.62	0.89	1.01	**0.43**	0	2.58

Table 5.22: Inverse reliability results, considering the limit state derived from failure mode 3, for the design situation F5.

	i	k_u	θ_u	ρ_c (kg/m^3)	$\tan\phi$	θ_R	θ_S	θ	$G_3(\boldsymbol{x},\theta)$	β
	0	0.25	1.00	2400.00	1.00	1.00	1.00	0.30	0.21	-
$\beta_t = 3.89$	17	0.55	1.02	2244.84	0.63	0.90	1.01	**0.46**	0	3.89
$\beta_t = 3.29$	21	0.48	1.02	2279.13	0.65	0.90	1.01	**0.44**	0	3.29
$\beta_t = 2.58$	31	0.39	1.01	2319.13	0.67	0.91	1.01	**0.42**	0	2.58

Table 5.23: Inverse reliability results, considering the limit state derived from failure mode 4, for the design situation F5.

	i	k_u	θ_u	ρ_c (kg/m^3)	$\tan\phi$	θ_R	θ_S	θ	$G_4(\boldsymbol{x},\theta)$	β
	0	0.25	1.00	2400.00	-	-	-	0.30	-127779.28	-
$\beta_t = 3.89$	9	0.62	1.03	2196.81	-	-	-	**0.40**	0	3.89
$\beta_t = 3.29$	10	0.57	1.03	2230.58	-	-	-	**0.39**	0	3.29
$\beta_t = 2.58$	6	0.50	1.02	2268.05	-	-	-	**0.37**	0	2.58

5.3.2.7 Design situation F6

Table 5.24 to 5.27 show the relevant results of the inverse reliability procedure, considering the limit states derived from failure modes 1 to 4, respectively, for the design situation F6.

Table 5.24: Inverse reliability results, considering the limit state derived from failure mode 1, for the design situation F6.

	i	k_u	θ_u	ρ_c (kg/m^3)	$\tan\phi$	θ_R	θ_S	θ	$G_1(\boldsymbol{x},\theta)$	β
	0	0.48	1.00	2400.00	1.00	1.00	1.00	0.30	0.37	-
$\beta_t = 3.89$	7	0.75	1.01	2345.04	0.50	0.85	1.01	**1.00**	0	3.89
$\beta_t = 3.29$	6	0.71	1.01	2357.23	0.56	0.87	1.01	**0.77**	0	3.29
$\beta_t = 2.58$	6	0.64	1.01	2370.28	0.62	0.90	1.01	**0.54**	0	2.58

Table 5.25: Inverse reliability results, considering the limit state derived from failure mode 2, for the design situation F6.

	i	k_u	θ_u	ρ_c (kg/m^3)	$\tan\phi$	θ_R	θ_S	θ	$G_2(\boldsymbol{x},\theta)$	β
	0	0.48	1.00	2400.00	1.00	1.00	1.00	0.30	0.33	-
$\beta_t = 3.89$	8	0.76	1.01	2339.57	0.51	0.85	1.01	**0.88**	0	3.89
$\beta_t = 3.29$	6	0.72	1.01	2352.96	0.56	0.87	1.01	**0.71**	0	3.29
$\beta_t = 2.58$	5	0.66	1.01	2366.74	0.63	0.90	1.01	**0.52**	0	2.58

Table 5.26: Inverse reliability results, considering the limit state derived from failure mode 3, for the design situation F6.

	i	k_u	θ_u	ρ_c (kg/m^3)	$\tan\phi$	θ_R	θ_S	θ	$G_3(\boldsymbol{x},\theta)$	β
	0	0.48	1.00	2400.00	1.00	1.00	1.00	0.30	0.20	-
$\beta_t = 3.89$	24	0.89	1.04	2231.63	0.64	0.90	1.01	**0.52**	0	3.89
$\beta_t = 3.29$	27	0.85	1.03	2277.55	0.66	0.91	1.01	**0.49**	0	3.29
$\beta_t = 2.58$	15	0.78	1.02	2325.81	0.69	0.92	1.01	**0.46**	0	2.58

Table 5.27: Inverse reliability results, considering the limit state derived from failure mode 4, for the design situation F6.

	i	k_u	θ_u	ρ_c (kg/m^3)	$\tan\phi$	θ_R	θ_S	θ	$G_4(\boldsymbol{x},\theta)$	β
	0	0.48	1.00	2400.00	-	-	-	0.30	-200446.15	-
$\beta_t = 3.89$	22	0.92	1.06	2171.24	-	-	-	**0.46**	0	3.89
$\beta_t = 3.29$	79	0.90	1.04	2217.31	-	-	-	**0.44**	0	3.29
$\beta_t = 2.58$	24	0.86	1.03	2269.98	-	-	-	**0.42**	0	2.58

5.3.3 Result analysis

Dams, as water-retaining structures, aim to create reservoirs to partially or totally accommodate the water inflow from a flood and later to discharge it, at a controlled rate, to downstream. The structure shall then ensure adequate levels of safety during the occurrence of a flood, when subjected to extreme load conditions characterized by a reservoir water level at the FWL, generally located one meter below the dam crest.

In this section, the design variable was quantified such that the safety requirements, representing by target reliability indexes, were fulfilled for all design situations covering the range of possible classifications of the rock mass foundation regarding its hydraulic and mechanical properties. These results are synthesized in Table 5.28.

Table 5.28: Syntheses of the inverse reliability results for all failure modes, design situations and target reliability indexes considered.

	$\beta_t = 3.89$				$\beta_t = 3.29$				$\beta_t = 2.58$			
Design	Failure mode				Failure mode				Failure mode			
situation	1	2	3	4	1	2	3	4	1	2	3	4
F1	0.38	0.40	**0.42**	0.40	0.21	0.30	**0.39**	0.39	-	0.18	0.33	**0.37**
F2	0.50	**0.50**	0.47	0.46	0.31	0.37	0.43	**0.44**	-	0.23	0.36	**0.42**
F3	**0.57**	0.54	0.44	0.40	0.41	0.42	**0.42**	0.39	0.21	0.29	**0.39**	0.37
F4	**0.71**	0.66	0.50	0.46	**0.52**	0.51	0.47	0.44	0.29	0.35	**0.43**	0.42
F5	**0.81**	0.72	0.46	0.40	**0.63**	0.58	0.44	0.39	0.43	**0.43**	0.42	0.37
F6	**1.00**	0.88	0.52	0.46	**0.77**	0.71	0.49	0.44	**0.54**	0.52	0.46	0.42

Regarding the influence of the hydraulic properties of the rock mass foundation upon the conception of proper structural solutions that fulfill the safety requirements, distinction was made between regular and unfavorable geologic conditions, such as described in the French guidelines (CFBR 2012). The optimum value for the downstream face slope is inversely proportional to the efficiency of the uplift reduction works carried out, since

design situations F1, F3 and F5 (for regular geologic conditions) result in smaller face slopes than design situations F2, F4 and F6 (for unfavorable geologic conditions), respectively, for any failure mode.

Regarding the influence of the mechanical properties of the rock mass foundation upon the conception of proper structural solutions that fulfill the safety requirements, distinction was made between the three classes defined in the Chinese standards (GB50199 1994) regarding the shear strength of the rock mass foundation. The optimum value for the downstream face slope is also inversely proportional to the structural capacity, characterized, for the failure modes 1 to 3, by the dam-foundation friction coefficient, since design situations F1 and F2 (rock mass class I) result in smaller face slopes than design situations F3 and F4 (rock mass class II), which, in turn, results in smaller face slopes than design situations F5 and F6 (rock mass class III). For the failure mode 4 (overturning), the solution is independent on the shear strength and a pattern of results is repeated for all rock mass classes.

Regarding the failure modes, the following conclusions might be drawn:

- The most conditioning failure mode depends on the target reliability index and the design situation. Since, for a smaller target reliability index, the corresponding downstream face slope is lower, failure mode 4 is more likely to be the conditioning failure mode, as obtained for the design situations F1 and F2 which considers the highest shear strength class;
- As the target reliability index increases, greater downstream face slope is required, specially to ensure stability conditions for the failure mode 1 and 2 which gain predominance;
- For the highest target reliability index, the failure mode 1 was only not conditioning for the design situations F1 and F2, since, given its higher shear strength, failure mode 2 or 3 become critical.

The sensitivity of the probability of failure to changes in random variables can be evaluated through the vector of direction cosines $\boldsymbol{\alpha}$ which indicates the direction to the design point located on the failure surface. This evaluation is important to identify which variables are worth to be further studied in order to reduce the associated uncertainties.

In Figure 5.3 the relative sensitivity of each random variable is illustrated using a bar graph, reflecting the variability over the design situations considered for each failure mode.

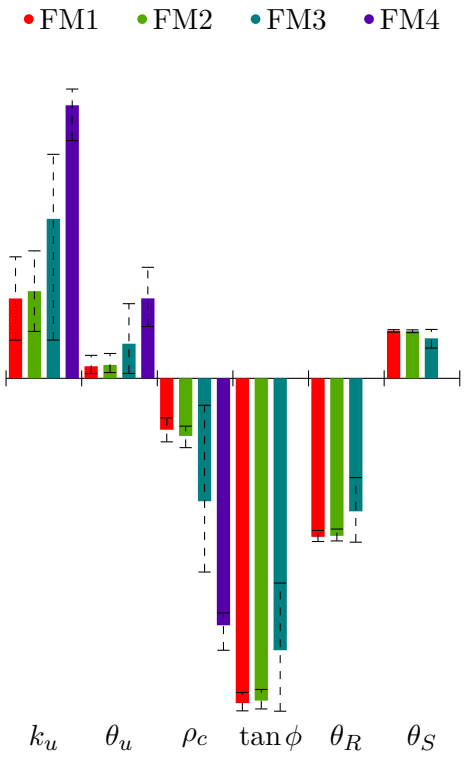

Figure 5.3: Representation of the variability of the relative sensitivity of each random variable for the design situations derived from the extreme hydrological combination.

For the extreme load combination, further information to reduce the uncertainty mostly related to the uplift factor and the friction coefficient would improve the estimation on the probability of failure.

5.4 Accidental earthquake combination (earthquake load event)

5.4.1 General considerations

The loading conditions for the accidental earthquake combination are obtained by overlapping the operational loads to the effects of the occurrence of the MDE (RSB 2018).

In earlier versions of the Portuguese dam safety regulation (RSB 1990; RSB 2007), specific seismologic studies would be necessary for the quantification of the MDE. In the last version (RSB 2018), MDE is characterized by a return period which is quantified, depending on the global seismic risk index, such as presented in Table 3.6. Only for exceptional cases, with high seismic risk index, the MDE is still taken from the MCE, deterministically quantified according to the local geological environmental considered (ICOLD 1989).

In the theoretical and generic case study analyzed, a return period of 1000 years, for a probability of exceedance of 10% during the structure service life (generally 100 years), is considered. Thus, the differentiation between dam implantation sites according to the regional seismology can be accounted considered the Portuguese seismic hazard maps (NP EN1998-1 2010). The seismic hazard maps, which divide the Portuguese mainland territory into zones with approximately constant seismic characteristics, were shown in Figure 3.16, for both seismic types.

In the case study presented, considering a return period of 1000 years (or equivalently a probability of annual occurrence of 0.001), the seismic accelerations for each seismic zone of the Portuguese territory, computed through the equation 3.19, are presented in Table 5.29.

Table 5.29: Seismic ground accelerations a_g (m/s^2) of a 1000-year return period earthquake for each seismic zone (NP EN1998-1 2010).

Zone	1	2	3	4	5	6
Type 1	4.11	3.29	2.46	1.64	0.99	0.57
Type 2	3.37	2.69	2.29	1.48	1.08	-

On one hand, the effects on the structure due to the occurrence of the MDE are, by simplicity, taken into account using the analytical pseudo-static or pseudo-dynamic load models which simulates the real structural response with approximation errors quantified at section 4.4.2. Given the lower standard deviation of the model uncertainty, the pseudo-static load model, which considers inertia forces as the product between mass and acceleration, is considered hereinafter.

On the other hand, the reservoir water level, in normal operation conditions, are characterized by the water inflow and outflow, depending on the environmental events but also on the dam exploitation management policy. Since the NWL, as a design data for each particular project, is targeted for optimum operation conditions, the variability of the relative reservoir water level, quantified in section 4.2.2 from data monitored in existing dams, depends on both the relation between the NWL and the dam height (k_{nwl}) and the project exploitation type. Although commonly varying, in practice, between 0.85 and 0.95, 11 levels of k_{nwl} (from $k_{nwl} = 0.79$ to $k_{nwl} = 0.99$ with a step of 0.02), each one with a different probability distribution, were considered in each design situation.

In order to cover all possible scenarios, regarding not only the project exploitation

type but also the hydraulic and mechanical properties of the foundation, the groups of the random variables were combined into 12 design situations E1 to E12, synthesized in Table 5.30.

Table 5.30: Design situations for the accidental earthquake load combination.

Design	k_u		k_r		$\tan\phi$		
situation	U1	U2	L1	L2	S1	S2	S3
E1	✓		✓		✓		
E2		✓	✓		✓		
E3	✓			✓	✓		
E4		✓		✓	✓		
E5	✓		✓			✓	
E6		✓	✓			✓	
E7	✓			✓		✓	
E8		✓		✓		✓	
E9	✓		✓				✓
E10		✓	✓				✓
E11	✓			✓			✓
E12		✓		✓			✓

Moreover, given the target values for the total probability of failure assumed and the return period of the MDE considered, the target conditional probabilities of failure for the earthquake load event are presented in Table 5.31.

Table 5.31: Target probabilities of failure (and reliability indexes) conditioned to the occurrence of the MDE with a return period of 1000 years.

p_{ft}	$p_{ft}\|E$ $(\beta_T\|E)$
10^{-8}	10^{-5} (4.26)
10^{-7}	10^{-4} (3.72)
10^{-6}	10^{-3} (3.09)

5.4.2 Inverse reliability results

5.4.2.1 General considerations

The inverse reliability procedure starts with the selection of an initial value for the downstream face slope and the design values. For convergence purposes, a small value for the

downstream face slope ($\theta_0 = 0.30$) and a design point given by the mean values of the random variables were considered.

The optimum downstream face slope, for the different design situations, is shown in the following sections. The conditioning failure mode is also represented.

5.4.2.2 Relevant results

Figures 5.4 to 5.9 show the design variable of the conditional failure mode for the design situations of the seismic type 1, seismic zones 1 to 6, respectively, and Figures 5.10 to 5.14 show the design variable of the conditional failure mode for the design situations of the seismic type 2, seismic zones 1 to 5, respectively. Since NWL is known in the design phase, different values of k_{nwl} were tested. The common range of practical values (between 0.85 and 0.95) was highlighted.

5.4.3 Result analysis

When comparing to other structural solutions, the typical geometry that makes concrete gravity dams economically competitive is characterized by downstream face slopes in the range of 0.7 to 0.8 (Corns *et al.* 1988), admitting a maximum value, depending on the loading conditions, of 1.0. The results obtained in this section, in which the design variable was quantified such that the safety requirements, representing by target reliability indexes, were fulfilled for all design situations, show increasing sensitivity to the exploitation type, the hydraulic and mechanical characteristics of the rock mass foundation and, above all, to the intensity of the seismic action considered.

For high intensity seismic zones, characterized by peak ground accelerations of considerable value, the minimum downstream face slope, which fulfills the safety requirements, increases to values that surely make this solution cost-prohibitive. Despite the validity of this conclusion, this fact may have been exacerbated by the consideration of the pseudo-static seismic load model to simulate the structural effects due to the occurrence of an earthquake, since this model, considering inertia forces proportional to the structure mass, may lose suitability for an exaggerated increase of the downstream face slope. In fact, the quantification of the analytical seismic load model uncertainty, made in section 4.4.2, was based on numerical models whose downstream face slope varied within a range of practical values (0.75 to 1.00). Its appropriateness for values far from that range cannot then be ensured. Consequently, in some extreme cases, for the most demanding design situations

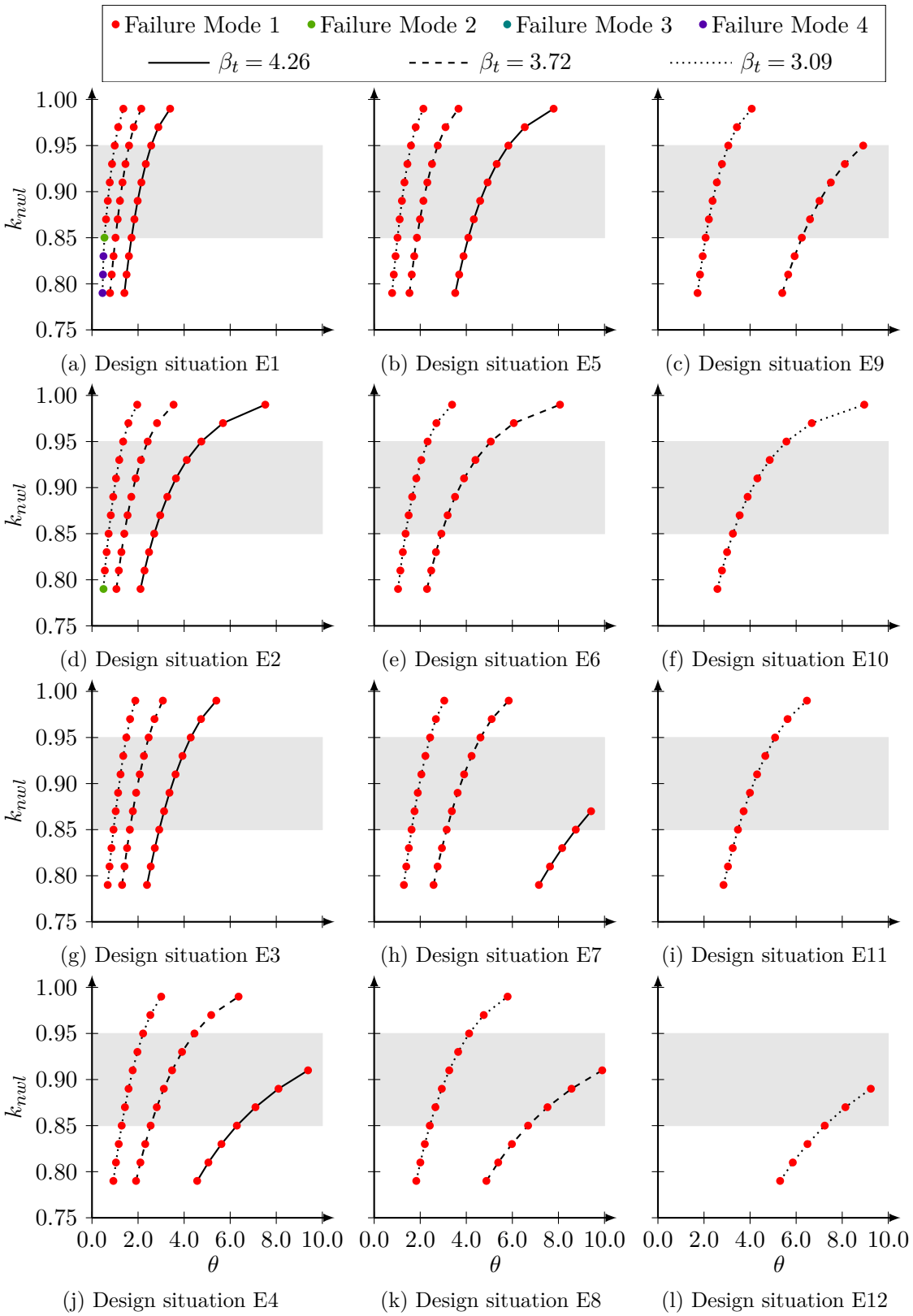

(a) Design situation E1 (b) Design situation E5 (c) Design situation E9

(d) Design situation E2 (e) Design situation E6 (f) Design situation E10

(g) Design situation E3 (h) Design situation E7 (i) Design situation E11

(j) Design situation E4 (k) Design situation E8 (l) Design situation E12

Figure 5.4: Optimum design variable for the design situations E1 to E12, considering the seismic zone 1.1.

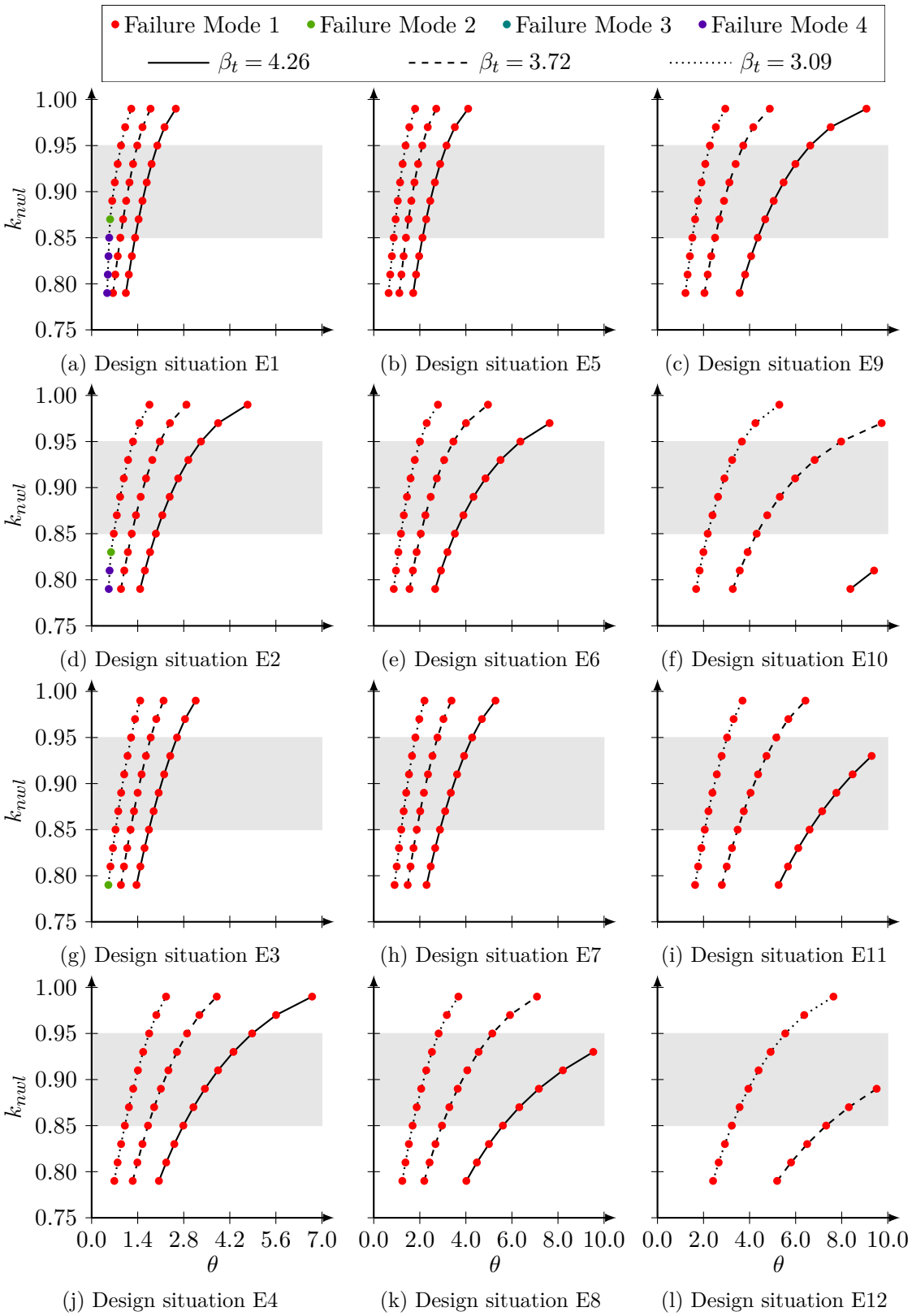

(a) Design situation E1 (b) Design situation E5 (c) Design situation E9

(d) Design situation E2 (e) Design situation E6 (f) Design situation E10

(g) Design situation E3 (h) Design situation E7 (i) Design situation E11

(j) Design situation E4 (k) Design situation E8 (l) Design situation E12

Figure 5.5: Optimum design variable for the design situations E1 to E12, considering the seismic zone 1.2.

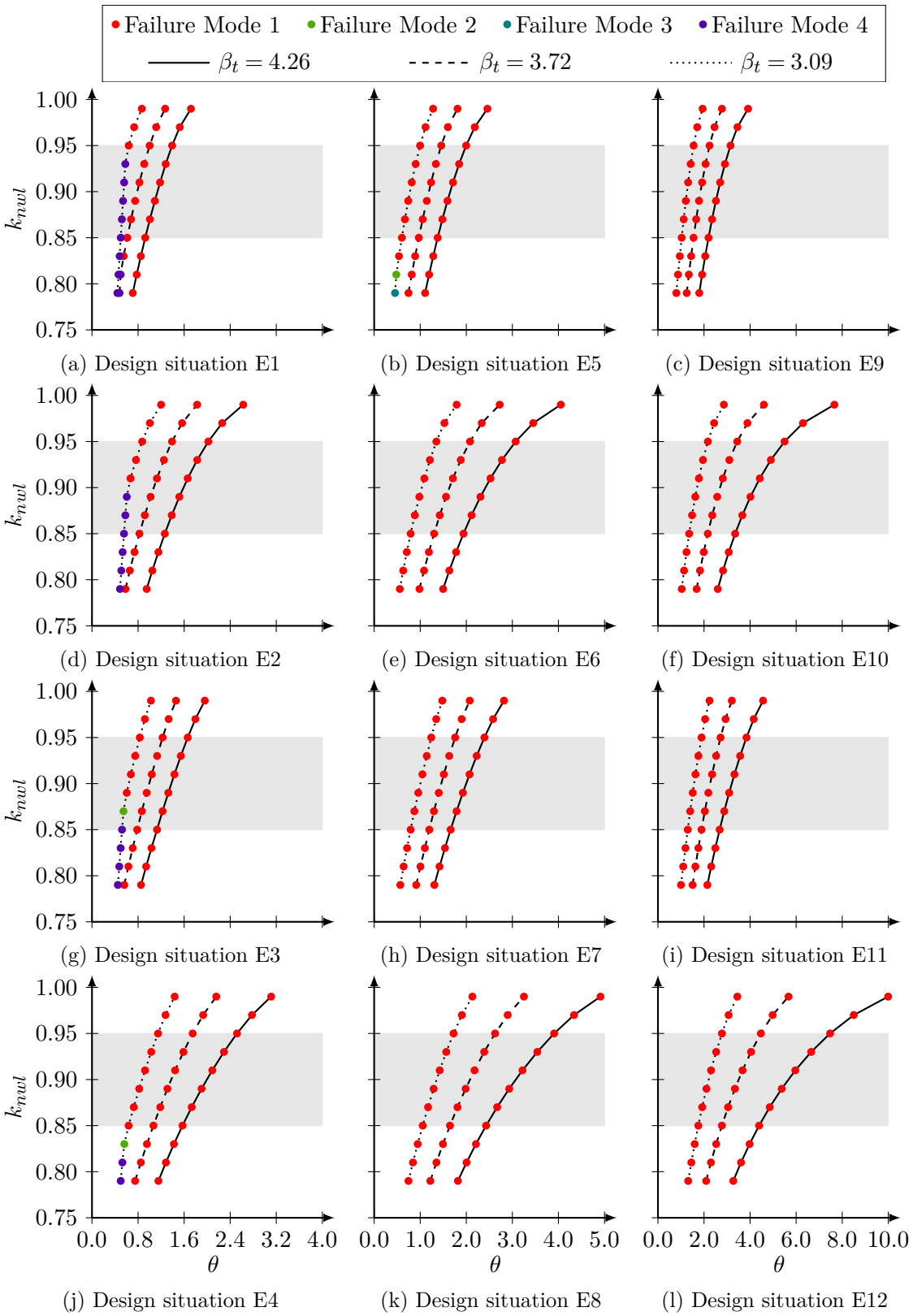

(a) Design situation E1 (b) Design situation E5 (c) Design situation E9

(d) Design situation E2 (e) Design situation E6 (f) Design situation E10

(g) Design situation E3 (h) Design situation E7 (i) Design situation E11

(j) Design situation E4 (k) Design situation E8 (l) Design situation E12

Figure 5.6: Optimum design variable for the design situations E1 to E12, considering the seismic zone 1.3.

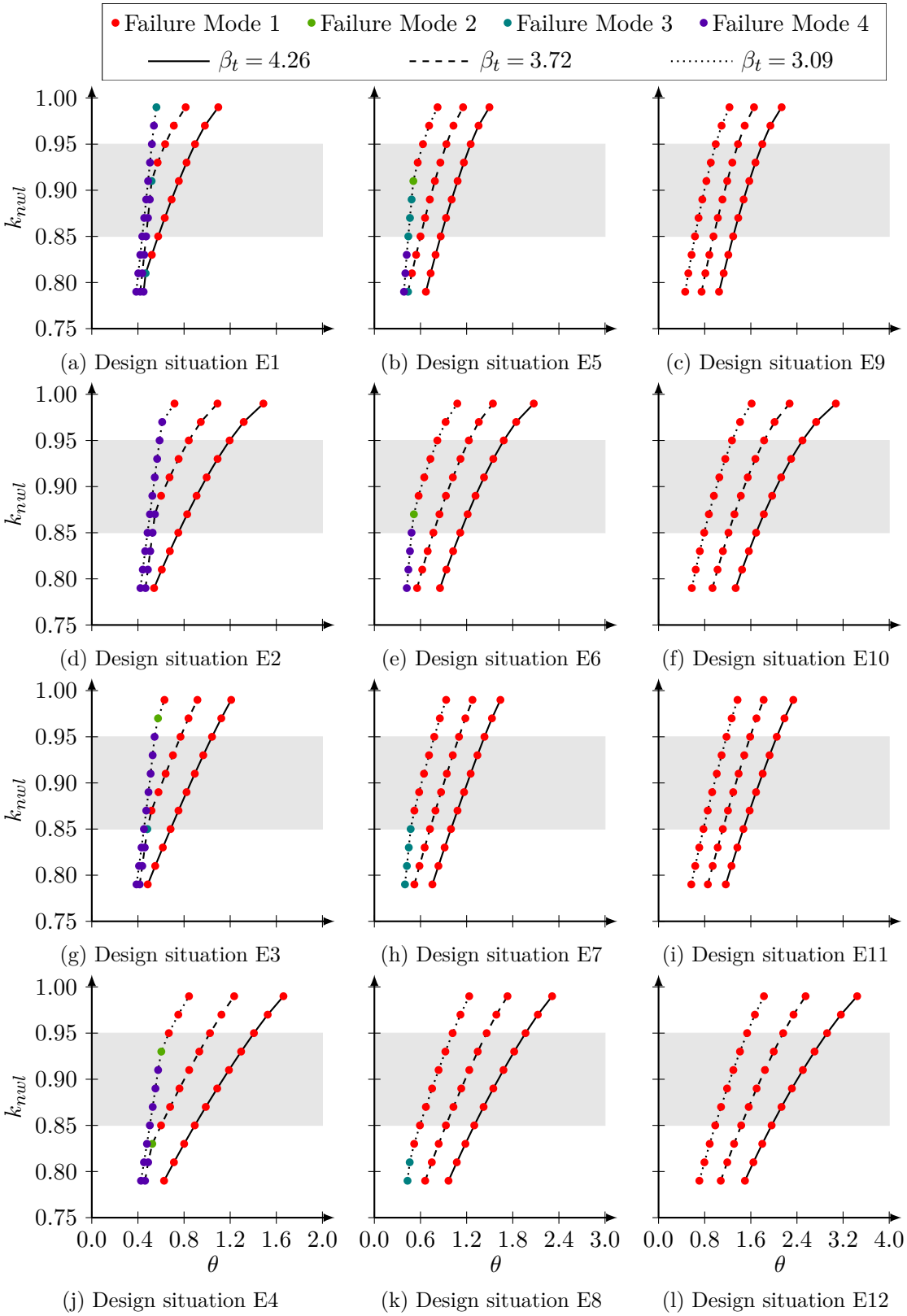

(a) Design situation E1 (b) Design situation E5 (c) Design situation E9

(d) Design situation E2 (e) Design situation E6 (f) Design situation E10

(g) Design situation E3 (h) Design situation E7 (i) Design situation E11

(j) Design situation E4 (k) Design situation E8 (l) Design situation E12

Figure 5.7: Optimum design variable for the design situations E1 to E12, considering the seismic zone 1.4.

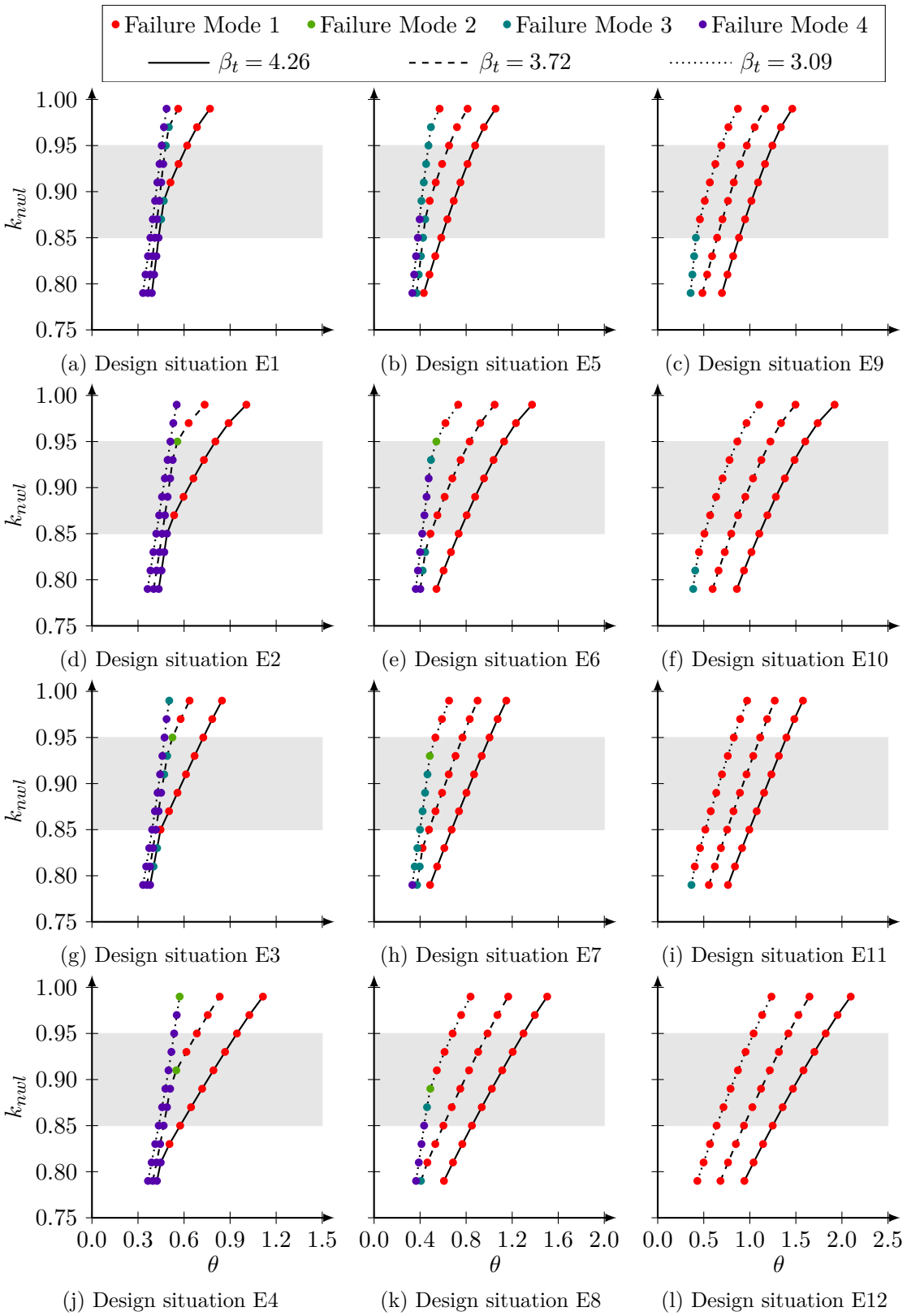

Figure 5.8: Optimum design variable for the design situations E1 to E12, considering the seismic zone 1.5.

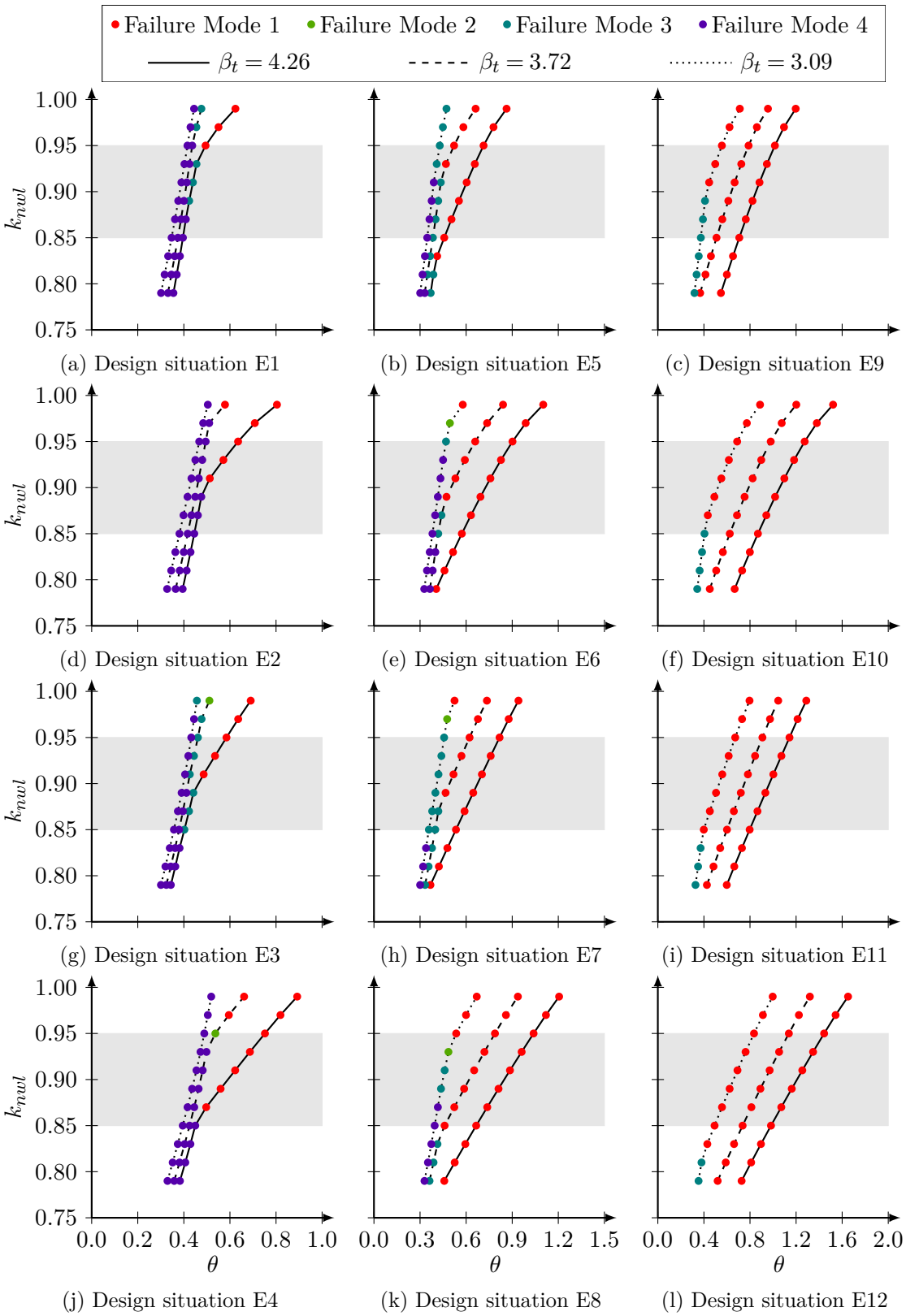

(a) Design situation E1 (b) Design situation E5 (c) Design situation E9

(d) Design situation E2 (e) Design situation E6 (f) Design situation E10

(g) Design situation E3 (h) Design situation E7 (i) Design situation E11

(j) Design situation E4 (k) Design situation E8 (l) Design situation E12

Figure 5.9: Optimum design variable for the design situations E1 to E12, considering the seismic zone 1.6.

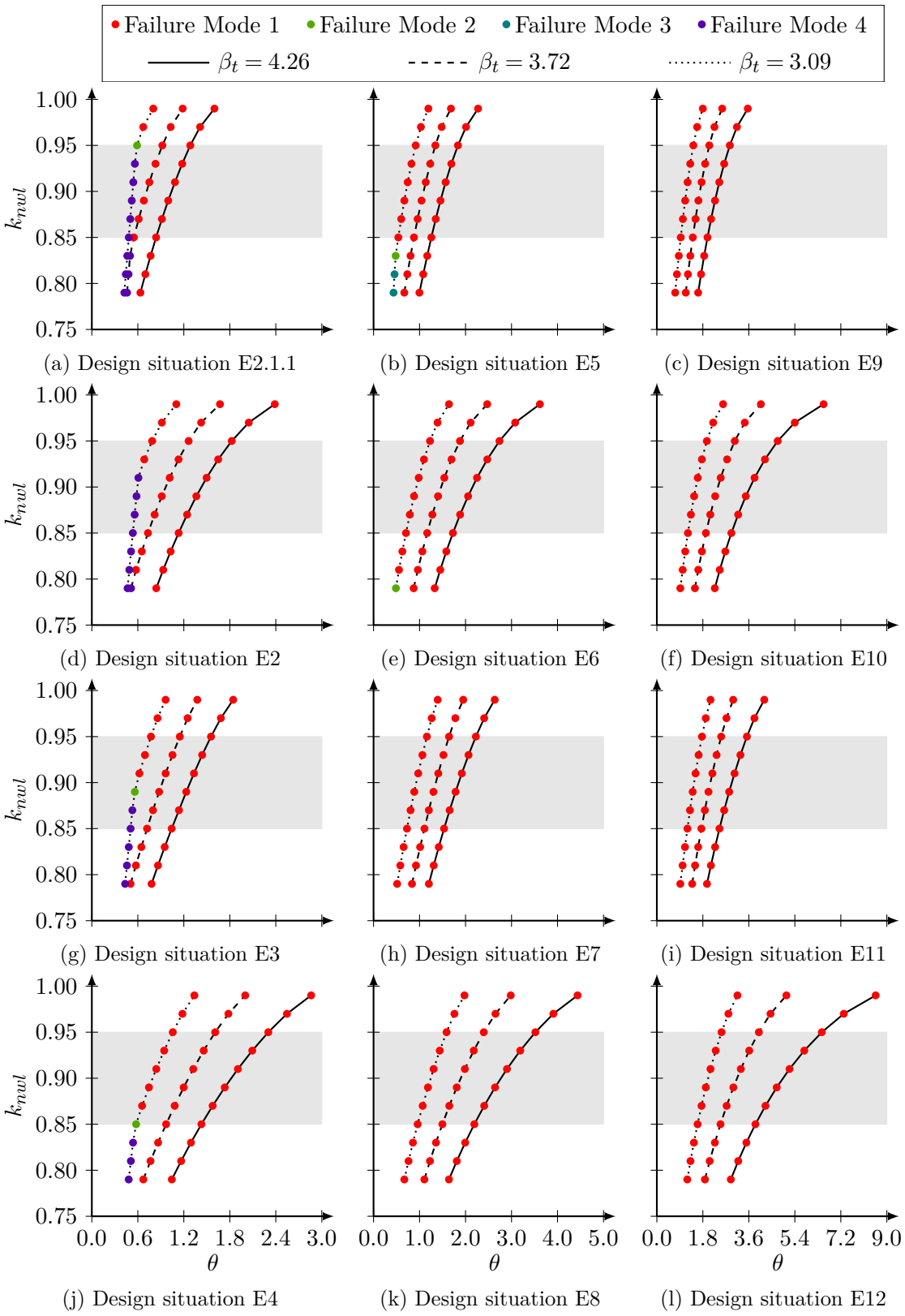

(a) Design situation E2.1.1 (b) Design situation E5 (c) Design situation E9

(d) Design situation E2 (e) Design situation E6 (f) Design situation E10

(g) Design situation E3 (h) Design situation E7 (i) Design situation E11

(j) Design situation E4 (k) Design situation E8 (l) Design situation E12

Figure 5.10: Optimum design variable for the design situations E1 to E12, considering the seismic zone 2.1.

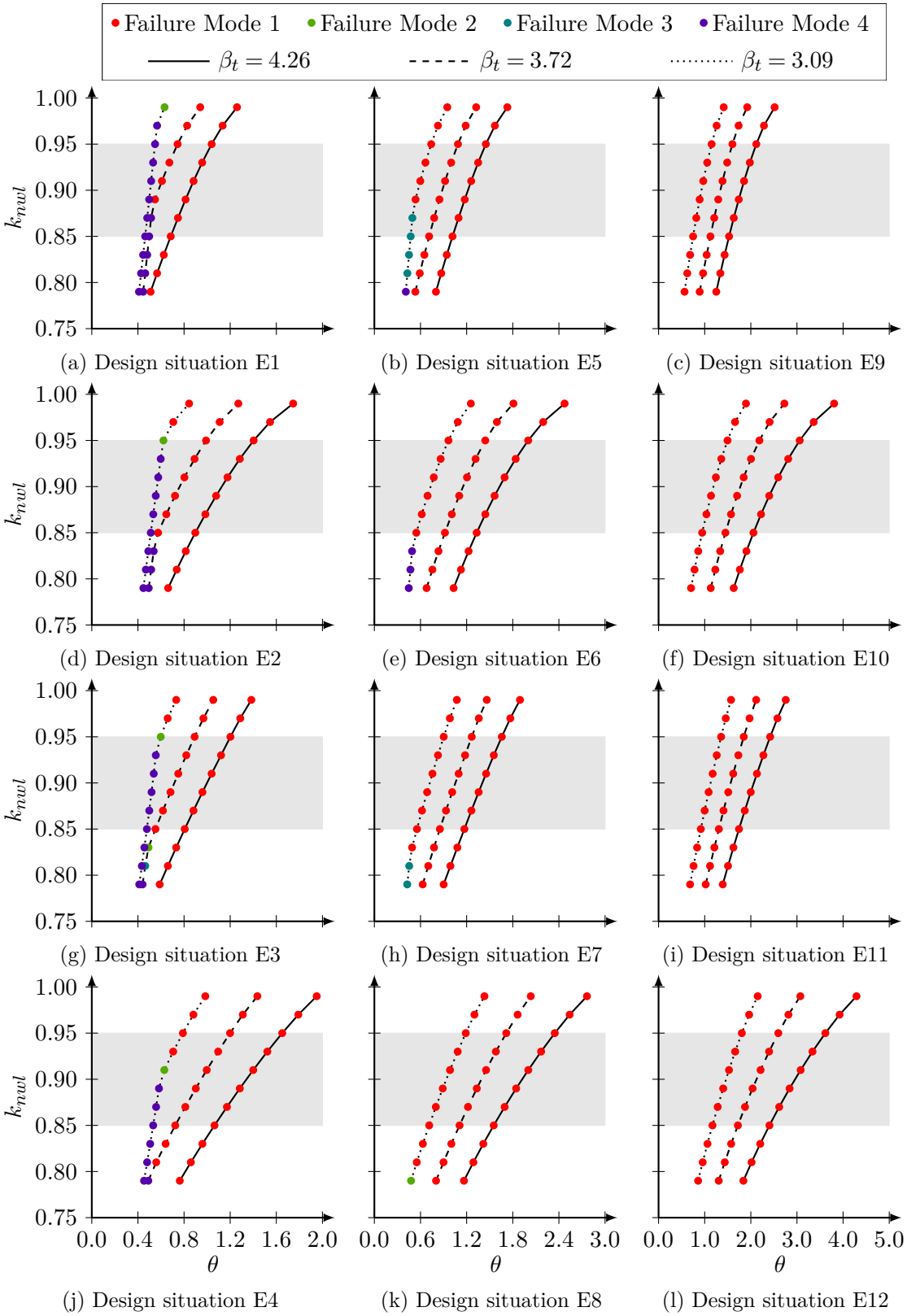

(a) Design situation E1 (b) Design situation E5 (c) Design situation E9

(d) Design situation E2 (e) Design situation E6 (f) Design situation E10

(g) Design situation E3 (h) Design situation E7 (i) Design situation E11

(j) Design situation E4 (k) Design situation E8 (l) Design situation E12

Figure 5.11: Optimum design variable for the design situations E1 to E12, considering the seismic zone 2.2.

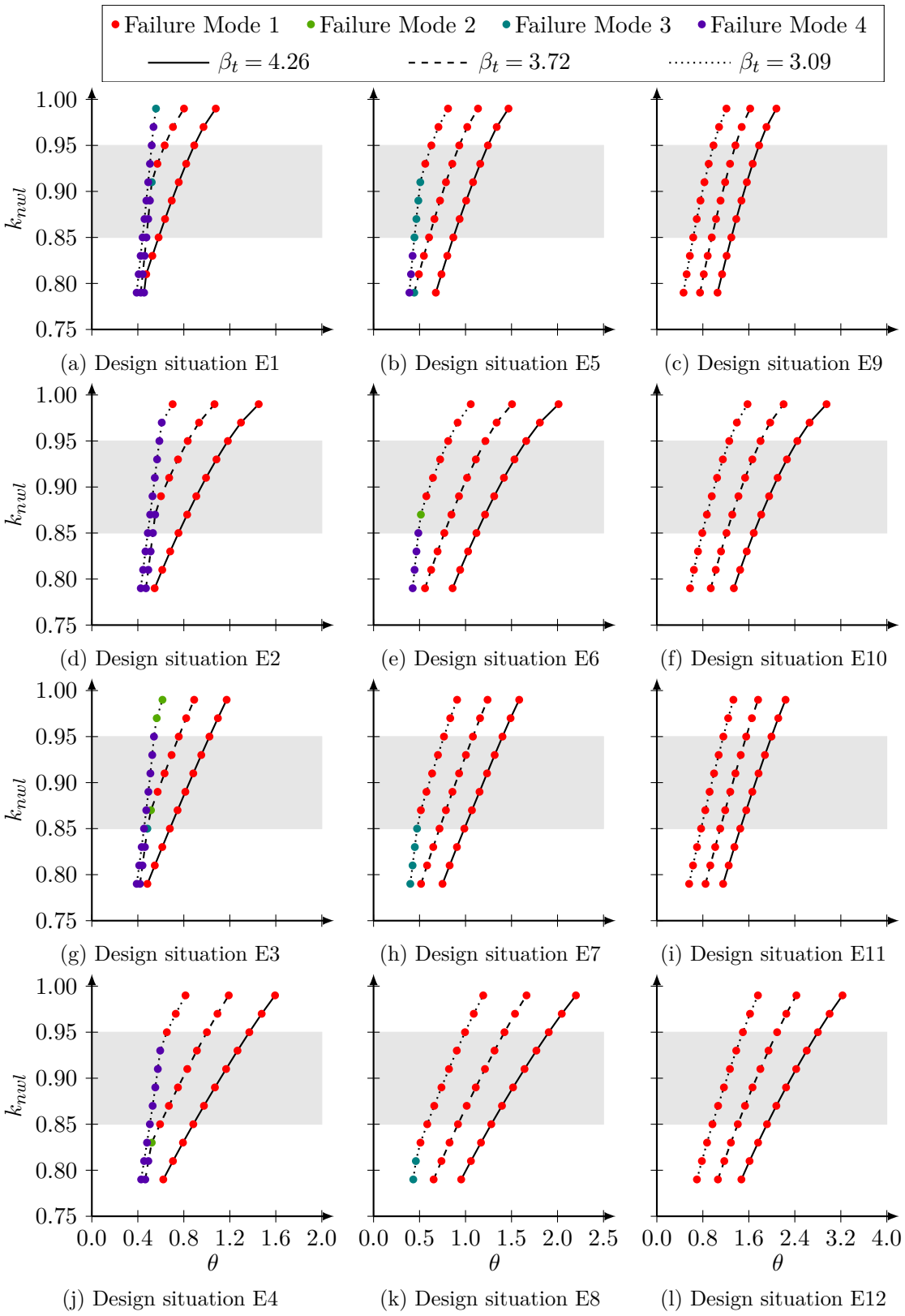

Figure 5.12: Optimum design variable for the design situations E1 to E12, considering the seismic zone 2.3.

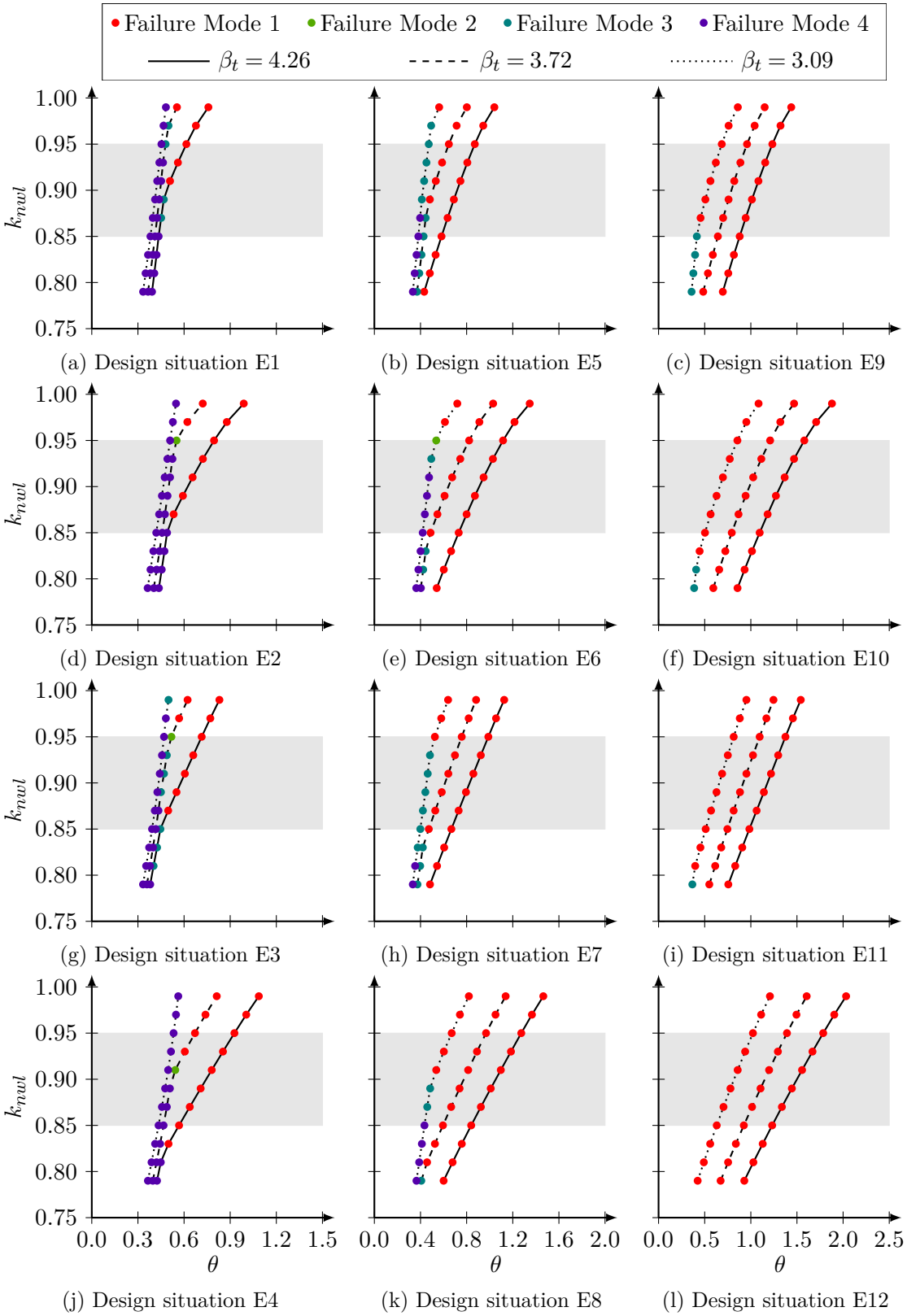

(a) Design situation E1 (b) Design situation E5 (c) Design situation E9

(d) Design situation E2 (e) Design situation E6 (f) Design situation E10

(g) Design situation E3 (h) Design situation E7 (i) Design situation E11

(j) Design situation E4 (k) Design situation E8 (l) Design situation E12

Figure 5.13: Optimum design variable for the design situations E1 to E12, considering the seismic zone 2.4.

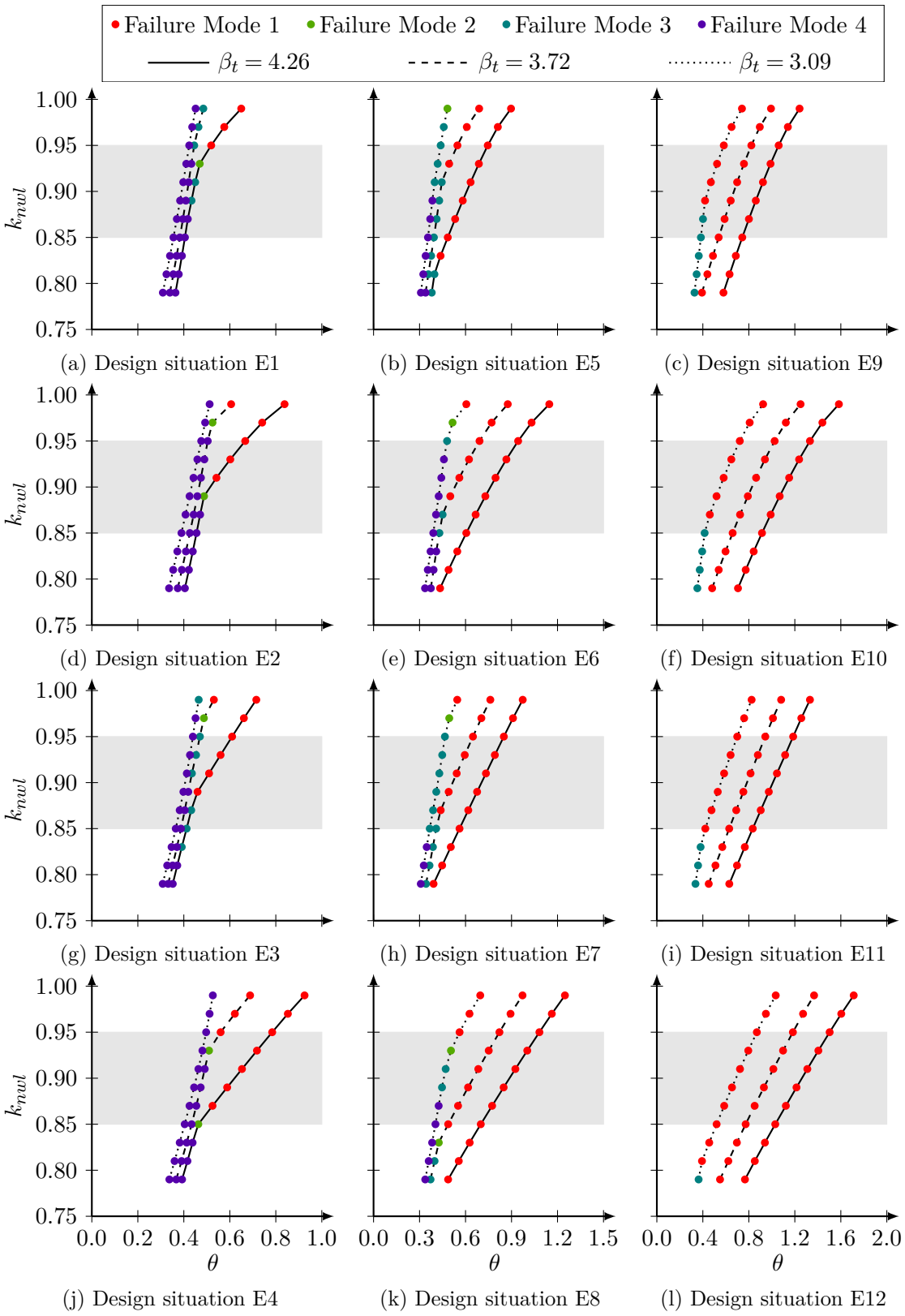

(a) Design situation E1 (b) Design situation E5 (c) Design situation E9

(d) Design situation E2 (e) Design situation E6 (f) Design situation E10

(g) Design situation E3 (h) Design situation E7 (i) Design situation E11

(j) Design situation E4 (k) Design situation E8 (l) Design situation E12

Figure 5.14: Optimum design variable for the design situations E1 to E12, considering the seismic zone 2.5.

and larger target reliability index, the inverse reliability procedure did not even converge to a stable solution since, from certain point, an increase in the downstream face slope led to a decrease in the reliability index because the dam weight increase do not compensate the increase in the equivalent inertia force.

The absence of concrete gravity dams built in high intensity seismic zones of the Portuguese territory, namely the seismic zones 1 to 3 of both seismic types, proves the difficulty in conceiving structural solutions which are economically more advantageous than other types of structures. To conceive cost-effective solutions, other constructive dispositions may be adopted, namely the consideration of a greater keyed depth, such as embraced in Pedrógão dam (located at Vidigueira, seismic zones 1.4 and 2.4), the consideration of a curvature in plan (arch-gravity dams) or, in particular cases, the use of post-tensioned anchors.

Also the influence of the hydraulic and mechanical properties of the rock mass foundation upon the conception of proper structural solutions that fulfill the safety requirements was tested considering, on one hand, the distinction made in the French guidelines (CFBR 2012) between regular and unfavorable geologic conditions and, on the other hand, the three classes defined in the Chinese standards (GB50199 1994) regarding the shear strength of the rock mass foundation. The optimum value for the downstream face slope is inversely proportional to:

- the efficiency of the uplift reduction works carried out, since design situations E1, E3, E5, E7, E9 and E11 (for regular geologic conditions) result in smaller face slopes than design situations E2, E4, E6, E8, E10 and E12 (for unfavorable geologic conditions), respectively; and

- the structural capacity, characterized, for the failure modes 1 to 3, by the dam-foundation friction coefficient, since design situations E1 to E4 (rock mass class I) result in smaller face slopes than design situations E5 to E8 (rock mass class II), which, in turn, results in smaller face slopes than design situations E9 to E12 (rock mass class III).

Before designing a concrete gravity dam, geotechnical investigations aiming to characterize the hydromechanical behavior and the mechanical properties of the rock mass foundation are then crucial to predict the efficiency of uplift reduction works and the shear strength, respectively, and estimate the downstream face slope.

Finally, the influence of the project exploitation type was also tested by considering the distinction between run-of-river and storage exploitation systems whose probability distributions of the relative reservoir water level, for the same k_{nwl}, are different. Although varying, in practice, between 0.85 and 0.95 (shadow area), 11 levels of k_{nwl} were tested, resulting in smaller downstream face slopes for the storage (design situations E1, E2, E5, E6, E9 and E10) than for run-of-river (E3, E4, E7, E8, E11 and E12) exploitation systems. Therefore, for the same exploitation conditions (k_{nwl}) and ignoring the environmental factors that influence the choice on the type of exploitation, a storage exploitation system is more economically attractive, due to both a more profitable use of the water resources and the smaller dimensions that the gravity structure must have to ensure adequate levels of safety.

Regarding the failure modes, the following conclusions might be drawn:

- Failure mode 1 is conditioning for most design situations. Although depending on the loading conditions, only for lower downstream face slopes (roughly lower than 0.5), other failure modes become relevant;

- Rarely, the failure mode 2 was the conditioning one. Even in those cases, the design variable for the failure modes 1 and 3 would not differ considerably from the obtained for the failure mode 2. This was also expected given the proximity of the limit equilibrium conditions between failure modes 1 and 2, such as illustrated in Figure 3.26;

- Failure mode 4 is less sensitive to loading variations, since the slope of the line representing the optimum downstream face slope, for different values of k_{nwl}, is nearly vertical. From failure mode 4 to failure mode 1 the sensitiveness to loading variations increases. Since the slope of the line representing the optimum downstream face slope is greater, failure mode 1 is the most sensitive to loading variations;

- Failure modes are also sensitive to the target reliability index. The degree of sensitiveness decreases from failure mode 1 to failure mode 4 the degree of sensitiveness decreases. For failure mode 4 small variations on the downstream face slope result in extreme variations on the reliability levels.

Regarding the relative sensitivity of each random variable, Figure 5.15 illustrates, using a bar graph, the variability over the design situations considered for each failure mode.

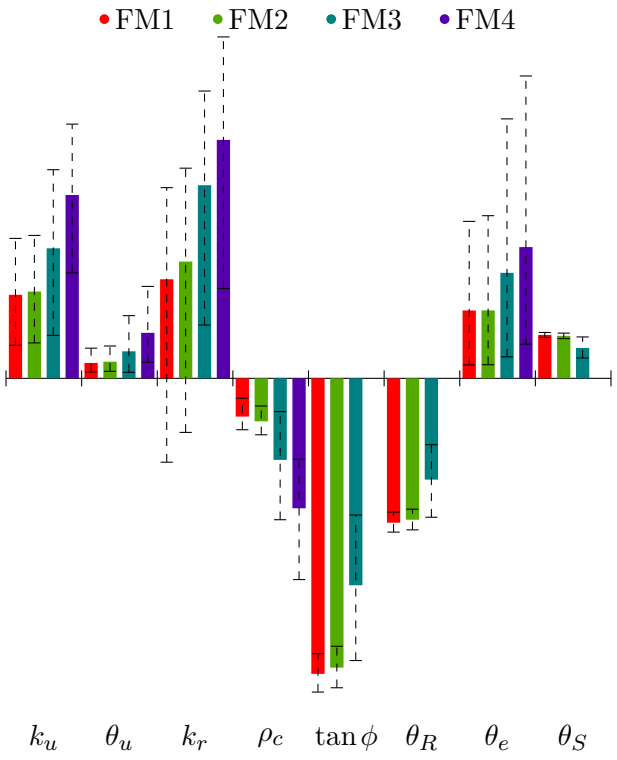

Figure 5.15: Representation of the variability of the relative sensitivity of each random variable for the design situations derived from the accidental earthquake combination.

For the accidental earthquake combination, further information to reduce the uncertainty mostly related to the uplift factor, relative reservoir water level , the seismic load model uncertainty and the friction coefficient would improve the estimation on the probability of failure.

5.5 Final considerations

After the decision upon the construction of a dam, invoking political and social reasons, the choice for concrete gravity dams, between other types of structures and materials, shall present engineering and/or economical advantages, since the fulfillment of performance requirements must not be achieved at disproportionate costs.

Regarding the structural safety, the trade-off between safety and economy is, according to the Portuguese dam safety regulation (RSB 2018), addressed subjectively by considering deterministic safety criteria representing the safety requirements, which shall accommodate a safety margin to account for the inherent uncertainties of the problem, as well as the severity of the consequences of a structural failure. The structural solution obtained shall

ensure adequate levels of safety for the most conditioning foreseeable load conditions arising during the intended service life of the structure, namely those derived from the occurrence of the design flood and the design earthquake, being naturally given by the most demanding case.

Alternatively, a RBDO procedure for the optimum design of concrete gravity dams, such that structural safety is analyzed from a reliability-based perspective explicitly considering the sources of uncertainty, was tested in this chapter covering all design situations derived from both load events that may plausibly compromise its safety.

When comparing to other structural solutions, the typical geometry that makes concrete gravity dams economically competitive is characterized by downstream face slopes in the range of 0.7 to 0.8 (Corns *et al.* 1988), admitting a maximum value, depending on the loading conditions, of 1.0. The results obtained, in which the design variable was quantified such that the safety requirements, representing by target reliability indexes, were fulfilled for all design situations, show increasing sensitivity to the exploitation type, the hydraulic and mechanical characteristics of the rock mass foundation and, above all, to the intensity of the seismic action considered.

The optimal structural solution that satisfies the safety requirements for both load events is almost always conditioned by the accidental earthquake combination, which requires greater values for the downstream face slope. Only in low intensity seismic zones, and for unusual relations between the NWL and the dam height (roughly $k_{nwl} < 0.85$), the extreme hydrological combination may condition the final solution. To attest that, Figure 5.16 compares the optimum values, for a total probability of failure of $1/10^7$, of the downstream face slope for equivalent design situations, namely, E1 or E3, depending on the type of exploitation system (run-of-river or storage), for the seismic load event and F1 for the flood load event, which refer to the case of a rock mass foundation with regular geologic characteristics (Group "U1" the uplift pressures) and rock mass class I (Group "S1" for the shear strength).

For high intensity seismic zones, characterized by peak ground accelerations of considerable value, the minimum downstream face slope, which fulfills the safety requirements, increases to values that surely make this solution cost-prohibitive. Despite the validity of this conclusion, this fact may have been exacerbated by the consideration of the pseudo-static seismic load model to simulate the structural effects due to the occurrence of an earthquake, since this model, considering inertia forces proportional to the structure mass,

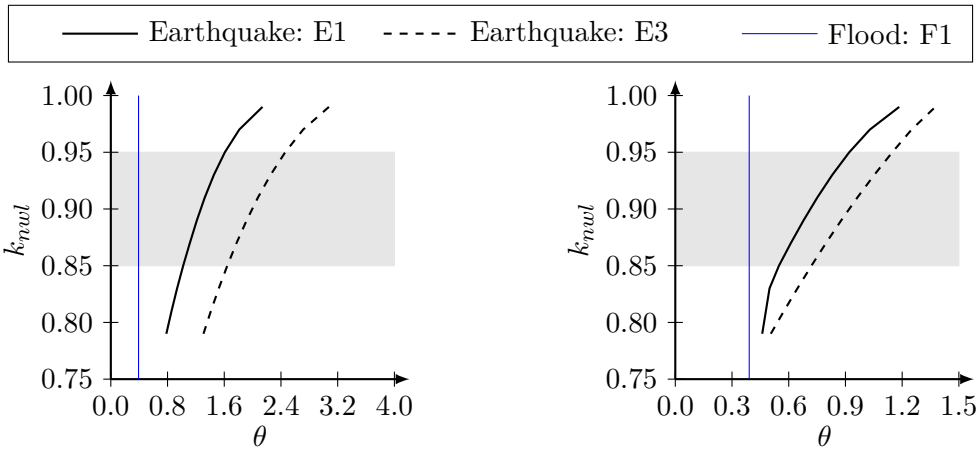

(a) Seismic zone 1.1

(b) Seismic zone 2.1

(c) Seismic zone 1.6

(d) Seismic zone 2.5

Figure 5.16: Comparison between the structural solution, characterized by the downstream face slope, having a total probability of failure of $1/10^7$, for the extreme hydrological combination and the accidental earthquake combination, considering the highest and lowest intensity seismic zones of each type of seismic action.

may lose suitability for an exaggerated increase of the downstream face slope. In fact, the quantification of the analytical seismic load model uncertainty, made in section 4.4.2, was based on numerical models whose downstream face slope varied within a range of practical values (0.75 to 1.00). Its appropriateness for values far from that range cannot then be ensured. Consequently, in some extreme cases, for the most demanding design situations and larger target reliability index, the inverse reliability procedure did not even converge to a stable solution since, from certain point, an increase in the downstream face slope led to a decrease in the reliability index because the dam weight increase do not compensate the increase in the equivalent inertia force.

The absence of concrete gravity dams built in high intensity seismic zones of the Portuguese territory, namely the seismic zones 1 to 3 of both seismic types, proves the

difficulty in conceiving structural solutions which are economically more advantageous than other types of structures. To conceive cost-effective solutions, other constructive dispositions may be adopted, namely the consideration of a greater keyed depth, such as embraced in Pedrógão dam (located at Vidigueira, seismic zones 1.4 and 2.4), the consideration of a curvature in plan (arch-gravity dams) or, in particular cases, the use of post-tensioned anchors.

The most conditioning failure modes depend on the magnitude of the downstream face slope. For gravity profiles characterized by downstream face slopes roughly greater than 0.5, including the range of practical values 0.7 to 1.00, the failure mode 1 is always the most conditioning case. This conclusion remains valid as the safety requirements increase, since gravity profiles shall expectedly be less inclined.

CHAPTER 6

Code calibration for ultimate limit states

6.1 General considerations

Historically, the design of concrete dams has been based on the traditional safety factor methodology, in which the geometric properties of the dam that satisfy a certain design equation, considering predicted values for the loads and material properties, are sought.

Before the formal definition of explicit safety criteria by national regulations, safety factors were selected by the practitioner (Donnelly 2006) such that reservations about the predicted structural capacity, the severity of the consequences of a possible structural failure and the magnitude of loads were implicitly taken into account.

The development of national safety regulations, in order to provide a regulatory framework to drive engineering decisions, were stimulated, when focus on dam safety was prioritized given (ICOLD 1987): (i) the incidents, caused by incompetent design or construction; (ii) the growing dimensions of new dams; (iii) the aging of older dams; and (iv) the increasing number of dams being constructed in countries with little experience in dam engineering. The common approach suggested (ICOLD 1987), denoted as classical approach to dam safety, evidence the importance of continuous surveillance as a tool for the early identification of anomalies and adverse structural behavior and establish explicit safety criteria, based on safety factors, for the dam safety analysis. Nonetheless, room was left for local interpretation and the national regulations quantified safety factors according to their own experience on dam engineering.

Given the inherent conservatism due to implicitly account for all sources of uncertainty on a global safety factor, studies on the applicability of probabilistic principles to dam safety analysis have been encouraged (ICOLD 1987) ever since. It is recognized that the logical trend and primarily goal goes from the predominantly deterministic concept of safety factors to the semi-probabilistic method of partial safety factors, which, although not including explicitly uncertainties and costs, it reduces the inherent conservatism imposed, compensating the increased complexity introduced.

In the semi-probabilistic design method, considering the LRFD format, a comparison between design values for resistance and load effects shall ensure that the designed structure is associated with adequate levels of safety (Faber and Sørensen 2003). Design values are introduced as characteristic values affected by partial safety factors. Furthermore, load combination factors can also multiply some variable loads to take into account the effect of simultaneously occurring variable load effects.

The method for assigning design values for resistance and loads evolved from an experience-based approach to a reliability-based approach after the development of structural reliability methods. This way, the calibration of a code applied to a class of structures, is a process of minimizing the deviations between the reliability of representative structures, designed according to the suggested code, and the target reliability, such that conservatism is minimized.

The factors that influence the choice of the target reliability index, such as the frequency of the load event, the suddenness of structural failure and the severity of the associated consequences, shall be shared within the class of structures such that the reliability of structures is approximately homogeneous. If such cannot be ensured, subdivision in several class of structures, to which the calibration problem is addressed separately, shall be considered.

The code calibration process (Figure 6.1) for ultimate limit states of concrete gravity dams, considering separately the main load events (flood and earthquake) which may compromise the structural safety, are detailed in the following sections. After the formulation of the code, introducing the code domain, code objective and the code formats tested, the partial safety factors for both load events are calibrated in a code optimization procedure. Later, the obtained code is checked by comparing the reliability of structures designed according to the code to the target reliability index.

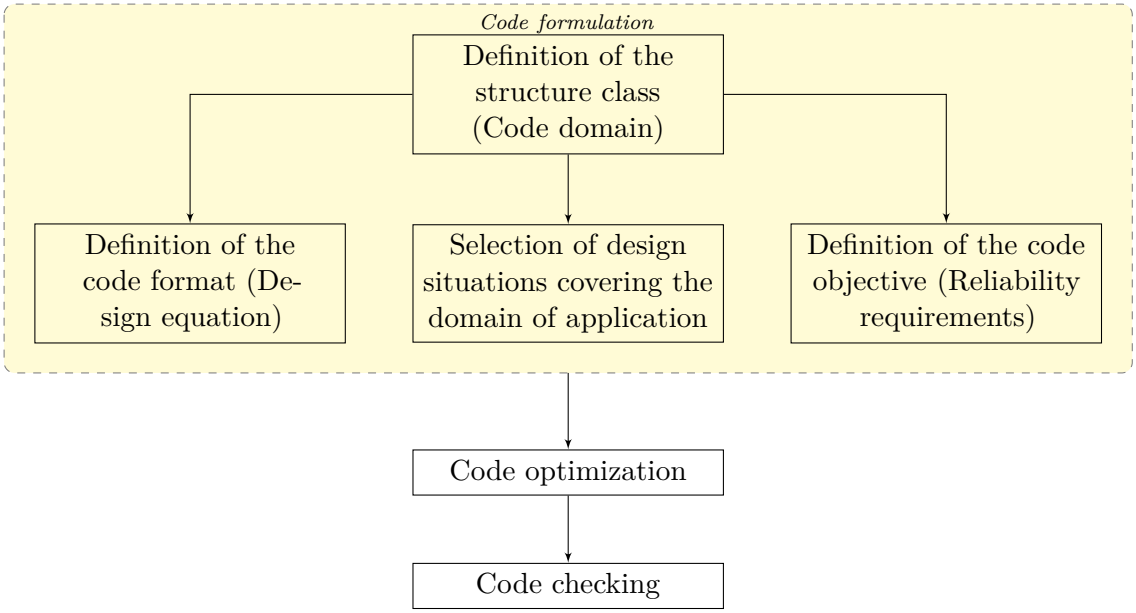

Figure 6.1: Code calibration task scheme.

6.2 Code formulation

6.2.1 Code domain

The definition of the code domain aims to identify the structure class on which the code should operate (Ditlevsen and Madsen 1996) defining not only the type of structures covered, but also geographical domains, failure modes, materials, etc.

Since, by definition, large dams encompass a vast group of structures, with heights above 15 meters or between 5 and 15 meters with large capacity reservoirs (ICOLD 2017), multiple structures, varying the dam height and key depth, must be considered. However, to keep the process simple and comprehensible, only the case study considered in Chapter 5 (a theoretical 100-meter-high gravity profile, keyed into the foundation at a depth corresponding to 10% of its height), is used for the code calibration.

Also, separation between the load events is considered so that one can judge independently the partial safety factors calibrated. A more complex code, including load combination factors, could be considered instead but would introduce redundancy and unpredictability in the optimization process which is intended to be avoided at this stage. Therefore, two code domains are considered: (i) one related to the flood load event; and (ii) other related to the earthquake load event.

6.2.2 Code objective

The code objective is any requirement that the referred class of structures shall fulfill. It is generally given by a target reliability index or a target failure probability, corresponding to the intended level of safety.

The derivation of a target reliability index, intrinsically related to tolerable risks, is a complex task taken in socio-political and/or institutional levels. The possibility of calibration to previous codes is often mentioned (Schneider 1997; Melchers 1999), assuming that the existing practice is optimal. The fact that, if structures designed according to previous codes have failed the codes/practice would have changed quickly (Westberg 2010), may attest the suitability of this approach. However, if implicit safety levels of previous codes were optimal, code reformulation would not be justified. In the case of concrete dams, since present codes are still based on safety factors and safety is then not measurable, only the inherent conservatism has ensured sufficient safety levels.

Since target failure probabilities for concrete dams shall be related to the severity of the consequences and the suddenness of failure (ductile or brittle), three values for the total failure probability are tested, such as in Chapter 5, assuming that the intended range of safety levels may thus be covered: $1/10^8$, $1/10^7$ and $1/10^6$.

6.2.3 Code format

The definition of the code format is the process of selecting the design elements (partial safety factors, load combination factors, etc) in which the code is formulated. Most of physical quantities (related to geometry, loads, material properties and load models) have some degree of uncertainty, which is concentrated in these elements.

Simpler code format consists of a specific set of characteristic values and corresponding partial safety factors. More complexly, code formats can be given by load combination factors (to cover several load combinations), importance factors (to cover other class of structures related to different severity of the consequences of failure) and/or partial safety factors defined explicitly in terms of mathematical expressions (Ditlevsen and Madsen 1996).

In general, since codes cover a wide class of structures and design situations, even the simplest code objective cannot be satisfied exactly by any chosen code format except possibly code formats of an unacceptable level of complexity (Ditlevsen and Madsen 1996).

A code shall then balance simplicity, avoiding misinterpretations, and optimality, ensuring the most optimal solutions.

Since structural codes usually consider the single failure mode checking format (Faber and Sørensen 2003), for the safety analysis of concrete gravity dams, according to the ultimate limit states derived from the failure modes identified, the design equations shall then be verified separately and the most conditioning one rules the safety level. For the ultimate limit states, the following design equations are suggested,

$$E_d \leq R_d \Leftrightarrow \begin{cases} S_1\left[W_k \cdot \gamma_W; I_k \cdot \gamma_I; U_k \cdot \gamma_U; (E_k \cdot \gamma_E)\right] \leq \tan(\phi)_k / \gamma_m \\ S_2\left[W_k \cdot \gamma_W; I_k \cdot \gamma_I; U_k \cdot \gamma_U; (E_k \cdot \gamma_E)\right] \leq \tan(\phi)_k / \gamma_m \\ S_3\left[W_k \cdot \gamma_W; I_k \cdot \gamma_I; U_k \cdot \gamma_U; (E_k \cdot \gamma_E)\right] \leq \tan(\phi)_k / \gamma_m \\ M_c\left[W_k \cdot \gamma_W; I_k \cdot \gamma_I; U_k \cdot \gamma_U; (E_k \cdot \gamma_E)\right] \leq 0 \end{cases} \tag{6.1}$$

where W_k, I_k, U_k and E_k are the characteristic values of the load effects (net force or resultant moment) due to the structure weight, the hydrostatic pressure, the uplift pressure and the seismic action, respectively, and γ_W, γ_I, γ_U and γ_E are the corresponding partial safety factors. $\tan(\phi)_k$ and γ_m are the characteristic value for the friction coefficient and the corresponding partial safety factor, respectively.

Characteristic values are often given by values associated with a fixed probability p of non-exceedance, i.e.,

$$X_k = F_X^{-1}(p) \tag{6.2}$$

where F_X^{-1} is the inverse distribution function of a random variable X and p is the probability arbitrarily selected but influenced by rational considerations (Thoft-Christensen 2001):

- characteristic values of loads are values which shall rarely be exceeded (often $p = 95\%$);
- characteristic values of material strength properties should normally be exceeded by actual properties (often $p = 5\%$);
- the values of p should neither be so large nor so small that the values X_k are not occasionally encountered.

Moreover, mean values are occasionally considered as characteristic values for quantities with low variability (such as permanent loads or geometrical features) or when advantages in the code construction can be taken therefrom.

The characteristic values considered in this work are defined in order to adapt the current design practice and to ensure that the partial safety factors calibrated in the following section are necessarily greater than one for unfavorable loads and smaller than one for favorable loads. Therefore:

- The same partial safety factor shall affect the three groups in which the residual friction coefficient, which characterizes the structural capacity, is divided, depending on the foundation characteristics. Thus, the 5th percentiles of the corresponding distribution function are considered as characteristic values ($\tan(\phi)_k = 0.98$ for the rock mass class I or group S1, $\tan(\phi)_k = 0.83$ for the rock mass class II or group S2, $\tan(\phi)_k = 0.70$ for the rock mass class III or group S3).

- The characteristic hydrostatic pressure I_k is given in terms of the characteristic value of a dimensionless variable $k_{r,k}$. In the current practice, deterministic values of the reservoir water level are used for the safety analysis (FWL for the flood events and NWL for normal operation), whose corresponding values of k_r are here considered, by simplicity, as characteristic values ($k_{r,k} = k_{fwl}$ for the flood events and $k_{r,k} = k_{nwl}$ for the normal operation), regardless the project type (group R1 for run-of river projects and group R2 for storage purposes);

- The characteristic value of the structure weight W_k is given in terms of the characteristic concrete density $\rho_{c,k}$, considered equal to the mean value of the distribution function ($\rho_{c,k} = 2400$ kg/m^3), such as recommended in the Eurocodes (EN1990 2002).

- The characteristic uplift pressure is given in terms of the characteristic value of the uplift factor $k_{u,k}$, which defines the pressure at the drainage line. Dam safety regulations indicate round-figure thresholds (0.25, 0.33, 0.50 and 0.66) for its quantification. From the uncertainty modeling presented in section 4.2.3, the mean values obtained for the uplift factor, opportunely close to 0.25 and 0.50, for regular (Group U1) and unfavorable (Group U2) foundation geologic conditions, respectively, are here considered as characteristic values ($k_{u,k} = 0.25$ for the group U1 and $k_{u,k} = 0.50$ for the group U2);

- The seismic action is computed through the pseudo-static load model as a function of the peak ground acceleration, given in the national annex of the Eurocode 8 (NP EN1998-1 2010), depending on the dam location. The partial safety factor proposed

shall be understood as a correction factor to account the uncertainties regarding: (i) the suitability of the model to represent the seismic load; and (ii) the random nature of the seismic load. Thus, the characteristic value of the seismic load E_k is computed directly from the pseudo-static load model considering the regulatory peak ground acceleration.

Regarding the distinction of partial safety factors between the design equations (failure modes), three approaches are tested:

- Code format CF1 considering different partial safety factors for all design equations;
- Code format CF2 considering partial safety factors grouped for the design equations mainly associated with sliding mechanisms (failure mode 1 and 2), and for the design equations associated with rotational mechanisms (failure mode 3 and 4);
- Code format CF3 considering the same set of partial safety factors for all design equations.

6.3 Code optimization

6.3.1 Optimization procedure

In the code optimization, the best set of partial safety factors $\boldsymbol{\gamma}$, which minimizes the deviations between the inherent reliability level of the structures designed according to the code and the reliability requirements (code objective), is sought.

The optimization procedure accounts for the relative importance of each design situation, which shall cover the code domain, through weight factors ω, and penalizes the deviations of the code from the objective ($\zeta - \zeta_t$ or $\zeta/\zeta_t - 1$), through a penalty function M (equation 2.61), which shall penalize more underdesigned than overdesigned structures, such that the total expected losses Δ (equation 2.62) are minimized. The optimization problem was detailed in section 2.7.2.

In this study, the numerical minimization routine is performed using the alternative design-value method proposed (Figure 2.15), based on the consideration of the design variable (downstream face slope) as degree-of-fit parameter $\zeta = \theta$, which avoids the difficulties of extracting information from the results of the original design-value method (Ditlevsen and Madsen 1996) and dispenses the performance of repeated reliability analysis at each

iteration, as opposite to the global optimization method. Also a relative measure of the deviations ($\zeta/\zeta_t - 1$) is used in order to account that gravity dams with large values of the downstream face slope would not probably be built, and gravity structures with other geometric provisions or other types of structures would be considered instead. Thus, the importance of achieving a good adjustment to design situations associated with smaller values of the downstream face slope is enhanced.

However, the relative importance of each design situation shall express, not only the importance of achieving a good adjustment to the code objective for a specific design situation ($\omega_j^{(1)}$), but also the influence of the variation of the design variable θ on the reliability index ($\omega_j^{(2)}$). For that, prior to the minimization routine, the weight factor ω_j, for the design situation j, shall be quantified using equation 2.68. Generally, except in particular cases, a good adjustment is equally important for all design situations (the greater importance posed on design situations associated with smaller downstream face slopes is masked by the selection of the relative measure of deviations). Therefore, the influence of the variation of the design variable on the reliability index ($\omega_j^{(2)}$), which is computed for each design situation using the results of the reliability-based design presented in Chapter 5, rules the order of magnitude of the associated weight factor ω_j.

The next section synthesize the results of the code optimization procedure (illustrated in Figure 2.15), applied to the structures under load conditions corresponding to the occurrence of: (i) the design flood; and (ii) the design earthquake.

6.3.2 Extreme hydrological combination (flood load event)

6.3.2.1 General considerations

The code calibrated shall cover not only the design situations F1 to F6, presented in Table 5.2 considering the different subgroups in which the random variables are divided, but also the failure modes that share the same set of partial safety factors. Therefore:

- For the code format CF1, since partial safety factors depend on the failure mode, the code optimization procedure is performed, and repeated for each failure mode, considering $N = 6 \times 1 = 6$ design situations;

- For the code format CF2, since partial safety factors are shared within two groups, one related to the failure modes 1 and 2 and other related to the failure modes 3

and 4, the code optimization procedure is performed, and repeated for each group, considering $N = 6 \times 2 = 12$ design situations;

- For the code format CF3, since all failure modes share the same partial safety factors, the code optimization procedure is performed considering $N = 6 \times 4 = 24$ design situations.

Furthermore, the code objective refers to the total probability of failure. The reliability requirements for non-permanent load events, characterized by a specific return period, is given by the probability of failure conditioned to their occurrence. For the flood load event (characterized by the occurrence of the design flood with, for instance, 5000 years of return period), such as considered for the reliability-based design (Chapter 5), the conditional probabilities of failure $p_{ft}|E = 5 \cdot 10^{-5}$ ($\beta_t|E = 3.89$), $p_{ft}|E = 5 \cdot 10^{-4}$ ($\beta_t|E = 3.29$) and $p_{ft}|E = 5 \cdot 10^{-3}$ ($\beta_t|E = 2.58$), corresponding to the code objective $1/10^8$, $1/10^7$ and $1/10^6$, respectively, are targeted.

6.3.2.2 Relevant results

From an initial set of partial safety factors based on the design points obtained in the reliability-based procedure, the code optimization led to the results presented in Tables 6.1, 6.2 and 6.3 for target reliability indexes of $\beta_t|E = 3.89$, $\beta_t|E = 3.29$ and $\beta_t|E = 2.58$, respectively.

Table 6.1: Code optimization results, considering the flood load event, for a target reliability index of $\beta_t|E = 3.89$.

	CF1				CF2		CF3
	FM1	FM2	FM3	FM4	FM1,FM2	FM3,FM4	FM1-FM4
γ_G	0.96	0.94	0.95	0.92	0.94	0.90	0.92
γ_I	1.07	1.11	1.05	1.11	1.10	1.08	1.11
γ_U	1.15	1.15	1.26	1.27	1.13	1.26	1.25
γ_m	1.55	1.46	1.40	-	1.48	1.30	1.36
$N \cdot \Delta$ (10^1)	< 0.01	< 0.01	0.03	0.00	0.01	0.93	1.67

The following aspects are concluded from these results:

- Structure weight, as a favorable load, shall be affected by a partial safety factors smaller than one. For the remain loads, partial safety factors greater than one were ensured;

Table 6.2: Code optimization results, considering the flood load event, for a target reliability index of $\beta_t|E = 3.29$.

	CF1				CF2		CF3
	FM1	FM2	FM3	FM4	FM1,FM2	FM3,FM4	FM1-FM4
γ_G	0.98	0.97	0.96	0.94	0.97	0.94	0.94
γ_I	1.03	1.08	1.03	1.09	1.06	1.08	1.08
γ_U	1.12	1.12	1.23	1.27	1.10	1.26	1.25
γ_m	1.44	1.36	1.35	-	1.40	1.27	1.27
$N \cdot \Delta$ (10^1)	< 0.01	< 0.01	0.04	0.00	0.01	1.03	1.31

Table 6.3: Code optimization results, considering the flood load event, for a target reliability index of $\beta_t|E = 2.58$.

	CF1				CF2		CF3
	FM1	FM2	FM3	FM4	FM1,FM2	FM3,FM4	FM1-FM4
γ_G	0.99	0.98	0.98	0.96	0.98	0.96	0.96
γ_I	1.02	1.04	1.01	1.06	1.04	1.06	1.06
γ_U	1.07	1.08	1.08	1.27	1.08	1.26	1.25
γ_m	1.26	1.22	1.25	-	1.23	1.21	1.20
$N \cdot \Delta$ (10^1)	< 0.01	< 0.01	0.04	0.00	< 0.01	0.90	1.54

- As expected, given the small number of design situations considered in the code format CF1, the reliability requirements are fulfilled almost perfectly since the total expected losses $N \cdot \Delta$ are very small;

- Naturally, the simplification from the code format CF1 to the code format CF2, and posteriorly from code format CF2 to code format CF3, comes at a cost of loss of optimality, given the higher losses.

- The grouping of failure modes 1 and 2, in the same code domain, is not as much penalizing as the grouping of failure modes 3 and 4, since, on one hand, the best set of partial safety factors is similar for both failure modes and, on the other hand, the smaller weight factors (listed in the following section) allows easier manipulation of the partial safety factors;

- As the reliability requirements decrease, the partial safety factors naturally get closer to one, reflecting the lower conservatism required in the code.

6.3.2.3 Code check

The code check, intending to evaluate the quality of the results and decide upon different alternatives regarding the code format, is performed by comparing the inherent reliability index of structures designed according to the new code, considering all design situations, to the target reliability index. Alternatively, the comparison can be made using the design variable, since the minimization routine considers the design variable as degree-of-fit parameter.

Tables 6.4, 6.5 and 6.6 compare the design variable (and reliability index) obtained using the calibrated code (θ_1 for the code format CF1, θ_2 for the code format CF2 and θ_3 for the code format CF3) to the optimum solution, obtained from the reliability-based design, for target reliability indexes of $\beta_t|E = 3.89$, $\beta_t|E = 3.29$ and $\beta_t|E = 2.58$, respectively.

Since an asymmetrical penalty function, penalizing more underdesigned than overdesigned structures, was considered, the difference between the inherent reliability index throughout the structure class shall be greater, in average, than the target reliability index. Accordingly, the computed mean values of this difference, using the code formats CF1, CF2 and CF3, are presented in Table 6.7.

Alternatively, for comparison purposes, the accuracy of codes calibrated using different code formats can be evaluated through the variation (i.e., the standard deviation) of the difference $\beta_j - \beta_t|E$, which are presented, for the code formats CF1, CF2 and CF3, in Table 6.8.

Naturally, as the code domain is extended to more design situations (from code format CF1 to code format CF2 and from code format CF2 to code format CF3), the standard deviation of the difference $\beta_j - \beta_t|E$ increases.

6.3.3 Accidental earthquake combination (earthquake load event)

6.3.3.1 General considerations

The loads due to the design earthquake shall overlap the existing loading conditions in normal operation periods. As mentioned, in those cases, the reservoir water level depends on the normal water level (NWL) of a specific dam. Also the magnitude of the seismic loads depends on the dam location, according to the Portuguese seismic map (Figure 3.16).

Therefore, the code calibrated shall cover not only the design situations E1 to E12, presented in Table 5.30 considering the different subgroups in which the random variables

Table 6.4: Comparison of the optimum design variable and the solution of the optimized code, for a target reliability index of 3.89.

	FM	$\omega^{(2)}$	$\theta^*\,(\beta^*)$	$\theta_1\,(\beta_1)$	$\theta_2\,(\beta_2)$	$\theta_3\,(\beta_3)$
F1	1	3.15	0.81 (3.89)	0.81 (3.90)	0.81 (3.89)	0.77 (3.76)
	2	4.10	0.72 (3.89)	0.72 (3.91)	0.73 (3.95)	0.71 (3.85)
	3	31.48	0.46 (3.89)	0.46 (3.86)	0.48 (4.65)	0.49 (4.79)
	4	42.54	0.40 (3.89)	0.40 (3.89)	0.40 (3.80)	0.40 (3.83)
F2	1	2.50	1.00 (3.89)	1.00 (3.89)	0.99 (3.87)	1.01 (3.92)
	2	3.19	0.88 (3.89)	0.88 (3.89)	0.89 (3.91)	0.92 (3.99)
	3	25.27	0.52 (3.89)	0.52 (3.82)	0.55 (4.63)	0.55 (4.70)
	4	35.40	0.46 (3.89)	0.46 (3.89)	0.45 (3.78)	0.45 (3.75)
F3	1	3.59	0.57 (3.89)	0.57 (3.90)	0.56 (3.87)	0.52 (3.71)
	2	4.73	0.54 (3.89)	0.54 (3.89)	0.55 (3.93)	0.52 (3.81)
	3	28.48	0.44 (3.89)	0.44 (4.01)	0.46 (4.57)	0.47 (4.82)
	4	42.54	0.40 (3.89)	0.40 (3.89)	0.40 (3.80)	0.40 (3.83)
F4	1	2.91	0.71 (3.89)	0.72 (3.91)	0.71 (3.88)	0.71 (3.88)
	2	3.73	0.66 (3.89)	0.66 (3.89)	0.67 (3.92)	0.68 (3.96)
	3	22.14	0.50 (3.89)	0.50 (4.00)	0.53 (4.58)	0.53 (4.76)
	4	35.40	0.46 (3.89)	0.46 (3.89)	0.45 (3.78)	0.45 (3.75)
F5	1	3.77	0.38 (3.89)	0.38 (3.88)	0.37 (3.83)	0.31 (3.63)
	2	5.37	0.40 (3.89)	0.40 (3.87)	0.41 (3.91)	0.38 (3.76)
	3	24.22	0.42 (3.89)	0.42 (3.84)	0.41 (3.79)	0.44 (4.41)
	4	42.54	0.40 (3.89)	0.40 (3.89)	0.40 (3.80)	0.40 (3.83)
F6	1	3.16	0.50 (3.89)	0.50 (3.91)	0.49 (3.86)	0.47 (3.81)
	2	4.27	0.50 (3.89)	0.50 (3.89)	0.50 (3.92)	0.50 (3.92)
	3	18.09	0.47 (3.89)	0.47 (3.91)	0.47 (3.92)	0.50 (4.43)
	4	35.40	0.46 (3.89)	0.46 (3.89)	0.45 (3.78)	0.45 (3.75)

are divided, but also: (i) the failure modes that share the same set of partial safety factors; (ii) different values of k_{nwl} (in the reliability-based design presented, 11 levels were tested), since probability distribution functions of the reservoir water level, during normal operation conditions, depend on this property; and (iii) any dam location. Since optimum solutions for seismic zones 1.1, 1.2, 2.1 and 2.2 usually imply large values for the design variable (downstream face slope), discouraging the choice to build concrete gravity dams in those locations, only the remain 7 seismic zones are considered (seismic zones 3 to 6, for seismic type 1, and seismic zones 3 to 5, for seismic type 2), avoiding unnecessary constraints in the optimization procedure. Therefore:

Table 6.5: Comparison of the optimum design variable and the solution of the optimized code, for a target reliability index of 3.29.

	FM	$\omega^{(2)}$	$\theta^*\,(\beta^*)$	$\theta_1\,(\beta_1)$	$\theta_2\,(\beta_2)$	$\theta_3\,(\beta_3)$
F1	1	3.48	0.63 (3.29)	0.63 (3.30)	0.63 (3.30)	0.61 (3.23)
	2	4.56	0.58 (3.29)	0.58 (3.30)	0.59 (3.33)	0.58 (3.30)
	3	31.64	0.44 (3.29)	0.44 (3.29)	0.47 (4.11)	0.46 (4.10)
	4	45.29	0.39 (3.29)	0.39 (3.29)	0.39 (3.19)	0.39 (3.17)
F2	1	2.82	0.78 (3.29)	0.77 (3.29)	0.76 (3.26)	0.81 (3.39)
	2	3.61	0.71 (3.29)	0.70 (3.27)	0.70 (3.27)	0.75 (3.45)
	3	24.00	0.49 (3.29)	0.49 (3.21)	0.52 (4.04)	0.52 (4.00)
	4	36.39	0.44 (3.29)	0.44 (3.29)	0.44 (3.12)	0.44 (3.08)
F3	1	3.78	0.41 (3.29)	0.41 (3.30)	0.41 (3.29)	0.37 (3.17)
	2	5.29	0.42 (3.29)	0.42 (3.29)	0.42 (3.33)	0.41 (3.26)
	3	26.63	0.42 (3.29)	0.42 (3.43)	0.44 (4.01)	0.44 (4.00)
	4	45.29	0.39 (3.29)	0.39 (3.29)	0.39 (3.19)	0.39 (3.17)
F4	1	3.17	0.52 (3.29)	0.52 (3.30)	0.51 (3.28)	0.53 (3.34)
	2	4.24	0.51 (3.29)	0.51 (3.28)	0.51 (3.29)	0.54 (3.42)
	3	19.45	0.47 (3.29)	0.47 (3.41)	0.50 (3.99)	0.50 (3.96)
	4	36.39	0.44 (3.29)	0.44 (3.29)	0.44 (3.12)	0.44 (3.08)
F5	1	3.03	0.22 (3.29)	0.21 (3.28)	0.20 (3.26)	0.11 (3.08)
	2	6.02	0.30 (3.29)	0.29 (3.28)	0.30 (3.32)	0.28 (3.22)
	3	19.03	0.39 (3.29)	0.39 (3.22)	0.38 (3.15)	0.38 (3.15)
	4	45.29	0.39 (3.29)	0.39 (3.29)	0.39 (3.19)	0.39 (3.17)
F6	1	3.01	0.31 (3.29)	0.31 (3.31)	0.30 (3.28)	0.29 (3.24)
	2	4.89	0.37 (3.29)	0.36 (3.29)	0.37 (3.31)	0.38 (3.38)
	3	13.83	0.43 (3.29)	0.43 (3.31)	0.43 (3.31)	0.43 (3.30)
	4	36.39	0.44 (3.29)	0.44 (3.29)	0.44 (3.12)	0.44 (3.08)

- For the code format CF1, since partial safety factors depend on the failure mode, the code optimization procedure is performed, and repeated for each failure mode, considering $N = 12 \times 11 \times 7 \times 1 = 924$ design situations;

- For the code format CF2, since partial safety factors are shared within two groups, one related to the failure modes 1 and 2 and other related to the failure modes 3 and 4, the code optimization procedure is performed, and repeated for each group, considering $N = 12 \times 11 \times 7 \times 2 = 1848$ design situations;

- For the code format CF3, since all failure modes share the same partial safety factors,

Table 6.6: Comparison of the optimum design variable and the solution of the optimized code, for a target reliability index of 2.58.

	FM	$\omega^{(2)}$	$\theta^*\,(\beta^*)$	$\theta_1\,(\beta_1)$	$\theta_2\,(\beta_2)$	$\theta_3\,(\beta_3)$
F1	1	3.76	0.43 (2.58)	0.43 (2.59)	0.43 (2.57)	0.48 (2.78)
	2	5.20	0.43 (2.58)	0.44 (2.59)	0.44 (2.59)	0.48 (2.83)
	3	29.97	0.42 (2.58)	0.42 (2.58)	0.44 (3.46)	0.44 (3.40)
	4	49.20	0.37 (2.58)	0.37 (2.58)	0.37 (2.52)	0.37 (2.47)
F2	1	3.18	0.54 (2.58)	0.53 (2.56)	0.53 (2.56)	0.65 (2.94)
	2	4.21	0.52 (2.58)	0.52 (2.56)	0.52 (2.57)	0.62 (2.98)
	3	21.14	0.46 (2.58)	0.46 (2.49)	0.50 (3.41)	0.50 (3.34)
	4	36.66	0.42 (2.58)	0.42 (2.58)	0.42 (2.48)	0.42 (2.41)
F3	1	2.92	0.21 (2.58)	0.21 (2.58)	0.20 (2.55)	0.25 (2.70)
	2	6.06	0.29 (2.58)	0.29 (2.58)	0.29 (2.59)	0.33 (2.80)
	3	19.80	0.39 (2.58)	0.39 (2.69)	0.42 (3.25)	0.41 (3.16)
	4	49.20	0.37 (2.58)	0.37 (2.58)	0.37 (2.52)	0.37 (2.47)
F4	1	3.00	0.29 (2.58)	0.29 (2.58)	0.29 (2.57)	0.38 (2.87)
	2	4.98	0.35 (2.58)	0.35 (2.57)	0.35 (2.58)	0.43 (2.95)
	3	14.37	0.43 (2.58)	0.43 (2.70)	0.47 (3.32)	0.46 (3.23)
	4	36.66	0.42 (2.58)	0.42 (2.58)	0.42 (2.48)	0.42 (2.41)
F5	1	-	- (-)	- (-)	- (-)	- (-)
	2	6.91	0.18 (2.58)	0.18 (2.57)	0.19 (2.59)	0.21 (2.77)
	3	6.92	0.33 (2.58)	0.32 (2.52)	0.31 (2.45)	0.29 (2.38)
	4	49.20	0.37 (2.58)	0.37 (2.58)	0.37 (2.52)	0.37 (2.47)
F6	1	-	- (-)	- (-)	- (-)	- (-)
	2	5.77	0.23 (2.58)	0.23 (2.58)	0.23 (2.59)	0.29 (2.91)
	3	6.01	0.36 (2.58)	0.36 (2.57)	0.35 (2.54)	0.33 (2.44)
	4	36.66	0.42 (2.58)	0.42 (2.58)	0.42 (2.48)	0.42 (2.41)

Table 6.7: Mean values of $\beta_j - \beta_t|E$, considering the code formats CF1, CF2 and CF3, for the flood load event.

	$\beta_t\|E = 3.89$	$\beta_t\|E = 3.29$	$\beta_t\|E = 2.58$
CF1	0.005	0.006	0.005
CF2	0.093	0.086	0.116
CF3	0.136	0.074	0.203

the code optimization procedure is performed considering $N = 12 \times 11 \times 7 \times 4 = 3696$ design situations.

Regarding the code objective, for the earthquake load event, such as considered for the

Table 6.8: Standard deviations of $\beta_j - \beta_t|E$, considering the code formats CF1, CF2 and CF3, for the flood load event.

	$\beta_t\|E = 3.89$	$\beta_t\|E = 3.29$	$\beta_t\|E = 2.58$
CF1	0.038	0.045	0.044
CF2	0.290	0.309	0.307
CF3	0.386	0.317	0.319

reliability-based design (Chapter 5), the conditional probabilities of failure $p_{ft}|E = 10^{-5}$ ($\beta_t|E = 4.26$), $p_{ft}|E = 10^{-4}$ ($\beta_t|E = 3.72$) and $p_{ft}|E = 10^{-3}$ ($\beta_t|E = 3.09$), corresponding to the code objective $1/10^8$, $1/10^7$ and $1/10^6$, respectively, are targeted.

6.3.3.2 Relevant results

Tables 6.9, 6.10 and 6.11 show the results of the code optimization for target reliability indexes of $\beta_t|E = 4.26$, $\beta_t|E = 3.72$ and $\beta_t|E = 3.09$, respectively.

Table 6.9: Code optimization results, considering the earthquake load event, for a target reliability index of $\beta_t|E = 4.26$.

	CF1				CF2		CF3
	FM1	FM2	FM3	FM4	FM1,FM2	FM3,FM4	FM1-FM4
γ_G	0.94	0.95	0.88	0.84	0.95	0.85	0.86
γ_I	1.14	1.15	1.14	1.30	1.14	1.24	1.25
γ_U	1.23	1.30	1.29	1.29	1.28	1.27	1.28
$\gamma_{E,1}$	1.18	1.21	1.23	1.30	1.17	1.29	1.28
$\gamma_{E,2}$	0.73	0.78	0.85	0.88	0.79	0.88	0.86
γ_m	1.59	1.54	1.53	-	1.58	1.26	1.30
$N \cdot \Delta$ (10^2)	0.70	0.42	0.26	0.44	1.14	1.08	2.52

In addition to similar conclusions to those made for the flood load event, regarding the optimality losses as the code domain is extended to other failure modes and the order of magnitude of the partial safety factors, other conclusions are taken:

- As the number of design situations increases, when compared to the optimization procedure for the flood load event, the total expected losses also increases, since in order to cover a wider code domain of application and keeping the simplicity of the code, optimality decreases;

Table 6.10: Code optimization results, considering the earthquake load event, for a target reliability index of $\beta_t|E = 3.72$.

	CF1				CF2		CF3
	FM1	FM2	FM3	FM4	FM1,FM2	FM3,FM4	FM1-FM4
γ_G	0.96	0.96	0.91	0.85	0.95	0.85	0.88
γ_I	1.08	1.09	1.13	1.23	1.07	1.18	1.21
γ_U	1.17	1.22	1.23	1.22	1.20	1.23	1.24
$\gamma_{E,1}$	1.13	1.15	1.22	1.26	1.12	1.29	1.25
$\gamma_{E,2}$	0.71	0.73	0.82	0.87	0.71	0.86	0.84
γ_m	1.48	1.44	1.35	-	1.48	1.20	1.23
$N \cdot \Delta$ (10^2)	1.25	0.63	0.20	0.35	1.76	1.56	2.67

Table 6.11: Code optimization results, considering the earthquake load event, for a target reliability index of $\beta_t|E = 3.09$.

	CF1				CF2		CF3
	FM1	FM2	FM3	FM4	FM1,FM2	FM3,FM4	FM1-FM4
γ_G	0.97	0.98	0.96	0.89	0.98	0.91	0.90
γ_I	1.06	1.05	1.12	1.20	1.05	1.18	1.06
γ_U	1.11	1.19	1.20	1.17	1.19	1.18	1.19
$\gamma_{E,1}$	1.12	1.12	1.18	1.25	1.10	1.24	1.24
$\gamma_{E,2}$	0.68	0.68	0.78	0.87	0.68	0.82	0.82
γ_m	1.32	1.31	1.26	-	1.32	1.20	1.22
$N \cdot \Delta$ (10^2)	1.82	1.48	0.21	0.25	3.35	1.11	4.12

- When grouping all the failure modes within the same set of partial safety factors (Code format CF3), the importance of a good adjustment to failure modes 3 and 4 are dominant since their weight factors are considerably greater than for the failure modes 1 and 2 (Figure 6.2 for $\beta_t|E = 4.26$, Figure 6.3 for $\beta_t|E = 3.72$ and Figure 6.4 for $\beta_t|E = 3.09$), reflecting the greater influence that the variation of the design variable has on the reliability index;

- Advantages are taken by considering different partial safety factors for seismic actions type 1 and 2, since the corresponding distribution functions are considerably different. Since the pseudo-static load model underestimates the structural response under seismic excitations type 1 and overestimates the structural response under seismic excitations type 2, the corresponding partial safety factors, seen as correction factors, are greater than one for the first and smaller than one for the latter.

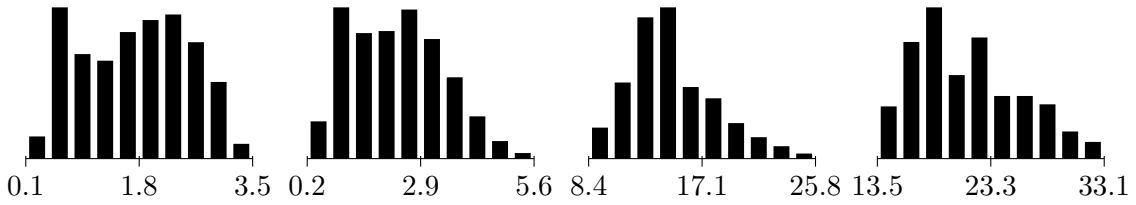

(a) Failure mode 1. (b) Failure mode 2. (c) Failure mode 3. (d) Failure mode 4.

Figure 6.2: Histogram of $\omega^{(2)}$ for the design situations of the earthquake load event, for a target reliability index of $\beta_t|E = 4.26$.

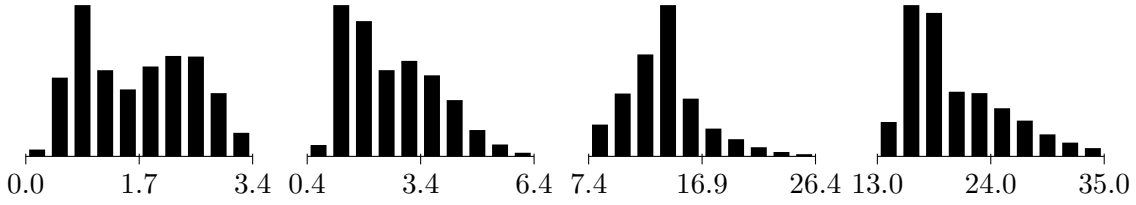

(a) Failure mode 1. (b) Failure mode 2. (c) Failure mode 3. (d) Failure mode 4.

Figure 6.3: Histogram of $\omega^{(2)}$ for the design situations of the earthquake load event, for a target reliability index of $\beta_t|E = 3.72$.

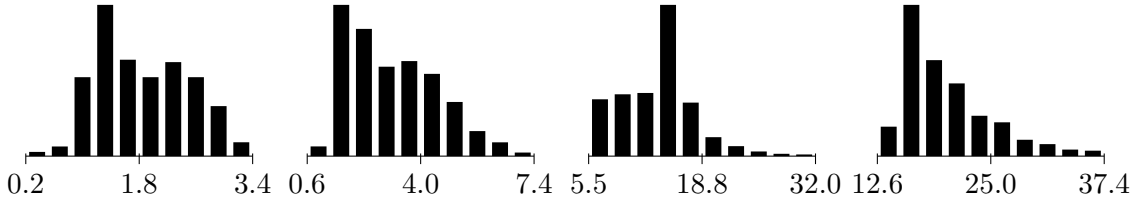

(a) Failure mode 1. (b) Failure mode 2. (c) Failure mode 3. (d) Failure mode 4.

Figure 6.4: Histogram of $\omega^{(2)}$ for the design situations of the earthquake load event, for a target reliability index of $\beta_t|E = 3.09$.

6.3.3.3 Code check

Since structural reliability analysis for such large number of design situations, code formats and target reliability indexes, would be a cumbersome task, the code is checked by comparing the design variable obtained through the calibrated code (θ_1 for the code format CF1, θ_2 for the code format CF2 and θ_3 for the code format CF3) to the optimum design variable θ^*, obtained by the reliability-based design (Chapter 5). This comparison is made in Figures 6.5 to 6.11, for the seismic zones considered.

Note that, from this comparison:

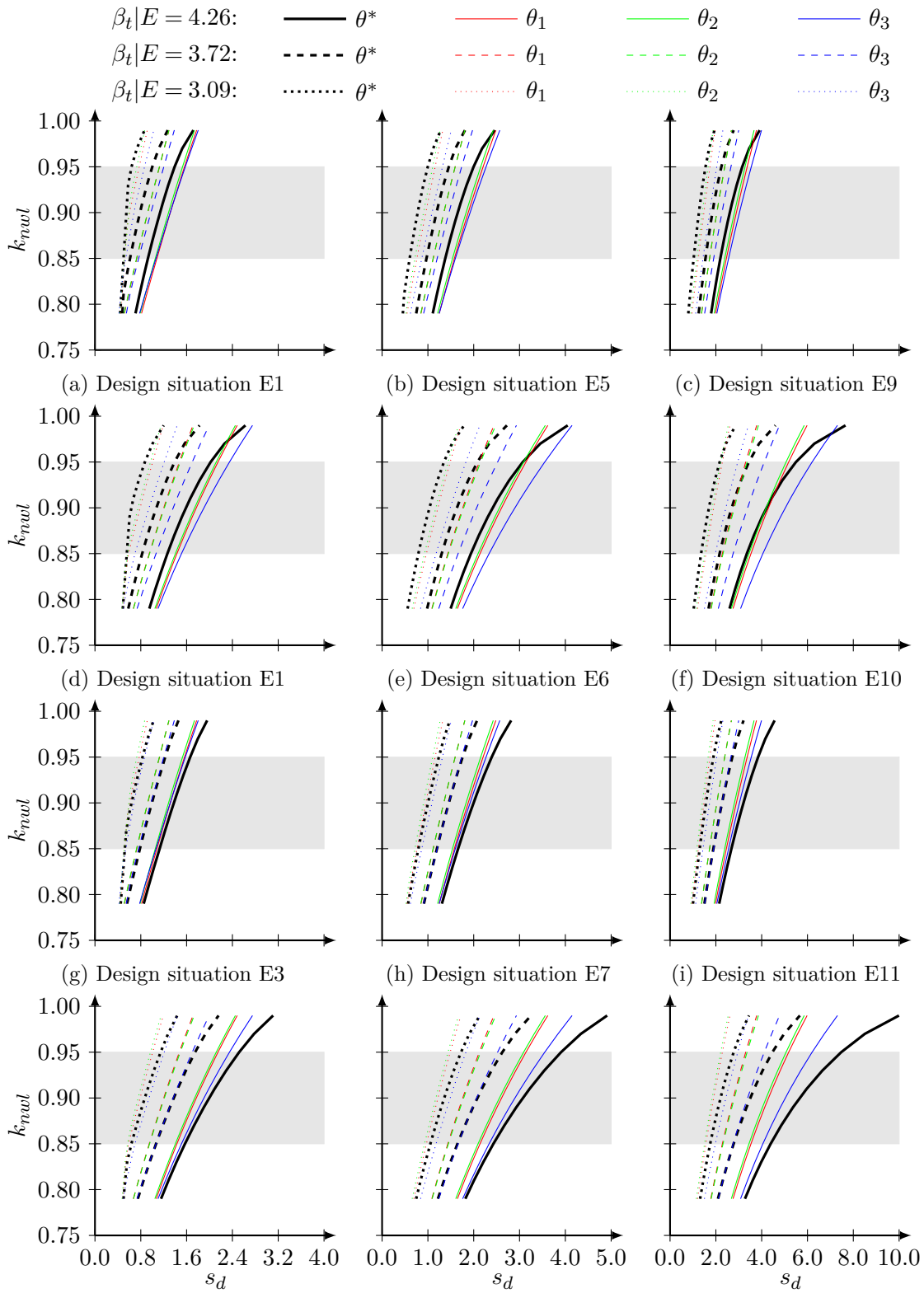

(a) Design situation E1 (b) Design situation E5 (c) Design situation E9

(d) Design situation E1 (e) Design situation E6 (f) Design situation E10

(g) Design situation E3 (h) Design situation E7 (i) Design situation E11

(j) Design situation E4 (k) Design situation E8 (l) Design situation E12

Figure 6.5: Comparison between the solution of code design to the solution of reliability-based design for seismic zone 1.3.

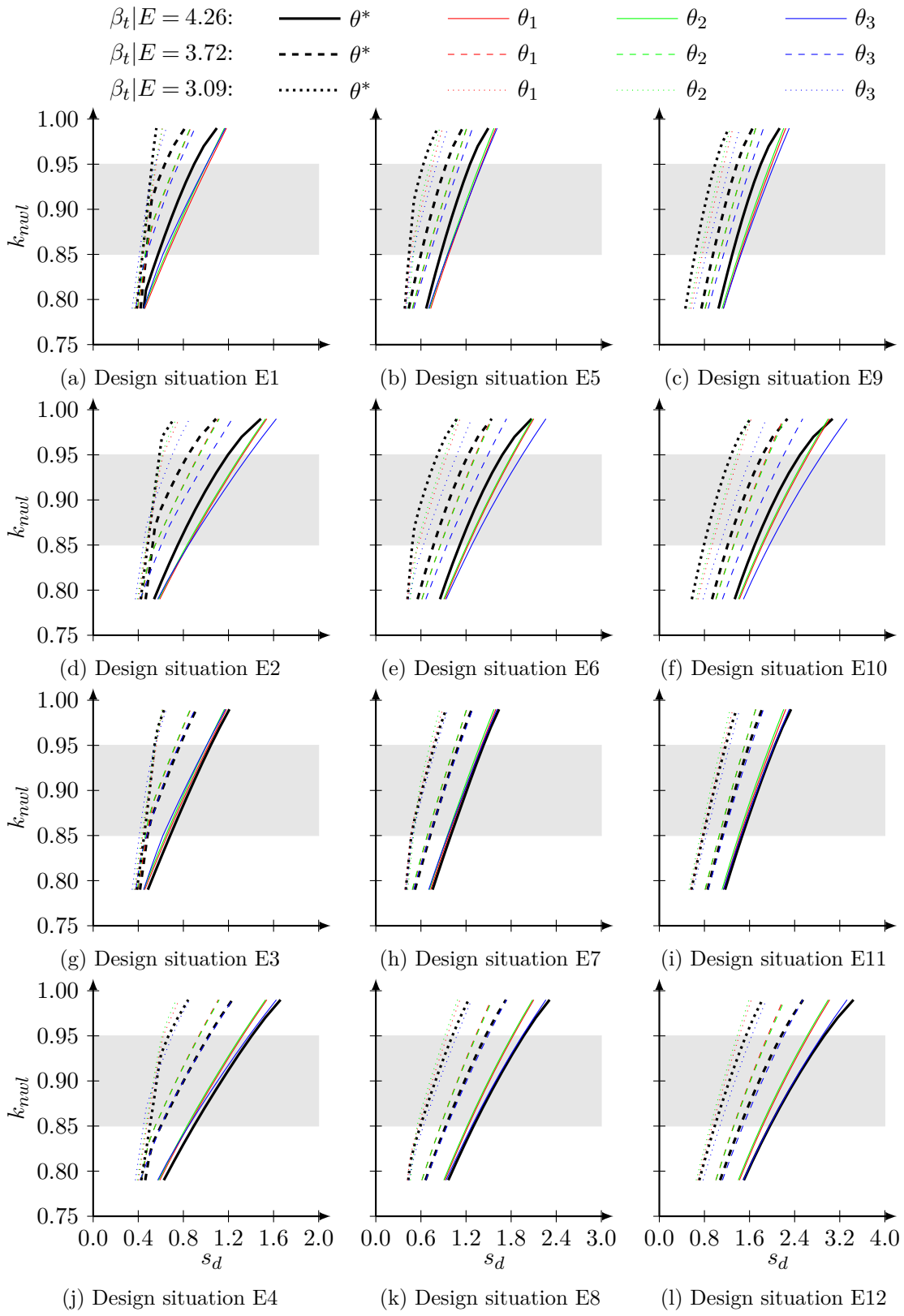

(a) Design situation E1 (b) Design situation E5 (c) Design situation E9

(d) Design situation E2 (e) Design situation E6 (f) Design situation E10

(g) Design situation E3 (h) Design situation E7 (i) Design situation E11

(j) Design situation E4 (k) Design situation E8 (l) Design situation E12

Figure 6.6: Comparison between the solution of code design to the solution of reliability-based design for seismic zone 1.4.

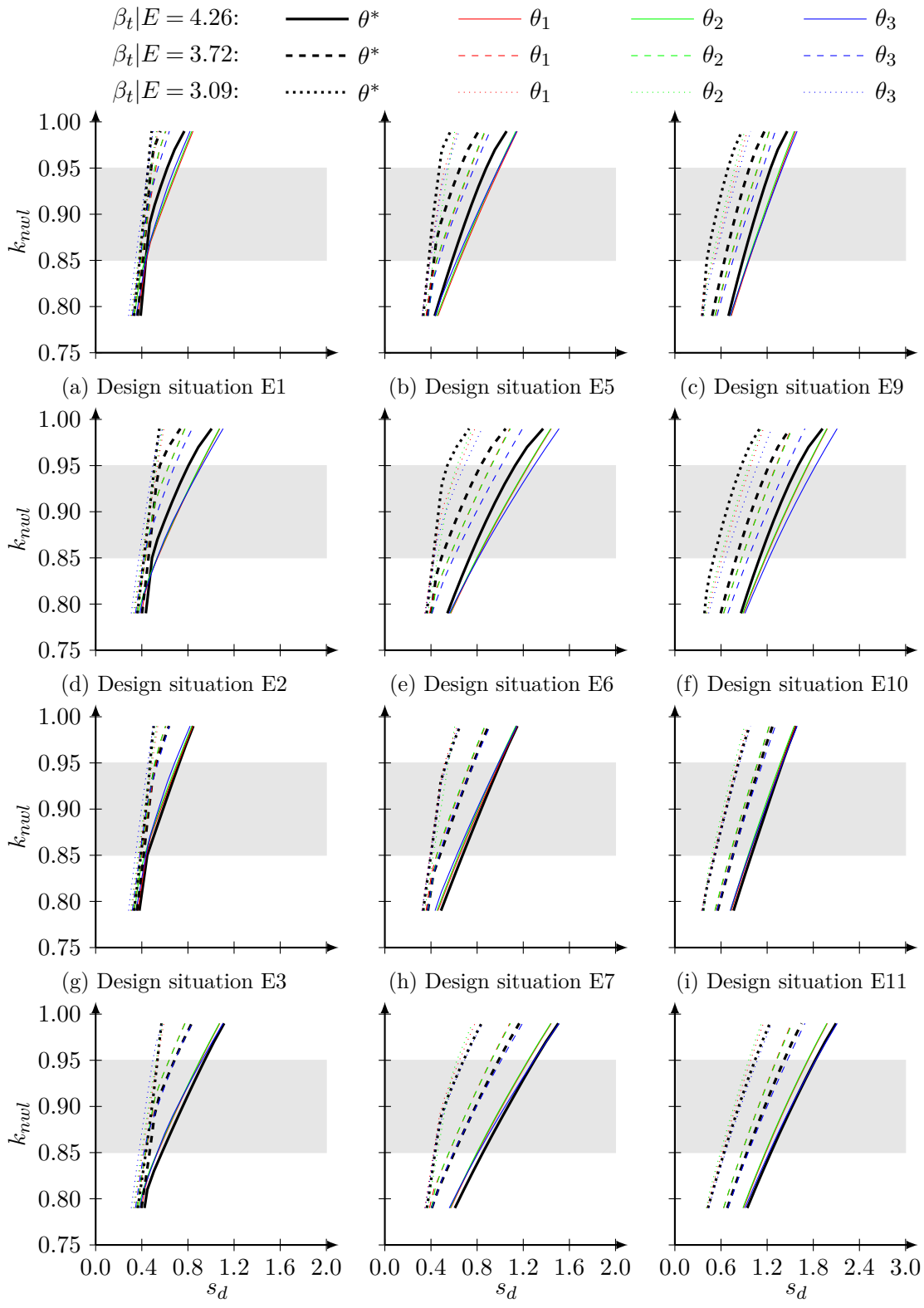

(a) Design situation E1 (b) Design situation E5 (c) Design situation E9

(d) Design situation E2 (e) Design situation E6 (f) Design situation E10

(g) Design situation E3 (h) Design situation E7 (i) Design situation E11

(j) Design situation E4 (k) Design situation E8 (l) Design situation E12

Figure 6.7: Comparison between the solution of code design to the solution of reliability-based design for seismic zone 1.5.

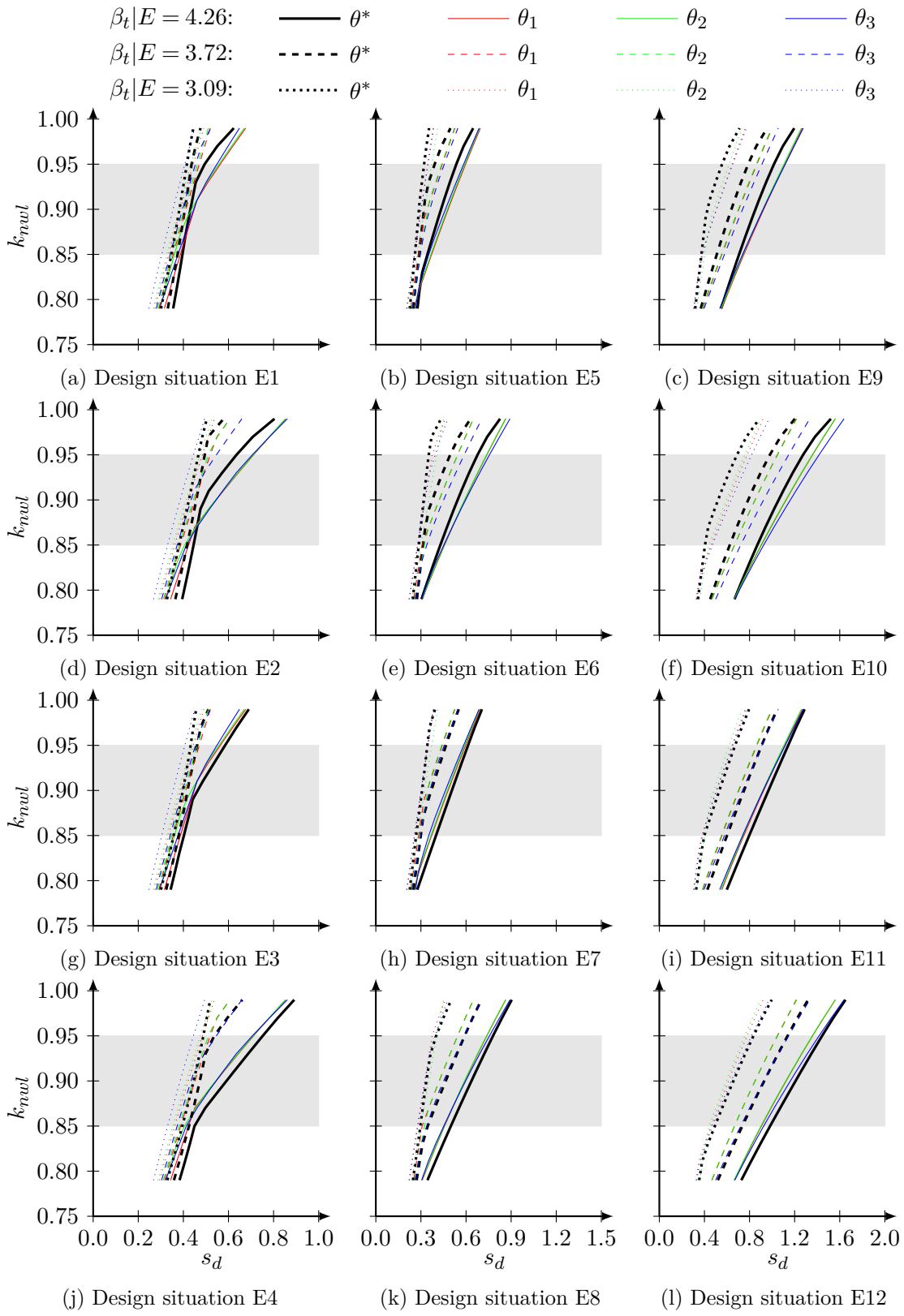

(a) Design situation E1 (b) Design situation E5 (c) Design situation E9

(d) Design situation E2 (e) Design situation E6 (f) Design situation E10

(g) Design situation E3 (h) Design situation E7 (i) Design situation E11

(j) Design situation E4 (k) Design situation E8 (l) Design situation E12

Figure 6.8: Comparison between the solution of code design to the solution of reliability-based design for seismic zone 1.6.

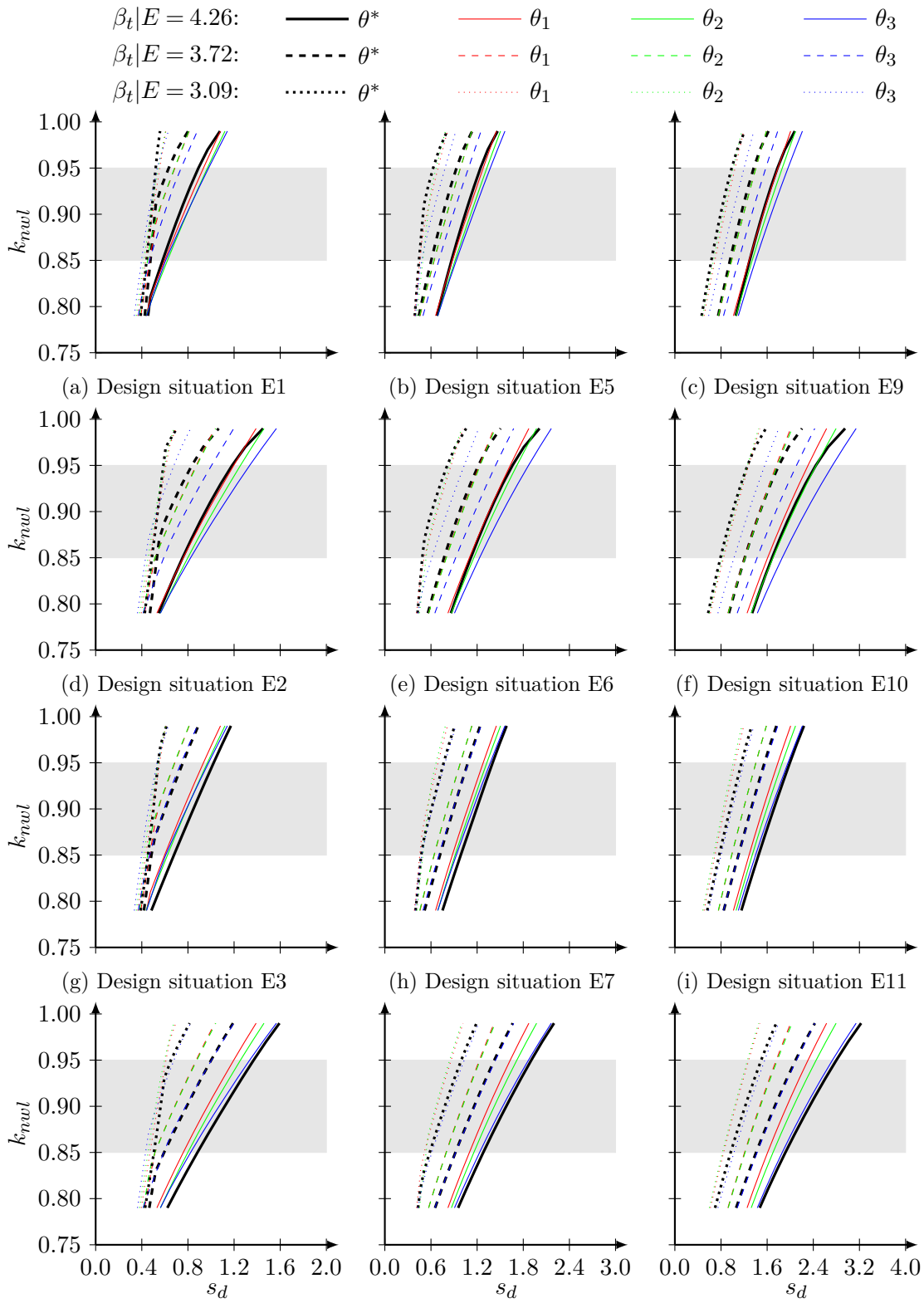

(a) Design situation E1 (b) Design situation E5 (c) Design situation E9

(d) Design situation E2 (e) Design situation E6 (f) Design situation E10

(g) Design situation E3 (h) Design situation E7 (i) Design situation E11

(j) Design situation E4 (k) Design situation E8 (l) Design situation E12

Figure 6.9: Comparison between the solution of code design to the solution of reliability-based design for seismic zone 2.3.

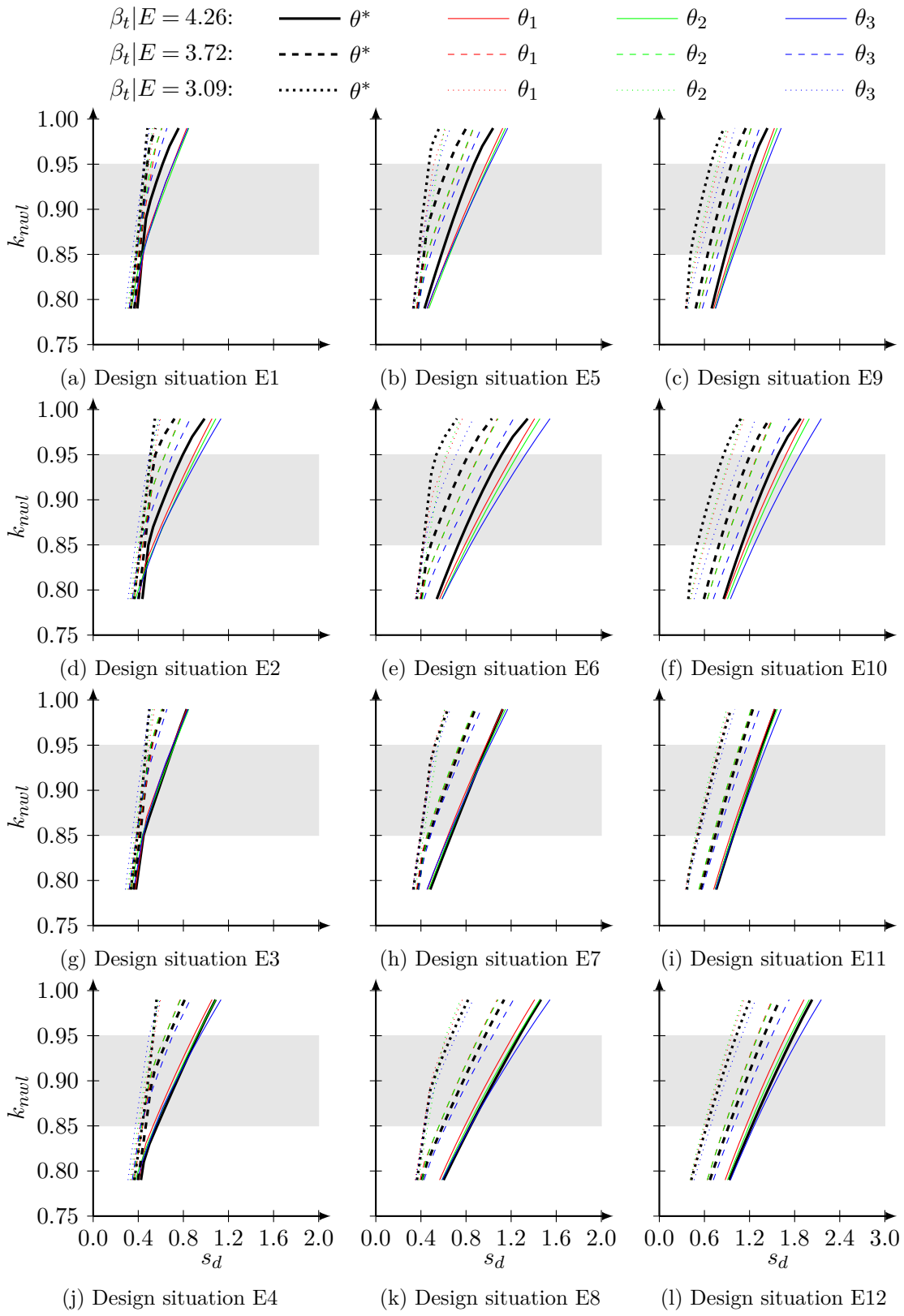

(a) Design situation E1 (b) Design situation E5 (c) Design situation E9

(d) Design situation E2 (e) Design situation E6 (f) Design situation E10

(g) Design situation E3 (h) Design situation E7 (i) Design situation E11

(j) Design situation E4 (k) Design situation E8 (l) Design situation E12

Figure 6.10: Comparison between the solution of code design to the solution of reliability-based design for seismic zone 2.4.

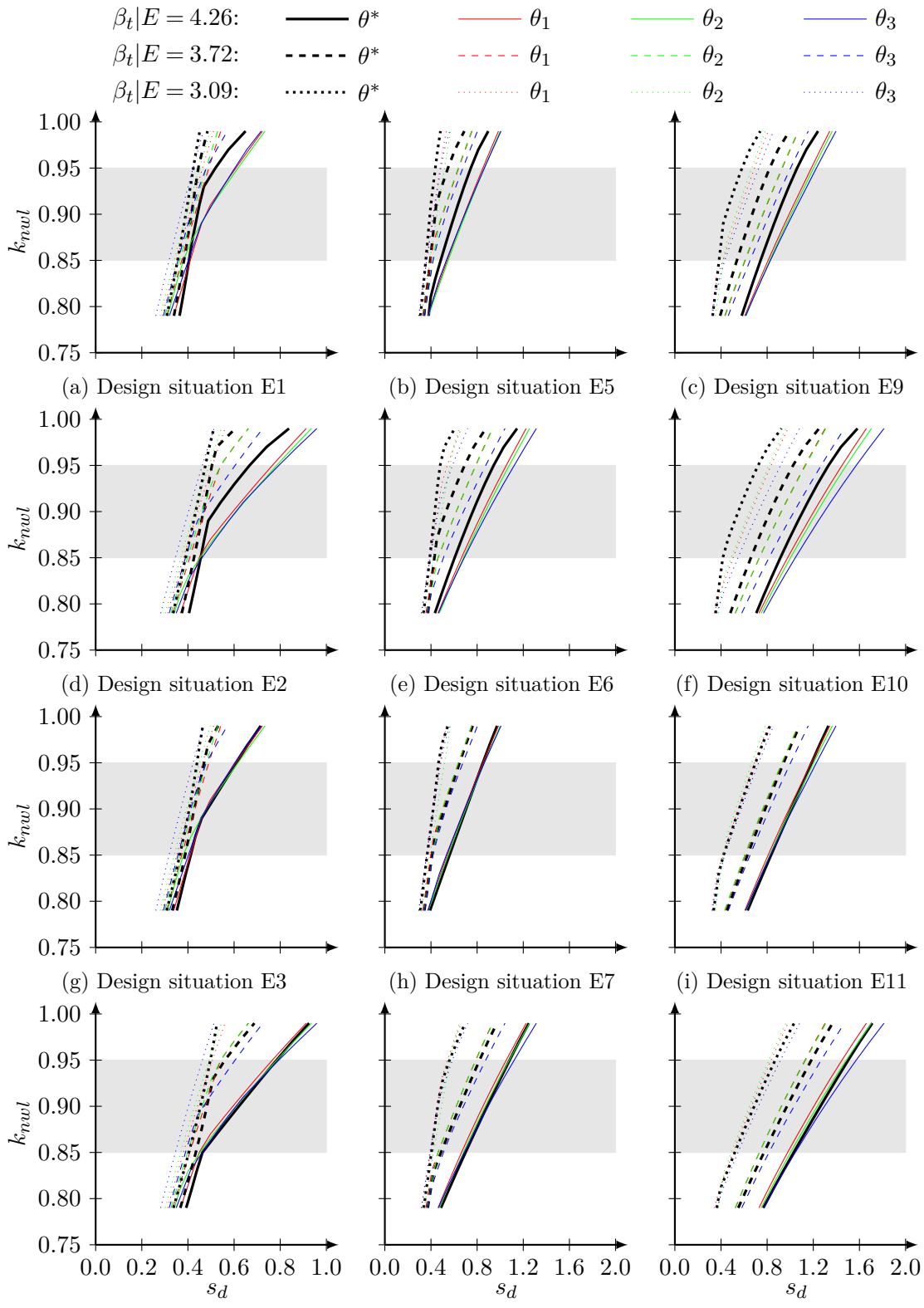

(a) Design situation E1 (b) Design situation E5 (c) Design situation E9

(d) Design situation E2 (e) Design situation E6 (f) Design situation E10

(g) Design situation E3 (h) Design situation E7 (i) Design situation E11

(j) Design situation E4 (k) Design situation E8 (l) Design situation E12

Figure 6.11: Comparison between the solution of code design to the solution of reliability-based design for seismic zone 2.5.

- The tested code formats lose suitability for larger values of k_{nwl} because they cannot reflect the non-linearity of the optimal solution due to the decreasing variance of the probability distribution of k_r as k_{nwl} tends to one (see Figure 4.3), suggesting that the corresponding partial safety factor given by a mathematical expression in terms of k_{nwl} could be more appropriate;
- Code formats CF1 and CF2 do not differ considerably regarding the adjustment quality. This is due to the similarities between the set of partial safety factors for failure modes 1 and 2 (code format CF1) which, when combined (code format CF2), do not lose their optimality;
- Code format CF3, although covering a wider domain (all failure modes) and present a greater conservatism than code formats CF1 and CF2 for some design situations (e.g. design situations E2, E6 and E10), is the format that best approaches the optimal solution in other cases (e.g. design situations E4, E8 and E12);
- The adjustment differences between design situations E1, E5 and E9 and E3, E7 and E11, respectively, and between design situations E2, E6 and E10 and E4, E8 and E12, respectively, is due to the different subgroups regarding the reservoir water level, suggesting that distinct partial safety factors for the hydrostatic pressure, depending on the project type, could be more appropriate.

The ratio θ/θ^* are synthesized in Figure 6.12, for different target reliability indexes and using different code formats.

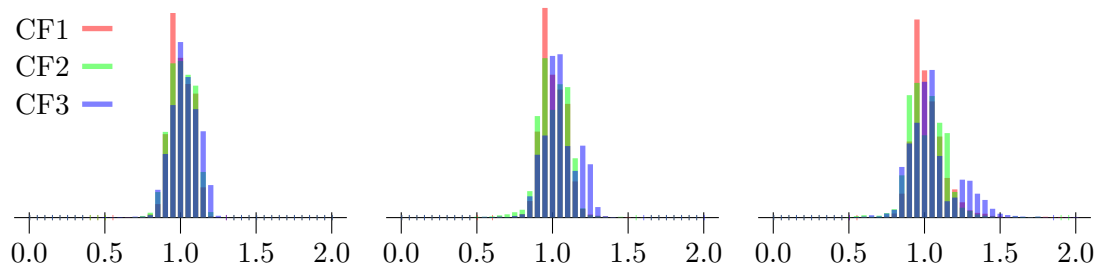

(a) $\beta_t|E = 4.29$ (b) $\beta_t|E = 3.72$ (c) $\beta_t|E = 3.09$

Figure 6.12: Histogram of the relative deviations $(\theta/\theta^*(\beta_t|E))$ between the code solution and the target values.

For comparison purposes, the accuracy of codes calibrated, using different code formats, can be evaluated through the standard deviations of the relative deviations presented in Table 6.12.

Table 6.12: Standard deviations of θ/θ^*, considering the code formats CF1, CF2 and CF3, for the earthquake load event.

	$\beta_t \vert E = 3.89$	$\beta_t \vert E = 3.29$	$\beta_t \vert E = 2.58$
CF1	0.074	0.088	0.123
CF2	0.082	0.103	0.128
CF3	0.093	0.113	0.168

Again, as the code domain is extended to more design situations (from code format CF1 to code format CF2 and from code format CF2 to code format CF3), the standard deviation of relative deviations θ/θ^* increases.

6.4 Final considerations

6.4.1 Synthesis

The adaptation from deterministic to semi-probabilistic safety criteria has been encouraged (ICOLD 1987) and has already been implemented in regulations or technical notes from some countries. Other regulators and/or institution have followed a risk-based approach, since the aging of dams became the main concern and maintenance and rehabilitation have surpassed the construction era.

This chapter addressed the code calibration for the semi-probabilistic safety analysis of concrete gravity dams, considering the ultimate limit states reflecting the loss of structural equilibrium, intending to reduce the inherent conservationism levels presented in the classical approach to dam safety, based on the concept of global safety factors.

The code calibration process required the code formulation and the code optimization tasks. Regarding the code formulation, the simple case study used in the previous chapter was considered for the representation of a structure class addressing large concrete gravity dams. Different code objectives were tested in order to evaluated its influence on the partial safety factors. Simple code formats, concentrating the sources of uncertainty in few partial safety formats, was considered, testing the effects of varying their application domain, from each failure mode individually or all failure modes together. Regarding the code optimization, the alternative procedure proposed in chapter 2 was considered. The procedure was applied to the extreme hydrological and accidental earthquake combinations separately in order to judge independently the partial safety factors for each case.

Although differing between load combinations, common values were obtained for the partial safety factors. The extension of the code domain to multiple failure modes has different effects when comparing the extreme hydrological to the accidental seismic combinations. While, for the first, the deviations from the optimum solutions increase considerably when the partial safety factors are shared by multiple failure modes, for the latter, this difference is not so abrupt.

6.4.2 Code proposal

In this work, it is intended to propose a semi-probabilistic criteria for the structural safety analysis of concrete gravity dams that, when applied to any design situation considering the failure modes identified, results in structural solutions close to those obtained by the RBDO procedure, considered as the optimum solutions.

It is known that, in practice, the typical geometry that makes concrete gravity dams economically competitive is characterized by downstream face slopes in the range of 0.7 to 0.8 (Corns *et al.* 1988), admitting a maximum value of 1.0. For more demanding design situations, to conceive cost-effective solutions, other constructive dispositions are preferred, such as the consideration of a greater keyed depth, the consideration of a curvature in plan (arch-gravity dams) or, in particular cases, the use of post-tensioned anchors. On the other hand, for less demanding design situations, the adoption of hollow gravity dams is also preferred, for economic reasons.

Furthermore, from the previous chapter, it was concluded that failure mode 1 is the most conditioning failure mode in the range of practical values of the downstream face slope. Therefore, since structural codes usually consider the single failure mode checking format (Faber and Sørensen 2003), the partial safety factors calibrated for the design equations derived from the failure mode 1 (code format CF1) can be used throughout the code domain, since it does not result, when applied to the remaining failure modes, in most demanding structural solutions characterized by greater values of the downstream face slope.

The partial safety factors proposed, obtained by rounding the partial safety factors calibrated for the design equations derived from the failure mode 1 (code format CF1) to the nearest significant and conservative value, are presented in Tables 6.13 and 6.14, for the extreme earthquake and accidental hydrological load combinations, respectively, considering the three targeted values of the total probability of failure tested for the code

objective.

Table 6.13: Partial safety factors proposed for the extreme earthquake load combination.

	$p_{ft} = 1/10^8$	$p_{ft} = 1/10^7$	$p_{ft} = 1/10^6$
γ_G	0.90	0.95	0.95
γ_I	1.15	1.10	1.10
γ_U	1.25	1.20	1.15
$\gamma_{E,1}$	1.20	1.15	1.15
$\gamma_{E,2}$	0.75	0.75	0.70
γ_m	1.60	1.50	1.35

Table 6.14: Partial safety factors proposed for the accidental hydrological load combination.

	$p_{ft} = 10^{-8}$	$p_{ft} = 10^{-7}$	$p_{ft} = 10^{-6}$
γ_G	0.95	0.95	0.95
γ_I	1.10	1.05	1.05
γ_U	1.15	1.15	1.10
γ_m	1.55	1.45	1.30

Comparing to the values proposed, the Portuguese dam safety regulation (RSB 2018), which considers a global safety coefficient applied to the frictional component of the shear strength with values between 1.2 and 1.5, should inherently target to a total probability of failure in the order of magnitude of 10^{-6}. Note that this value is larger than the probability of failure admitted, in the Eurocodes (EN1990 2002), for structures of the consequence class CC3.

However, the results obtained in this chapter may have been conditioned both by: (i) the consideration of the pseudo-static seismic load model, which underestimates the structural response under seismic actions type 1 and overestimates the structural response under seismic actions type 2; and (ii) the consideration of a single case study corresponding to a 100 meter high concrete gravity dam.

CHAPTER 7

Conclusions

7.1 Summary and main conclusions

The main objective of this thesis was to explore the applicability of probabilistic principles to structural safety of concrete gravity dams. The intermediate tasks to perform a reliability-based design of concrete gravity dams and to calibrate safety criteria, based on the semi-probabilistic approach, for ultimate limit states, namely the failure mode and uncertainty modeling, enabled the success of this work.

Firstly, introductory notes were presented. The role of dams in society, in general, and in Portugal, in particular, was reviewed. The structural safety of dams was framed by a historical perspective. After the propagation of dam construction for hydropower generation, since the industrial revolution, dam safety gained importance. The formation of the International Commission on Large Dams (ICOLD) encouraged advances in planning, design, construction, operation and maintenance of large dams. When focus was put on sujects of current concern such as safety, monitoring, aging and environmental impacts, a common approach to dam safety, denoted as classical approach, came formally (ICOLD 1987), introducing the lessons taken from experience and collaboration of several national members. The theoretical development of classical structural reliability motivated developments in other areas of civil engineering and discussions regarding its application in dam engineering was also taken, recognizing that the logical trend goes from a predominantly deterministic concept of safety factors to the semi-probabilistic method of partial safety

factors. Since then, studies have been developed and probabilistic approaches to dam safety are already implemented either in national regulations/technical rules or in guidelines for dam safety management.

In the second chapter the formulation of the structural safety problem, from a probabilistic perspective, was presented. Again, a historical background on structural design was mentioned. Themes such as the uncertainty modeling, the approaches for the structural safety analysis and reliability methods were detailed in order to frame the standards-based approach for the structural design, whose link to probabilistic approach is set on the theory of code calibration. Procedures for the reliability-based design and the code calibration, that latter were applied, was also presented. Regarding the code optimization, an alternative method was proposed, reducing the computational demand.

In the third chapter, the aspects related to the structural safety of concrete gravity dams are presented. After a review on the historical background on concrete dam design and construction, the constructive aspects and design principles, the loads acting on concrete gravity dams and the philosophy of the design codes are detailed. At the end, failure modes are derived by comparing analytical and numerical solutions of a representative, though generic, case study.

In the forth chapter, the tasks related to the modeling of the relevant sources of uncertainty associated with the safety of concrete gravity dams, were detailed. Data from monitoring and quality control tests were used to derive probabilistic models for the water loads and the concrete mechanical properties, respectively. The quantification of other sources of physical uncertainties, such as the concrete unit weight and concrete-rock interface shear strength, was based on the literature. Sources of model uncertainty were also analyzed, mainly those related to the consideration of analytical seismic load model for the representation of the structural response to seismic actions.

The advances made allowed the quantification of the relevant sources of uncertainty involved in the concrete dam safety which will enable, in the following chapters, both the studies on the reliability-based design and the code calibration for ultimate limit states.

In the fifth chapter, probabilistic principles for the reliability-based design were applied. The objective was to obtain the structural solution that ensures adequate levels of safety for the most conditioning foreseeable load conditions arising during the intended service life of the structure, namely those derived from the occurrence of the design flood and the design earthquake, being naturally given by the most demanding case. Therefore, a

theoretical case study, representing the structural class of large concrete gravity dams, and the design situations derived from the flood (extreme hydrological load combination) and earthquake (accidental earthquake load combination) load events were considered.

The results obtained, in which the design variable was quantified such that the safety requirements, representing by target reliability indexes, were fulfilled for all design situations, show increasing sensitivity to the exploitation type, the hydraulic and mechanical characteristics of the rock mass foundation and, above all, to the intensity of the seismic action considered. While the structural characteristics required to face the accidental earthquake load combination are frequently the conditioned ones, the predominance of this conclusion varies with the dam location.

For high intensity seismic zones zones, characterized by peak ground accelerations of considerable value, the minimum downstream face slope, which fulfills the safety requirements, increases to values that surely make this solution cost-prohibitive (practical values are in the range of 0.7 to 0.8, admitting a maximum value of 1.0). Despite the validity of this conclusion, this fact may have been exacerbated by the consideration of the pseudo-static seismic load model to simulate the structural effects due to the occurrence of an earthquake, since this model, considering inertia forces proportional to the structure mass, may lose suitability for an exaggerated increase of the downstream face slope.

For low intensity seismic zones, the extreme hydrostatic combination may condition the structural solution, even though, the required downstream face slope is small when compared to the current practice. Regarding the failure modes, the failure mode 1, involving the sliding of the dam body while pushing the downstream rock wedge, is often the conditioning one. Only for less demanding design situations, frequently those coming from the flood load event, other failure modes may become prominent.

Regarding the failure modes, the most conditioning one depends on the magnitude of the downstream face slope. For gravity profiles characterized by downstream face slopes roughly greater than 0.5, including the range of practical values 0.7 to 1.00, the failure mode 1 is always the most conditioning case. This conclusion remains valid as the safety requirements increase, since gravity profiles shall expectedly be less inclined.

From the results obtained, it was evident the advantages that can be taken from the reliability-based design of concrete gravity dams, since safety levels can be controlled and different thresholds can easily be achieved by updating the design variable (downstream face slope). The algorithm developed for that purpose was based, on one hand, on the

limit states derived from the construction aspects and design principles of this type of structures and, on other hand, on robust theoretical reliability methods.

In the sixth chapter, a code calibration procedure was applied to derive partial safety factors, for ultimate limit states, such that the inherent conservationism levels presented in the classical approach to dam safety, may be reduced.

The code calibration process required the code formulation and the code optimization tasks. Regarding the code formulation, the simple case study used in chapter 5 was considered for the representation of a structure class addressing large concrete gravity dams. Different code objectives were tested in order to evaluated its influence upon the partial safety factors. Simple code formats, concentrating the sources of uncertainty in few partial safety formats, were considered, testing the effects of varying their application domain, from each failure mode individually or all failure modes together.

The extension of the code domain to multiple failure modes was found to produce different effects when comparing the extreme hydrological to the accidental seismic combinations. While, for the first, the deviations from the optimum solutions increase considerably when the partial safety factors are shared by multiple failure modes, for the latter, this difference is not so abrupt.

A set of partial safety factors, for the load and material properties were proposed considering that the failure mode 1 is the most conditioning one in the range of practical values of the downstream face slope. For more demanding design situations, to conceive cost-effective solutions, other constructive dispositions are preferred, such as the consideration of a greater keyed depth, the consideration of a curvature in plan (arch-gravity dams) or, in particular cases, the use of post-tensioned anchors. On the other hand, for less demanding design situations, the adoption of hollow gravity dams is also preferred, for economic reasons.

In the seventh chapter, the summary and main conclusions are presented, as well as, the future developments.

7.2 Future developments

Being this work a first step towards the adoption of probabilistic principles, the development of full risk analysis tools to dam safety management may, at this moment, seem a distant objective. Several accessory subjects, namely probabilistic models that relates

the magnitude of load events with the respective probability of occurrence and models to estimate the consequences in terms of the flood wave from a dam break, must be studied and a discussion on institutional and political levels should first be taken.

Nonetheless, reliability-based tools for the assessment of existing structures, providing valuable information for the decision-making process, may apparently be prioritized. These tools may be specifically useful for the estimation of the service life of deteriorated structures, either for the planning and scheduling of interventions or for the allocation of financial, material and environmental resources on a prioritized basis.

Meanwhile, in order to go through the necessary tasks aiming at a definitive adoption of semi-probabilistic approach to structural safety of concrete dams, which would also be required for the development of reliability-based tools, some extensions must be taken, namely:

- Extension to the rock mechanics, in order to account the possible failure modes involving the movement of considerable volumes of rock;
- Extension to other types of concrete dams. Arch dams and buttress dams must also be analyzed in similar way. For that, the procedure followed in this thesis to the concrete gravity dams must be generalized to theoretical arch and buttress dams;
- Extension to other limit states corresponding, essentially, to the serviceability and durability requirements. Extreme or accidental situations are fortunately extremely rare and the reliability principles can also be advantageously considered in the continuous monitoring of concrete dams, aiming at supporting the decision-making regarding their maintenance;
- For that, it is essential to develop an algorithm for the continuous (bayesian) updating of the uncertainty models as soon as data from monitoring become available.

It was shown that the application of the partial safety factor method to the design of concrete gravity dams can be sought. However, in order to built new paradigm-shifted safety regulation, renouncing the working stress philosophy to the detriment of limit state philosophy, several aspects must be also studied:

- The definition of the structural class, namely the application field of the desired designed criteria;

- The definition, on institutional and political levels, of the code objective, i.e. the required levels of safety, given in terms of probability of failure or reliability index, that this type of structures shall ensured.

- The code format by establishing structural coefficients, in order to differentiate reliability requirements for different types of structures, combinations coefficients, in order to represent adequately the realistic load combinations defined and partial safety factors using a methodology similar to the presented in this study.

Bibliography

ACI (1996). *Mass concrete*. ACI 207.1R-96. American Concrete Institute (ACI).

ACI (2005). *Guide to mass concrete*. ACI 207.1R-05. American Concrete Institute (ACI).

Almeida, F. (1969). "Sobre a barragem romana de Olisipo e seu aqueduto (On the Olisipo Roman dam and its aqueduct)." Portuguese. In: *O arqueólogo Português* 3, pp. 179–189.

Altarejos, L. G. (2009). "Contribuición a la estimación de la probabilidad de fallo de presas de hormigón en el contexto del análisis de riesgos (Contribution to the estimation of the probability of failure of concrete gravity dams in the risk analysis context)." Spanish. Doctoral dissertation. Spain: Universidad Politécnica de València.

Altarejos, L. G., I. B. Escuder, and A. M. Torres (2015). "Advances on the failure analysis of the dam-foundation interface of concrete dams." In: *Materials* 8, pp. 8255–8278.

ANCOLD (2003). *Guidelines on risk assessment*. Australia: Australian National Committee on Large Dams (ANCOLD).

Anderson, N. and Å. Björck (1973). "A new high order method of regula falsi type for computing a root of an equation." In: *BIT Numerical Mathematics* 13.3, pp. 253–264.

Andrade, R. M. (1982). *A drenagem nas fundações das estruturas hidráulicas: análise e intrepertação prática (Drainage in the foundation of hydraulic structures: analysis and practical interpretation)*. Portuguese. Engevix.

Ang, A. H.-S. (2011). "An application of quantitative risk assessment in infrastructures engineering." In: *Quantitative risk assessment (QRA) for natural hazards*. Ed. by N. Uddin and A. H.-S. Ang. ASCE.

Ang, A. H.-S. and D. de Leon (1997). "Determination of optimal target reliabilities for design and upgrading of structures." In: *Structural safety* 89.1, pp. 91–103.

APA (2001). *Curso de exploração e segurança de barragens (Course on operation and safety of dams)*. Portuguese. Agência Portuguesa do Ambiente (APA).

Baravalle, M. (2017). "Risk and reliability based calibration of structural design codes. Principles and applications." Doctoral dissertation. Trondheim, Norway: Norwegian University of Science and Technology.

Barla, G., M. Bonini, and G. Cammarata (2004). "Stress and seepage analyses for a gravity dam on a jointed granitic rock mass." In: *1st International UDEC/3DEC Symposium*. Bochum, Germany, pp. 263–268.

Batista, A. L. (1998). "Análise do comportamento ao longo do tempo de barragens abóbada (Analysis of arch dams behavior over time)." Portuguese. Doctoral dissertation. Lisbon, Portugal: Instituto Superior Técnico (IST).

Batista, A. L. and M. L. B. Farinha (2011). *Curso de projecto, construção e exploração de pequenas barragens: Dimensionamento estrutural e controlo da segurança de pequenas barragens de betão (Course on design, construction and operation of small dams: Structural design and safety control of small concrete dams)*. Portuguese. Laboratório Nacional de Engenharia Civil (LNEC).

Beck, A. T. and W. J. S. Gomes (2012). "A comparison of deterministic, reliability-based and risk-based structural optimization under uncertainty." In: *Probabilistic Engineering Mechanics* 88, pp. 18–29.

Bernard, P. and M. Fogli (1986). "Un calcul probabiliste en génie civil. Évaluation de la probabilité de ruine des structures par une méthode de Monte-Carlo fondée sur une technique de conditionnement (A probabilistic calculus in engineering. Evaluation of failure probability for structures by a Monte-Carlo method based on a conditioning technique)." French. In: *Annales scientifiques de l'Université de Clermont-Ferrand 2. Série Annales scientifiques de l'Université de Clermont-Ferrand 2. Série Probabilités et applications* 89.23, pp. 47–90.

Bernardo, J. M. (2009). "Bayesian methodology in statistics." In: *Comprehensive chemometrics*. Ed. by S. D. Brown, R. Tauler, and B. Walczak. Elsevier.

Billington, D. P., D. C. Jackson, and M. V. Melosi (2005). *The history of large federal dams. Planning, design, and construction in the era of big dams*. USACE and USBR.

Bjerager, P. (1988). "Probability integration by directional simulation." In: *Journal of Engineering Mechanics* 14.8, pp. 1285–1302.

Blitzstein, J. K. and J. Hwang (2004). *Introduction to probability*. Chapman & Hall/CRC.

Bowles, D. S., L. R. Anderson, and T. F. Glover (1998). "The practice of dam safety risk assessment and management: Its roots, its branches and its fruit." In: *Eighteenth USCOLD Annual Meeting and Lecture*. Buffalo, New York, United States of America.

Brahtz, J. H. A. (1936). "Pressures due to percolating water and their influence upon stresses in hydraulic structures." In: *Translations of the 2nd Congress on Large Dams* 5, pp. 43–71.

Breitung, K. (1984). "Asymptotic approximations for multinormal integrals." In: *Journal of Engineering Mechanics* 110.3, pp. 357–366.

Brent, R. P. (1971). "An algorithm with guaranteed convergence for finding a zero of a function." In: *The Computer Journal* 14.4, pp. 422–425.

Bretas, E., A. L. Batista, J. V. Lemos, and P. Léger (2014). "Seismic analysis of gravity dams: a comparative study using a progressive methodology." In: *Proceedings of the 9th International Conference on Structural Dynamics, EURODYN 2014*. Porto, Portugal, pp. 3707–3714.

Bretas, E. M. (2012). "Desenvolvimento de um modelo de elementos discretos para o estudo de barragens gravidade em alvenaria (Development of a discrete element model for masonry gravity dams analysis)." Portuguese. Doctoral dissertation. Guimarães, Portugal: Universidade do Minho.

Brown, E. T. (2015). "Rock engineering design of post-tensioned anchors for dams: A review." In: *Journal of Rock Mechanics and Geotechnical Engineering* 7.1, pp. 1–13.

Bucher, C. G. (1988). "Adaptive sampling - an iterative fast Monte Carlo procedure." In: *Structural safety* 5.2, pp. 119–126.

Caldeira, L. (2005). *Análises de riscos em geotecnia: Aplicação a barragens de aterro (Risk analysis in geotechnics: Application to embankment dams)*. Portuguese. Programa de Investigação. Lisbon, Portugal: Laboratório Nacional de Engenharia Civil (LNEC).

Calgaro, J.-A. (2011). "Safety philosophy of Eurocodes." In: *ISGSR 2011 - Geotechnical Safety and Risk*. Munich, Germany.

Carvalho, A. (2007). "Modelação estocástica da acção sísmica em Portugal Continental (Stochastic modeling of seismic action in mainland Portugal)." Portuguese. Doctoral dissertation. Lisbon, Portugal: Instituto Superior Técnico (IST).

Casaca, J. M. and R. Pereira (2017). *Parametric inference in the context of beta mixtures*. ICT Barragens 24. Lisbon, Portugal: Laboratório Nacional de Engenharia Civil (LNEC).

Casagrande, A. (1961). "Control of seepage through foundations and abutments of dams." In: *Géotechnique* 3.11, pp. 161–182.

CDA (2007). *Dam safety guidelines*. Toronto, Ontario, Canada: Canadian Dam Association (CDA).

CFBR (2012). *Guidelines for the justification of the stability of gravity dams*. Comité Français des Barrages et Réservoirs (CFBR).

Chen, S.-H. (2015). *Hydraulic structures*. Springer.

Chopra, A. K. (1978). "Earthquake resistant design of concrete gravity dams." In: *Journal of the Structural Division* 104.6, pp. 953–971.

Chopra, A. K. and P. Chakrabarti (1973). "The Koyna earthquake and the damage to Koyna dam." In: *Bulletin of the seismological society of America* 63.2, pp. 381–397.

Chopra, A. K. and L. Zhang (1991). "Earthquake-induced base sliding of concrete gravity dams." In: *Journal of the Structural Division* 117.12, pp. 3698–3719.

Cornell, A. C. (1969). "A probabilistic based structural code." In: *Journal of the American Concrete Institute* 66.12, pp. 974–985.

Corns, C. F., G. S. Tarbox, and E. K. Schrader (1988). "Gravity dam design and analysis." In: *Advanced dam engineering for design, construction, and rehabilitation*. Ed. by R. B. Jansen. Van Nostrand Reinhold, pp. 466–492.

Costa, F. V. (1948). "Notions de probabilité dans l'étude de la sécurité des constructions (Notions of probability in the study of structures' safety)." French. In: *IABSE congress report*. Liège, Belgium.

Coutinho, A. S. and A. Gonçalves (1994). *Fabrico e propriedades do betão: Volume III (Manufacturing and properties of concrete: Volume III)*. Portuguese. 2nd Edition. LNEC.

Cundall, P. A. (1971). "A computer model for simulating progressive large scale movements in blocky rock systems." In: *Proceedings of the Symposium of the International Society for Rock Mechanics*. Nancy, France, pp. II–8.

Cundall, P. A., J. Marti, P. Beresford, N. Last, and M. Asgian (1978). *Computer modeling of jointed rock masses*. Technical report 78-4. Vicksburg, Mississipi, USA: U.S. Army Engineers Waterways Experiment Station.

Dachler, R. (1936). *Grundwasserströmung (The flow of water in ground)*. German. Springer.

Darcy, H. (1856). *Les fontaines publiques de la ville de Dijon. Exposition et application des principes à suivre et des formules à employer dans les questions de distribution d'eau*

(The public fountains of the city of Dijon: Exposition and application of principles to follow and formulas to use in questions of water distribution). French. Victor Dalmont.

Dekker, T. J. (1969). "Finding a zero by means of successive linear interpolation." In: *Constructive Aspects of the Fundamental Theorem of Algebra*. Bruno Dejon and Peter Henrici. Wiley-Interscience.

Delocre, E. (1866). "Mémoire sur la forme du profil à adopter pour les grands barrages en maçonnerie des résèrvoirs (Report on the profile shape to be adopted for large masonry reservoir dams)." French. In: *Analles de Ponts et Chaussées*, pp. 212–272.

Diamantidis, D. and M. Holický (2010). "Reliability differentiation in the Eurocodes." In: *SEMC 2010 - The 4th international conference on structural engineering, mechanics and computation*. Cape Town, South Africa.

Ditlevsen, O. (1981). "Principle of normal tail approximation." In: *Journal of the Engineering Mechanics Division* 107.6, pp. 1191–1208.

Ditlevsen, O. and H. O. Madsen (1996). *Structural reliability methods*. Wiley.

Ditlevsen, O., P. Bjerager, R. Olsen, and A. M. Hasofer (1988). "Directional simulation in gaussian processes." In: *Probabilistic Engineering Mechanics* 3.4, pp. 207–217.

Donnelly, R. C. (2006). "Safe and secure: Risk-based techniques for dam safety." In: *International Water Power & Dam Construction*.

Dowell, M. and P. Jarratt (1971). "A modified regula falsi method for computing the root of an equation." In: *BIT Numerical Mathematics* 11.2, pp. 168–174.

Efron, B. and R. J. Tibshirani (1993). *An introduction to the bootstrap*. Chapman & Hall.

Elingwood, B. R. (1994). "Probability-based codified design: past accomplishments and future challenges." In: *Structural Safety* 13.3, pp. 159–176.

Elishakoff, I. (2004). *Safety factors and reliability: friends or foes?* Springer.

EN1990 (2002). *Eurocode 0: Basis of structural design*. European Standard 1990. Brussels, Belgium: European Committee for Standardization (CEN).

EN1990 (2018). *Eurocode: Basis of structural and geotechnical design*. European Standard (On-going working document) 1990. Brussels, Belgium: European Committee for Standardization (CEN).

EN1992 (2004). *Eurocode 2: Design of concrete structures*. European Standard 1992. Brussels, Belgium: European Committee for Standardization (CEN).

EN1998 (2004). *Eurocode 8: Design of structures for earthquake resistance*. European Standard 1992. Brussels, Belgium: European Committee for Standardization (CEN).

EPRI (1990). *Investigation of uplift pressures and shear and tensile strength for concrete gravity dams*. Interim Report GS-7100. Palo Alto, California, USA: Eletric Power Research Institute (EPRI).

EPRI (1992). *Uplift pressures, shear strengths and tensile strengths for stability analysis of concrete gravity dams. Volume 1*. Final Report TR-100345. Palo Alto, California, USA: Eletric Power Research Institute (EPRI).

Escuder, I. B., L. G. Altarejos, and A. L. Serrano (2011). "Theme C: Estimation of the probability of failure of a gravity dam for the sliding failure mode." In: *Proceedings of the 11th ICOLD benchmark workshop on numerical analysis of dams*. Valencia, Spain.

European Commission (2012). *M/515 Mandate for amending existing Eurocodes and extending the scope of structural Eurocodes*. Mandate M515 EN. European Commission - Enterprise and industry directorate-general.

Faber, M. H. (2012). *Statistics and probability theory: in pursuit of engineering decision support*. Springer.

Faber, M. H. and J. D. Sørensen (2003). "Reliability-based code calibration." In: *Applications of Statistics and Probability in Civil Engineering: Proceedings of the 9th international conference on applications of statistics and probability in civil engineering (Volume 2)*. Ed. by A. D. Kiureghian, S. Madanat, and J. M. Pestana. San Francisco, California, United States: Millpress, pp. 927–935.

Farinha, M. L. B. (2010). "Hydromechanical behaviour of concrete dam foundations. In situ tests and numerical modelling." Doctoral dissertation. Lisbon, Portugal: Instituto Superior Técnico (IST).

Farinha, M. L. B., L. Caldeira, and E. M. Neves (2014). "Block modelling of rock masses." In: *Structure and Infrastructure Engineering: Maintenance, Management, Life-Cycle Design and Performance* 11.10, pp. 1306–1322.

Fenves, G. and A. K. Chopra (1985). "Effects of reservoir bottom absorption and dam-water-foundation rock interaction on frequency response function for concrete gravity dams." In: *Earthquake Engineering and Structural Dynamics* 13.1, pp. 13–31.

Fenves, G. and A. K. Chopra (1986). *Simplified analysis for earthquake resistant design of concrete gravity dams*. Report UCB/EERC-85/10. California, USA: Earthquake Engineering Research Center, College of Engineering, University of California.

FERC (2002). *Engineering guidelines for the evaluation of hydropower projects. Chapter 3: Gravity dams*. Washington, USA: Federal Energy Regulatory Commission (FERC).

Ferrari, S. and F. Cribari-Neto (2004). "Beta regression for modelling rates and proportions." In: *Journal of Applied Statistics* 31.7, pp. 197–208.

Ferry-Borges, J. (1954). *O dimensionamento de estruturas (The design of structures).* Portuguese. Memória 54. Lisbon, Portugal: Laboratório Nacional de Engenharia Civil (LNEC).

Ferry-Borges, J. (1997). "Probability based structural codes: past and future." In: *Probabilistic methods for structural design.* Ed. by C. G. Soares. Springer.

Ferry-Borges, J. and M. Castanheta (1983). *Structural Safety.* 3rd Edition. Laboratório Nacional de Engenharia Civil (LNEC).

FIB (2010). *Model Code 2010: Volume 1.* Bulletin 65. Fédération Internationale du Béton (FIB).

Fiessler, B., R. Rackwitz, and H.-J. Neumann (1979). "Quadratic limit states in structural reliability." In: *Journal of the Engineering Mechanics Division* 105.4, pp. 661–676.

Forbes, C., M. Evans, N. Hastings, and B. Peacock (2000). *Statistical distributions.* Wiley.

Freudenthal, A. M. (1947). "The safety of structures." In: *Transactions of the American Society of Civil Engineers* 112.1, pp. 125–159.

Friis-Hansen, P. and J. D. Sørensen (2002). "Reliability-based code calibration of partial safety factors." In: *JCCS Workshop on Code calibration.* Zurich, Switzerland.

Gayton, N., A. H. Mohamed, J. D. Sørensen, M. Pendola, and M. Lemaire (2004). "Calibration methods for reliability-based design codes." In: *Structural Safety* 26.1, pp. 207–217.

GB50199 (1994). *Unified design standard for reliability of hydraulic engineering structures.* GB 50199-1994. Beijing, China: Research Institute of Standards and Norms of the Ministry of Construction of the People's Republic of China.

Gomes, J. M. P. (2005). "Análise experimental de cenários de rotura em fundações de barragens de betão: Ensaios estáticos e dinâmicos (Experimental analysis of failure scenarios for concrete dams foundations: Static and dynamic tests)." Portuguese. Doctoral dissertation. Rio de Janeiro, Brazil: Universidade Federal do Rio de Janeiro (UFRJ).

Gomes, J. M. P., C. P. Costa, J. V. de Lemos, and C. A. B. Pina (1997). *Study on geomechanical model of the failure of a gravity dam due to sliding along the foundation.* Memória 810. Lisbon, Portugal: Laboratório Nacional de Engenharia Civil (LNEC).

Gonçalves, A. (1999). *Durabilidade real e potencial do betão (Concrete real and potential durability)*. Programa de Investigação. Lisbon, Portugal: Laboratório Nacional de Engenharia Civil (LNEC).

Goodman, R. E., R. L. Taylor, and T. L. Brekke (1968). "A model for the mechanics of jointed rock." In: *Journal of the Soil Mechanics and Foundations Division* 94.3, pp. 637–660.

Grenoble, B. A., C. W. Harris, J. K. Meisenheimer, and D. I. Morris (1995). "Influence of rock joint deformations on uplift pressure in concrete gravity dam foundations: Field measurements and interpretation." In: *Fractured and Jointed Rock Masses*. Ed. by L. R. Myer, N. G. W. Cook, R. E. Goodman, and C. F. Tsang. Balkema, Rotterdam.

Guiducini, G. and R. M. Andrade (1988). "Seasonal oscillation of uplift pressures in hydraulic structure foundations due to environmental thermal variations." In: *Rock mechanics and power plants*. Ed. by M. Romana. Balkema, pp. 467–471.

Haldar, A. and S. Mahadevan (2000). *Probability, reliability and statistical methods in engineering design*. Wiley.

Harbitz, A. (1986). "An efficient sampling method for probability of failure calculations." In: *Structural safety* 3.2, pp. 109–115.

Hariri-Ardebili, M. A. (2018). "Risk, reliability, resilience (R3) and beyond in dam engineering: A state-of-the-art review." In: *International Journal of Disaster Risk Reduction* 31, pp. 806–831.

Hasofer, A. M. and N. C. Lind (1974). "Exact and invariant second-moment code format." In: *Journal of Engineering Mechanics* 100.EM1, pp. 111–121.

Herzog, M. A. M. (1989). "Spatial action of straight gravity dams in narrow valleys." In: *Journal of Structural Engineering* 115.3, pp. 698–706.

Higginson, E. C., G. B. Wallace, and E. L. Ore (1963). "Effect of maximum size of aggregate upon compressive strength of concrete." In: *Symposium on mass concrete*. ACI, Michigan, Detroit, pp. 219–246.

Hohenbichler, M. and R. Rackwitz (1988). "Improvement of second-order reliability estimates by importance sampling." In: *Journal of Engineering Mechanics* 114.12, pp. 2195–2199.

Hohenbichler, M., S. Gollwitzer, W. Kruse, and R. Rackwitz (1987). "New light on first- and second-order relaibility methods." In: *Structural safety* 4.4, pp. 267–284.

HSE (2001). *Reducing risks, protecting people: HSEs Decisionmaking process*. Health and Safety Executive (HSE).

ICOLD (1987). *Dam safety: Guidelines*. Bulletin 59. International Commission on Large Dams (ICOLD).

ICOLD (1988). *Dam design criteria: the philosophy of their selection*. Bulletin 61. International Commission on Large Dams (ICOLD).

ICOLD (1989). *Selecting seismic parameters for large dams - Guidelines*. Bulletin 72. International Commission on Large Dams (ICOLD).

ICOLD (1990). *Dams in Europe and USSR: a geographical approach*. ICOLD/Water Power & Dam Construction.

ICOLD (1993). *Rock foundations for dams*. Bulletin 88. International Commission on Large Dams (ICOLD).

ICOLD (1998). *Technical dictionary on dams*. ICOLD.

ICOLD (2000). *The gravity dam: a dam for the future. Review and recommendations*. Bulletin 117. International Commission on Large Dams (ICOLD).

ICOLD (2005). *Risk assessment in dam safety management. A reconnaissance of benefits: Methods and current applications*. Bulletin 130. International Commission on Large Dams (ICOLD).

ICOLD (2008). *The physical properties of hardened conventional concrete in dams*. Bulletin 145. International Commission on Large Dams (ICOLD).

ICOLD (2011). *Constitution status*. International Commission on Large Dams (ICOLD).

ICOLD (2017). *Dam safety legislation*. Final report. International Commission on Large Dams (ICOLD) - European Club.

ICOLD (2018). *World register of dams*. ICOLD.

ISO 2394 (2015). *ISO 2394:2015 - General principles on reliability for structures*. Geneva, Switzerland: International Organization for Standardization (ISO).

Itasca (2011). *UDEC - Universal Distinct Element Code, Version 5.0, User's manual*. Minneapolis, USA: Itasca Consulting Group.

Jaky, J. E. (1948). "Pressure in silos." In: *Proceedings of the Second International Conference on Soil Mechanics and Foundation Engineering*. Rotterdam, Netherlands, pp. 103–107.

Jansen, R. B. (1983). *Dams and public safety*. The Bureau of Reclamation of the U.S. Department of Interior.

Jansen, R. B. (1988). "Introduction." In: *Advanced dam engineering for design, construction, and rehabilitation*. Ed. by R. B. Jansen. Van Nostrand Reinhold, pp. 1–7.

JCSS (2001). *Probabilistic model-code*. Joint Committee on Structural Safety (JCSS).

JCSS (2008). *Risk assessment in engineering: principles, system representation & risk criteria*. Joint Committee on Structural Safety (JCSS).

JRC (2015). *State of implementation of the Eurocodes in the European Union*. Scientific and Technical Research Report 97893. Joint Research Centre (JRC).

Kalkani, E. C. (1992). "Ambient temperature effect in concrete dam foundation seepage." In: *Journal of Geotechnical Engineering* 118.1, pp. 1–11.

Kim, J.-K., S.-T. Yi, C.-K. Park, and S.-H. Eo (1999). "Size effect on compressive strength of plain and spirally reinforced concrete cylinders." In: *ACI Structural Journal* 96.1, pp. 88–94.

Kiureghian, A. D. and O. Ditlevsen (2009). "Aleatory or epistemic? Does it matter?" In: *Structural safety* 31, pp. 105–112.

Kiureghian, A. D., Y. Zhang, and C.-C. Li (1994). "Inverse reliability problem." In: *Journal of Engineering Mechanics* 120.5, pp. 1154–1159.

Kreuzer, H. (2005). "Assessing uncertainty in dam engineering." In: *Proceedings of the 73rd Annual Meeting of ICOLD*. Tehran, Iran.

Krounis, A., F. Johansson, and S. Larsson (2015). "Effects of spatial variation in cohesion over the concrete-rock interface on dam sliding stability." In: *Journal of Rock Mechanics and Geotechnical Engineering* 6.7, pp. 659–667.

Krounis, A., F. Johansson, and S. Larsson (2016). "Shear strength of partially bonded concreterock interfaces for application in dam stability analyses." In: *Rock Mechanics and Rock Engineering* 49.7, pp. 1–54.

Kübler, O. (2007). "Applied decision-making in civil engineering." Doctoral dissertation. Zürich, Switzerland: Institute of Structural Engineering, Swiss Federal Institute of Technology.

Labadie, J. W. (2004). "Optimal operation of multireservoir systems: state-of-the-art review." In: *Journal of Water Resources Planning and Management* 130.2, pp. 93–111.

LAH (1926). *Lei dos aproveitamentos hidráulicos (Law for the hydraulic exploitation)*. Portuguese. Decreto 12:559.

Leclerc, M., P. Léger, and R. Tinawi (2001). *CADAM - User's manual. Version 1.4.3*. École Polytechnique de Montréal.

Leclerc, M., P. Léger, and R. Tinawi (2003). "Computer aided stability analysis of gravity dams - CADAM." In: *Advances in Engineering Software* 34.7, pp. 403–420.

Léger, P., M. Cotê, and R. Tinawi (1995). "Thermal protection of concrete dams subjected to freeze-thaw cycles." In: *Canadian Journal of Civil Engineering* 22, pp. 588–602.

Leliavsky, S. (1945). "Uplift pressure in and beneath dams: experiments on effective uplift area in gravity dams." In: *Transactions of the American Society of Civil Engineers* 71, pp. 1474–1517.

Lemaire, M. (2009). *Structural reliability*. ISTE and Wiley.

Lemos, J. V. (1987). "A distinct element model for dynamic analysis of jointed rock with applications to dam foundation and fault motion." Doctoral dissertation. Minneapolis, USA: University of Minnesota.

Lemos, J. V. (2008). "Block modelling of rock masses." In: *European Journal of Environmental and Civil Engineering* 12.7/8, pp. 915–949.

Lemos, J. V. (2012). "Modelling the failure modes of dams' rock foundations." In: *MIR 2012 - Nuovi metodi di indagine, monitoraggio e modellazione degli amassi rocciosi*. Politecnico di Torino, Italy, pp. 259–278.

Lévy, M. (1895). "Quelques considérations sur la construction des grands barrages (Some considerations on the construction of large dams)." French. In: *Comptes Rendus de l'Académie de Sciences* 121.6, pp. 288–300.

Lim, J., B. Lee, and I. Lee (2014). "Second-order reliability method-based inverse reliability analysis using Hessian update for accurate and efficient reliability-based design optimization." In: *International journal for numerical methods in engineering* 100, pp. 773–792.

Lind, N. C. (1973). "The design of structural design norms." In: *Journal of Structural Mechanics* 1.3, pp. 357–370.

Lind, N. C. (1977). "Reliability-based structural codes, practical calibration." In: *Safety of Structures Under Dynamic Loading*. Trondheim, Norway.

LNEC (2007). *O betão compactado com cilindros usado na barragem de Pedrógão (The roller-compacted concrete used in Pedrógão dam)*. Portuguese. Relatório 126/2007. Lisbon, Portugal: Laboratório Nacional de Engenharia Civil (LNEC).

LNEC (2014). *Barragem de montante do Aproveitamento Hidroelétrico do Baixo Sabor. Análise das causas da abertura de juntas de betonagem às cotas 185 m e 186 m, na zona central do paramento de montante, no final da construção, e apreciação da solução*

de reabilitação (Upstream dam of hydroelectric exploitation of Baixo Sabor: Analysis of causes for the opening of concrete lift joints at 185 m and 186 m of elevation, in the central zone of the upstream face, at the end of construction, and comments on the rehabilitation solution). Portuguese. Relatório 452/2014. Lisbon, Portugal: Laboratório Nacional de Engenharia Civil (LNEC).

Lo, K. Y., T. Ogawa, B. Lukajic, G. F. Smith, and D. Dupak (1991). "The evaluation of stability of existing concrete dams on rock foundations and remedial measures." In: *Proceedings of the 17th International Congress on Large Dams. Volume 2*. Vienna, Austria, pp. 963–990.

Lombardi, G. (1993). "Concrete dams and their foundation. Evaluation for static loading." In: *Proceedings of the International Workshop on Dam Safety Evaluation. Volume 4: Keynote lectures*. Grindelwald, Switzerland, pp. 77–90.

Londe, P. (1987). "The Malpasset dam failure." In: *Engineering geology* 24, pp. 295–329.

Mascarenhas, A. (2005). *Searching for hydraulic quality in concrete dam foundations*. LNEC.

Mata, J. (2013). "Structural safety control of concrete dams aided by automated monitoring systems." Doctoral dissertation. Lisbon, Portugal: Instituto Superior Técnico (IST).

Mayer, M. (1926). *Die sicherheit der bauwerke und ihre berechnung nach grenzkräften anstatt nach zulässigen spannungen (The safety of structures and their design according to ultimate forces instead of allowable stresses)*. German. Springer.

McCullagh, P. and J. A. Nelder (1989). *Generalized linear models*. 2nd Edition. Chapman & Hall/CRC.

McKay, M. D., R. J. Beckman, and W. J. Conover (1979). "A comparison of three methods for selecting values of input variables in the analysis of output from a computer code." In: *Technometrics* 21.2, pp. 239–245.

Melchers, R. E. (1999). *Structural reliability analysis and prediction*. 2nd Edition. John Wiley & Sons.

Mier, J. G. M. van and M. B. Nooru-Mohamed (1990). "Geometrical and structural aspects of concrete fracture." In: *Engineering fracture mechanics* 25.4/5, pp. 617–628.

Muller, D. E. (1956). "A method for solving algebraic equations using an automatic computer." In: *Mathematical Tables and Other Aids to Computation* 10.56.

Muralha, J. (1995). "Abordagem probabilística do comportamento mecânico de descontinuidades de maciços rochosos (Probabilistic approach to the mechanical behavior

of rock mass joints)." Portuguese. Doctoral dissertation. Lisbon, Portugal: Instituto Superior Técnico (IST).

Nataf, A. (1962). "Détermination des distributions de probabilités dont les marges sont données (Determination of probability distribution whose marginals are given)." French. In: *Comptes rendus de l'Académie des Sciences* 225, pp. 42–43.

NCB (1998). *Normas de construção de barragens (Code of practice for construction of dams)*. Portuguese. Portaria 246/98.

Nicholson, G. A. (1983). *Design of gravity dams on rock foundations: sliding stability assessment by limit equilibrium and selection of shear strength parameters*. Report GL-83-13. Washington, USA: United States Army Corps of Engineers (USACE).

NOIB (1993). *Normas de observação e inspecção de barragens (Code of practice for observation and inspection of dams)*. Portuguese. Portaria 847/93.

Novak, P., I. Moffat, C. Nalluri, and R. Narayanan (2007). *Hydraulic structures*. 4th Edition. Taylor & Francis.

NP EN1998-1 (2010). *Eurocódigo 8: Projecto de estruturas para resistência aos sismos (Eurocode 8: Design of structures for earthquake resistance)*. Portuguese. Norma portuguesa NPEN1998. Caparica, Portugal: Instituto Português da Qualidade (IPQ).

NP EN206-1 (2007). *Betão - Parte 1: Especificação, desempenho, produção e conformidade (Concrete Part I: Specification, performance, production and conformity)*. Portuguese. Norma portuguesa NP EN206-1. Caparica, Portugal: Instituto Português da Qualidade (IPQ).

NPB (1993). *Normas de projeto de barragens (Code of practice for dam design)*. Portuguese. Portaria 846/93.

NTPCS (2014). *Norme tecniche per la progettazione e la costruzione degli sbarramenti di ritenuta (Technical rules for the design and construction of dams)*. Italian. Decreto. Rome, Italy: Ministero delle Infrastrutture e dei Trasporti.

Paolino, P. (2001). "Maximum likelihood estimation of models with beta-distributed dependent variables." In: *Political Analysis* 9.4, pp. 325–346.

Paté-Cornell, M. E. (1996). "Uncertainties in risk analysis: Six levels of treatment." In: *Reliability engineering and system safety* 54, pp. 95–111.

Patton, F. D. (1966). "Multiple modes of shear failure in rock and related materials." In: *Proceedings of the 1st International Congress on Rock Mechanics. Volume 1*. Lisbon, Portugal.

Pedro, J. O. (1977). *Dimensionamento das barragens abóboda pelo método dos elementos finitos (Design of arch dams by the finite element method)*. Portuguese. Memória 479. Lisbon, Portugal: Laboratório Nacional de Engenharia Civil (LNEC).

Pedro, J. O. (1999). "Safety and performance of arch dams." In: *Arch dams: Designing and monitoring for safety*. Ed. by J. O. Pedro. Springer-Verlag Wien GmbH.

Pedro, J. O. (2007). *Barragens abóbada - Coeficientes de funcionalidade e segurança e probabilidades de incidente e acidente, para cenários de degradação do betão (Arch dams - Functionality and safety factors and incident and accident probabilities, for concrete degradation scenarios)*. Portuguese. ITB 35. Lisbon, Portugal: Laboratório Nacional de Engenharia Civil (LNEC).

Pedro, J. O. (2018). *As barragens portuguesas enquadradas pelos regulamentos de segurança (The Portuguese dams covered by the safety regulation)*. Portuguese. Unpublished. Lisbon, Portugal: Laboratório Nacional de Engenharia Civil (LNEC).

Pereira, R., A. L. Batista, and L. C. Neves (2014). "Verificação da segurança ao deslizamento de barragens gravidade considerando a variabilidade das propriedades hidráulicas e mecânicas do maciço rochoso de fundação (Safety evaluation of concrete gravity dam sliding considering the variability of rock mass foundation hydraulic and mechanical properties)." Portuguese. In: *5as Jornadas Portuguesas de Engenharia de Estruturas*. Lisbon, Portugal.

Pereira, R., A. L. Batista, and L. C. Neves (2015). "Safety evaluation of concrete gravity dam sliding considering the variability of rock mass foundation hydraulic and mechanical properties." In: *Proceedings of the Second International Conference Dam World*. Lisbon, Portugal.

Pereira, R., A. L. Batista, and L. C. Neves (2016a). "Modelo probabilístico para a representação das subpressões nas fundações de barragens de betão (Probabilistic model for the representation of the uplift pressures in the concrete dam foundations)." Portuguese. In: *Encontro Nacional Betão Estrutural*. Coimbra, Portugal.

Pereira, R., A. L. Batista, and L. C. Neves (2016b). "Modelo probabilístico para a representação do nível de água na albufeira em análises de fiabilidade de barragens de betão (Probabilistic model for the representation of the reservoir water level in reliability analysis of concrete dams)." Portuguese. In: *Encontro Nacional Betão Estrutural*. Coimbra, Portugal.

Pereira, R., A. L. Batista, and L. C. Neves (2016c). "Quantificação das propriedades estruturais do betão de barragens. Parte 1 Caracterização probabilística das propriedades potenciais a partir de resultados de ensaios (Quantification of the dam concrete structural properties. Part 1 - Probabiistic characterization of the potential properties based on test results)." Portuguese. In: *Encontro Nacional Betão Estrutural*. Coimbra, Portugal.

Pereira, R., A. L. Batista, and L. C. Neves (2016d). "Quantificação das propriedades estruturais do betão de barragens. Parte 2 Estimativa das propriedades reais a partir das propriedades potenciais (Quantification of the dam concrete structural properties. Part 2 - Estimation of the real properties from the potential properties)." Portuguese. In: *Encontro Nacional Betão Estrutural*. Coimbra, Portugal.

Pereira, R., A. L. Batista, and L. C. Neves (2017). "Reliability analysis of a concrete gravity dam. Contribution for discussion on Theme D: Risk Analysis-assessment of reliability for concrete dams." In: *Proceedings of the 14th ICOLD benchmark workshop on numerical analysis of dams*. Stockholm, Sweden.

Pereira, R., A. L. Batista, and L. C. Neves (2018). "Probabilistic model for the representation of the reservoir water level of concrete dams during normal operation periods." In: *Water Resources Management* 9.32, pp. 3041–3052.

Peyras, L., P. Royet, L. Deroo, R. Albert, J.-P. Becue, S. Aigouy, E. Bourdarot, D. Loudiere, and J.-B. Kovarik (2008). "French recommendations for limit-state analytical review of gravity dam stability." In: *European Journal of Environmental and Civil Engineering* 12.9-10, pp. 1137–1164.

Pimenta, L. (2009). "Abordagens de riscos em barragens de aterro (Risk approach to embankment dams)." Portuguese. Doctoral dissertation. Lisbon, Portugal: Instituto Superior Técnico (IST).

Pina, C. A. B., C. P. Costa, J. V. de Lemos, and J. M. P. Gomes (1994). *An experimental study of failure of a gravity dam on a jointed rock foundation*. Memória 798. Lisbon, Portugal: Laboratório Nacional de Engenharia Civil (LNEC).

Plesha, M. E. (1987). "Constitutive models for rock discontinuities with dilatancy and surface degradation." In: *International Journal for Numerical and Analytical Methods in Geomechanics* 11.4, pp. 345–362.

PNBEPH (2007). *Programa nacional de barragens com elevado potencial hidroeléctrico (National programme for dams of great hydroelectric potential)*. Portuguese. Memória. COBA/PROCESL.

Ponslet, E. (1994). "Analytical and experimental comparison of probabilistic and deterministic optimization." Doctoral dissertation. Virginia, USA: Faculty of the Virginia, Polytechnic Institute and State University.

Pugsley, A. G. (1951). "Concepts of safety in structural engineering." In: *Journal of the Institution of Civil Engineers* 36.5, pp. 5–31.

Rackwitz, R. and B. Fiessler (1978). "Structural reliability under combined random load sequences." In: *Computers & Structures* 9.5, pp. 489–495.

Raj, D. (1968). *Sampling theory*. McGraw-Hill.

Ramos, J. M. (1994). *Fiabilidade e monitoramento de barragens de betão (Reliability and monitoring of concrete dams)*. Portuguese. Programa de Investigação. Lisbon, Portugal: Laboratório Nacional de Engenharia Civil (LNEC).

Ramos, J. M. (2004). *Observação do comportamento estrutural de barragens de betão (Monitoring of the structural behavior of concrete dams)*. Portuguese. LNEC.

Rankine, W. J. M. (1872). "Report on the design and construction of masonry dams." In: *The Engineer* 33, pp. 1–2.

Raphael, J. M. (1984). "Tensile strength of concrete." In: *ACI Journal Proceedings* 81.2, pp. 158–165.

Ravindra, M. K. and T. V. Galambos (1978). "Load and resistance factor design for steel." In: *Journal of the Structural Division* 104.9, pp. 1337–1353.

Ridders, C. (1979). "A new algorithm for computing a single root of a real continuous function." In: *IEEE Transactions on Circuits and Systems* 26.11, pp. 979–980.

Rissler, P. (2001). "Dimensioning of the design flood as part of a reservoir safety concept." In: *Hydropower & Dams* 4, pp. 98–105.

Rocha, M. (1965). *Structural model techniques: Some recent developments*. Memória 264. Lisbon, Portugal: Laboratório Nacional de Engenharia Civil (LNEC).

Rocha, M., J. L. Serafim, and A. F. Silveira (1958). *A method of quantitative interpretation of the results of the observation of concrete dams*. Memória 128. Lisbon, Portugal: Laboratório Nacional de Engenharia Civil (LNEC).

Rosenblatt, M. (1952). "Remarks on a multivariate transformation." In: *The Annals of Mathematical Statistics* 23.3, pp. 470–472.

RSB (1990). *Regulamento de segurança de barragens (Dam safety regulation)*. Portuguese. Decreto-Lei 11/90. Ministério das Obras Públicas, Transportes e Comunicações.

RSB (2007). *Regulamento de segurança de barragens (Dam safety regulation)*. Portuguese. Decreto-Lei 344/2007. Ministério das Obras Públicas, Transportes e Comunicações.

RSB (2018). *Regulamento de segurança de barragens (Dam safety regulation)*. Portuguese. Decreto-Lei 21/2018. Ministério do Planeamento e das Infrastruturas.

Ruggeri, G. (2004a). *Sliding safety of existing gravity dams*. Final Report. International Commission on Large Dams (ICOLD) - European Club.

Ruggeri, G. (2004b). *Uplift pressures under concrete dams*. Final Report. International Commission on Large Dams (ICOLD) - European Club.

Rutqvist, J. and O. Stephansson (2003). "The role of hydromechanical coupling in fractured rock engineering." In: *Hydrogeology Journal* 11, pp. 7–40.

Sazilly, J. A. T. de (1853). "Sur un type de profil d'égale resistance proposé pour les murs des résèrvoirs deau (On a type of profile of equal resistance proposed for the walls of the water reservoirs)." French. In: *Analles de Ponts et Chaussées*, pp. 191–222.

Schneider, J. (1997). *Introduction to safety and reliability of structures*. IABSE.

Serra, C. (2017). "Prediction of dam concrete structural properties based on wet-screened test results and mesoscale modeling." Doctoral dissertation. Lisbon, Portugal: Faculdade de Ciências e Tecnologia da Universidade Nova de Lisboa (FCT/UNL).

Serra, C., A. L. Batista, and N. M. Azevedo (2016). "Effect of wet screening in the elastic properties of dam concrete: Experimental in situ test results and fit to composite models." In: *Journal of Materials in Civil Engineering* 28.12, pp. 04016146–1–04016146–10.

Serrano, A. L. (2011). "Desarrollo de una herramienta completa de análisis y evaluación de riesgos en seguridad de presas (Development of a complete tool of risk analysis and assessment in dam safety)." Spanish. Doctoral dissertation. Spain: Universidad Politécnica de València.

Sims, G. P. (1994). "Ageing of masonry dams." In: *ICE Proceedings Water Maritime and Energy* 106.1, pp. 61–70.

Smith, N. A. F. (1994). "The failure of the Bouzey Dam in 1895." In: *Construction History* 10, pp. 47–65.

Sørensen, J. D., I. B. Kroon, and M. H. Faber (1994). "Optimal reliability-based code calibration." In: *Structural Safety* 15.3, pp. 197–208.

SPANCOLD (2013). *Technical guide on operation of dams and reservoirs: Risk analysis applied to management of dam safety. Volume 1.* Madrid, Spain: Spanish National Committee on Large Dams (SPANCOLD).

Steffensen, J. F. (1933). "Remarks on iteration." In: *Scandinavian Actuarial Journal* 1, pp. 64–72.

Tanchev, L. (2014). *Dams and appurtenant hydraulic structures.* 2nd Edition. CRC Press.

Tang, B. (1993). "Orthogonal array-based latin hypercubes." In: *Journal of the American Statistical Association* 88.424, pp. 1392–1397.

Teles, M. (1985). "Comportamento térmico de barragens de betão (Thermal behavior of concrete dams)." Portuguese. Doctoral dissertation. Porto, Portugal: Faculdade de Engenharia da Universidade do Porto (FEUP).

Terzaghi, K. and L. Rendulic (1934). "Die wirksame flaechenporositäat des betons (Effective porosity of concrete)." German. In: *Zeitschrift des Öesterreichischen Ingenieur und Architekten Vereines* 86.1/2, pp. 1–9.

The Mathworks Inc. (2010). *MatLab.* Natick, Massachusetts, USA.

Thoft-Christensen, P. (2001). "Risk analysis in civil engineering." In: *Module 1 of a short course on risk and reliability in civil engineering at the international conference on safety, risk and reliability: Trends in Engineering (IABSE).* Malta.

Thoft-Christensen, P. and M. J. Baker (1982). *Structural reliability theory and its applications.* Prentice-Hall.

Thomas, H. H. (1976). *Engineering of Large Dams.* Wiley.

Tvedt, L. (1990). "Distribution of quadratic forms in normal space - application to structural reliability." In: *Journal of Engineering Mechanics* 116.6, pp. 1183–1197.

Underwood, L. B. and N. A. Dixon (1976). "Dams on rock foundations." In: *Rock Engineering for Foundations and Slopes.* Vol. 2. Boulder, Colorado, United States, pp. 125–146.

Underwood, P. (1983). "Dynamic Relaxation." In: *Computational Methods for Transient Analysis.* Ed. by T. Belytschko and T. Hughes. North Holland, pp. 245–265.

USACE (1995). *Gravity dam design.* Manual 1110-2-2200. Washington, USA: United States Army Corps of Engineers (USACE).

USBR (1976). *Design of gravity dams.* Denver, Colorado, USA: United States Bureau of Reclamation (USBR).

USBR (1981). *Concrete manual: A water resources technical publication*. 8th Edition. USBR.

USBR (2011). *Dam safety public protection guidelines: A risk framework to support dam safety decision-making*. Denver, Colorado, USA: United States Bureau of Reclamation (USBR).

Vrouwenvelder, T. (1997). "JCSS probabilistic model code." In: *Structural safety* 19.3, pp. 245–251.

Vrouwenvelder, T. (2008). "Treatment of risk and reliability in the Eurocodes." In: *Structures & Buildings* 161.4, pp. 209–214.

Vrouwenvelder, T. and A. Siemes (1987). "Probabilistic calibration procedure for the derivation of partial safety factors for the Netherlands building codes." In: *Heron* 32.4, pp. 9–29.

Vrouwenvelder, T., R. Lovegrove, M. Holický, P. Tanner, and G. Canisus (2001). "Risk assessment and risk communication in civil rngineering." In: *Safety, Risk, and Reliability - Trends in Engineering*. Malta.

Weaver, W. (1932). "Uplift pressure on dams." In: *Journal of mathematics and physics* 11.1-4, pp. 114–145.

Wegmann, E. (1908). *The design and construction of dams*. 5th Edition. John Wiley & Sons.

Westberg, M. (2009a). "Geostatistical approach for statistical description of uplift pressures: Part I." In: *Dam Engineering* 19.4, pp. 241–256.

Westberg, M. (2009b). "Geostatistical approach for statistical description of uplift pressures: Part II." In: *Dam Engineering* 20.1, pp. 39–58.

Westberg, M. (2010). "Reliability-based assessment of concrete dam stability." Doctoral dissertation. Sweden: Lund University.

Westberg, M. and F. Johansson (2016). *Probabilistic model code for concrete dams*. Report 2016:292. Energiforsk.

Westberg, M., F. Johansson, F. R. Bayona, and L. G. Altarejos (2017). "Theme D: Risk analyis-assessment of reliability for concrete dams." In: *Proceedings of the 14th ICOLD benchmark workshop on numerical analysis of dams*. Stockholm, Sweden.

Westergaard, H. M. (1933). "Water pressure on dams during earthquakes." In: *Transactions of the American Society of Civil Engineers* 98, pp. 418–472.

Wittke, W. (1990). *Rock mechanics: Theory and applications with case histories*. Springer-Verlag.

Wyllie, D. C. (1999). *Foundations on rock*. 2nd Edition. CRC Press.

You, J.-Y. and X. Cai (2008a). "Hedging rule for reservoir operations: A numerical model." In: *Water resources research* 44.1.

You, J.-Y. and X. Cai (2008b). "Hedging rule for reservoir operations: A theoretical analysis." In: *Water resources research* 44.1.

Zangar, C. N. (1952). *Hydrodynamic pressures on dams due to horizontal earthquake effects*. Engineering Monograph 11. United States Bureau of Reclamation (USBR).

Zienkiewicz, C. (1947). "The stress-distribution in gravity dams." In: *Journal of the Institution of Civil Engineers* 27.3, pp. 244–271.

APPENDIX

Pseudo-dynamic seismic load model

A.1 General considerations

Chopra (1978) suggested the pseudo-dynamic seismic load model, as a simplified version of a general dynamic analysis procedure, to overcome the unrealistic assumptions of the pseudo-static model, namely, the rigid dam and water incompressibility.

Based on simplified analysis in which the maximum response is estimated directly from the seismic design spectrum and response history of finite element idealizations of the dam monolith, the procedure proposed involves the computation of equivalent lateral forces associated with the fundamental vibration mode of the dam and includes the effects of the dam-reservoir interaction and compressibility of water.

Later, Fenves and Chopra (1986) extended this procedure to account both the effects of dam-foundation interaction and the response contribution of higher vibration modes, through the "static correction" concept, which shall make this procedure sufficiently accurate for the elastic analysis for the design phase and safety evaluation of concrete gravity dams.

In the following sections the computation of the equivalent lateral forces for the fundamental and higher mode response is described.

A.2 Simplified analysis for the fundamental mode response

A.2.1 Vibrational properties

Although the analysis of the fundamental mode response of the concrete dam is complicated due to the frequency-dependent and complex-valued hydrodynamic and foundation terms in the response governing equations (Fenves and Chopra 1986), a equivalent single degree-of-freedom (SDF) system can be considered to represent approximately the fundamental mode response of concrete gravity dams, since it corresponds to a shear deformation of the cross-section.

The vibrational properties (period and damping ratio) of the equivalent SDF system can be represented by the corresponding approximated properties of the concrete gravity dam monolith.

The fundamental vibration period T_1 of a standard nonoverflow cross-section of concrete gravity dams on rigid foundation with empty reservoir is, according to finite-element tests (Chopra 1978), given by,

$$T_1 = 0.38 \cdot \frac{H}{\sqrt{E_c}} \tag{A.1}$$

where H is the dam height in meters and E_c is the Young's modulus of the dam in MPa.

After forced vibration tests (Chopra 1978), it was concluded that the viscous damping ratio ξ_1, in the same conditions, is in the range of 1% to 3%. However, for large motions and high stresses expected in a dam during intense earthquakes, $\xi_1 = 5\%$ is recommended for lower vibration modes of concrete gravity dams (Chopra and Chakrabarti 1973; Chopra 1978).

The effect of the impounded water on the vibration period and damping ratio of the dam on rigid foundation is accounted, respectively, by,

$$\tilde{T_r} = T_1 \cdot R_r \tag{A.2}$$

and,

$$\tilde{\xi_r} = \frac{1}{R_r} \cdot \xi_1 + \xi_r \tag{A.3}$$

where R_r and ξ_r are the period lengthening ratio and the additional damping due to the added hydrodynamic mass from dam-water interaction and reservoir bottom absorption,

respectively. Values of R_r are given in Table A.1, in terms of the relative reservoir water height k_r, for a wave reflection coefficient $\alpha = 1$, such as recommended for nonabsorptive reservoir bottom of new or recent dams (Chopra 1978).

Table A.1: Standard values for the period lengthening ratio R_r due to dam-reservoir interaction, for $\alpha = 1$ (Fenves and Chopra 1985).

	E (10^6 psi) ≈E (GPa)×0.145							
k_r	5.0	4.5	4.0	3.5	3.0	2.5	2.0	1.0
1.00	1.454	1.409	1.37	1.341	1.32	1.301	1.286	1.263
0.95	1.368	1.323	1.289	1.259	1.241	1.224	1.212	1.193
0.90	1.289	1.247	1.214	1.191	1.176	1.164	1.154	1.140
0.85	1.215	1.179	1.152	1.136	1.126	1.117	1.110	1.100
0.80	1.148	1.121	1.104	1.095	1.087	1.081	1.077	1.071
0.75	1.092	1.078	1.070	1.063	1.059	1.055	1.053	1.049
0.70	1.055	1.048	1.044	1.041	1.039	1.037	1.035	1.033
0.65	1.033	1.031	1.028	1.026	1.025	1.024	1.023	1.022
0.60	1.020	1.020	1.017	1.016	1.016	1.016	1.016	1.014
0.55	1.013	1.012	1.010	1.010	1.01	1.009	1.009	1.009
0.50	1.009	1.008	1.006	1.006	1.006	1.006	1.006	1.005

The effect of the rock mass foundation flexibility on the vibration period and damping ratio of the concrete gravity dam with impounded reservoir is accounted, respectively, by,

$$\tilde{T}_1 = T_1 \cdot R_r \cdot R_f \tag{A.4}$$

and,

$$\tilde{\xi}_1 = \frac{1}{R_r} \cdot \frac{1}{R_f^3} \cdot \xi_1 + \xi_r + \xi_f \tag{A.5}$$

where R_f and ξ_f are the period lengthening ratio and the additional damping due to the dam-foundation interaction. Their values are given in Table A.2, in terms of the ratio between the Young's modulus of the foundation and the dam materials (E_f/E_c) and a constant hysteretic damping factor $\eta = .10$, such as recommended in the absence of information on damping properties of the rock mass foundation (Fenves and Chopra 1985).

Equation A.5, shows that the dam-water and dam-foundation interactions reduce the effectiveness of the structural damping, although the overall damping of the system is

Table A.2: Standard values for the period lengthening ratio R_f, and added damping ratio ξ_f due to the dam-foundation interaction, for $\eta_f = 0.10$ (Fenves and Chopra 1985).

E_f/E_c	R_f	ξ_f
5.0	1.044	0.014
4.5	1.049	0.016
4.0	1.054	0.018
3.5	1.061	0.020
3.0	1.070	0.024
2.5	1.083	0.028
2.0	1.102	0.035
1.5	1.131	0.047
1.4	1.139	0.050
1.3	1.149	0.053
1.2	1.159	0.057
1.1	1.172	0.062
1.0	1.187	0.067
0.9	1.204	0.074
0.8	1.225	0.082
0.7	1.252	0.091
0.6	1.286	0.103
0.5	1.332	0.118
0.4	1.396	0.138
0.3	1.495	0.166
0.2	1.670	0.208

increased due to these effects.

A.2.2 Lateral forces

The maximum response of the concrete gravity dam, given in terms of lateral equivalent forces, is then estimated from the seismic design spectrum, based on the vibration properties and the fundamental mode shape, obtained through the response history of finite element idealizations of the dam monolith.

The lateral equivalent forces include both the dynamic amplification of the inertia forces along the dam height but also the hydrodynamic forces due to the effects of water

compressibility, expressed by the period ratio R_w,

$$R_w = \frac{T_1^r}{\tilde{T}_r} \tag{A.6}$$

where $T_1^r = 4 \cdot H_r / C$ is the fundamental vibration period of the impounded water, and $C = 1440\, m/s$ is the velocity of pressure waves in water.

For the computation of the lateral equivalent forces, the generalized mass $\tilde{M}_1$, including the hydrodynamic added mass, and the earthquake force coefficient $\tilde{L}_1$ must be computed, such as, respectively,

$$\tilde{M}_1 = M_1 \cdot (R_r)^2 \tag{A.7}$$

and,

$$\tilde{L}_1 = L_1 + \frac{1}{g} \cdot I_w \cdot \left(\frac{H_r}{H} \right)^2 \cdot A_p \tag{A.8}$$

where $I_w = \gamma_w \cdot H_r^2 / 2$ is the total hydrostatic force on the dam, A_p is the hydrodynamic force coefficient, given in Table A.3 in terms of R_w, and the generalized mass M_1 and earthquake force coefficient L_1, with empty reservoir, are, respectively, given by,

$$M_1 = \frac{1}{g} \cdot \int_0^{H_r} w(y) \cdot \phi^2(y)\, \partial y \tag{A.9}$$

and,

$$L_1 = \frac{1}{g} \cdot \int_0^{H_r} w(y) \cdot \phi(y)\, \partial y \tag{A.10}$$

where $w(y)$ is the dam weight per unit height, and $\phi(y)$ is the displacement of the fundamental mode shape of a standard monolith, given in TableA.4.

Finally, the lateral equivalent forces are given by,

$$f_1(y) = \frac{\tilde{L}_1}{\tilde{M}_1} \cdot \frac{S_a\left(\tilde{T}_1, \tilde{\xi}_1\right)}{g} \cdot \left[w(y) \cdot \phi(y) + g \cdot p\left(y, \tilde{T}_r\right) \right] \tag{A.11}$$

where $S_a\left(\tilde{T}_1, \tilde{\xi}_1\right)$ is the pseudo-acceleration ordinate of the design spectrum evaluated at the vibration period $\tilde{T}_1$, and $p\left(y, \tilde{T}_r\right)$ is a function representing the hydrodynamic pressure of a full reservoir on the upstream face due to a harmonic acceleration of period $\tilde{T}_r$, extracted from the Table A.5, based on a nondimensional form $g \cdot p(\hat{y}) / (\gamma_w \cdot H)$, where $\hat{y} = y/H$. For reservoir water levels lower than a full reservoir, the values of $p(y)$ must be

Table A.3: Standard values for the hydrodynamic force coefficient A_p.

R_w	A_p
0.99	1.242
0.98	0.893
0.97	0.739
0.96	0.647
0.95	0.585
0.94	0.539
0.93	0.503
0.92	0.474
0.9	0.431
0.85	0.364
0.8	0.324
0.7	0.279
$\leq$0.5	0.237

multiplied by $\left(H_r/H\right)^2$.

A.3 Static correction for higher mode response

Since periods of higher vibration modes of concrete gravity dams are very short, the corresponding ordinates of the pseudo-acceleration response spectrum for the design earthquake are close to the peak ground acceleration, with little dynamic amplification, responding statically as a rigid body.

The maximum earthquake effects associated with the contribution of the nth vibration mode can by represented by equivalent lateral forces (Fenves and Chopra 1986), such as,

$$f_n(y) = \frac{L_n}{M_n} \cdot S_{an} \cdot m(y) \cdot \phi_n(y) \tag{A.12}$$

where $S_{an} \approx \bar{a}_g$ is the pseudo-acceleration ordinate of the design spectrum which, due to the very short vibration period, is very close to the maximum ground acceleration $\bar{a}_g$, $m(y) = w(y)/g$ is the dam mass per unit height and ω_n and $\phi_n(y)$ are the natural frequency and the horizontal component nth vibration mode shape.

The maximum earthquake response is given by overlapping the maximum response of all higher vibration modes, since they are attained at the same instant when the ground

Table A.4: Standard fundamental mode shape $\phi(y)$ for concrete gravity dams.

y/H	$\phi(y)$
1.00	1.000
0.95	0.866
0.90	0.735
0.85	0.619
0.80	0.530
0.75	0.455
0.70	0.389
0.65	0.334
0.60	0.284
0.55	0.240
0.50	0.200
0.45	0.165
0.40	0.135
0.35	0.108
0.30	0.084
0.25	0.065
0.20	0.047
0.15	0.034
0.10	0.021
0.05	0.010
0.00	0.000

acceleration is at its maximum value $\bar{a}_g$, i.e.,

$$f_{sc}(y) = \sum_{n=2}^{\infty} f_n(y) = \sum_{n=2}^{\infty} \frac{L_n}{M_n} \cdot m(y) \cdot \phi_n(y) \cdot \bar{a}_g \tag{A.13}$$

Since the deformation response of a dam to ground acceleration $a_g(t)$ is identical to the response of a structure on fixed base to external forces equal to the product between mass per unit height and ground acceleration (Fenves and Chopra 1986), these forces can be expressed as the summation of modal contributions given, for the maximum ground acceleration, by

$$m(y) \cdot \bar{a}_g = \sum_{n=1}^{\infty} \frac{L_n}{M_n} \cdot m(y) \cdot \phi_n(y) \cdot \bar{a}_g \tag{A.14}$$

Table A.5: Standard values for the nondimensional hydrodynamic pressure function $g \cdot p(\hat{y}) / (\gamma_w \cdot H)$, for full reservoir, due to harmonic acceleration of period $\tilde{T}_r$.

$\hat{y}$	R_w												
	≤0.50	0.70	0.80	0.85	0.90	0.92	0.93	0.94	0.95	0.96	0.97	0.98	0.99
1.00	.000	.000	.000	.000	.000	.000	.000	.000	.000	.000	.000	.000	.000
0.95	.070	.073	.076	.079	.083	.086	.088	.090	.092	.096	.102	.111	.133
0.90	.112	.118	.124	.129	.138	.143	.147	.151	.157	.164	.176	.195	.238
0.85	.127	.135	.144	.152	.164	.172	.178	.184	.193	.204	.221	.249	.313
0.80	.133	.144	.155	.165	.182	.193	.200	.208	.220	.235	.257	.295	.379
0.75	.141	.154	.168	.180	.201	.214	.223	.234	.248	.267	.294	.340	.445
0.70	.145	.161	.178	.192	.216	.232	.242	.255	.272	.294	.327	.382	.506
0.65	.143	.161	.180	.197	.224	.242	.254	.269	.288	.313	.351	.414	.558
0.60	.139	.159	.180	.199	.230	.250	.264	.280	.301	.330	.373	.444	.605
0.55	.137	.159	.183	.203	.237	.260	.274	.293	.316	.348	.395	.473	.651
0.50	.135	.159	.184	.206	.244	.269	.284	.304	.329	.364	.415	.500	.694
0.45	.130	.155	.182	.206	.246	.272	.289	.310	.338	.375	.430	.522	.730
0.40	.124	.151	.179	.204	.247	.275	.293	.315	.345	.384	.442	.540	.762
0.35	.121	.149	.179	.205	.250	.279	.298	.322	.353	.395	.456	.559	.793
0.30	.118	.147	.178	.206	.252	.283	.303	.328	.360	.403	.467	.575	.820
0.25	.113	.143	.175	.204	.252	.284	.304	.330	.363	.408	.475	.587	.840
0.20	.109	.139	.172	.202	.252	.284	.305	.332	.366	.412	.481	.596	.856
0.15	.107	.138	.172	.202	.252	.286	.307	.334	.369	.417	.487	.604	.871
0.10	.106	.137	.172	.202	.253	.287	.309	.337	.372	.420	.491	.611	.881
0.05	.103	.135	.169	.200	.252	.286	.308	.336	.372	.420	.492	.613	.886
0.00	.100	.133	.168	.198	.251	.285	.307	.335	.371	.420	.492	.613	.886

which can be used to rewrite equation A.13 such as,

$$f_{sc}(y) = \frac{\bar{a}_g}{g} \cdot w(y) \cdot \left[1 - \frac{L_1}{M_1} \cdot \phi(y)\right] \tag{A.15}$$

In the "static correction" concept, the effects of the impounded water are introduced as additional hydrodynamic force, since inertia and damping terms are neglected, leading to a generalization of the maximum earthquake response (equation A.13) into,

$$f_{sc}(y) = \sum_{n=2}^{\infty} \frac{L_n}{M_n} \cdot m(y) \cdot \phi_n(y) \cdot \bar{a}_g + \sum_{n=2}^{\infty} \frac{B_n}{M_n} \cdot m(y) \cdot \phi_n(y) \cdot \bar{a}_g \tag{A.16}$$

where B_n, representing the added hydrodynamic pressure is given by,

$$B_n = \int_0^{H_r} p_0(y)\,\phi_n(y)\;\partial y \tag{A.17}$$

where $p_0(y)$ is a real-valued and frequency-independent function for hydrodynamic pressure on a rigid dam under unit acceleration, with water compressibility neglected, given in Table A.6, based on a nondimensional form $g \cdot p_0(\hat{y}) / (\gamma_w \cdot H)$, where $\hat{y} = y/H$.

Table A.6: Standard values for the nondimensional hydrodynamic pressure function $g \cdot p_0(\hat{y}) / (\gamma_w \cdot H)$ on a rigid dam, for full reservoir, undergoing unit acceleration.

$\hat{y}$	$g \cdot p_0(\hat{y}) / (\gamma_w \cdot H)$
1.00	0.000
0.95	0.137
0.90	0.224
0.85	0.301
0.80	0.362
0.75	0.418
0.70	0.465
0.65	0.509
0.60	0.546
0.55	0.580
0.50	0.610
0.45	0.637
0.40	0.659
0.35	0.680
0.30	0.696
0.25	0.711
0.20	0.722
0.15	0.731
0.10	0.737
0.05	0.741
0.00	0.742

Again, the maximum response value is given by the summation of modal contributions, i.e.,

$$p_0(y) \cdot \bar{a}_g = \sum_{n=1}^{\infty} \frac{B_n}{M_n} \cdot m(y) \cdot \phi_n(y) \cdot \bar{a}_g \tag{A.18}$$

which can be used to extended the equation A.15, introducing the effects of the impounded

water, such as,

$$f_{sc}(y) = \frac{\bar{a}_g}{g} \cdot \left\{ w(y) \cdot \left[1 - \frac{L_1}{M_1} \cdot \phi(y) \right] + \left[g \cdot p_0(y) - \frac{B_1}{M_1} \cdot w(y) \cdot \phi(y) \right] \right\} \tag{A.19}$$

where B_1 provides a measure of the portion of $p_0(y)$ that acts in the fundamental vibration mode, given by,

$$B_1 = 0.20 \cdot \frac{I_w}{g} \cdot \left(\frac{H_r}{H} \right)^2 \tag{A.20}$$

APPENDIX B

Deduction of the failure mode equations

B.1 Failure mode 1

The limit stability conditions, considering the failure mode 1, can be obtained by solving, in order to the critical friction coefficient $\tan\phi_c$, the following system of equations,

$$\begin{cases} \sum M_{icr} = F_v \cdot x_0 - F_h \cdot (L/\tan\alpha - y_0) + R_{v,A} \cdot \tan\phi_c \cdot L/\tan\alpha + \\ \qquad \left(R_{n,B} \cdot \tan\phi_c + x\right) \cdot L/\sin\alpha = 0 & \text{(B.1a)} \\ \sum F_{t,h} = R_{v,A} \cdot \tan\phi_c + R_{n,B} \cdot \sin\alpha + \left(R_{n,B} \cdot \tan\phi_c + x\right) \cdot \cos\alpha = F_h & \text{(B.1b)} \\ \sum F_{t,v} = R_{v,A} + R_{n,B} \cdot \cos\alpha - \left(R_{n,B} \cdot \tan\phi_c + x\right) \cdot \sin\alpha = F_v & \text{(B.1c)} \\ \sum F_{t,t,w} = F_{t,w} + x - F_{n,w} \cdot \tan\phi_c = 0 & \text{(B.1d)} \end{cases}$$

where $\sum M_{irc}$ expresses the equilibrium of moments around the point *icr*, located at the intersection point between lines perpendicular to the movement of points A and B, $\sum F_{t,h}$ and $\sum F_{t,v}$ express the equilibrium of horizontal and vertical forces, respectively and $\sum F_{t,t,w}$ express the equilibrium of tangential moments at the downstream rock wedge. Apart from the friction coefficient $\tan\phi_c$, the remain unknown variables are the vertical reaction at point A ($R_{v,A}$), the normal reaction at point B ($R_{n,B}$) and the unbalanced force that pushes the downstream rock wedge (x).

From equation B.1d, x is given by,

$$x = F_{n,w} \cdot \tan\phi_c - F_{t,w} \tag{B.2}$$

Replacing x in equation B.1a, $R_{v,A}$ is given by,

$$\begin{aligned}
&c_1 + R_{v,A} \cdot \tan\phi_c \cdot L/\tan\alpha + \Big(R_{n,B} \cdot \tan\phi_c + F_{n,w} \cdot \tan\phi_c - F_{t,w}\Big) \cdot L/\sin\alpha = 0 \\
\iff &-R_{v,A} \cdot \tan\phi_c \cdot L/\tan\alpha = c_1 + \Big(R_{n,B} \cdot \tan\phi_c + F_{n,w} \cdot \tan\phi_c - F_{t,w}\Big) \cdot L/\sin\alpha \\
\iff &R_{v,A} = -\frac{c_1 + \Big(R_{n,B} \cdot \tan\phi_c + F_{n,w} \cdot \tan\phi_c - F_{t,w}\Big) \cdot L/\sin\alpha}{\tan\phi_c \cdot L/\tan\alpha} \iff \\
&R_{v,A} = -\left(\frac{R_{n,B}}{\cos\alpha} + \frac{F_{n,w}}{\cos\alpha} + \frac{c_2}{\tan\phi_c}\right)
\end{aligned} \tag{B.3}$$

where c_1 is given by,

$$c_1 = F_v \cdot x_0 - F_h \cdot (L/\tan\alpha - y_0) \tag{B.4}$$

and c_2 is given by,

$$c_2 = \frac{c_1}{L/\tan\alpha} - \frac{F_{t,w}}{\cos\alpha} \tag{B.5}$$

Replacing x and $R_{v,A}$ in equation B.1c, $R_{n,B}$ is given by,

$$\begin{aligned}
&-\left(\frac{R_{n,B}}{\cos\alpha} + \frac{F_{n,w}}{\cos\alpha} + \frac{c_2}{\tan\phi_c}\right) + R_{n,B} \cdot \cos\alpha - \Big(R_{n,B} \cdot \tan\phi_c + F_{n,w} \cdot \tan\phi_c - F_{t,w}\Big) \\
&\cdot \sin\alpha = F_v \iff -\frac{R_{n,B}}{\cos\alpha} - \frac{F_{n,w}}{\cos\alpha} - \frac{c_2}{\tan\phi_c} + R_{n,B} \cdot \cos\alpha - R_{n,B} \cdot \tan\phi_c \cdot \sin\alpha \\
&-F_{n,w} \cdot \tan\phi_c \cdot \sin\alpha + F_{t,w} \cdot \sin\alpha = F_v \overset{\cdot\tan\phi_c}{\iff} R_{n,B} \cdot \tan\phi_c \cdot \cos\alpha - \frac{R_{n,B} \cdot \tan\phi_c}{\cos\alpha} \\
&-R_{n,B} \cdot \tan^2\phi_c \cdot \sin\alpha = F_{n,w} \cdot \tan^2\phi_c \cdot \sin\alpha + \frac{F_{n,w} \cdot \tan\phi_c}{\cos\alpha} - F_{t,w} \cdot \tan\phi_c \cdot \sin\alpha \\
&+F_v \cdot \tan\phi_c + c_2 \iff R_{n,B} \cdot \Big(c_3 \cdot \tan\phi_c - \sin\alpha \cdot \tan^2\phi_c\Big) = F_{n,w} \cdot \sin\alpha \cdot \tan^2\phi_c \\
&+c_4 \cdot \tan\phi_c + c_2 \iff R_{n,B} = \frac{F_{n,w} \cdot \sin\alpha \cdot \tan^2\phi_c + c_4 \cdot \tan\phi_c + c_2}{-\sin\alpha \cdot \tan^2\phi_c + c_3 \cdot \tan\phi_c}
\end{aligned} \tag{B.6}$$

where c_3 and c_4 are given, respectively, by,

$$c_3 = \cos\alpha - 1/\cos\alpha \tag{B.7}$$

$$c_4 = \frac{F_{n,w} \cdot \tan\phi_c}{\cos\alpha} - F_{t,w} \cdot \sin\alpha \tag{B.8}$$

Finally, replacing x, $R_{v,A}$ and $R_{n,B}$ in equation B.1b, $\tan\phi_c$ is given by,

$$
\begin{aligned}
&-\left(\frac{R_{n,B}}{\cos\alpha}+\frac{F_{n,w}}{\cos\alpha}+\frac{c_2}{\tan\phi_c}\right)\cdot\tan\phi_c+R_{n,B}\cdot\sin\alpha+\Big(R_{n,B}\cdot\tan\phi_c+F_{n,w}\cdot\tan\phi_c\\
&-F_{t,w}\Big)\cdot\cos\alpha=F_h\Longleftrightarrow-\frac{R_{n,B}\cdot\tan\phi_c}{\cos\alpha}-\frac{F_{n,w}\cdot\tan\phi_c}{\cos\alpha}-c_2+R_{n,B}\cdot\sin\alpha\\
&+R_{n,B}\cdot\cos\alpha\cdot\tan\phi_c+F_{n,w}\cdot\cos\alpha\cdot\tan\phi_c-F_{t,w}\cdot\cos\alpha=F_h\Longleftrightarrow\\
&R_{n,B}\cdot(\sin\alpha+c_3\cdot\tan\phi_c)=c_5-F_{n,w}\cdot c_3\cdot\tan\phi_c\Longleftrightarrow\\
&\frac{F_{n,w}\cdot\sin\alpha\cdot\tan^2\phi_c+c_4\cdot\tan\phi_c+c_2}{-\sin\alpha\cdot\tan^2\phi_c+c_3\cdot\tan\phi_c}\cdot(\sin\alpha+c_3\cdot\tan\phi_c)=-F_{n,w}\cdot c_3\cdot\tan\phi_c\\
&+c_5\Longleftrightarrow\Big(F_{n,w}\cdot\sin\alpha\cdot\tan^2\phi_c+c_4\cdot\tan\phi_c+c_2\Big)\cdot(\sin\alpha+c_3\cdot\tan\phi_c)\\
&=(-F_{n,w}\cdot c_3\cdot\tan\phi_c+c_5)\cdot\Big(-\sin\alpha\cdot\tan^2\phi_c+c_3\cdot\tan\phi_c\Big)\Longleftrightarrow\\
&F_{n,w}\cdot\sin^2\alpha\cdot\tan^2\phi_c+\cancel{F_{n,w}\cdot\sin\alpha\cdot c_3\cdot\tan^3\phi_c}+c_4\cdot\sin\alpha\cdot\tan\phi_c\\
&+c_4\cdot c_3\cdot\tan^2\phi_c+c_2\cdot\sin\alpha+c_2\cdot c_3\cdot\tan\phi_c=\cancel{F_{n,w}\cdot\sin\alpha\cdot c_3\cdot\tan^3\phi_c}\\
&-F_{n,w}\cdot c_3^2\cdot\tan^2\phi_c-c_5\cdot\sin\alpha\cdot\tan^2\phi_c+c_5\cdot c_3\cdot\tan\phi_c\Longleftrightarrow\\
&c_6\cdot\tan^2\phi_c+c_7\cdot\tan\phi_c+c_8=0\Longleftrightarrow\tan\phi_c=\frac{-c_7\pm\sqrt{c_7^2-4\cdot c_6\cdot c_8}}{2\cdot c_6}
\end{aligned}
\tag{B.9}
$$

where c_5, c_6, c_7 and c_8 are given, respectively, by,

$$c_5=c_2+F_{t,w}\cdot\cos\alpha+F_h \tag{B.10}$$

$$c_6=F_{n,w}\cdot\sin^2\alpha+c_4\cdot c_3+F_{n,w}\cdot c_3^2+c_5\cdot\sin\alpha \tag{B.11}$$

$$c_7=c_4\cdot\sin\alpha+(c_2-c_5)\cdot c_3 \tag{B.12}$$

$$c_8=c_2\cdot\sin\alpha \tag{B.13}$$

B.2 Failure mode 2

The critical friction coefficient $\tan\phi_c$, expressing the limit equilibrium conditions considering the failure mode 2, is given by,

$$\tan\phi_c=\frac{F_{t,w}+F_t}{F_{n,w}+F_n} \tag{B.14}$$

where $F_{t,w}$ and $F_{n,w}$ are the tangential and normal forces acting on the downstream rock wedge, respectively, and F_t and F_n are the tangential and normal components of the total forces acting on the dam projected to the sliding plane, respectively, given by,

$$F_t = F_h \cdot \cos\alpha - F_v \cdot \sin\alpha \tag{B.15}$$

$$F_n = F_h \cdot \sin\alpha + F_v \cdot \cos\alpha \tag{B.16}$$

B.3 Failure mode 3

The critical friction coefficient $\tan\phi_c$, expressing the limit equilibrium conditions considering the failure mode 3, is obtained by solving the following equation,

$$F_{t,w} + F_t = (F_{n,w} + F_n) \cdot \tan\phi_c \tag{B.17}$$

where $F_{t,w}$ and $F_{n,w}$ are the tangential and normal forces acting on the downstream rock wedge, respectively, and F_t and F_n are the tangential and normal components, respectively, of the reaction forces at the point contact C, given by,

$$F_t = R_{h,C} \cdot \cos\alpha + R_{h,C} \cdot \tan\phi_c \cdot \sin\alpha \tag{B.18}$$

$$F_n = -\left(R_{h,C} \cdot \sin\alpha + R_{h,C} \cdot \tan\phi_c \cdot \cos\alpha\right) \tag{B.19}$$

where $R_{h,C}$ is the horizontal component of the reaction at the contact point C, given, considering the equilibrium of the dam body, by,

$$R_{h,C} = \frac{M_B}{h_w} = \frac{F_h \cdot y_0 - F_v \cdot (L - x_0)}{h_w} \tag{B.20}$$

Equation B.17 is then re-written as a quadratic function, whose roots define the the limit equilibrium conditions through the critical friction coefficient $\tan\phi_c$, given by,

$$a \cdot \tan\phi_c^2 + b \cdot \tan\phi_c + c = 0 \Longleftrightarrow \tan\phi_c = \frac{-b \pm \sqrt{b^2 - 4 \cdot a \cdot c}}{2 \cdot a} \tag{B.21}$$

where a, b and c are the quadratic polynomial parameters given, respectively, by,

$$a = R_{h,C} \cdot \cos\alpha \tag{B.22}$$

$$b = 2R_{h,C} \cdot \sin\alpha - F_{n,w} \tag{B.23}$$

$$c = F_{t,w} + R_{h,C} \cdot \cos\alpha \tag{B.24}$$

B.4 Failure mode 4

The limit conditions are expressed by a null moment around the point C.

APPENDIX C

Discrete element method

C.1 General considerations

Structural analysis methods, aiming to determine the effects of loads on structures, must be able to model properly the geometry, support conditions, material properties and loads. Apart from simple linear elastic models of particular structures, whose structural response can be obtained analytically using classical mechanic principles and elasticity theory, numerical methods are used to approximate solutions of large systems of differential equations generated by the application of those principles to more complex structures.

Finite-element method (FEM) is the most widespread numerical method for structural analysis. It considers a subdivision of a large model into a mesh of smaller finite-elements interconnected by nodal points. The solution of the system equilibrium is approximated by solving a large system of partial differential equations, composed by the simple equations related to each finite element, that models the structural response. Several authors used FEM for structural analysis of concrete dams (e.g. Pedro (1977) and Wittke (1990)), considering equivalent continuum models.

However, concrete dams should not be analysed as independent structures but integrated in dam-reservoir-foundation systems characterized by the interaction between materials and the existence of discontinuities which control its structural behaviour, namely in the case of gravity dams, since they represent low-resistance paths that govern failure

mechanisms. In the case of the explicit consideration of the discontinuities into discontinuous models, FEM with joint elements can be used for that purpose (Goodman *et al.* 1968). However, discrete-element method (DEM), which emerged as an alternative to FEM for applications in the field of rock mechanics (Cundall 1971) since it intends to analyse especially discontinuous media, has been successfully used for the structural analysis of concrete dams and dam foundations.

It differs, advantageously in these cases, from FEM more from the numerical than the conceptual point of view, namely (Lemos 2008; Lemos 2012): (i) contact logic based on point contacts, suitable for large displacements; (ii) ease of generation of complex block patterns with the automatic contact detection; (iii) explicit solution algorithms using dynamic relaxation, for both static and dynamic analysis, instead of matrix solutions; and (iv) more satisfactory representation of failure modes involving complete block separation.

In the following sections, the basic principles of the method, the software currently used for dam structural analysis (e.g. Barla *et al.* 2004; Farinha 2010), its application to static and dynamic analysis, the contact representation and the solution procedure are presented.

C.2 Basic principles

In DEM, the structural system consists of an assembly of interacting polygonal blocks. In the earlier versions, only rigid blocks could be used. Later, the method was extended to deformable blocks (Cundall *et al.* 1978), discretizing each block into an internal finite-element mesh. Hybrid models with both block types are also available.

Nonetheless, rigid block models still have their field of application, being appropriate for problems involving strong materials or when the installed stress field is not relevant for the analysis. In these models, deformation is concentrated at the discontinuities, being even possible to adapt the joint stiffness to account for block elastic deformation, if it is not negligible. Rigid block models present a significant time-consuming advantage, especially for dynamic analysis.

For deformable blocks, FEM is applied to solve partial differential equations, given the boundary conditions, in order to compute nodal displacements, the stress field and equivalent nodal forces.

The solution algorithm of DEM is based on the integration of the equations of motion

of each block. In two-dimension analysis, the three equations of motion, related to the centroid of a rigid block or the nodal points of each finite-element of a deformable block, are separated in translational equations in the x-y plane expressed by,

$$m \cdot \ddot{u} + c \cdot \dot{u} = f \tag{C.1}$$

and a rotational equation expressed by,

$$I \cdot \ddot{\theta} + c \cdot \dot{\theta} = M \tag{C.2}$$

where m is the block mass, c is the damping coefficient, I is the moment of inertia around z-axis, u and θ are the corresponding displacement and angle of rotation, and f and M are the forces and moment at the degree-of-freedom, which include the contact forces and external loads, respectively.

Other innovation of this method is the modelling of mechanical contacts by means of interaction constitutive laws.

C.3 Software: Universal Distinct Element Code (UDEC)

The developments on DEM, since Cundall (1971), were the basis of the commercial software named Universal Distinct Element Code (UDEC), for two-dimensional analysis, whose first version was released in 1980. After several contributions and related studies, continuously improved versions have been released.

UDEC is intended for analysis of progressive failure and study of the influence of discontinuities. Therefore, UDEC is ideally suited to study potential modes of failure directly related to the presence of discontinuous features.

The general features of UDEC are (Itasca 2011):

- Manual and automatic joint generators built to create sets of discontinuities which represent jointed structures;
- Different material behaviour models are available: (i) Coulomb slip criterion which assigns elastic stiffness, frictional, cohesive and tensile strengths, and dilation characteristics to a joint; (ii) additional displacement weakening, as a result of loss in

cohesive and tensile strength at the onset of shear failure, can be included; (iii) continuously yielding joint model simulating continuous weakening behavior as a function of accumulated plastic shear displacement; (iv) Barton-Bandis joint model; and (v) additional properties that can be assigned individually.

- Rigid and deformable blocks, with several built-in materials;
- Assumes a two-dimensional plane-strain state;
- Explicit solution algorithm, which considers the central-difference method to integrate the equations of motion, allowing either dynamic or static analysis using the same calculation scheme;
- Both stress (force) and displacement (velocity) boundary conditions, which may differ throughout the model, are available;
- Fluid flow through discontinuities and voids can be simulated and mechanical-hydraulic analysis can be performed with different flow idealisation models;
- Reinforcement and thermal models are available;
- Contains a built-in programming language, FISH, which enables the user to define new variables and functions, allowing: (i) user-prescribed property variations in the grid; (ii) implementation of special joint generators; (iii) servo-control of numerical tests; (iv) specification of unusual boundary conditions, varying in time and space; and (v) automation of parameter studies.

In UDEC, the internal finite-element discretisation is based on uniform strain triangular elements. The choice of internal elements with a linear displacement field guarantees the block boundary to remain a polygonal line which simplifies contact calculations. It also has the advantage of fitting arbitrary block geometries, making use of well-tested procedures for automatic generation.

An user-friendly graphical interface is available in the last versions, with an extensive plotting facility built directly in UDEC. The history plots are especially helpful in monitoring the equilibrium or failure state during transient calculations. Data exporting is also possible which allows the interaction with other post-analysis software.

In this work, UDEC 5.0 (Itasca 2011) is used.

C.4 Contact representation

The representation of contact between blocks is based on the point contact approach, i.e. the interaction between blocks is represented by a set of contact points. Contrary to the joint element approach where the stresses in the joint elements are obtained directly from displacement differences between adjacent continuum elements, in point contacts the stress at a point depends solely on the joint displacement at that point, leading to a discontinuous stress distribution on the joint plane (Lemos 2008). Consequently, the accuracy of the stress distribution obtained on the joint plane is lower with this approach, requiring a larger number of contact points for rigorous stress analysis.

Three types of contact are available in UDEC (Figure C.1): vertex-vertex, vertex-edge and edge-edge. A great advantage of point contacts lies in the handling of large displacements with the system connectivity automatically updated during a simulation, due to contact detection technique. Point contacts may be relocated as the vertices move on the joint plane, and the transition between vertex-to-edge and edge-to-edge interactions is smooth (Figure C.2), due to the original logic implemented in UDEC of rounding corner contacts, as one of the contacts remains and its force can vary continuously.

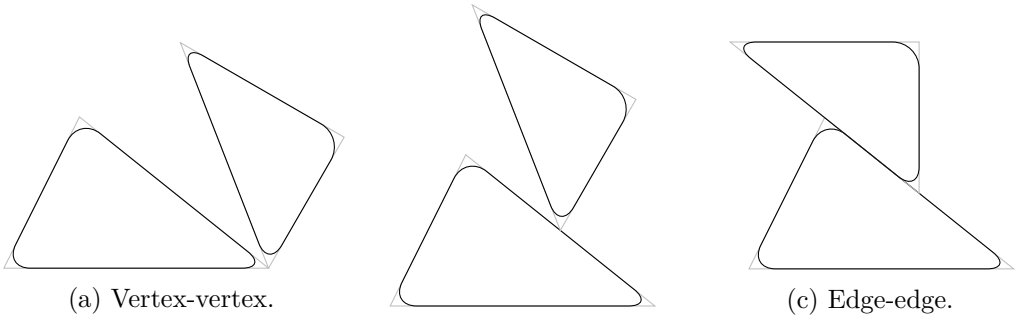

(a) Vertex-vertex. (b) Vertex-edge. (c) Edge-edge.

Figure C.1: Types of contact considered in UDEC.

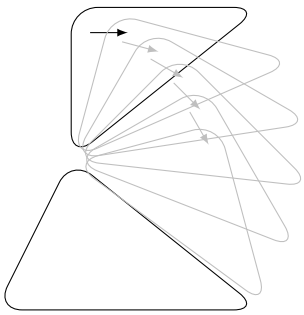

Figure C.2: Transaction between contact types: from vertex-vertex to edge-edge.

C.5 Static analysis

In static analysis, the aim is to find the final steady-state equilibrium conditions of the model. For that, in the transient phase, dynamic relaxation algorithms (Underwood 1983) are typically used in order to eliminate the vibrational response by introducing energy dissipation, thus allowing the convergence to equilibrium or the development of a failure mechanism. This leads to the so-called quasi-static solution.

Due to the difference in block and element size and stiffness, artificial damping is intended to improve the convergence to the final solution, since transient response is meaningless. For that purpose, high mass-proportional viscous damping is often use, by replacing the mass and the moment of inertia in the equations of motion (equations C.1 and C.2) by their scaled values (Lemos 2008).

C.6 Dynamic analysis

For dynamic analysis, Rayleigh damping is typically used, composed by mass-proportional and stiffness-proportional components,

$$c = \alpha \cdot m + \beta \cdot k \tag{C.3}$$

Optimal convergence is usually achieved by adjusting Rayleigh damping to a minimum frequency corresponding to the dominant mode in the response. Traditionally, minimum Rayleigh damping is set to 5% (Figure C.3), as recommended for the lower modes of concrete gravity dams (Chopra and Chakrabarti 1973).

The mass-proportional component, which affects mostly the lower frequencies, is included in the equations of motion. In an explicit algorithm, the stiffness-proportional component, responsible for damping the higher frequencies, is added to the contact forces and the element stresses (Lemos 2008).

The reduction of the time step due to the inclusion of the stiffness-proportional damping may be substantial, leading to excessively high run times. This term is often left out, specially in deformable block models, which increases the high frequency noise in the response. Bretas (2012) suggests that the type of damping chosen (mass-proportional, stiffness-proportional, or Rayleigh damping) depends on the sensitivity of the model to this parameter. In some cases, the consideration of the mass-proportional damping is the

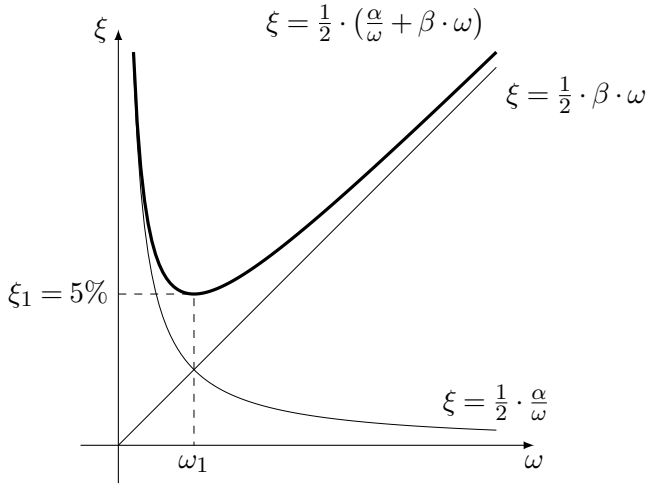

Figure C.3: Rayleigh damping definition.

best approach, since it significantly reduces the run time while not affecting considerably the system response.

C.7 Solution procedures

In order to ensure numerical stability, the time step of an explicit algorithm cannot be larger than a critical value. This may be a significant drawback in dynamic analysis, as very stiff joints or thin elements imply small time steps. For deformable blocks, smaller the maximum dimension of a finite-element, slower became the analysis. On the other hand, for static problems, scaled damping mitigates the problem, but large contrasts in stiffness or element size may still cause longer solution times. For that reason, very stiff blocks should be represented as rigid, and very stiff elastic joints should be attached to the adjacent blocks.

At each time step, when equations of motion must be solved for time-independent (static) or time-dependent (dynamic) external forces, the following cycle is repeated: (i) the application of the equations of motion, defining the differential equations based on the Newton's second law, produces new velocities and displacements; and (ii) the application of the constitutive models of the continuum elements (deformable blocks), interfaces and contacts, provides new stresses, nodal and contact forces, resulting in unbalanced forces which causes new velocities and displacements.

APPENDIX D

Root-finding methods

D.1 General considerations

Root-finding methods are iterative procedures that find approximated roots of a continuous function $f(x)$ which is not expressed in a closed-form.

The root-finding methods are distinguished, according to the concept followed, into:

- Bracketing methods that determine successively smaller intervals (brackets) containing the root;
- Interpolation methods that replace the original function by low-degree polynomials, which match the last computed values, to approximate its root.

The number of iterations needed is usually related to the accuracy required for the approximation of the root and/or the properties of the function.

Some methods for finding the roots of unknown continuous functions are detailed in the following sections.

D.2 Bracketing methods

D.2.1 General considerations

Bracketing methods are based on the intermediate value theorem which states that, at least, one root exists if a continuous function $f(x)$ has opposite sign at the end points of

an interval $[a, b]$, i.e. $f(a)/f(b) < 0$.

In the following sections, bracketing methods, such as bisection and false position methods, are detailed.

D.2.2 Bisection method

In the bisection method, the initial bracketing interval $[a, b]$ is successively bisected in equal subintervals by evaluating the function $f(x)$ at the end and middle points and selecting the subinterval in which the root must lie.

Although this method presents a slow convergence rate, its main advantages are the guaranteed convergence and the ability of predicting the necessary number of iterations N to find the root, given the maximum admissible error ϵ, such as,

$$N \geq \log_2 \frac{(a-b)}{\epsilon} \tag{D.1}$$

D.2.3 False position method

In the false position method, not only the sign but also the values of the function $f(x)$ computed at the end points of the interval are used. In each iteration, the root of the function is approximated by the x-intercept of the line that connects $f(a)$ to $f(b)$.

Although this method has a higher convergence rate than the bisection method, improvements, such as Anderson & Björk's (Anderson and Björck 1973), Illinois (Dowell and Jarratt 1971), and Ridders (Ridders 1979) methods, can be useful in slow-convergence conditions.

D.3 Interpolation methods

D.3.1 General considerations

Interpolation methods consist in approximate, iteratively, the continuous function $f(x)$ by a low-degree polynomial whose root is used as an approximation of the root of the original function.

D.3.2 Newton-Raphson method

Newton-Raphson method, such as other similar derivative-based methods, needs the explicit description of the derivative function to estimate a root. The function $f(x)$ is approximated by its tangent line around the previous guess point whose x-intercept point is easily computed. Apart from cases which may diverge due to derivative issues, the method obtains successively better estimates of the root, within an iterative procedure, given by,

$$x_i = x_{i-1} - \frac{f(x_{i-1})}{f'(x_{i-1})} \tag{D.2}$$

D.3.3 Secant method

In the secant method, the derivative of the function $f(x)$ required in the Newton-Raphson method is replaced by its finite-difference approximation, i.e. the secant line between two computed values of $f(x)$.

The estimation of the root, that follows an iterative process based on the two last computed values, is given by,

$$x_i = x_{i-1} - f(x_{i-1}) \cdot \frac{x_{i-1} - x_{i-2}}{f(x_{i-1}) - f(x_{i-2})} \tag{D.3}$$

This method requires two initial computed values $f(x_0)$ and $f(x_1)$ that, unlike the false position method, do not need to have opposite signs. Consequently, convergence is not guaranteed.

D.3.4 Steffensen's method

Steffensen's method (Steffensen 1933) is similar to Newton-Raphson's, since both have quadratic convergence rate, but it does not require the derivation of the function $f(x)$. Its disadvantage, when compared to the secant method, is that it needs double function evaluation to estimated the root, in an iterative process, since,

$$x_i = x_i - \frac{f(x_{i-1})}{g(x_{i-1})} \tag{D.4}$$

where,

$$g(x_{i-1}) = \frac{f\left(x_{i-1} + f(x_{i-1})\right) - f(x_{i-1})}{f(x_{i-1})} \tag{D.5}$$

Although the convergence rate is lower, secant method may converge faster than Steffensen's since it may need less function evaluations.

D.3.5 Muller's method

Muller's method (Muller 1956) replaces the function $f(x)$ by a parabola, i.e. a second-order polynomial, and takes its x-interception as the approximation of the root. The estimation of the root, that follows an iterative process based on the three last computed values, is given by,

$$x_i = x_{i-1} - \frac{2 \cdot f(x_{i-1})}{w \pm \sqrt{w^2 - 4 \cdot f(x_{i-1}) \cdot f[x_{i-1}, x_{i-2}, x_{i-3}]}} \tag{D.6}$$

where,

$$w = f[x_{i-1}, x_{i-2}] + f[x_{i-1}, x_{i-3}] - f[x_{i-2}, x_{i-3}] \tag{D.7}$$

and $f\left[x_v, \cdots, x_{v+j}\right]$ denotes divided difference given by,

$$f\left[x_v, \cdots, x_{v+j}\right] = \frac{f\left[x_{v+1}, \cdots, x_{v+j}\right] - f\left[x_v, \cdots, x_{v+j-1}\right]}{x_{v+j} - x_v} \tag{D.8}$$

This method requires three initial computed values $f(x_0)$, $f(x_1)$ and $f(x_2)$.

D.3.6 Inverse quadratic interpolation

In inverse quadratic interpolation, the function $f(x)$ is replaced by an inverse quadratic function, by applying the Lagrange interpolation formula using the three last computed points, whose root is given by,

$$\begin{aligned} x_i = & \frac{f(x_{i-2}) \cdot f(x_{i-1})}{(f(x_{i-3}) - f(x_{i-2})) \cdot (f(x_{i-3}) - f(x_{i-1}))} \cdot x_{i-3} + \\ & + \frac{f(x_{i-3}) \cdot f(x_{i-1})}{(f(x_{i-2}) - f(x_{i-3})) \cdot (f(x_{i-2}) - f(x_{i-1}))} \cdot x_{i-2} + \\ & + \frac{f(x_{i-3}) \cdot f(x_{i-2})}{(f(x_{i-1}) - f(x_{i-3})) \cdot (f(x_{i-1}) - f(x_{i-2}))} \cdot x_{i-1} \end{aligned} \tag{D.9}$$

This method also requires three initial computed values $f(x_0)$, $f(x_1)$ and $f(x_2)$. This method is seldom used by itself since its behaviour depends on the initial values chosen.

D.3.7 Brent's method

Since inverse quadratic interpolation converges fast, since it get close to the root, but performs poorly otherwise, Brent (1971) proposed a method that combines the bisection method, the secant method and inverse quadratic interpolation. Previously, Dekker (1969) had already suggested the combination of bisection and secant methods, but Brent's method also benefits from the inverse quadratic interpolation faster convergence rate in the vicinity of the root.

During Brent's method, tests are performed in order to determine which method is used in the next iteration. Initially, two brackets a and b, with opposite sign, are selected. A third point c is initially set equal to a. In the iterative procedure, b is interpreted as the best guess of the root, a is the previous guess, and c is the best guess with opposite sign. The new guess, computed from inverse quadratic interpolation (if $f(a) \neq f(c)$) or secant method (if $f(a) = f(c)$) is rejected if it does not lie up to three-quarters or half the way from b to c, respectively. In that case, the new guess is computed using bisection method. This process is repeated until convergence.